FABRICATION AND MASS TRANSPORT IN HIGH T_c SUPERCONDUCTORS

Ioannis Kontoulis, Dipl. Eng.

A thesis submitted for the degree of
Doctor of Philosophy of the University of London
and for the Diploma of Imperial College (DIC)

Department of Materials,
Imperial College, University of London

- August 1990 -

To my wife, Eleia,
for her patience and support

TITLE: FABRICATION AND MASS TRANSPORT IN HIGH T_c SUPERCONDUCTORS

ABSTRACT

This work investigates the behaviour of the high critical temperature (T_c) superconductors $YBa_2Cu_3O_{7-\delta}$ (YBCO) and $Bi_{1.7}Pb_{0.3}Sr_2CaCu_2O_x$ (BPSCCO) but only preliminary experiments are reported for BPSCCO. Fabrication, cation substitution, oxygen-ion concentration and conductivity/ diffusion related properties have been examined.

Several methods of fabrication have been investigated for YBCO in order to optimize the phase purity and the properties of the material. Solid state reaction has shown to be a simple and efficient method, while evaporation from nitrates and freeze drying did not produce good quality material. Material produced with mist pyrolysis, however, was of very good quality.

Replacement of the rare earth (R.E.) cation Y by Er, Gd and Nd has been attempted simultaneously with either barium deficiency or doping of the Ba site with potassium. In all cases the undoped (R.E.)$Ba_2Cu_3O_{7-\delta}$ material had a T_c of around 90 K while Ba-deficiency or K-doping resulted in a drop of T_c, except for $YBa_{2-x}K_xCu_3O_{7-\delta}$.

Oxygen stoichiometry in YBCO determines the phase (orthorhombic or tetragonal) and also whether the material is a superconductor. Therefore, the orthorhombic to tetragonal (O-T) transition temperature was examined by XRD in quenched material or in-situ by neutron diffraction. Potassium doped material had a higher O-T transition temperature than undoped YBCO when examined by X-ray diffraction (XRD) in quenched material, but no difference was detected by *in situ* neutron diffraction.

Oxygen conductivity at 400-800 C was determined by a solid state electrochemical method using a cell consisting of a mixed conductor (Ag, YBCO or BPSCCO) between two electronically blocking, ionically reversible electrolyte pellets (Yttium Stabilized Zirconia-YSZ or $Bi_{1.75}Sm_{0.25}O_3$-BiSm). Using DC and AC (impedance) techniques, the oxygen conductivity and therefore the diffusion coefficient was obtained and compared with results from other investigations.

ACKNOWLEDGEMENTS

I would like to thank my supervisor Professor B.C.H. Steele for his guidance and support throughout this study, as well as for filling numerous forms and reference letters for me (and probably more to come...).

I am pleased to thank Xavier Turrillas, Dan Waters, Kevin Ley and Francis Saba for their help, collaboration and useful discussions. I am also grateful to Bob Rudkin, Richard Sweeney, Nalin Salpadoru, Gordon Hicks, Mike Haddon and other staff of the department of Materials for providing their technical expertise.

I want to thank John Laverty and Sula Bungre from the Dept. of Physics; Bob Cywinski and Sue Kilcoyne from Univ. of Reading; Jerry Maiers from Rutherford Lab.; Prof. Schoonman and colleagues from Delft Univ. of Technology for their collaboration.

To the colleagues in B435, for all the funny, relaxed or frustrating moments we shared, I give my best wishes for the future, with special thanks to Steven Golden, Nasrullah Khan and Michael Priestnall for their support and advice.

Last but not least, I wish to acknowledge financial support for my first year from the Evgenidis Foundation, providing a scholarship awarded by the Governing Body of the Technical Univ. of Athens; for my second year for a NATO scientific fellowship and for my third year the British Council (fees) and the Commission of the European Communities for the award of a sectoral grant.

CONTENTS

LIST OF FIGURES

LIST OF TABLES:

LIST OF SYMBOLS

Latin

A – area

B_i – absolute mobility of species i

C – capacitance

c – concentration per unit volume

d – spacing

D_i^* – self diffusion coefficient of species i

$\tilde{D}_i$ – chemical diffusion coefficient of species i

e – charge of electron (1.602×10^{-19} Cb)

E – electric field

f – force

f – frequency

h – hole

H_{c1} – lower critical field

H_{c2} – upper critical field

I – current

J – flux

J_c – critical current density

j_i – current density of species i

k – Boltzman's constant (1.381×10^{-23} J/deg K)

ℓ – thickness

L – distance

M – atomic mass

m_n – mass of neutrons

M_w – molar weight

N – Avogadro's number

n_i – concentration of species i

p_n – momentum of neutrons

q – charge

R – resistance

R – Gas constant (8.314 J/deg K)

t – time

t[i] – tranference number of species i

T_c – critical temperature

u_i – drift velocity of species i

V – voltage

v_n – velocity of neutrons

Vo – oxygen vacancy

x – distance

Z – impedance

z – valence

Greek

γ – surface tension

ϵ – dielectric constant

ϵ_o – permittivity of free space

θ – diffraction angle

λ – wavelength

λ_L – London penetration depth

μ_i – mobility of species i

μ_i – chemical potential

ξ – coherence length

π – 3.14159

ρ – density

ρ – resistivity

σ_i – conductivity of species i

φ – angle

ω – period

LIST OF ABBREVIATIONS

BCS theory – Bardeen, Cooper and Schrieffer
BiSm – $Bi_{1.75}Sm_{0.25}O_3$
BPSCCO or BSCCO – $Bi_{0.2}Pb_{1.8}SrCa_2Cu_2O_x$
EDAX – Energy Dispersive Analysis of X-rays
HTS – High Temperature Superconductors
O-T – Orthorhombic-to-Tetragonal
R.E. or RE – Rare Earth
SEM – Scanning Electron Microscopy
SQUID – Superconducting Quantum Interference Device
t-o-f – time-of-flight
TGA – Thermogravimetric Analysis
XRD – X-Ray Diffraction
YBCO – $YBa_2Cu_3O_{7-\delta}$
YSZ or 8YSZ – 8% Yttrium Stabilized Zirconia
123 – $YBa_2Cu_3O_{7-\delta}$
124 – $YBa_2Cu_4O_8$
132 – $YBa_3Cu_2O_x$
211 – Y_2BaCuO_5

1. INTRODUCTION

Electrical ceramics are a relatively new field that emerged with the development of ceramic technology during the last four decades [1]. They have a large variety of applications and a quickly growing share of the market [2]. The applications range from the area of electronics (substrates, capacitors) to transducers, sensors and magnets [3]. New technologies and new products emerge as the result of development of new materials with interesting properties. Ceramic materials can be insulators, semiconductors, metallic conductors or even superconductors.

Ceramic high temperature superconductors have been a major scientific breakthrough for the last three years. Even though superconductivity was discovered by K. Onnes in 1911 [4] at 4.2 K for Hg, it was not until 1986 that high temperature superconductivity was found by Bednorz and Müller [5] at IBM Laboratories in Zurich in the $La_{2-x}Ba_xCuO_4$ ceramic superconductors at around 30 K.

Superconductivity is not a rare phenomenon. Until 1986, about twenty eight elements of the periodic system and approximately 700 compounds and alloys had been found to be superconducting [6]. Alloys such as Nb_3Sn with a transition temperature of 18 K and high critical current, enabled commercial applications.

The highest transition temperature until then was 23.2 K with the superconductor Nb_3Ge. Other materials that were known to display superconductivity, were organic compounds with low transition temperatures (1–2 K) and oxides. Sleight et al. [7] found $Ba(Pb,Bi)O_3$ to be superconducting at approximately 12 K in 1975. Their work motivated Bednorz and Müller [5] who discovered superconductivity in the La–Ba–Cu–O system near 30 K at 1986. This was a start to an enormous development of superconductivity. As it can be seen from figure 1.1, the average increase of critical temperature due to discovery of new materials, was 4 degrees per decade until 1986. Later, the new ceramic superconductors such as $La_{(2-x)}Sr_xCuO_4$ [8,9], $YBa_2Cu_3O_{7-\delta}$ discovered by Chu et al. [10], $Bi_2Sr_2CaCu_2O_x$ by Maeda [11] and $Tl_2Ba_2CaCu_2O_x$ by Sheng and Hermann [12] raised the critical temperature to 125 K.

Applications such as powerful magnets, sensitive magnetometers (SQUID's – Superconducting Quantum Interference Devices) and other devices, would have been impossible without superconductivity. Today, the discovery of new materials with much higher transition temperatures will

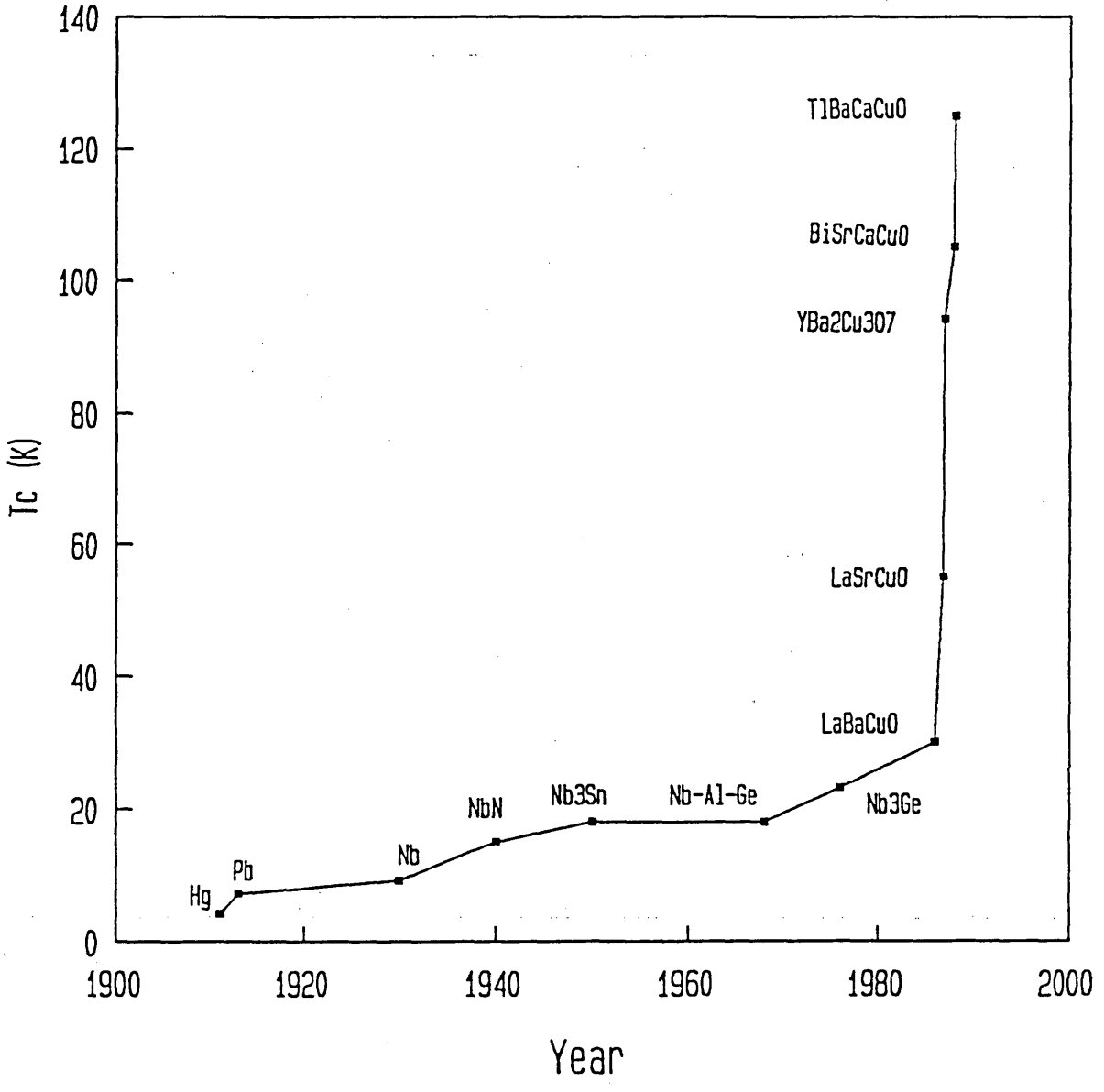

Figure 1.1: The increase of critical temperature due to the discovery of new materials.

open the way for other applications and make much cheaper the existing ones.

Superconductivity at temperatures greater than 77 K gives the prospect of replacing liquid helium with liquid nitrogen as a coolant. This will result in applications/ devices with smaller size and capital cost since liquid nitrogen does not require the sophisticated refrigeration and insulation systems used for liquid helium and also smaller operating cost since the price of liquid nitrogen is a tenth of the price of liquid helium.

Main objectives of research for the application of these novel materials are the optimization of critical temperature T_c, critical current J_c and physical properties through the development of fabrication techniques and the knowledge of their structure and behaviour.

Much work is therefore being done in the investigation of fundamental superconductive, magnetic, structural, chemical and other properties. Attempts to produce a new theory that can explain and predict superconductivity are under way, but with no success for the time being.

Various substitutions of the cations have been attempted in $YBa_2Cu_3O_{7-\delta}$ (YBCO) in order to improve the superconductive properties but in most of the cases there was a decrease of T_c. Oxygen content has been identified as a crucial factor for superconductivity and much work has been devoted to the structural changes that occur with the variation of oxygen content and their relation to superconductivity, as well as the oxygen kinetics of YBCO.

Control of the microstructure has also been an important field, since impurities and grain boundaries apparently act as weak links limiting the values of J_c, especially under the influence of magnetic fields. Highly oriented thin films with good J_c have been prepared, while lower J_c values are obtained for bulk samples. Considerable effort is being done for the fabrication of oriented bulk samples in order to improve their current-carrying capability.

This thesis is concerned with the fabrication and investigation of the properties of bulk ceramic superconductor $YBa_2Cu_3O_{7-\delta}$ (YBCO). Several fabrication techniques have been examined, mist pyrolysis being the most promising. Chemical substitution/doping of the Y and Ba cations and its effects on the structure, superconductivity and orthorhombic-to-tetragonal (O-T) transition was investigated. A solid state electrochemical technique was employed for the determination of oxygen conductivity and the diffusion coefficient was calculated. Oxygen kinetics were also examined for the $Bi_{2-x}Pb_xCa_2SrCu_2O_8$ (BPSCCO) ceramic superconductor.

2. LITERATURE SURVEY

2.1. Superconductivity

2.1.1. General

As a metallic material is cooled, its electrical resistivity decreases, since the lattice vibrations, and therefore the electron scattering, decrease. As the temperature approaches 0 K, the resistivity tends to a constant (residual) value, caused by impurities and other defects which destroy/distort the perfect periodicity of the lattice [13].

In the case of a superconductor, at a sufficiently low temperature, the resistivity drops suddenly to zero (figure 2.1) and the material undergoes a second order phase transition from the normal to the superconductive state. This temperature is called the critical or transition temperature (T_c).

The onset of superconductivity (T_c^{onset}) is usually defined as the temperature at which the resistivity is 90% of the normal and midpoint ($T_c^{midpoint}$) the temperature at the midpoint between 10%–90% of the normal resistivity (figure 2.1). Alternatively, it can be defined as the point were the second derivative of the resistivity becomes zero. Finally, the zero resistance transition temperature ($T_c^{R=0}$) is another very important characteristic, especially from the application point of view.

The magnetic properties of a superconductor are different from those of a normal conductor. A bulk superconductor will eject all the flux lines of a weak magnetic field, behaving as a perfect diamagnet (figure 2.2) [4], so that there is no magnetic field well within the specimen. This is the Meissner effect, first observed in 1933 by Meissner and Oschenfeld and is achieved by persistent surface currents which flow in a layer of finite thickness λ_L and hence the field does penetrate a distance λ_L which is called the *London penetration depth.*

If the magnetic field increases, materials behave in two ways: they either cease suddenly to be superconductors above a critical magnetic field H_c and the flux lines penetrate the material completely (type I superconductors) or the flux starts penetrating the material at a field H_{c1}, but part of it remains superconductive up to a value of H_{c2} (type II superconductors). The two types of behaviour are illustrated in figure 2.3, where the applied magnetic field is plotted against magnetization. H_{c2} has a very high value compared to the H_c of type I materials.

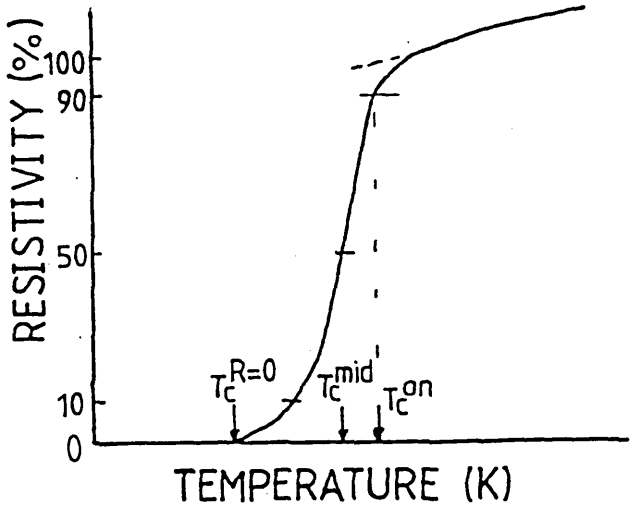

Figure 2.1: The change of resistivity during the superconductive transition

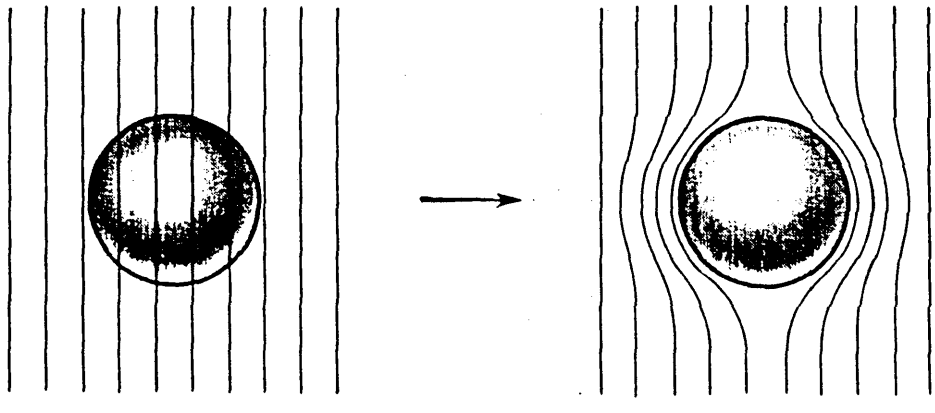

Figure 2.2: The Meissner effect: the magnetic field is expelled by the superconductor [4].

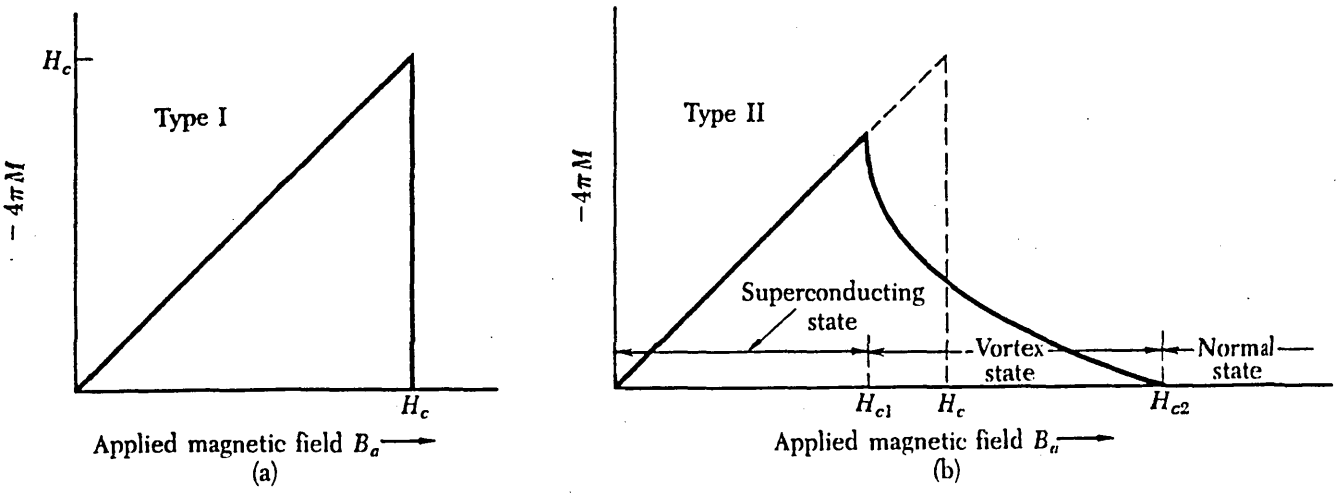

Figure 2.3: Magnetization versus applied magnetic field in type I and type II superconductors.

The distance over which superconducting electrons behave in a rigid way is called *coherence length* (ξ). The relative magnitude of λ_L and ξ determines whether the material is type I or II superconductor. If $\xi/\lambda_L>1$, the surface energy between normal and superconducting regions in an external magnetic field is positive and the transition to the normal state is sharp – type I behaviour. If $\xi/\lambda_L<1$, the energy is negative and the transition is gradual – type II behaviour [14].

The current that passes through a superconductor is associated with a magnetic field. If the produced field exceeds the critical magnetic field, the material returns to the normal state. The current density at which this occurs is called the critical current density (J_c). Only some of the type II superconductors for which J_c is sufficiently large, are useful for commercial applications.

Other phenomena characteristic of superconductivity are: a discontinuity of the specific heat at T_c, reflecting the second order transition from a relatively disordered (normal) state to a more highly ordered (superconducting) state of lower entropy [15], and the "isotope effect", the dependence of T_c on atomic mass. In conventional superconductors the relation is T_c $(M^{1/n})$ = constant, where M=atomic mass, n≈0.5.

2.1.2. Theories of Superconductivity

All the theories developed, attempted to explain the above phenomena (R=0, Meissner effect, specific heat discontinuity, isotope effect). The first theories developed by London, Landau–Ginzburg and Pippard were phenomenological and their equations gave a satisfactory macroscopic description of superconductivity and introduced important parameters such as the *London penetration depth* (λ_L) and the *coherence length* (ξ).

This work provided the base upon which Bardeen, Cooper and Schrieffer [16] formed a theory in 1957, known as the BCS theory, that incorporated the previous work, but furthermore, could explain the mechanism of superconductivity.

The BCS "microscopic" theory is based on the fact that the conduction electrons in a superconductor, pair up with one another due to an attractive interaction. The zero resistivity can be explained by assuming that a pair can only be scattered if the energy involved is sufficient to break it up into two single electrons. In general, this energy is not

available and so the electron passes on without any scattering.

As an electron is passing close to an ion, there will be a momentary interaction which might slightly modify the vibration of the ion. This in turn could interact with a second electron nearby which will also be attracted to the ion. The net effect of these two interactions is that there is an apparent attractive force between the two electrons, which appears due to the existence of the ion [14]. At low enough temperatures, this interaction dominates over the Coulomb repulsive force and the electrons form pairs of opposite spins and momentum ("Cooper pairs"). The distance between an electron pair, or the minimum length over which the wave-function can significantly change is the coherence length (ξ).

According to the BCS theory the energy of the electron pairs is lower than that of single electrons in the normal metal. This energy gap can justify the specific heat anomaly of conventional superconductors. The superconductive phenomena are explained by this theory and the predicted values of isotope effect, energy gap and other characteristic parameters relating to superconductivity agree well with experimental ones, as far as the conventional superconductive materials (metals and alloys) are concerned.

Modifications of the BCS theory have been proposed as well as completely different theories [17] involving the concept of bipolarons.

No theory however, can explain superconductivity in the new high temperature superconductive ceramics. It has been proved experimentally that electrons form pairs [18], but the order of magnitude of the isotope effect is small compared to that predicted from BCS theory [19]. As a result, all theories like BCS, based on a relatively strong electron-lattice interaction, have to be excluded or properly modified.

Referring to YBCO in particular, the structural change from orthorhombic (superconducting) to tetragonal (semiconducting) behaviour and the existence of Cu-O chains in the orthorhombic phase which do not exist in the tetragonal one, initially gave rise to theories attributing superconductivity to these chains.

Later on, Cu substitution experiments [20] with Fe and Co produced superconductive tetragonal YBCO, suggesting that CuO_2 planes (see chapter 2.3 for structure) are responsible for superconductivity. The subsequent discovery of Bi and Thallium compounds confirmed that the CuO_2 planes common to the three structures (figure 2.4) are the most possible place for superconductivity to occur.

Several theories, based on the two-dimensional character of the planes have been suggested [21,22]. They incorporate or are based on

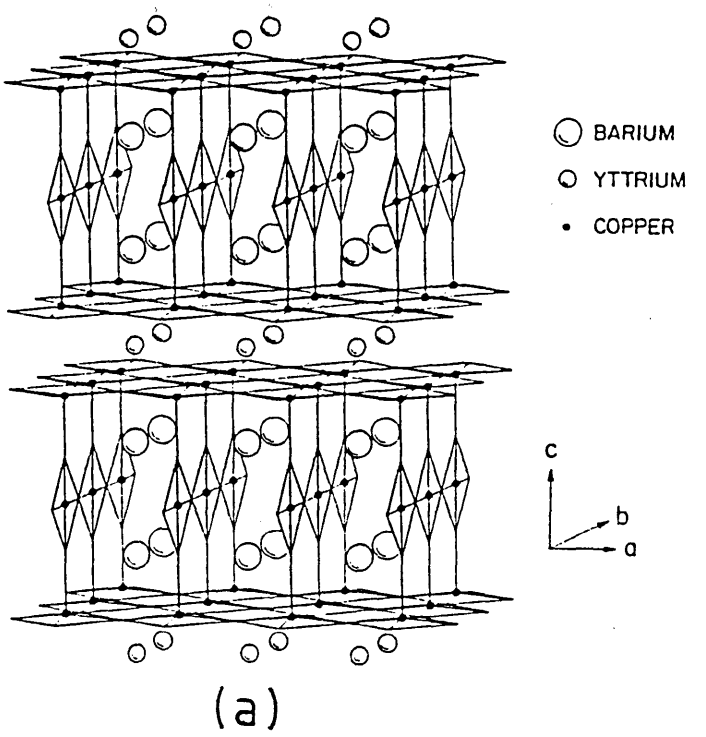

(a)

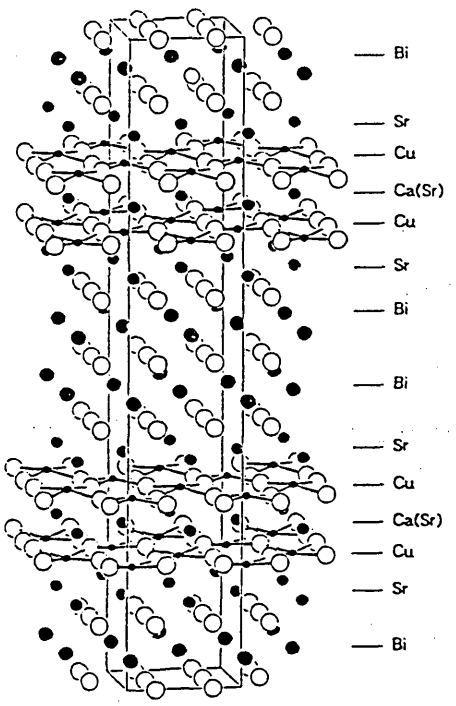

(b)

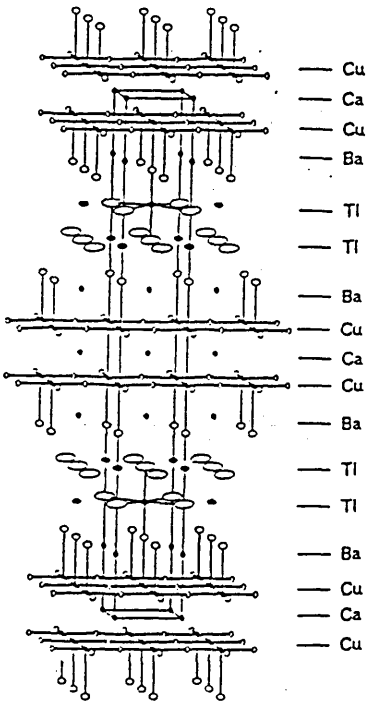

(c)

Figure 2.4: The layered structure of the superconductive compounds (a) $YBa_2Cu_3O_{7-\delta}$, (b) $Bi_2Sr_2CaCu_2O_8$ and (c) $Tl_2Ba_2CaCu_2O_8$

electronic and magnetic mechanisms (since strong electron–phonon interactions are unlikely), none of them however gives a satisfactory quantitative explanation.

2.1.3. Ceramic Superconductors

Ceramics can be insulators such as silicon dioxide (SiO_2) and aluminium oxide (Al_2O_3), semiconductors such as copper and zinc oxides [23], or oxides which have an electrical conductivity comparable to metals. ReO_3 [23] has a conductivity close to that of pure metallic copper at room temperature.

Therefore the existence of metallic – superconductive ceramics should not be surprising. In table 2.1 a list of known oxide superconductors is given along with the transition temperature and the possible substitutions with increasing critical temperatures.

TABLE 2.1: Ceramic superconductors

Formula	A	T_c (K)	Ref.
$SrTiO_{3-x}$		.7	24
TiO, NbO		1	25
Ag_7O_8X		1	26
Bronzes: A_xMoO_3	Na	4	27
A_xWO_3	or	6	28
A_xReO_3	K	4	28
$Bi(Pb_{1-x}Ba_x)O_3$		12	7
$Li_{1+x}Ti_{2-x}O_4$		13	29
$BiK_{0.4}Ba_{0.6}O_3$		28	30
$A_{2-x}Ce_xCuO_4$	Pr,Nd,Sm	24	31
$Nd_{2-x-y}Ce_ySr_xCuO_4$		22	32
$La_{2-x}A_xCuO_4$	Ba,Sr,Na,Ca	30,35,18,18	5,8,33,34
$Pb_2Sr_2Ln_{1-x}A_xCu_3O_{8+\delta}$	Sr,Ca	68	35
$ABa_2Cu_3O_{7-\delta}$ ("123")	Y,Ho,Dy,Er, Gd,Sm,Eu,Nd	94	36
$Bi_mSr_2Ca_{n-1}Cu_nO_{2n+m+2}$	m=1,2 n=1–3	12,22,85,110	33,11
$Tl_mBa_2Ca_{n-1}Cu_nO_{2n+m+2}$	m=1–3 n=1–3	80,100,125	38,12

A peculiarity of the latest superconductive compounds Bi-Sr-Ca-Cu-O / Tl-Ba-Ca-Cu-O is the variety of structures that have been observed. In order to identify easily the individual compounds they are denoted as 1201, 1212, 1223, 2212, 2223 etc.

Some of these oxide superconductors have common characteristics such as structural similarities and the departure from stoichiometry. Oxides such as $SrTiO_{3-x}$, $La_{2-x}Sr_xCuO_{4-\delta}$, $YBa_2Cu_3O_{7-\delta}$ have properties depending significantly on changes in stoichiometry. Moreover, the high temperature superconductors (HTS) have perovskite related structures which could be visualised as layered structures, with the copper - oxygen sublattice playing the most important part.

In most of the HTS the conducting species are holes (or hole-pairs at the superconductive state), with the exception of $A_{2-x}Ce_xCuO_4$ (A=Pr, Nd, Sm) which conduct through electrons.

2.1.4. YBCO: Superconducting Properties

The $YBa_2Cu_3O_{7-\delta}$ superconductor has a transition temperature which depends on the quality of the material and the oxygen content, that can be optimized by careful control of the fabrication procedure. Reported values give an onset of 90-94 K and zero resistivity of 86-92 K for oxygen content near 7 ($\delta \simeq 0$).

Magnetization curves usually show a transition temperature slightly lower than resistivity measurements and wider transitions. As the temperature becomes lower, more material superconducts and the diamagnetism is stronger. When magnetization stabilizes, the "saturation" point is said to be reached.

The isotope effect has been investigated for YBCO either by oxygen or copper substitution by their isotopes. Substitution of ^{16}O with ^{18}O gave a shift of 0.3 to 0.6 K [39,40] which is very small compared to the expected value of 5 K from the BCS theory. Use of ^{63}Cu and ^{65}Cu did not give any change in the transition temperature within the experimental error of ±0.2 K [41]. Both results indicate that the electron-lattice interaction is not as strong as the BCS theory predicts.

YBCO is a type II superconductor for which H_{c1} is very low but H_{c2} is high. Values given for the upper critical field H_{c2} do not agree well. For polycrystalline material it is 34-80 T at 77 K [42,43]. Single crystal studies have proved that there is an anisotropy of the critical field

perpendicular and parallel to the ab-plane, which is of the order of 5 times at 77 K and greater at lower temperatures. The highest values for the upper critical field at 0 K have been estimated at 240-330 T, when the field is parallel ($H_{c2_{||}}$) to the Cu-O planes (see figure 2.4) and 30-70 T when it is perpendicular ($H_{c2\perp}$) [42-47]. For the lower critical field, $H_{c1_{||}}$ is 5-24 mT and $H_{c1\perp}$ is 100-500 mT [46,48].

The anisotropy is not only limited to critical fields but also affects most of the properties of YBCO. For penetration depth, $\lambda_{L\perp}$=4500-7000 Å and $\lambda_{L_{||}}$=1300-1400 Å [48]. The large discrepancies for many parameters (H_c,λ_L,ξ) are mainly due to the difference in sample quality and to a smaller extent due to different experimental techniques/arrangements.

The value of coherence length is given as $\xi_\perp$=6-7 Å (perpendicular) and $\xi_{||}$=22-34 Å (parallel to the Cu-O planes) [45,46]. According to a review by Malozemoff [48] these values are 1.5-7 Å and 15-30 Å respectively. In general, it can be observed that the coherence length is smaller than that of conventional superconductors.

The critical current and its relation to the applied magnetic field, depends on the sample quality and whether it is in thin film or bulk form. J_c and the problems associated with it, will be presented in the next chapter.

2.1.5. Critical Current

In order for a type II superconductor to have a high critical current, it is not enough to have a large upper critical field.

If the applied field is greater than H_{c1}, a part of the material becomes normal and a network of vortices is formed where the magnetic flux penetrates the superconductor. If the field is uniform, the vortices are uniformly distributed, but if there is a field gradient, they tend to move across the material from a region of high field to one of low field. Reaching the low field region, vortex currents decay and vortices are annihilated, while on the high field region new vortices are being formed. This process, called *flux creep* results in power dissipation in the form of heat and eventually reduction of J_c and is most pronounced in defect-free conventional superconductors [49]. Depending on the way and the conditions that the flux lines move, this process is described as *flux flow* or *flux jumping*.

In the presence of lattice irregularities, the vortices are "pinned" so

that they do not move under the influence of Lorentz forces. Flux pinning, either by precipitating small normal or magnetic particles in the metallic matrix, or by dislocations produced by cold working of the alloys, resulted in an increase of the critical current density of conventional superconductors [50].

Another problem encountered for the low-T_c materials was flux-jump stability. It was found that flux jumping was suppressed when the diameter of a superconducting wire was decreased [51]. By optimization of the diameter of the wires, the multifilamentary superconductors were developed.

In the high temperature superconductors, problems for high critical current are of different nature.

Magnetization measurements of J_c in bulk or powdered YBCO [52], BSCCO and TBCCO material [53] give values of the order of 10^5-10^6 A/cm^2, while transport measurements give much smaller values. Usually reported values for bulk polycrystalline material at 77 K, 0 T, are less than 500 A/cm^2 and they drop by two orders of magnitude at fields between 0.1 and 1 mT. Therefore, even though the materials can have high J_c (as indicated by magnetization measurements), the transport current is limited by the inhomogeneities segregated at the grain boundaries, which act as weak link regions in the bulk material.

Thin films, however, have a different behaviour. The critical current in oriented thin films has reached values of 10^6 A/cm^2 at zero field and 77 K. By increasing the field to 4 T (77 K) its value drops to 10^2-10^5 A/cm^2 depending on the direction of the magnetic field [54], indicating the considerable effect of anisotropy of these materials.

Therefore, the main problems for J_c in HTS (High T_c Superconductors) are weak link regions -the grain boundaries- and the inherent anisotropy of these materials.

It is well known that impurities tend to segregate at grain boundaries. Furthermore, the formation of a carbon containing phase at YBCO grain boundaries has been demonstrated by Zhang et al. [55].

Direct measurements of the critical current density within grains and across grain boundaries in YBCO films showed a difference of two orders of magnitude (J_c grain bound.= 3.1x10^3 A/cm^2, J_c grains= 5x10^5 A/cm^2) [56]. More detailed experiments [57] in grains with controlled orientation on films grown on $SrTiO_3$ bicrystals, showed that the critical current along grain boundaries can reach 10^6 A/cm^2 if they have the same orientation along the a,b and c-axis. If they are aligned along the c-axis but the angle between the a-axis of the grains is more than 20^o, J_c

drops to 10^4 A/cm^2.

This behaviour is probably connected with the coherence length (ξ) of YBCO material. Commercial alloy superconductors have coherence lengths of 30–50 Å and lattice parameters of 4–5 Å [58,59], so that atomic scale defects have negligible effect on the transport J_c. In the case of YBCO, however, the coherence length $\xi_\perp$ is very small (1.5–7 Å) and if it is compared with the lattice spacing in the c–direction (11.7 Å), it is evident that any atomic scale defects such as in grain boundaries, will serve as weak–link barriers, reducing J_c.

In the a–b (CuO_2) plane, however, the coherence length is $\xi_{||}$=15–30 Å, larger than the a,b lattice parameters (3.8–3.9 Å) and therefore this direction should be favourable for high J_c's. This is demonstrated in the J_c values obtained for oriented thin films, with conduction taking place in the a–b plane.

In order to improve J_c in bulk HTS, special fabrication techniques, such as firing in a temperature gradient, are being used to induce orientation. Values of up to 10^4 A/cm^2 have been obtained for oriented polycrystalline YBCO material. This value drops to 10^3 A/cm^2 when a field of 1 T is applied [60].

Critical currents for thin films are very encouraging for commercial applications. Considerable improvement, however, will be necessary for bulk materials, through careful control of fabrication and microstructure.

2.1.6. Applications and Prospects

Commercial applications of superconductivity today are implemented with the conventional low T_c superconductors and they include high magnetic field generation for medical imaging systems (70% of the market), high energy physics and magnetic separation, as well as laboratory instruments and sensors [2,61].

There are several applications that have been demonstrated but they have not been commercialized such as electric current transmission lines, lossless interconnects and very fast switches in integrated circuits, high frequency applications, infrared sensors and transport systems (levitating trains) [22].

The new high temperature superconductors are candidates not only for these, but also a range of other applications as well. Considering the problems of critical current in bulk HTS materials, applications can be distinguished between heavy current and electronic ones [62].

Heavy current applications include high field magnets, homopolar motors and generators, power transmission lines, and energy storage devices. Unless considerable improvements are made, the HTS will not be able to operate at the high currents and fields that are required for these applications.

Judging by the progress in thin film technology however, it seems that electronic applications will be made possible. SQUID's (Superconductive Quantum Interference Devices) are being used for very sensitive detection of magnetic fields. SQUID behaviour has already been demonstrated with HTS and performance levels are approaching commercially useful values. A SQUID-cardiographer has been fabricated [63] and many laboratories around the world are experimenting with HTS SQUID's. A significant amount of work is also under way for high frequency (microwave) devices such as RF cavities and antennas.

Novel devices are also an interesting prospect, such as a superconducting lens, where a ring of HTS was used successfully to focus an electron beam [64].

Further developments in HTS technology will make many of these applications available commercially, creating essentially a large market for ceramic superconductors.

2.2. Phase Diagrams

2.2.1. The Y-Ba-Cu-O System in Air.

The study of the phase diagram for Y_2O_3-BaO-CuO is essential if a proper understanding of the relevant phase relations is to be achieved.

The pseudo-ternary diagram of $YO_{1.5}$-BaO-CuO at 950 C is shown in figure 2.5. The collected data [65-67] generally agree, even though some of the details are different.

Apart from the border phases such as $BaCuO_2$ and $Y_2Cu_2O_5$, there are three more phases: the superconducting $YBa_2Cu_3O_{7-\delta}$ ("123") and the non-superconducting Y_2BaCuO_5 ("211") and $YBa_3Cu_2O_x$ ("132").

The $YBa_2Cu_3O_{7-\delta}$ (YBCO) compound appears in two forms: the orthorhombic superconducting phase with oxygen stoichiometry near seven and the tetragonal non-superconducting phase with oxygen near six. Accurate diffraction patterns (position, indexing and intensity of peaks) can be found in references 67 and 68 for both phases. X-ray data for Y_2BaCuO_5 (211) and $YBa_3Cu_2O_x$ (132) phases which are the usual impurities of YBCO can be found in reference 67.

In the ternary diagram of figure 2.5, partial melting occurs [69] in the Cu rich region as indicated. If the original composition corresponds to that of YBCO and the temperature exceeds 980 C, the melting region is extended and includes YBCO which then melts incongruently. The products are 211 and a Cu and Ba rich liquid:

$$YBa_2Cu_3O_{7-\delta} \longrightarrow Y_2BaCuO_5 + L$$

The liquid consists of $BaCuO_2$ and CuO_x. The ternary diagram has been examined in detail in order to find possible solid solutions by Wagner et al. [70] and to determine the effect of slight variations in stoichiometry on T_c by Kogashi et al. [71]. In figure 2.6, the effect of stoichiometry on T_c is shown. Circles are used when the material exhibited superconductivity with T_c^{onset}=90-93.5 K, triangles when 77 K$\leq T_c^{onset} \leq$90 K and squares when the material showed semiconducting behaviour. It is evident that superconducting material is still formed even if a higher amount of Cu is used.

This effect along with the fact of incongruent melting mentioned

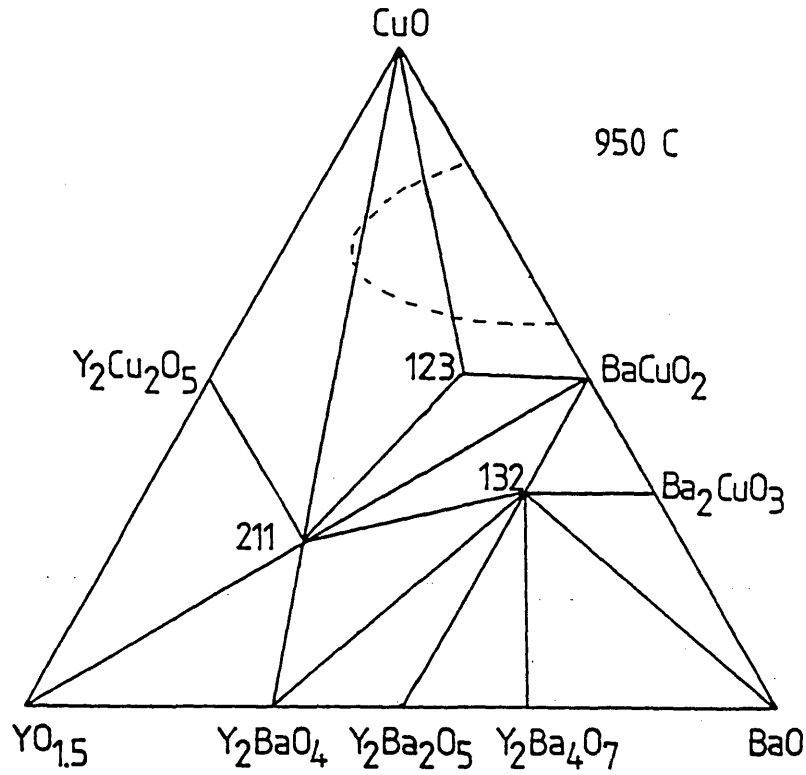

Figure 2.5: The pseudo-ternary $YO_{1.5}$-BaO-CuO phase diagram at 950 C in air. In the region enclosed by the broken line, a liquid is formed [65-67].

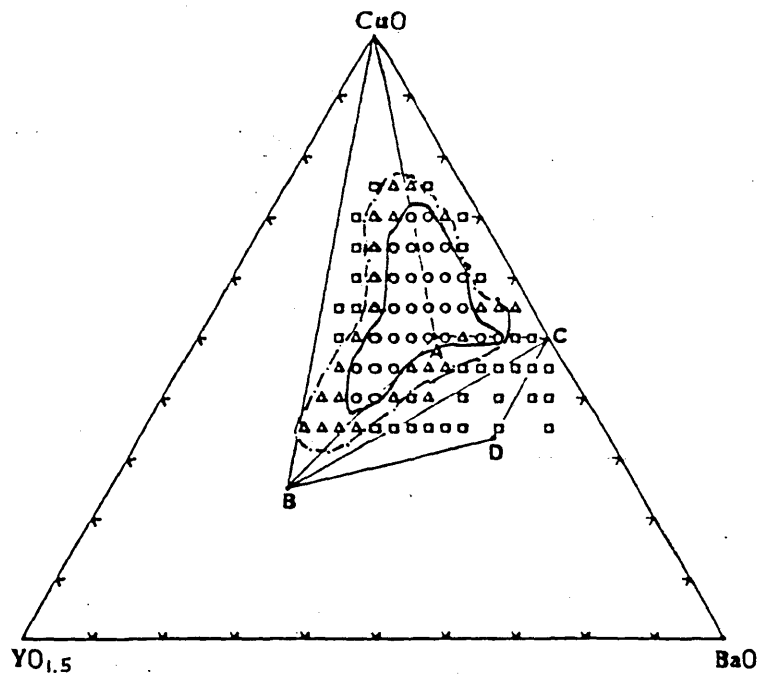

Figure 2.6: Pseudo-ternary diagram indicating the compositions for which superconductivity is observed. Circles show material with T_c>=90 K, triangles T_c>=77 K and squares T_c<77 K [71].

above, has found application for growing single crystals from the melt [72]. The starting composition has more Cu and Ba than the ratio 1:2:3, so that when the Ba–Cu rich liquid forms, the remaining material gives crystals of YBCO.

2.2.2. The Y–Ba–Cu–O System in Oxygen.

The oxygen partial pressure has an effect on the temperature of phase formation and decomposition. Sintering in oxygen atmosphere (P_{O_2}=1) has been found to stabilize YBCO against decomposition near the melting point [73]. High pressure studies of phase diagrams by Karpinski et al. [74] have shown that the melting point of YBCO, usually around 980 C, can be increased to 1100 C at pressures (P_{O_2}) around 100 atm. Furthermore, it has been found that the YBCO ("123") phase decomposes to two new phases, the 1–2–4 ($YBa_2Cu_4O_8$) and 1–2–3.5 ($YBa_2Cu_{3.5}O_{8-\delta}$) which are stable at P_{O_2}>110 atm. In figure 2.7 a log P vs. 1/T phase diagram shows these phase relations, as well as oxygen stoichiometry (x).

A preparation method for the 1–2–4 phase was devised by Cava et al. [75], where only one atmosphere of oxygen pressure is needed. This phase has a lower T_c of 80 K approximately but also the advantage that the superconducting properties do not depend on oxygen content. According to Miyatake [76], the T_c can reach 90 K by partial substitution of Y by Ca ($Y_{0.9}Ca_{0.1}Ba_2Cu_4O_8$).

Using oxygen atmosphere for sintering of YBCO, higher temperatures can be used, since the melting/ decomposition point is increased by 30 degrees, compared to sintering in air. It has been suggested [77] that better superconducting properties are obtained by annealing in oxygen at temperatures as high as 1030 C. Phase purity, normal state resistivity and critical current density are improved. This has been attributed to faster atomic motion which helps in producing better quality crystalline grains.

The atmosphere during the formation of YBCO is very important and it has been shown that even small quantities of CO_2 result in the formation of second phases, which are quite stable once they have formed [55,78].

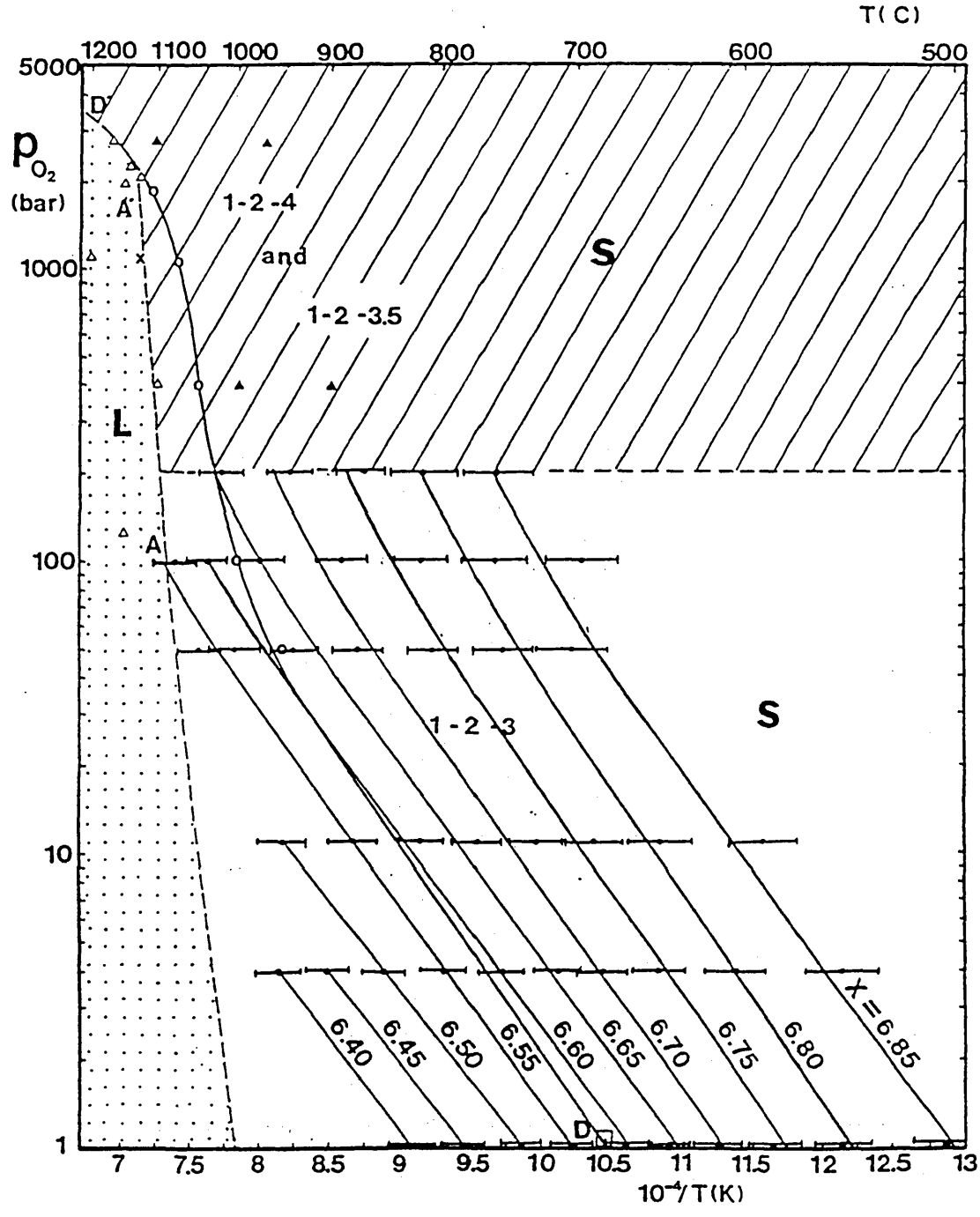

Figure 2.7: Log P_{O_2} vs. 1/T diagram showing the equilibrium between 1-2-3 ($YBa_2Cu_3O_{7-\delta}$)- S (solid), L (liquid) and 1-2-4, 1-2-3.5 ($YBa_2Cu_4O_8$, $YBa_2Cu_{3.5}O_{7+x}$)- S (solid), with parameter x the oxygen stoichiometry [74].

2.3. Structure of YBCO.

2.3.1. Perovskite Structure

The YBCO structure can be defined as a distorted, oxygen deficient, perovskite structure [79]. The simple perovskite structure is found in compounds with the formula ABO_3, where A is a relatively large cation in the centre of a cube and B is a smaller ion at the corners, while oxygen ions are at the unit cell edges [80]. A characteristic example is the one of $BaTiO_3$ in figure 2.8. The small ions B (Ti in figure 2.8) at the edges are in the centre of corner shared octahedra formed by oxygen ions.

In perovskites there are two main requirements: The A–O distance should be approximately $\sqrt{2}$ times the B–O distance (from geometrical considerations) and the electrostatic balance must be kept. The following A+B charge combinations are possible: 1+5 ($KNbO_3$), 2+4 ($BaTiO_3$) and 3+3 ($LaAlO_3$) so that a sum of 6 (for 3 oxygen ions) is always kept. Oxygen deficiency is sometimes possible as in $SrVO_{2.5}$ when the small cation B is forced to have an intermediate oxidation state.

The superconductive compound $YBa_2Cu_3O_{7-\delta}$ is a derivative of the cubic perovskite structure, tripled along one axis with cell parameters $a \approx b \approx a_0$, $c \approx a_0/3$, where a_0 is a typical perovskite cell parameter.

Depending on the oxygen content of the formula, two phases appear: the orthorhombic superconductive $YBa_2Cu_3O_7$ and the semiconducting phase $YBa_2Cu_3O_6$. The two phases can be fabricated reversibly by controlling the thermal treatment (temperature, atmosphere) and they display different electrical and physical properties.

2.3.2. The $YBa_2Cu_3O_7$ Orthorhombic Structure

The YBCO structure can be derived from the stacking of three simple perovskite blocks as shown in figure 2.9. Y and Ba are the large A ions and Cu is the small B ion surrounded octahedrally by oxygen ions. According to this, the stoichiometry should be:

$$ABO_3 \longrightarrow A_3B_3O_9 \longrightarrow \text{"}(YBa_2)Cu_3O_9\text{"}$$

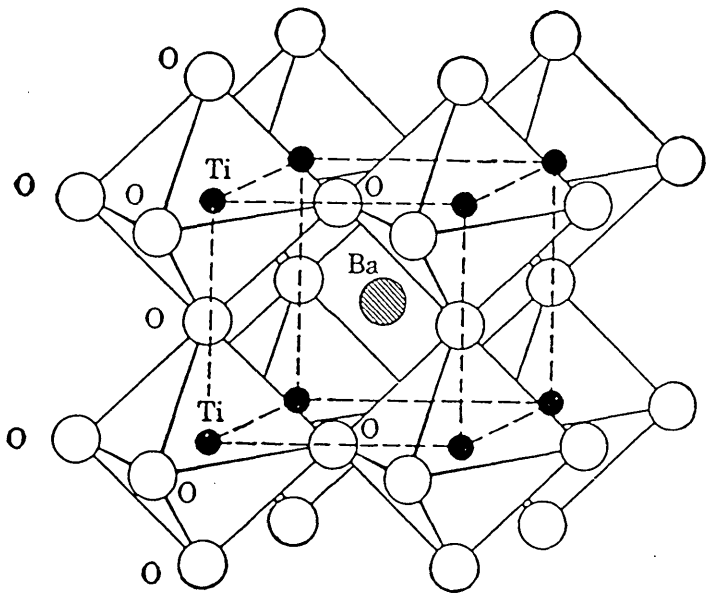

Figure 2.8: The $BaTiO_3$ perovskite structure showing the octahedra of oxygen surrounding titanium atoms.

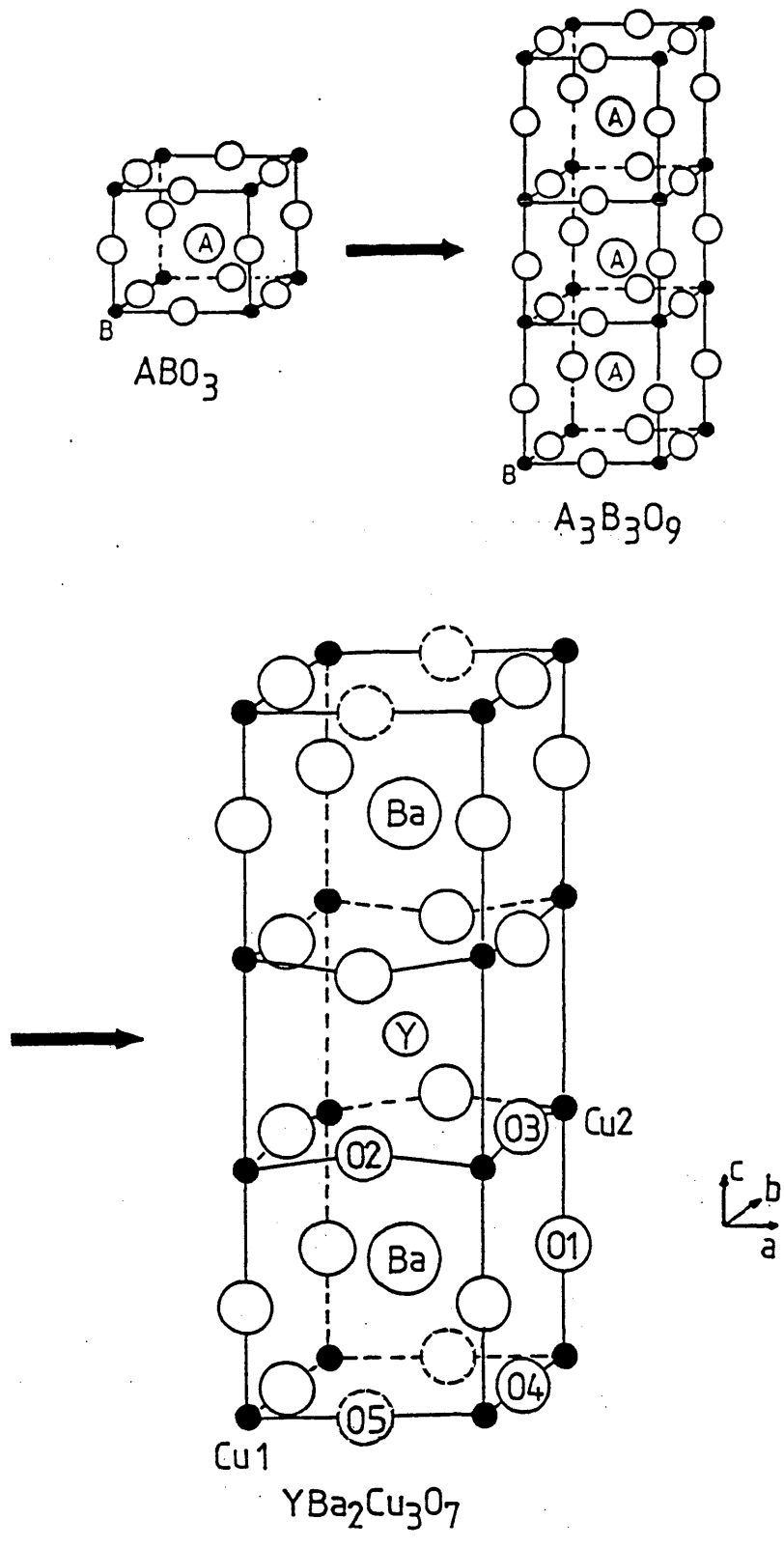

Figure 2.9: The orthorhombic $YBa_2Cu_3O_{7-\delta}$ (123) structure, as derived from the simple perovskite

Since Ba has a valence of 2+, unlike Y (3+), the oxygen stoichiometry should be reduced to 8. Furthermore, it is very difficult for copper to be at a 3+ state, so it maintains a valence between 2+ and 3+. The result is that more oxygen vacancies are created and the oxygen stoichiometry of the ideal YBCO structure becomes 7. In the real structure, the oxygen stoichiometry can vary between 6 and 7:

$$\text{"}(YBa_2)Cu_3O_9\text{"} \longrightarrow YBa_2Cu_3O_7 \longrightarrow YBa_2Cu_3O_{7-\delta} \longrightarrow YBa_2Cu_3O_6$$

The bigger ions Ba and Y occupy positions in the structure so that a Ba–Y–Ba sequence is formed along the c–axis. The a and b–axis are of the order 3.8Å which is the usual basic size for a perovskite cell. The c–axis is tripled, being 3.8x3=11.4Å approximately.

Considering the ideal "$YBa_2Cu_3O_9$", Cu atoms would all be in octahedral coordination. Because of the existence of oxygen vacancies, Cu atoms are surrounded of either 5 or 4 oxygen atoms instead of 6. According to their position they are characterised as Cu1 or Cu2.

Cu1 atoms are at the edge of the cell, in square–planar (four–fold), coordination forming linear chains of corner shared square planes oriented along the b–axis [81]. Cu2 atoms are located near the centre of the cell, they have pyramidal (five–fold) coordination and they form two dimensional layers of corner shared square pyramids. These layers are usually called "the Cu–O planes" in contrast with "the Cu–O chains" formed by Cu1.

There are five different positions for the oxygen atoms. O1 lies between Cu1 and Cu2 at the same plane as Ba atoms and it is the apex of the square pyramidal Cu2, while O2 and O3 atoms form the base of the pyramid.

The Cu–O "chains" are made from Cu1 along with the O4 atoms. The O5 site is the position between the chains and it is almost totally vacant (it has a very small occupancy factor) [82]. The occupancy of the O4 site, on the other hand, is almost 1 in the orthorhombic structure, resulting in an overall stoichiometry of 7. In the tetragonal phase, the O4 occupancy is 0, so the overall oxygen stoichiometry is 6.

Many structural refinements have been carried out by using either neutron or X–ray diffraction of single crystals or polycrystalline powders [79,82–87]. Slight variations of the results are due to differences in oxygen stoichiometry and fitting procedures. In one case, refinement of Cu occupancy in single crystals gave a copper deficiency of 4–8% [87].

The orthorhombic structure of YBCO has a Pmmm symmetry. The

atom positions are: Cu1 at (0 0 0), Cu2 at (0 0 z), Ba at (1/2 1/2 z), Y at (1/2 1/2 1/2), O1 at (0 0 z), O2 at (1/2 0 z), O3 at (0 1/2 z), O4 at (0 1/2 0) and O5 at (1/2 0 0). Cell parameters along with the value of z, the temperature factor B($\AA^2$) and the site occupancy (N) are given in table 2.2 from results of four different groups [79,82,88,89]. It can be observed that the results agree very well.

2.3.3. The $YBa_2Cu_3O_6$ Tetragonal Structure.

The tetragonal phase results either from the removal of the O4 atoms from the CuO chains (so that both O1 and O4 sites are vacant) or when the oxygen in the basal plane is disordered and evenly distributed in the O4 and O5 sites; something that usually occurs at oxygen stoichiometry lower than 6.5.

In both cases, the b-axis shrinks and at the same time a-axis expands so that eventually the structure becomes tetragonal (a=b), as shown in figure 2.10. The transition from the orthorhombic to tetragonal phase is gradual since oxygen stoichiometry can take any value from 6 to 7. As the stoichiometry decreases, the orthorhombic distortion of the cell (a-b) decreases until it becomes zero.

The tetragonal phase is not superconductive and has a very high room temperature resistivity. It behaves like a semiconductor, so its resistivity increases with decreasing temperature. The space group is P4/mmm and the cell parameters are approximately a=3.858 and c=11.78 $\AA$ respectively [84,90] and they depend on the exact oxygen stoichiometry.

At the temperature of approximately 950 C required for the formation and sintering of YBCO, the material has the tetragonal structure. In order to increase the oxygen stoichiometry and form the orthorhombic structure, slow cooling and a step of oxygen annealing at low temperature (400-500 C) is necessary.

X-ray diffractograms can be easily used for the distinction of the orthorhombic from the tetragonal phase. Four sets of peaks at 27-28, 32-33, 46-48 and 58-59 degrees 2θ respectively, (Cu $K\alpha$ radiation) show an inversion of intensities.

The orthorhombic to tetragonal (O-T) transition is a very important feature since it defines whether the material will be superconductive or not. The various effects of oxygen stoichiometry and transport have received much attention and will be presented in a separate chapter.

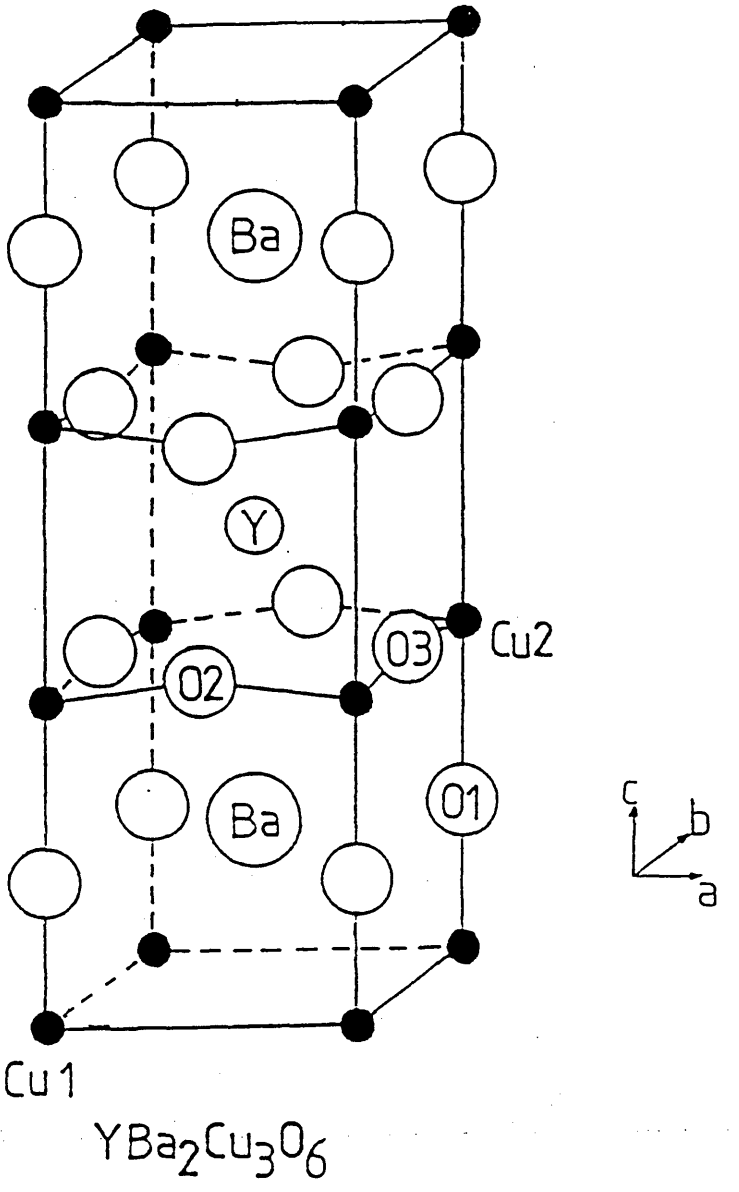

Figure 2.10: The tetragonal structure $YBa_2Cu_3O_6$

Table 2.2: Results of Rietveld refinement for YBa2Cu3O7.

Atom	Parameter	Cox et al.[82]	Capponi et al. [79]	Beno et al.[88]	Beech et al. [89]
Ba	z	0.189(3)	0.1841(3)	0.1843(3)	0.1839(2)
	B(Å^2)	0.4(1)	0.6(1)	0.54(5)	0.65(5)
Y	B(Å^2)	0.2(1)	0.6(1)	0.46(4)	0.56(4)
Cu(1)	B(Å^2)	0.2(1)	0.4(1)	0.50(5)	0.55(4)
Cu(2)	z	0.3546(2)	0.3549(9)	0.3556(1)	0.3547(1)
	B(Å^2)	0.3(1)	0.5(1)	0.29(4)	0.49(4)
O(1)	z	0.1589(3)	0.1581(4)	0.1584(2)	0.1581(2)
	B(Å^2)	0.5(2)	0.9(1)	0.67(5)	0.78(5)
	N	2.01(3)	2.0	2.0	2.0
O(2)	z	0.3783(3)	0.3779(4)	0.3773(2)	0.3779(2)
	B(Å^2)	0.5(2)	0.1(1)	0.56(5)	0.57(5)
	N	2.01(3)	2.0	1.89(2)	2.0
O(3)	z	0.3780(3)	0.3777(5)	0.3789(3)	0.3776(2)
	B(Å^2)	0.4(2)	0.3(1)	0.37(5)	0.55(5)
	N	2.02(3)	2.0	2.0	2.0
O(4)	B(Å^2)	1.6(3)	2.4(3)	1.35(5)	1.73(9)
	N	0.96(2)	1.0	0.92(2)	1.0
O(5)	B(Å^2)	1.6	–	–	–
	N	0.04(1)	–	–	–
	a	3.8172(1)	3.8206(1)	3.8231(1)	3.8198(1)
	b	3.8822(2)	3.8851(1)	3.8863(1)	3.8849(1)
	c	11.6707(4)	11.6757(4)	11.6809(2)	11.6762(3)

2.3.4. Comparison with Other Superconductors

Most of the high temperature superconductors contain copper and they have some common structural characteristics. The copper position in the lattice is the most important, since in all these structures there are planes composed of Cu and O ions. In figure 2.11 a very generalized picture of the structures of $La_xSr_{2-x}CuO_4$, $YBa_2Cu_3O_7$, Bi/Tl-2201, 2212 and 2223, and $Pb_2Sr_2Ln_{1-x}Ca_xCu_3O_{8+\delta}$ phases is given. All these phases can be approximately described as a sequence of Cu-O layers (usually Cu in pyramidal co-ordination) and layers containing Ba-O or Sr-O and possibly Bi-O or Tl-O. The CuO layers, can be separated by a cation layer (no oxygen) such as Y, Pr or Ca.

The combination that appears to be present in all these phases is the Cu-O layers having Ba-O or Sr-O in the near space. It has been suggested that even though the Cu-O planes appear to be mainly responsible for superconductivity, the accompanying layers (Ba/Sr - Bi/Tl - Ba/Sr, drawn as solid blocks in figure 2.11) appear to play an essential rôle as "charge reservoirs", controlling the electron hole concentration on the planes and, hence, also controlling T_c [91].

Even though it is not feasible to "design" similar structures of Cu-O planes coupled with "charge reservoirs", this observation can probably be of value as a general guideline in experimental and also theoretical investigations for superconductivity.

In the case of YBCO the importance of the (Ba-Cu chains-Ba) layers is well known since the oxygen deficient, tetragonal phase is not superconducting. The Cu-O chains are destroyed when oxygen is removed from them and so the "charge reservoir" cannot provide the required hole concentration for the material to be superconducting.

Another very important common characteristic for HTS is the average valency for Cu (in the Cu-based materials) and for Bi (in phases such as $Ba_{1-x}K_xBiO_3$) and the nature of their bond with O (oxygen). The cation valency is an average between 2+ and 3+ for Cu and between 3+ and 5+ for Bi. Sleight [92] has suggested a mechanism for superconductivity based on disproportionation reactions such as:

$$2Cu^{II} \longrightarrow Cu^{I} + Cu^{III}$$

and

$$2Bi^{IV} \longrightarrow Bi^{III} + Bi^{V} ,$$

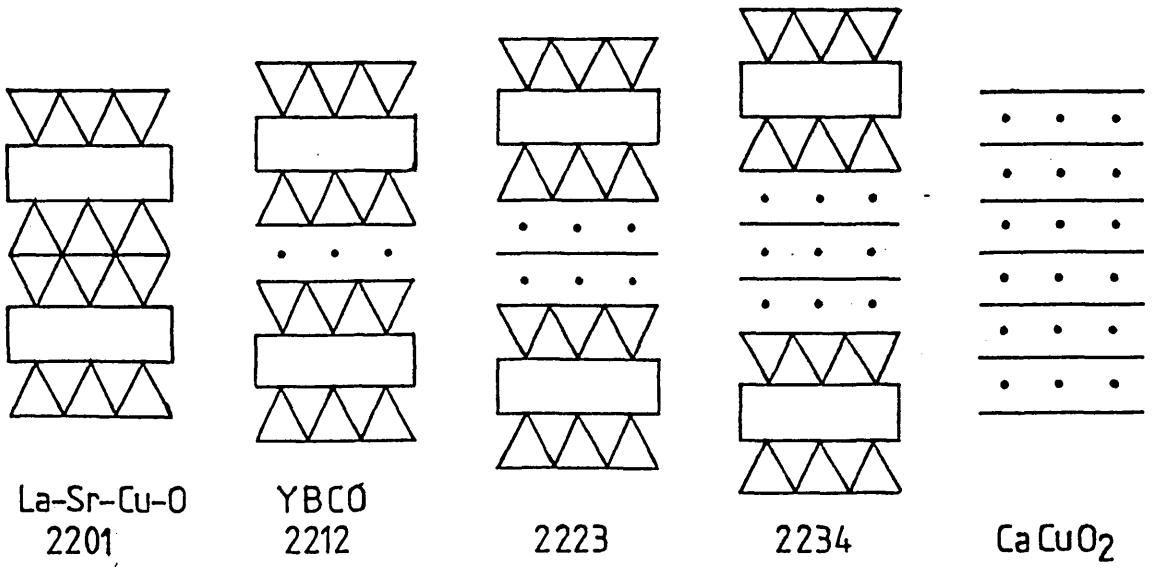

Figure 2.11: Common structural characteristics of superconductive compounds: CuO layers are coupled with Ba/Sr - [Bi/Tl] - Ba/Sr plane assemblies. Triangles represent Cu surrounded by O in pyramidal coordination, rectangles Ba or Sr - O assemblies, straight lines CuO planes and lines of dots rare earth or Ca cation layers. The 2201–2234 are the Bi–containing superconductors.

in relation with spin pairing reactions.

In this way, the behaviour of YBCO and $La_xSr_{2-x}CuO_4$, with superconducting properties drastically changing with oxygen stoichiometry, can be explained, since through oxygen, the overall charge and therefore the aforementioned reactions, are affected.

In most of the other HTS, however, the amount of oxygen that exists in their structure does not change significantly and therefore the dependence of superconducting properties on oxygen stoichiometry is much smaller.

2.4. High Temperature Defect Chemistry and Mass Transport

2.4.1. Oxygen stoichiometry and superconductivity

Oxygen stoichiometry depends on the annealing temperature and atmosphere of YBCO. In figure 2.12, oxygen content is plotted against temperature, varying the partial pressure of oxygen [93]. It can be seen that a maximum stoichiometry of 6.9 approximately is achieved when the temperature is around 400 C and the atmosphere is oxygen (P_{O_2}=1 atm). At temperatures lower than 400 C there is no change in oxygen stoichiometry.

The importance of oxygen content in the superconducting properties can be realized from figure 2.13 where T_c is lowered significantly as the annealing temperature in oxygen is increased [35]. Using an atmosphere with a lower P_{O_2}, a similar effect is observed, in fact, superconductivity can be suppressed altogether if the material becomes tetragonal.

The formation of the ceramic YBCO requires temperatures around 950 C that result in a low initial oxygen content and poor superconductive properties. In consequence, slow cooling and annealing at around 400 C in oxygen is necessary in order to maximize the oxygen content and hence optimize the superconductive properties of the material.

2.4.2. Determination of Oxygen Stoichiometry

TGA

The most usual method of determination of the oxygen stoichiometry is Thermogravimetric Analysis (TGA). Gallagher et al [94] used forming gas (10%H_2, 90%N_2) to create a reducing atmosphere at approximately 900 C. After identification of the phases present with X-ray diffraction, the following reaction was proposed:

$$YBa_2Cu_3O_{7-\delta} + (3.5-\delta)/2H_2 \longrightarrow 1/2Y_2O_3 + 2BaO + 3Cu + (3.5-\delta)H_2O$$

As a result, the remaining weight after the reduction corresponds to a fixed stoichiometry of 3.5 oxygen atoms per formula. In this way it is possible to calculate the original oxygen stoichiometry and data such as in

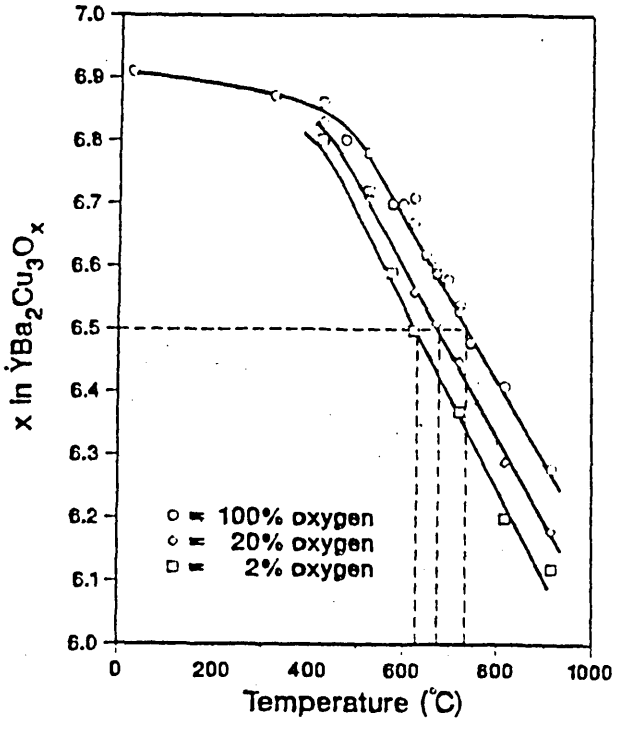

Figure 2.12: Oxygen content against temperature with varying atmosphere (calculated from TGA results) [93].

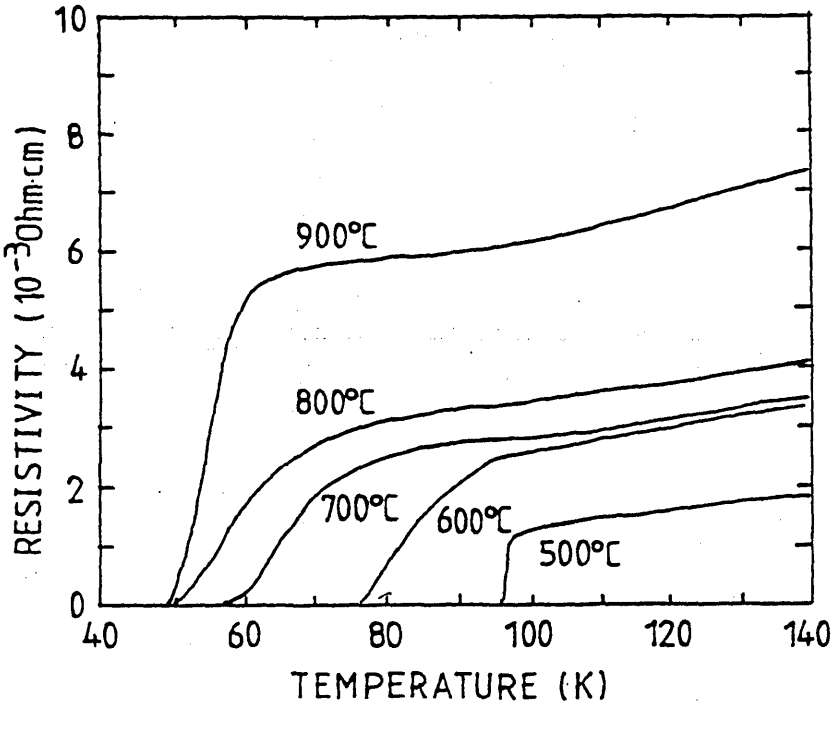

Figure 2.13: Variation of superconductive properties with annealing temperature and oxygen atmosphere [35].

figure 2.12 are obtained.

Neutron or X-Ray Diffraction

Another way to calculate oxygen stoichiometry is by neutron or in some cases X-ray diffraction [82-90]. The diffracted radiation is observed and with the help of Rietveld refinement programs, the occupancy factors for each atom are found. This method has the advantage that it takes into account only the oxygen that exists in the YBCO structure and not in other impurity phases. However, preferred orientation and different requirements from the refinement program may reduce the accuracy of these measurements.

Iodometric titration

In this method, the average copper oxidation state is determined and from this, the oxygen stoichiometry can be calculated [95-97]. In the first step, the total Cu content is determined. The YBCO material is dissolved in boiling HCl acid so that all Cu is converted to Cu^{2+}. Adding KI, CuI is formed and the released I_2 is measured through titration with sodium thiosulfate.

$$Cu^{2+},Cu^{3+}(\text{in YBCO}) \xrightarrow{(HCl)} Cu^{2+}\ (aq)$$

$$Cu^{2+}(aq) + 2I^- \longrightarrow CuI(s) + 1/2I_2\ (aq)$$

$$S_2O_3^{2+} + 1/2I_2 \longrightarrow S_4O_6^{2+} + I^-$$

In the second step, in a nitrogen atmosphere, another YBCO sample (from the same batch) reacts with diluted HCl containing KI, so that any Cu^{3+} will react with three I ions, instead of been converted to Cu^{2+} as in the first step. As a result, more sodium thiosulfate will be necessary to titrate the released I_2. From the difference of the thiosulfate necessary for the titration in these two steps, the Cu^{3+}/Cu^{2+} ratio can be determined.

$$Cu^{2+}(\text{in YBCO}) + 2I^- \longrightarrow CuI(s) + 1/2I_2\ (aq)$$

$$Cu^{3+}(\text{in YBCO}) + 3I^- \longrightarrow CuI(s) + I_2\ (aq)$$

This method has been used extensively in order to provide higher accuracy than the reduction/TGA method.

Other techniques

A variety of other techniques has also been developed such as the volumetric measurement of gases evolving from the dissolution of YBCO in dilute HCl acid [98], the charged particle activation method [99] and coulometric titration [100], although they have not been used by many research groups.

2.4.3. Orthorhombic-to-Tetragonal (O-T) Transition

Oxygen stoichiometry can change in YBCO at temperatures higher than 400 C. Any variation of the stoichiometry is necessarily connected with an effect on the structure of the material. Oxygen can be removed from the base plane containing the Cu-O chains appearing in figure 2.14(a).

The site occupancies of O4 and O5 versus temperature from in situ neutron diffraction data in oxygen are shown in figure 2.15 [93]. The O4 site loses oxygen if the temperature is higher than 400 C and a partial occupancy of the O5 site begins. When the oxygen stoichiometry becomes very low, the two site occupancies become equal and from the ordered orthorhombic structure, the disordered tetragonal phase results, where a=b. This process is illustrated in figure 2.14 (a)-(c).

The 90 K superconducting orthorhombic phase with $a<b\approx c/3$, is usually referred to as Oi, while the still orthorhombic ($a<b<c/3$) but slightly disordered phase with lower T_c, is referred to as Oii. The tetragonal phase (T) with $a=b<c/3$ is not superconducting.

Studies of T_c [101] and structure [102,103] versus the oxygen content have revealed that under certain circumstances, an oxygen ordered, orthorhombic phase with T_c=60 K can be formed at stoichiometry 6.5-6.7. In figure 2.16 the superconductive transition temperature versus oxygen content is shown [101]. In this case the samples became oxygen deficient with a low temperature (Zr-gettering) technique, therefore, maintainance of oxygen ordering was favoured. Indeed, TEM and electron diffraction studies of the 60 K phase by Chaillout et al. [104] showed indications of a superstructure due to oxygen ordering, with doubling of the a-axis when only half of the O4 sites where occupied.

The study of cell parameter variation can yield information about the O-T transition. This transition is mainly influenced by the temperature and the atmosphere. In figure 2.17 the effect of ambient oxygen on cell parameters is shown from neutron diffraction data [93]. It is obvious that

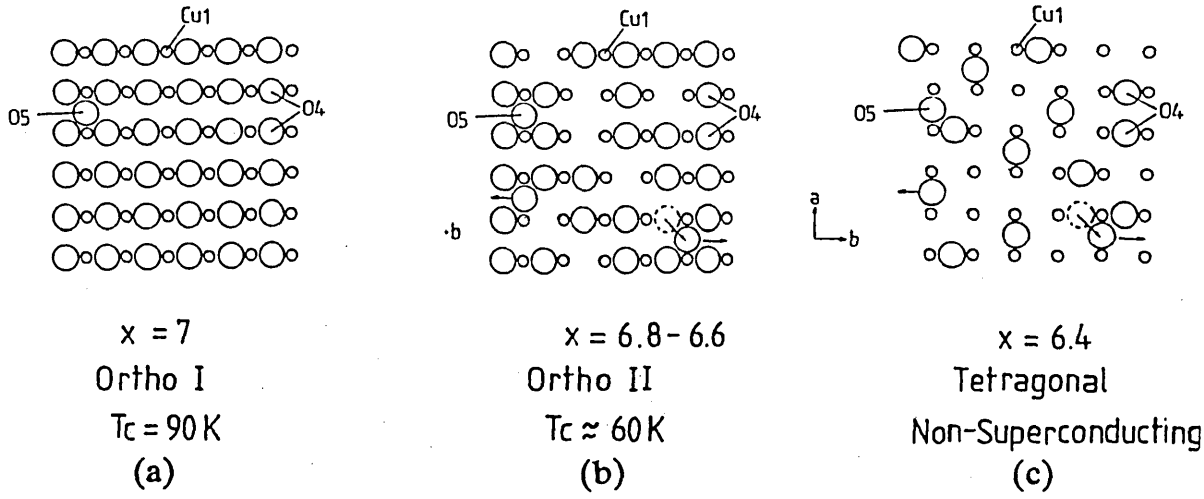

Figure 2.14: The Cu–O base plane: (a) Oi orthorhombic structure with Cu–O chains, (b) Oii disordered orthorhombic and (c) T tetragonal phase.

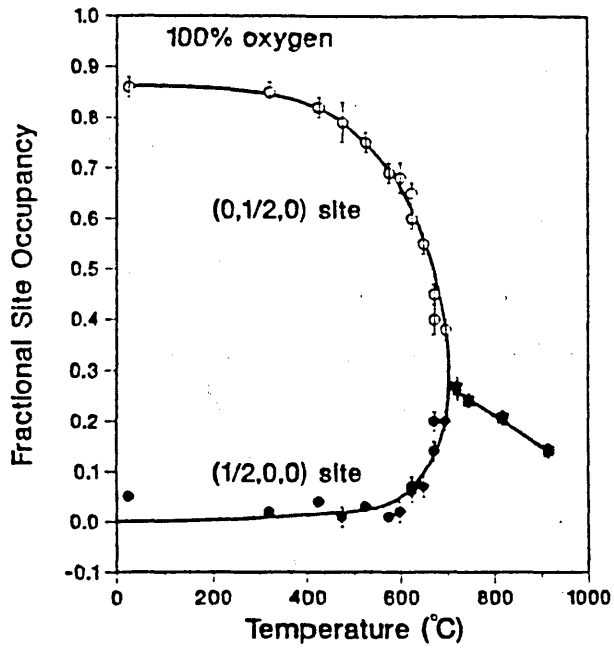

Figure 2.15: Temperature dependence of the site occupancies of O4 $(0,\frac{1}{2},0)$ and O5 $(\frac{1}{2},0,0)$ in oxygen atmosphere [93].

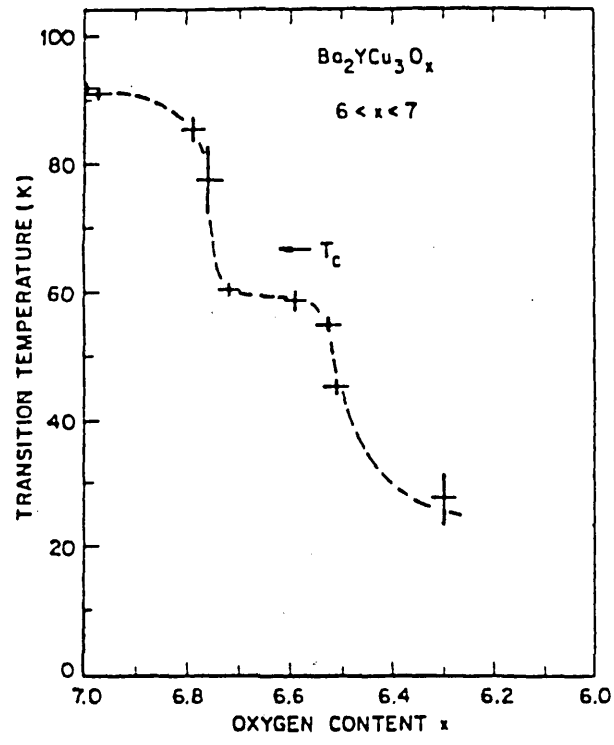

Figure 2.16: Oxygen content dependence of the superconductive transition. Vertical bars indicate the 10%– 90% transition width, horizontal bars the midpoint [101].

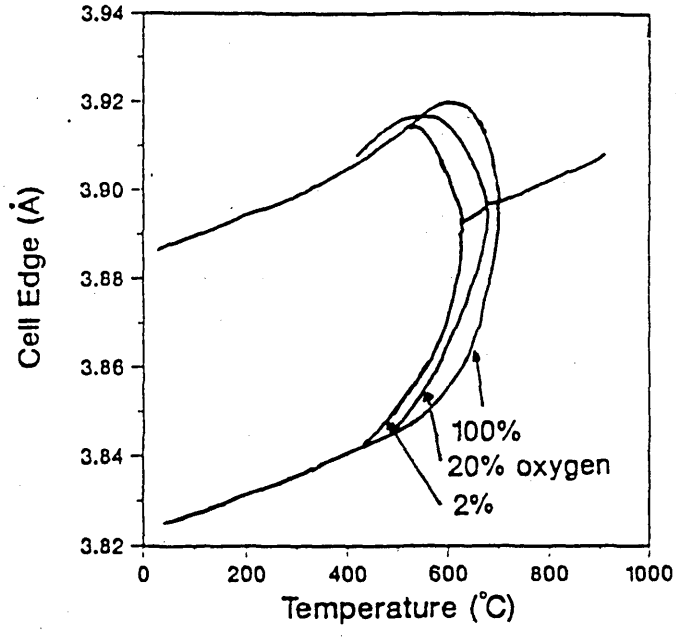

Figure 2.17: The a and b cell parameters versus temperature. The effect of partial oxygen pressure can be observed [93].

the O–T transition occurs at higher temperatures when the oxygen partial pressure is higher, but the difference from 2%–100% O_2 is not more than 80 C; from 610 (2% O_2) to 690 C (100% O_2).

However, when data from various studies [105–110,94] are compared (figure 2.18), it can be seen that they are quite scattered and form two groups. The first, represented with empty symbols has O–T transition temperatures in the range 750–820 C, and the second group represented with filled symbols has transition temperatures between 600–675 C. A set of data from another research group [111] was out of scale in the same diagram. It must be noted that all data are from X-ray or neutron diffraction in air. A similar comparative study [112], listing O–T transition temperatures, also shows considerable discrepancies between references. These differences, therefore, indicate that either the material has a very unpredictable behaviour and/or the method of determination of cell parameters for each group leads to systematic errors.

Reasons that could lead to systematic errors are: (a) Appreciably different time for the equilibration at a certain temperature, (b) Cell parameter determination with small accuracy (no internal standard, limited number of peaks taken into account etc.), (c) Difference in quenching speed. Some quench their samples with liquid nitrogen and some just quench them in air or between Cu plates or (d) Quenched samples could possibly behave differently than in *"in situ"* observations, examination of the data, however, shows no distinctive trend.

Another argument explaining the lack of reproducibility in HTS, suggested by Sleight [113], was that YBCO as well as other HTS, are thermodynamically stable only at high temperatures and only due to entropy. As "entropy stabilized phases", their properties are very dependent on processing and therefore reproducibility is difficult.

The conclusion that can be drawn is that it would be unsafe to make direct, quantitative comparisons between cell parameter results unless all conditions are held constant. Therefore it is absolutely essential that such results are self-consistent as these of figure 2.15.

2.4.4. Thermal Expansion Coefficient

Since the orthorhombic and tetragonal phase of YBCO are essentially different materials, different behaviour is observed for many physical properties. The thermal expansion coefficient has been measured by O'Bryan and Gallagher [94,110] and was found to be affected by changes

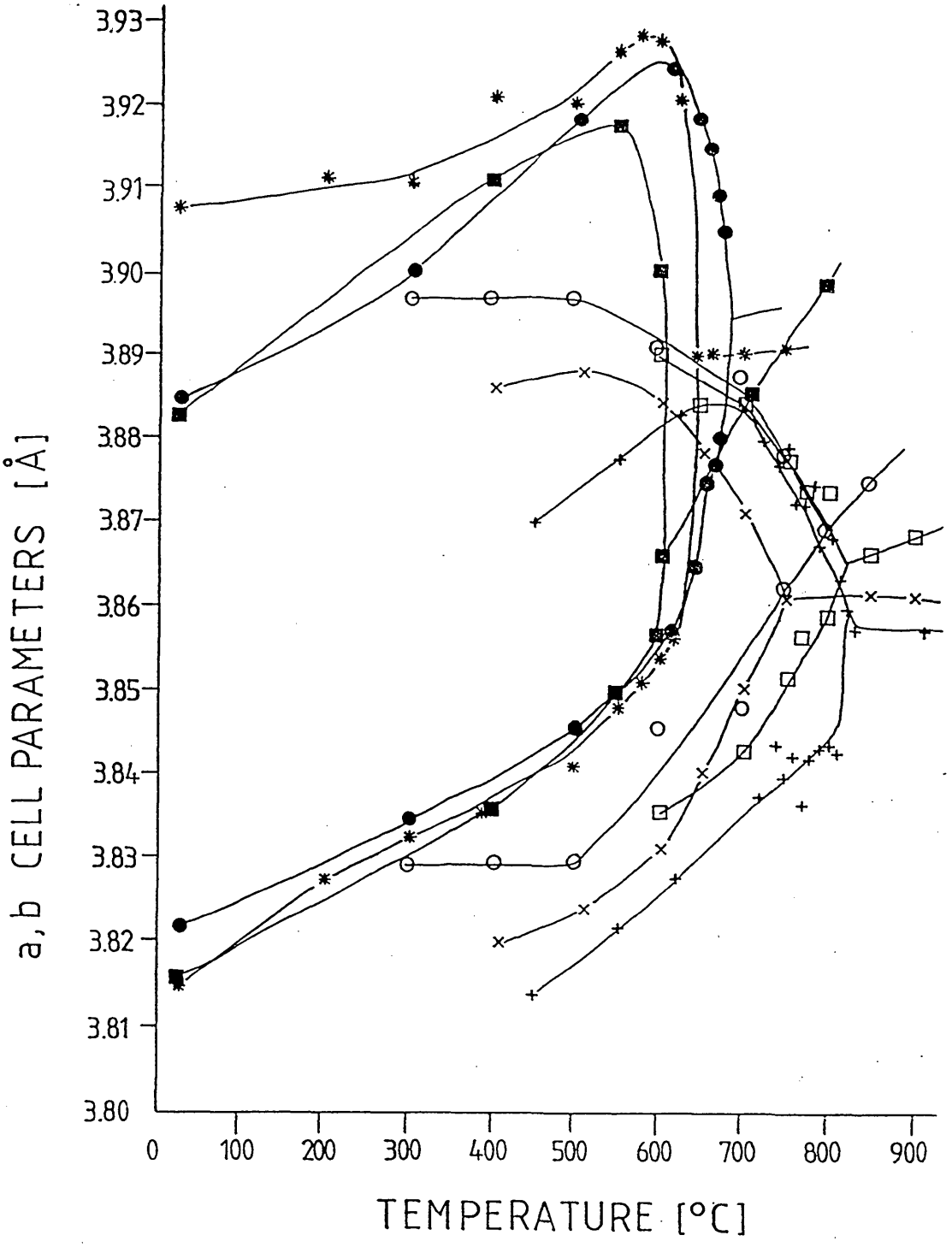

Figure 2.18: The temperature dependence of the a and b cell parameters of YBCO. Data collected from references: o 105, + 106, × 107, □ 108, ● 109, ■ 110, ✱ 94.

in oxygen stoichiometry.

There are three regimes for the thermal expansion coefficient over the temperature range 25 to 800 C:

I:	25-400 C	$a=12.9x10^{-6}$/ C
II:	400-635 C	$a=25.0x10^{-6}$/ C
III:	635-800 C	$a=20.0x10^{-6}$/ C

From X-ray data on the cell parameters variation, it is found that the thermal expansion coefficients are anisotropic with $a_a=22x10^{-6}$, $a_b=3.5x10^{-6}$ and $a_c=30x10^{-6}$/ C from 25 to 600 C. These values give an average that agrees well with dilatometry data. It can be observed that a_b is much smaller than a_a or a_c. This is because there is no significant change along the b-axis, during the O-T transition, while the removal of O4 affects both a and c-axes severely.

The result of this pronounced anisotropy and also of the temperature dependence of thermal expansion coefficient is thermal contraction stress. This stress is alleviated by twinning and the formation of microcracks at grain boundaries.

Both situations have been observed by microscopy studies. Twinning gives characteristic images when observed with TEM [104] or with polarised light under the optical microscope [112]. Twins have been found to appear always with the orthorhombic phase and to disappear when the material becomes tetragonal.

The connection between thermal stress and twinning has been demonstrated since thermomechanical detwinning was achieved in single crystals. After the application of a uniaxial compressive stress along an a/b axis at elevated temperatures, no twins were observed and the crystals remained superconducting [114].

Microcracks are a very important problem for the commercial applications since they cause deterioration of the mechanical properties of the material, in addition to affecting the superconductive properties. The problem is evident especially with very high density samples. When the density is more than 96%, the material has an abnormally low Young's modulus [115].

2.4.5. Electronic Conductivity

The application of an electric field to a material results in a current which reaches an equilibrium "direct current" value. The total electrical conductivity σ is the sum of the conductivities σ_i of each of the moving species i (electrons, holes, ions, vacancies).

$$\sigma = \Sigma \sigma_i = t_1\sigma + t_2\sigma + \ldots \qquad (2.4.1)$$

where t_i is the transference number for the species i, giving a measure of how much each of the species contributes to the total conductivity.

The conductivity σ_i is defined by the relationship:

$$\sigma_i = \frac{j_i}{E} \qquad (2.4.2)$$

where E is the electric field strength and j_i is the electric current density for the moving species i. The current density j is defined as the charge transported through a unit area in a unit of time and depends on the concentration of the charged particles (number per unit volume, n), their drift velocity v and the charge per particle $q = ze$ (z is valence and e the electronic charge):

$$j_i = n_i \, v_i \, z_i \, e \qquad (2.4.3)$$

Combining the last two equations,

$$\sigma_i = n_i \, z_i \, e \, \frac{v_i}{E} \qquad (2.4.4)$$

The drift velocity is directly proportional to the local electric field and the following ratio is defined as the mobility μ_i:

$$\mu_i = \frac{v_i}{E} \qquad (2.4.5)$$

Therefore the conductivity can be expressed as:

$$\sigma_i = n_i z_i e \mu_i = n_i q_i \mu_i \qquad (2.4.6)$$

This relation can be applied either to electrons/holes (electronic) or to ions/vacancies (ionic conductivity).

The ceramic superconductor $YBa_2Cu_3O_{7-\delta}$ is a mixed conductor, for which the moving species are holes and oxygen ions (depending on the temperature). The majority carriers are holes so the material can be described as a predominantly electronic conductor:

$$t\ (YBCO) = t_{[h^\cdot]} + t_{[O^{2-}]} \approx t_{[h^\cdot]} \qquad (2.4.7)$$

At temperatures >400 C oxygen ionic conductivity appears, but has a very small, insignificant contribution to the total conductivity.

The oxygen concentration on the other hand, has a very important effect on the hole conductivity since it determines the hole concentration through the following reaction:

$$V_O^{\cdot\cdot} + 1/2\ O_2 \longrightarrow O_O^X + 2h^\cdot \qquad (2.4.8)$$

Measurements of electrical resistivity of YBCO at temperatures between 20 and 900 C and various O_2 pressures showed a strong dependence on oxygen deficiency δ [116,117]. As it is shown in figure 2.19 the resistivity increases sharply at temperatures higher than 500 C since at these temperatures there is oxygen loss. The dependence of conductivity on oxygen partial pressure shown on this figure can be modelled using eq. 2.4.8 . Assuming that concentrations can be used instead of activities, the reaction constant is:

$$k = \frac{[O_O^X]\ [h^\cdot]^2}{(P_{O_2})^{\frac{1}{2}}\ [V_O^{\cdot\cdot}]} \qquad (2.4.9)$$

The oxygen concentration $[O_O^X]$ is large enough to be considered as constant. On the first model, using eq. 2.4.8 the relation $[V_O^{\cdot\cdot}]=2[h^\cdot]$ can be considered. Applying both arguments to 2.4.9, the following is obtained:

$$k' = \frac{[h^\cdot]^2}{(P_{O_2})^{\frac{1}{2}}\ \ 2[h^\cdot]} = \frac{[h^\cdot]}{2\ (P_{O_2})^{\frac{1}{2}}} \qquad (2.4.10)$$

As a result the hole concentration $[h^\cdot]$ and, therefore, conductivity is

proportional to $(P_{O_2})^{\frac{1}{2}}$.

Model I : $\sigma \propto [h^{\cdot}] \propto (P_{O_2})^{\frac{1}{2}}$ (2.4.11)

In the second model, if $[V_{\dot{O}}^{\cdot}]$ is large enough to be considered constant as well as $[O_O^X]$, the relation 2.4.9 will become:

$$k'' = \frac{[h^{\cdot}]^2}{(P_{O_2})^{\frac{1}{2}}} \qquad (2.4.12)$$

leading to :

Model II : $\sigma \propto [h^{\cdot}] \propto (P_{O_2})^{\frac{1}{4}}$ (2.4.13)

Both situations have been observed in different regimes. As shown in figure 2.20 [118], where the log of conductivity is plotted against the log of oxygen partial pressure, at low oxygen pressures where $[V_{\dot{O}}^{\cdot}]$ is small enough to follow the model I behaviour, the slope is 1/2, while at lower temperatures and oxygen pressures between 0.01 and 1 atm. the slope slowly changes, approaching the value 1/4, as suggested from model II.

High temperature resistivity also provides information about the orthorhombic to tetragonal (O–T) transition temperature. A change in slope in the resistivity curves of figure 2.19, which can be observed more easily when the resistivity–temperature logarithmic derivative is plotted against temperature as in figure 2.21, signifies the O–T transition. Results from two studies [116,117] agree well as shown in figure 2.22, where the transition temperature is plotted against the logarithm of partial pressure of oxygen. *In situ* neutron diffraction data [93] included in the same figure are in good agreement as well, even though they give slightly higher values (20–30 degrees) for the temperature.

High temperature defect chemistry data, including the electronic carrier (hole) generation mechanism and the O–T transition temperature can be obtained through conductivity measurements. Information on oxygen kinetics has also been derived and it will be examined in the next section.

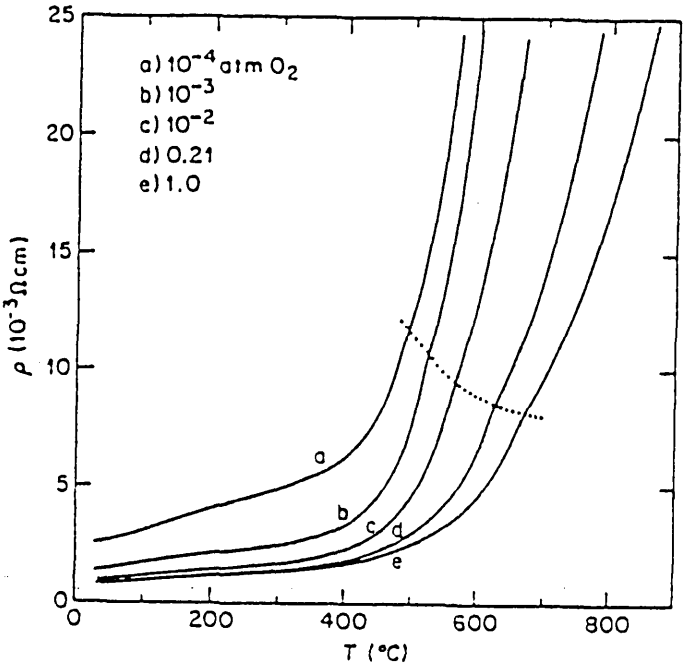

Figure 2.19: Temperature dependence of resistivity of YBCO at various oxygen partial pressures. The dotted curve shows the change in slope due to the O–T transition [116].

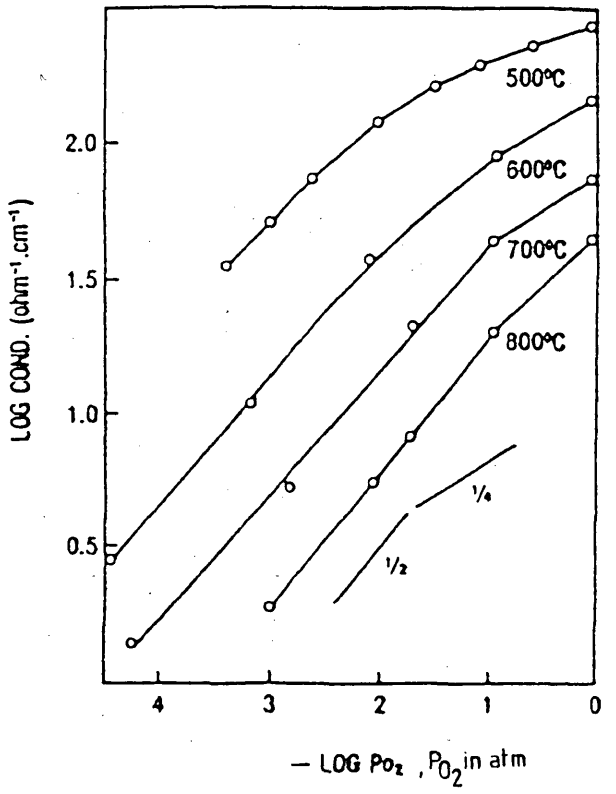

Figure 2.20: Equilibrium electrical conductivity as a function of oxygen partial pressure at 500–800 C. The slopes ½ and ¼ predicted by models I and II are indicated [118].

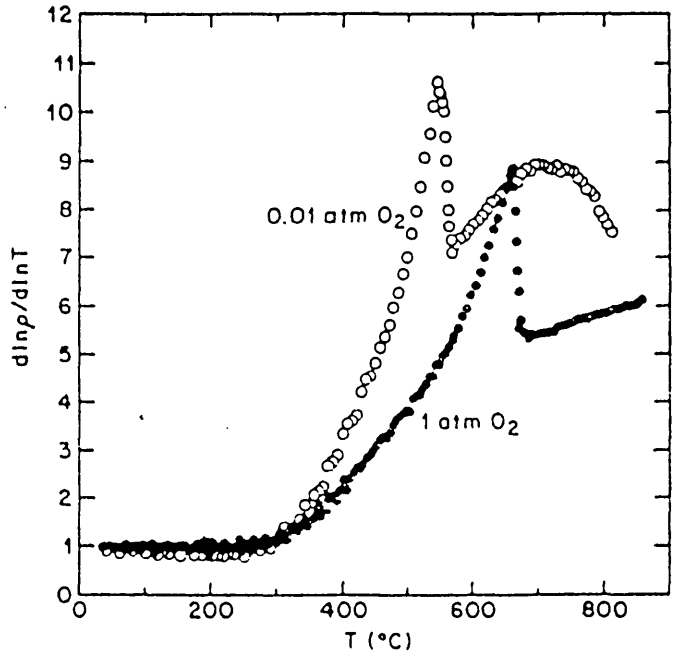

Figure 2.21: Temperature dependence of the resistivity logarithmic derivative [116].

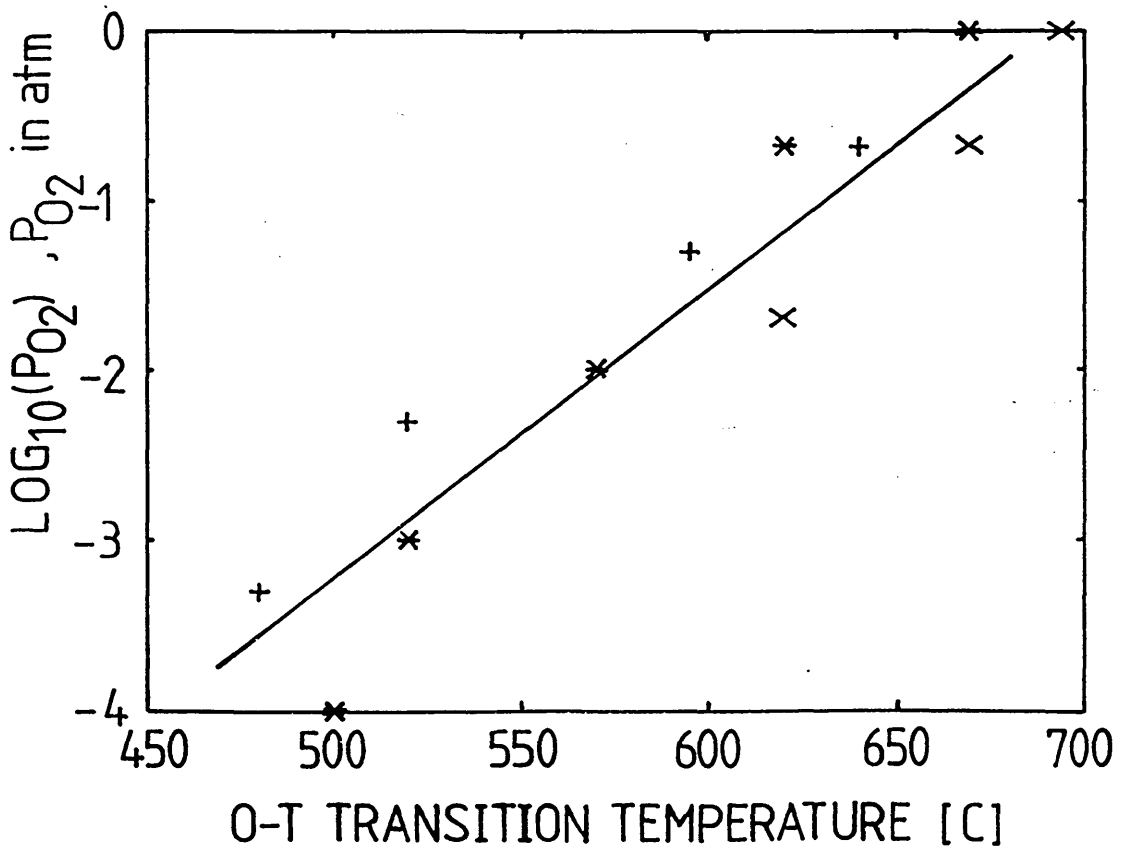

Figure 2.22: The orthorhombic to tetragonal transition temperature versus partial pressure of oxygen. Data from references: [* 116, + 117, x 93].

2.4.6. Oxygen Mass Transport

All the fabrication routes of YBCO bulk superconducting ceramics involve fabrication of the tetragonal phase with oxygen stoichiometry approximately 6, followed by a final stage of O_2 annealing at low temperatures so that the oxygen content reaches a value of 6.9–7. In this way the superconductive properties are optimized. The transfer of oxygen occurs in such a way that the concentration gradients (chemical potential gradients) are reduced. For any similar system where concentration gradients are present, Fick's first law states that the flux (J) – the quantity of the diffusing material which passes per unit time through a unit area normal to the direction of diffusion is proportional to the concentration gradient. Considering an isotropic medium under conditions of constant pressure and temperature, this is expressed as:

$$J = - D \frac{\partial c}{\partial x} \qquad (2.4.14)$$

where c is the concentration per unit volume and x the direction of diffusion. The diffusion coefficient D, usually given in units of cm^2/s is a proportionality factor specific to the given material.

From the technological point of view it is interesting to know the change in concentration at any point with time. Considering two parallel planes at a distance dx, the flux through the first plane (J_1) is as in eq. 2.4.14, while the flux through the second plane is:

$$J_2 = J + \frac{\partial J}{\partial x} dx = -D \frac{\partial c}{\partial x} - \frac{\partial}{\partial x} \left(D \frac{\partial c}{\partial x} \right) dx \qquad (2.4.15)$$

Subtracting,

$$J_2 - J_1 = \frac{\partial J}{\partial x} = - \frac{\partial}{\partial x} \left(D \frac{\partial c}{\partial x} \right) dx \qquad (2.4.16)$$

Since the change in flux with distance is equal to $-\partial c/\partial t$, the following relation results:

$$\frac{\partial c}{\partial t} = - D \frac{\partial^2 c}{\partial x^2} \qquad (2.4.17)$$

which is Fick's second law. An approximation of the solution of this equation can be obtained by $x \approx \sqrt{Dt}$.

Einstein first suggested that even though Fick's laws are expressed in terms of concentration, the force (f) for diffusion (in the absence of electric field or thermal gradients) is the chemical potential or partial molar free energy gradient $d\mu_i/dx$. The flux J can be expressed as the product of concentration and velocity. Using the definition of absolute mobility B_i = velocity/force,

$$J_i = - c_i \, v_i = - c_i \, B_i \, f = - c_i \, B_i \frac{1}{N_A} \frac{d\mu_i}{dx} \qquad (2.4.18)$$

where N_A is Avogadro's number. The change in chemical potential, assuming that concentration can be used instead of activity, is:

$$d\mu_i = R \, T \, d\ln c_i \qquad (2.4.19)$$

Substituting in 2.4.18, the following relation results:

$$J_i = - B_i \frac{R \, T}{N_A} \frac{dc_i}{dx} = - B_i \, k \, T \frac{dc_i}{dx} \qquad (2.4.20)$$

where k is Boltzmann's constant. Comparing this equation with Fick's first law (eq. 2.4.14), the Nerst-Einstein relation (connecting diffusion coefficient and mobility) can be obtained:

$$D_i^* = k \, T \, B_i \qquad (2.4.21)$$

Another way of presenting the Nerst-Einstein equation including the conductivity σ and can be derived: Using the definition of mobility $\mu = v/E$ (2.4.5) and the fundamental equation $E = f/q$ where v is th drift velocity, E is the electric field and f the force generated by it,

$$\mu_i = \frac{v_i \, q_i}{f} \qquad (2.4.22)$$

Please note that μ_i-chemical potential, used in eq. 2.4.18, 2.4.19, is different from the μ_i-mobility in 2.4.5, 2.4.6, 2.4.22-2.4.24 etc.

Substituting this in the eq. B=υ/f (definition of absolute mobility) gives:

$$B_i = \frac{\mu_i}{q_i} \qquad (2.4.23)$$

Eventually, using eq.2.4.23 along with the Einstein relation (2.4.21),

$$D_i^* = k\ T \frac{\mu_i}{q_i} \qquad (2.4.24)$$

where D_i^* is the *self diffusion coefficient* (referring to diffusion in the absence of a concentration gradient). Dividing both sides of the conductivity equation (2.4.6) with both sides of (2.4.24),

$$\frac{\sigma_i}{D_i^*} = \frac{n_i\ q_i^2}{k\ T} \qquad (2.4.25)$$

In this way the self diffusion coefficient is related to the conductivity of the moving species.

The diffusion coefficient when there is a concentration gradient is larger than the self diffusion coefficient and it is called the *chemical diffusion coefficient* ($\tilde{D}$). The two coefficients are connected by the relation:

$$\tilde{D}_i = D_i^* \frac{d\ln a_i}{d\ln c_i} \qquad (2.4.26)$$

where a_i is the activity and c_i the concentration of the diffusing species. The dlna/dlnc ratio is called thermodynamic factor. The derivation of this relation is given in Appendix 1.

A large number of techniques have been used to derive oxygen transport data and they will be briefly presented below:

$^{16}O/^{18}O$ exchange–SIMS profiling [119,120]:

An accurate but expensive technique, measuring D^* by tracing the profile of ^{18}O in a sample equilibrated first in ^{16}O and then left for a specified time in ^{18}O at the same temperature. The measured profile is fitted to an analytical solution of Fick's second law.

Thermal analysis [121,122,123]:

Measuring either weight changes during stepwise changes of oxygen pressure or the heat involved during absorption of oxygen and analysing the data according to a particular model, chemical diffusion coefficients can be estimated.

In situ resistivity [124,125]:

Measurements are made in isothermal or constant heating rate conditions and the results are modelled to provide $\tilde{D}$ (chem).

Electrochemical techniques [126,127,128]:

Different experimental arrangements involving ionic, electron blocking electrolytes such as $(Y)ZrO_2$ are used. A variety of measurements have been performed resulting in estimations of self diffusion coefficients.

Other methods [129,130,131]:

Using optical microscopy, magnetic or current transport measurements, the order of magnitude of chemical diffusivity has been roughly approximated.

$^{16}O/^{18}O$ exchange–SIMS measurements in single crystals [132] have shown pronounced anisotropy for diffusion in the ab plane and along the c–axis. Diffusion along the c axis (D^*_c) was four to six orders of magnitude smaller than in the ab plane (D^*_{ab}): $D^*_{ab} \approx 10^4$–10^6 D^*_c.

The diffusion mechanism is therefore suggested to be two dimensional, with oxygen moving through the basal plane and especially through the vacant O5 sites, as shown in figure 2.14.

In figure 2.23 a compilation of the data on oxygen self diffusion coefficient in polycrystalline YBCO is presented. Chemical diffusion coefficient data have been included, using the thermodynamic factor and equation (2.4.26) to calculate the equivalent self diffusion coefficient. The derivation and calculation of thermodynamic factor from thermogravimetric data by Kishio et al [121] is presented in detail in Appendix 2.

There is considerable disagreement between these results, of about 4–6 orders of magnitude. This and especially the differences in activation energy indicate that a possible explanation can be the fact that different processes are being measured by different techniques. This can be due to the actual experimental techniques or to the methods that in each case have been used to assess the results and calculate the diffusion coefficient. It should also be noted that where solid–gas equilibrium reactions are involved, the surface exchange process may be rate controlling.

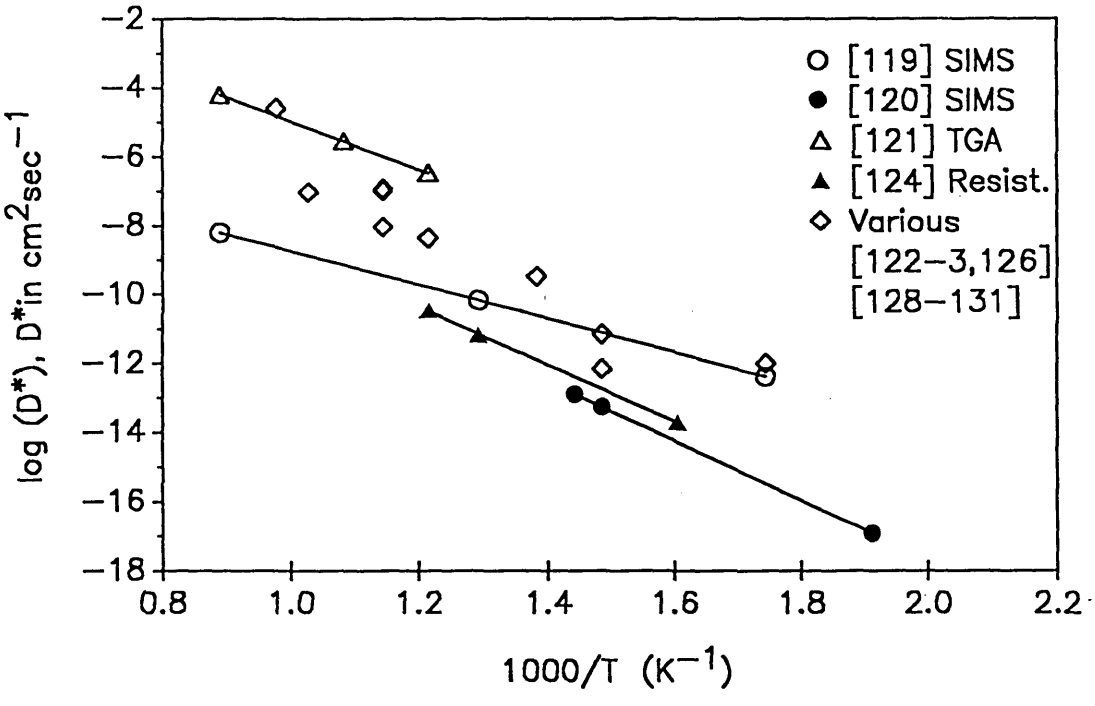

Figure 2.23: Oxygen diffusion coefficient versus temperature. Data from refs. [119–131].

Nevertheless, the approximate magnitude of the oxygen diffusivity at 400 C has in practice being recognized as a limiting factor for the fabrication of very dense YBCO. It has been reported that using fabrication techniques resulting in almost theoretical density material, had produced YBCO with critical current densities lower than for less dense material [131]. The reason for this was that it was not possible to fully oxygenate and transform to the orthorhombic superconducting phase the original tetragonal material in a reasonable time. As a result, after annealing at around 400 C the samples for several hours, only a very thin sheath around the sample had become orthorhombic, leaving the bulk of it in the tetragonal non-superconductive phase. It is, therefore, possible that a porosity of around 10% is necessary so that oxygen circulating through the pores will transform the material to orthorhombic. The determination of diffusivity will enable the quantitative assessment of this problem and the study of methods to overcome it.

2.5. Ceramic Fabrication

Since the discovery of YBCO many efforts have been made to improve its properties through better methods of fabrication.

The ideal conditions for ceramic fabrication require powders that fulfil the following requirements [133]:

i . Small particle size
ii . Uniform particle size
iii . Equiaxed shapes
iv . Weakly agglomerated
v . High purity
vi . Constant composition

As a result many methods of fabrication of bulk YBCO have been developed either by modifying the conventional ceramic fabrication or by using wet chemical preparation methods which have been proved very efficient in the fabrication of ceramics. These methods will be reviewed with the exception of chemical and physical techniques for thin films. In table 2.3, the general techniques for bulk ceramic fabrication are summarized with some of the most successful routes and typical references.

Table 2.3: Typical methods for ceramic fabrication of bulk YBCO

			Ref.
Bulk	Conventional Related	Conventional	135,136
		Viscous processing	115
		Hot pressing	134
	Wet Chemical Routes	Oxalates	86,144
		Sol Gel	145
		Spray/mist pyrolysis	143
	Alternative techniques	Alloy oxidation	146
		Shock compression	147
		Composites with Ag	149

2.5.1. Conventional fabrication and related methods

The conventional route involves mixing and thorough grinding of Y_2O_3, $BaCO_3$ and CuO. After firing at temperatures near 950 C the YBCO phase is formed. The grinding procedure is repeated. The material is compacted and fired again followed by slow cooling so that it can soak oxygen and become orthorhombic. There are several suggestions about the atmosphere and duration of annealing, as well as the number of times that the grinding/sintering procedure should be repeated. In all cases however, a post annealing at 400–450 C in oxygen is necessary in order to transform all the tetragonal phase to orthorhombic.

One modification by Alford et al. [131] was the use of viscous processing. After the formation of YBCO by calcination of the precursors and reduction of the particle size by milling in a high energy vibro mill, it is mixed with a viscous polymer solution. The mixture is processed on a two roll mill for homogenization and extruded in a ram extruder. The resulting material is dried at 80 C and fired. The final product is material with 95–99% of the X-ray density. The success of this method is due to the fact that the powder used had a very small particle size and the agglomerates were broken by the viscous processing. Another important advantage is that various shapes such as wires, tapes and springs can be easily produced.

Another modification is hot pressing which according to Grader et al. [134] gave dense (>95%), oriented and mechanically good samples. To avoid microcracks they produced tetragonal YBCO using an N_2 atmosphere and later, using small O_2-annealing times, oxidized (transformed to orthorhombic) only a small surface layer, which had a Jc of 3000 A/cm^2 approximately.

Using barium peroxide (BaO_2) instead of carbonate ($BaCO_3$) has been also found to improve the superconducting properties [135] (diamagnetism) and the homogeneity [136] of the bulk material when the conventional method of preparation is used. The advantage of using BaO_2 over $BaCO_3$ is the faster reaction rate achieved, since the former decomposes at a temperature less than 600 C and the latter at 1400 C approximately.

2.5.2. Wet chemical preparation methods

The synthetic preparation of powders from solutions can produce materials which fulfil the requirements mentioned at the beginning of the chapter: small/uniform particle size, equiaxed shape, high purity and homogeneity, without agglomerates.

Aqueous or organic solutions of the starting materials are formed, containing the cations in the correct ratios. The water or other solvent is removed so that homogeneity is maintained. The product is a mixture of salts which are calcined for decomposition so that agglomeration is avoided or minimized. Subsequently it is lightly ball-milled to break any hard agglomerates and finally pressed and fired for the production of the ceramic.

In most of the cases nitrate salts are used since their preparation is simple and they are soluble in water. A solution of Y, Ba and Cu nitrates was evaporated to dryness and the product was fired first at 400-500 C for the decomposition of nitrates and at 750-800 C for the formation of YBCO. After sintering at 900-950 C [137,138] the material was reported to have very good superconducting properties because of the lower temperature at which nitrates produced YBCO, compared to the $BaCO_3$ route.

Freeze-drying (lyophilisation) has been used successfully in the past for ceramic fabrication producing homogeneous powders of high surface area and reactivity [139,140]. The principle of the process is to freeze a solution quickly so that ions are immobilized and remove the water (or other solvent) by sublimation. For the YBCO, a nitrate solution is frozen by spraying it on liquid nitrogen. The resulting small frozen spheres are transferred to a vacuum chamber. Ice is sublimed and the nitrate salts are calcined at 830 C for decomposition and formation of the YBCO phase. After grinding, sintering is carried out at 900-930 C. Prepared material [141,142] has been reported to be dense with very sharp resistivity drop and large Meissner effect.

Spray/mist pyrolysis was also used and it seems very promising since the product of this technique is YBCO powder composed of spherical particles of uniform size ready for the final firing. In this method a nitrate solution of the powder precursors is passed through an aerosol generator to form fine droplets of the solution. These droplets are then carried through a furnace where the solvent evaporates and the precursor compound decomposes to form particles which are then collected on a

filter. If the temperature of the furnace is 1000 C and the average dwell time of the powder 20–100 seconds, at least 99% of the powder reacts producing YBCO. Kodas et al. [143] produced submicron powder of YBCO chemically homogeneous which sintered to dense, fine grained ceramics with sharp transitions at 90 K.

Coprecipitation of cation oxalates has also given powder of YBCO with small particle size [144]. A nitrate solution was added in oxalic acid adjusting the pH by dilute ammonia and a slurry was formed containing the oxalates. After washing, drying and grinding it was fired at 780 C. The YBCO phase was formed and because of the low temperature there was no sintering. As a result the powder was very fine, non–agglomerated and homogeneous, therefore a very good starting material for sintering.

Another successful method for the production of good quality YBCO is sol–gel [145], which produced submicron powders (<=0.2 μm) at temperatures as low as 750 C, sintering in bulk material with sharp superconducting transition.

2.5.3. Alternative techniques

Certain alternative methods have been reported using techniques borrowed from metallurgy. Yurek et al. [146] made an alloy of Eu–Ba–Cu and oxidized it at 800–900 C in an O_2 atmosphere producing a dense ceramic with good superconducting properties. Adding gold in the melt, the final product was a microcomposite containing two separate phases: the gold and the superconductor. This microcomposite displayed zero resistivity at 77 K but it had better mechanical properties than the ceramic. The advantage offered by these techniques is that the original alloy can be formed easily to any shape before oxidation, something that is not possible for a ceramic.

Murr et al. [147] applied a shock–compression technique for superconductor/metal composite monoliths. With the help of ammonium nitrate explosives, YBCO powder was enclosed in a copper or aluminium matrix, giving a continuous superconducting path. In this form the material can be machined, processed and protected from the environment as well.

A very popular technique, especially for wire fabrication, is silver (Ag) addition to YBCO. It has been shown that Ag has little or no effect to T_c, while the room temperature resistivity decreases (probably due to better connectivity). The main advantage, however, is that the mechanical

properties are much better [148]. Ag_2O has been also used in powder-in-tube techniques, acting as an oxygen donor as well as improving the flexibility of the wires [149].

2.5.4. Melt processing for textured YBCO

Despite the variety of techniques for preparing single phase YBCO with sharp superconducting transitions, the resulting randomly oriented polycrystalline material has usually a critical current in the order of 500 A/cm^2. Information on the anisotropic properties of YBCO along with the high J_c's obtained in oriented/ epitaxial thin films suggested that in order to improve the critical current in bulk materials, preferred orientation had to be induced.

The existing fabrication techniques for production of oriented material with improved J_c's usually involve heating above 985 C, so that there is liquid formation and fast grain growth. Several techniques, mainly borrowed from the field of crystal growing, have been employed [150] such as zone melting, melt quenching, laser melt processing, or slow cooling of the melt through the peritectic transformation temperature.

Oriented-grain materials have J_c that in some cases reach $7x10^4$ A/cm^2 [151], significantly larger than for randomly oriented ones. It is also significant that even at high fields considerable currents are sustained, in the order of $1.5x10^4$ A/cm^2 (H $\parallel$ a-b plane, 77 K, 1.25 T) [152] or more, while with randomly oriented material J_c drops to less than 5 A/cm^2 in similar fields.

Fabrication of textured bulk ceramics is therefore a promising approach, even though further improvement for critical current is necessary for practical applications.

2.6. Cation Substitution

The YBCO phase was discovered when Wu et al. [10] substituted successfully Y for La in the superconductive compound $La_{2-x}Ba_xCuO_{4-\delta}$. Following this example, research groups tried various cation substitutions, both searching for new superconductive materials with higher transition temperatures and also studying the effect of substitutions on superconductivity.

2.6.1. Y Substitution

Yttrium substitution was the first to be attempted because of the similarity of rare earth elements. Lu and Yb were initially selected because of their small or non-existent magnetic moment since it was well known that small amounts of magnetic impurities depress superconductivity significantly in conventional superconductors. However, Hor et al. [36] discovered that La, Nd, Sm, Eu, Gd, Ho and Er give high temperature superconductors as well as Y, Lu and Yb. The critical temperature in these compounds was found to be around 90 K, essentially the same as for $YBa_2Cu_3O_{7-\delta}$. This result indicates that the magnetic ions do not interact with the conduction electrons but ionic radius and valence are more important, since Ce, Pr and Tb with a valence of 4+ did not form superconductive compounds.

A more systematic study by Tarascon et al. [153] provided accurate critical temperature measurements, cell parameters and magnetic data for the Y-substituted compounds. Kistenmacher [154] studied these results and revealed that apart from the expected relation between cell parameters and ionic radius, critical temperature was also found to be slightly dependent on ionic radius as shown in figure 2.24.

Substitution of Y was also attempted with aliovalent cations such as Ca and Na. In the case of Ca, substitution of Y of up to 20% has been deduced from neutron diffraction data [155], in agreement with other reports. In the case of Na, however, Greaves et al. [155] suggests that no substitution could be achieved, even though previous workers [156,157] claimed single phase material for up to 50-60% Na from X-ray diffraction patterns. This could be explained by the high volatility of Na (it boils at 883 C [158]). If proper precautions are not taken, it is possible

that only little amount of Na remains in the sintered material.

Comparing the behaviour of Na and Ca in Y substitution and the effective ionic radii after Shannon [159] given at table 2.4, it is clear that formal valence is much more important than the ionic radius, as far as partial substitution is concerned.

Table 2.4

Valence and effective ionic radii for Y and doping cations*

Ion	Valence	Ionic radius (Å)
Y	3+	1.109
Ca	2+	1.260
Na	1+	1.180

*Coordination number = 8

Substitution of Y has thus provided the following information:
(a) Ions with magnetic moment do not destroy superconductivity,
(b) The valence of the central cation is crucial for the formation of YBCO phase and superconductivity,
(c) The ionic radius of the RE cation slightly influences T_c and cell parameters.

2.6.2. Substitution of Ba

The elements that have been used in order to substitute Ba are La, Sr and K.

Ba can be substituted by La up to 20% at. [160] ($YBa_{1.6}La_{0.4}Cu_3O_7$) but the T_c drops below 80 K for 10% at. substitution. The effect on cell parameters is a decrease in cell volume with doping and also the transformation from the orthorhombic to the tetragonal phase.

Substitution of Ba by Sr however, is possible up to 50% at. without the presence of any second phase [161]. The material remains orthorhombic and the T_c drops slowly as shown in figure 2.25. It is mentioned that even for x=1.5 (75% at. substitution) T_c is quite high (>75 K). Wu et al. [162] have discovered superconductivity in the Y-Sr-Cu-O system (transitions at 80 and 40 K), even though it is not certain that any of the phases produced is of the "123" structure.

Potassium doping experiments by Chen et al. [163] showed that up to

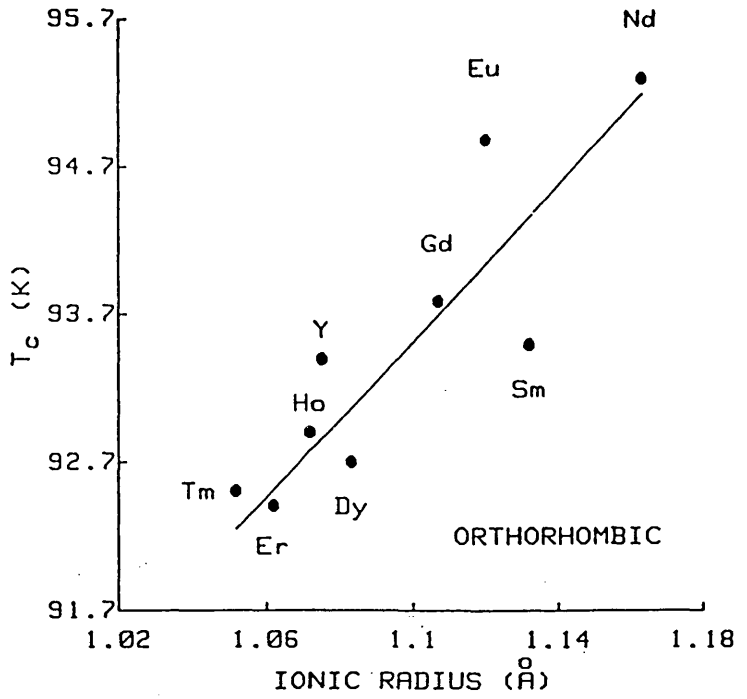

Figure 2.24: The variation of T_c with ionic radius of the rare earth cation for the R.E.$Ba_2Cu_3O_{7-\delta}$ system [154].

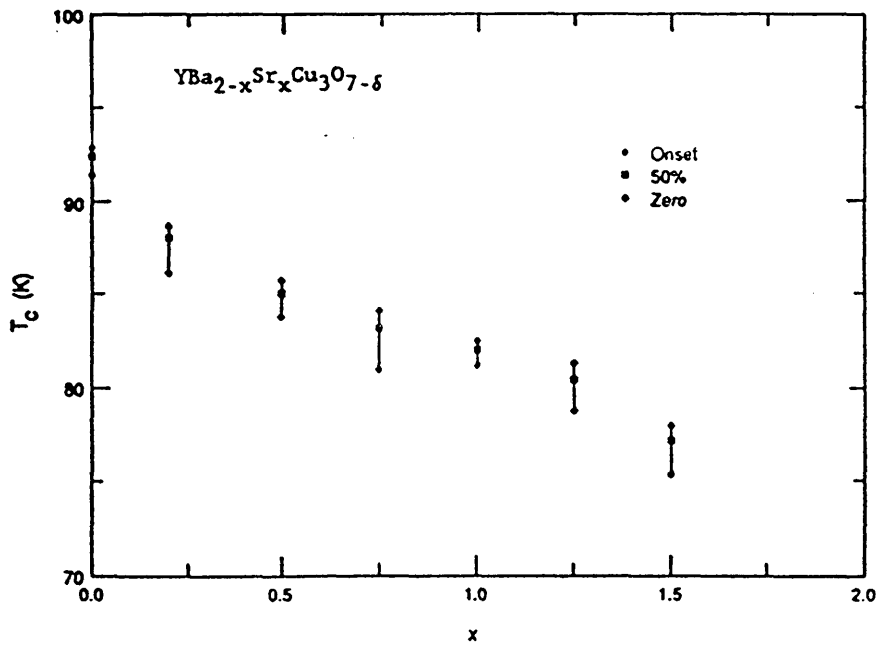

Figure 2.25: Critical temperature versus Sr-doping for $YBa_{2-x}Sr_xCu_3O_{7-\delta}$ [161].

3.5% at. K there was no significant change in T_c and more importantly, there was a tendency for the stabilization of the orthorhombic phase at higher temperature. Tallon et al. [164] suggested that substitution of Ba by K was possible up to 10% at. and that the orthorhombic phase was stabilized at 80 degrees higher when doping was 10% at. K ($YBa_{1.8}K_{0.2}Cu_3O_7$) than for the pure material. This fact has a great importance since oxygen annealing can be carried out at higher temperature and in this way annealing time can be also shortened. Moreover, if it is possible to remove the O-T transition at temperatures higher than those required for the formation of YBCO, there will be no microcracking due to the difference in thermal expansion coefficient of the tetragonal and the orthorhombic phase. Potassium doping has been also carried out by Felner and Barbara [165] and Moure et al. [166] with similar observations as far as the oxygen is concerned. Samples with up to 50% at. K in the place of Ba, were shown to be single phase, orthorhombic, with T_c dropping to 40 K at the highest K content [167]. In a previous paper [163] it was suggested that potassium improved sinterability and densification; however, it was claimed later [166] that no densification enhancement occurs. It appears there is considerable disagreement in the rôle of potassium and further work is needed to examine in detail the effects of K-doping.

The attempted substitution of Ba has shown that it cannot be replaced entirely as in the case of Y (in the 123 structure); however, successful partial substitution depends mainly on the valence combined with the ionic radius of ions. As can be seen in table 2.5, Sr has a greater difference to Ba in ionic radius than K but since it has the same valence it is accepted to a much larger extent. La however has an even bigger difference in ionic radius and a different valence as well and in this way the effect on T_c and structure is explained.

Table 2.5

Valence and ionic radii of Ba and doping cations*

Ion	Valence	Ionic radius (Å)
Ba	2+	1.52
Sr	2+	1.36
La	3+	1.27
K	1+	1.59

*Coordination number = 10

2.6.3. Cu Substitution

Substitution of Cu is of great importance since there are indications of a relation between Cu–O structure and superconductivity. In figure 2.26, superconducting transition temperatures as a function of dopant concentration are given [168] for Fe, Co, Al, Ga (3+), Zn, Ni (2+) and structural information can be seen at table 2.6.

Table 2.6: Effect of Cu substitution

Element	Subst. limit x M_xCu_{3-x}	Stru- cture	Preference in site occupancy	Method	Ref.
Fe	0.8	T	Cu1	Mossbauer spectr.	20,169
Co	1	T	Cu1	Neutron diffr.	20,170
Al	0.3	T	Cu1	TGA, XRD, crystall.	20
Ga	0.3	T	Cu1	XRD, crystall.	169
Zn	0.3	O	Cu2	Neutron diffr.	20,170
Ni	0.3	O	Cu2	TGA, XRD, crystall.	20,169
Ag	3	?	Cu1,Cu2	-	171,172

For the trivalent dopants Fe, Co, Al and Ga, a structural transition from orthorhombic to the tetragonal structure occurs with doping, without, however, loss of superconductivity. The fact that the tetragonal, doped material is superconducting indicates that superconductivity is not necessarily connected with the Cu–O chains.

Several studies indicate preferential occupancy of the Cu1 site (chains) by these ions, which tend to accumulate oxygen ions around them disordering, therefore, the Cu–O chains. This is confirmed by an increase in the total oxygen content [20]. In contrast, the divalent Zn and Ni possibly occupy the Cu2 site and do not change the oxygen content, the material remaining orthorhombic.

In conventional superconductors, atoms with magnetic moment were found to "break" the superconducting electron pairs (Cooper pairs), having a serious effect on superconductivity. Comparing the behaviour of the magnetic atoms Fe, Co, Ni and the diamagnetic atoms Al, Ga, Zn, no obvious trend can be deduced.

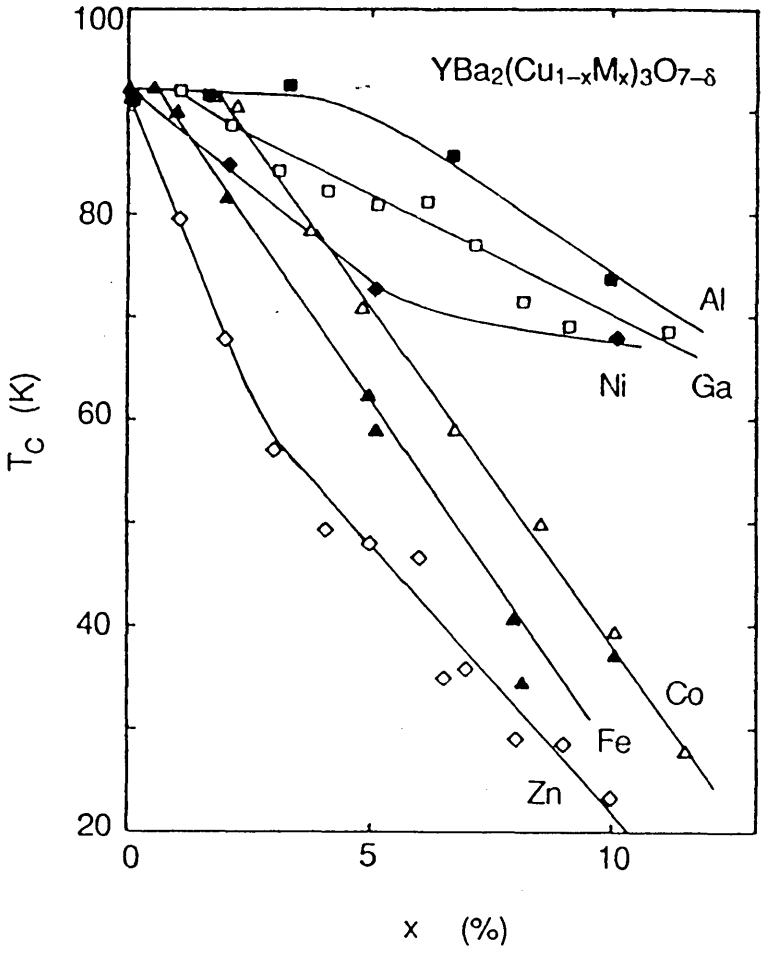

Figure 2.26: The superconductive transition temperature as a function of dopant concentration x for $YBa_2(Cu_{1-x}M_x)_3O_{7-\delta}$ [168].

2.7. Effect of Water on $YBa_2Cu_3O_{7-\delta}$

A very important problem for the application of the YBCO superconductors is the reaction with water. Even though the Bi-superconductor does not exhibit similar sensitivity, the superconductive properties of YBCO are gradually lost when it is immersed in water or exposed in a humid environment.

After twenty minutes in water at a temperature of 85 C superconductivity is lost, according to Dominec et al. [173], in general agreement with data from Dexin et al. [174]. Results of tests in a humid atmosphere, monitoring degradation through room temperature resistivity, showed similar behaviour [175].

The reactivity of YBCO is mainly due to Ba^{2+} and two reactions have been proposed [174,175]:

$$2YBa_2Cu_3O_7 + 3H_2O \longrightarrow 5CuO + 3Ba(OH)_2 + Y_2BaCuO_5 + 1/2O_2$$

and/or

$$2YBa_2Cu_3O_7 + 7H_2O \longrightarrow 6CuO + 4Ba(OH)_2 + 2Y(OH)_3 + 1/2O_2$$

Reaction of YBCO with water means that in any application the efficient protection of the material has to be taken into account and either dry atmosphere or an efficient protective coating should be provided.

An attempt by Barns et al. [175] to protect YBCO using an epoxy coating showed that their protection would not last more than 40 days. A passivation technique using vacuum deposition of CaF_2 on the superconductor [176] has been successfully applied and a plastic coating developed by Jin et al. [177] has also provided promising results.

2.8. Conclusions

High temperature superconductors have attracted a considerable number of researchers and a plethora of papers, often overlapping, has been published since the beginning of 1987. A large amount of information on YBCO, part of which was presented here, shows that it is an interesting material from both the scientific and the technological point of view.

This work started around the end of 1987 and therefore progressed simultaneously with research from other groups around the world. The limited knowledge available at the time, dictated an approach to research that would permit flexibility and continuous adjustment of the work direction through a variety of subjects being pursued in parallel.

The optimization of the fabrication of the material is necessary and high quality powder preparation routes must be developed in order to provide an adequate starting material. This powder could be used for the melt processing technique for texturing of YBCO which at present gives the best results as far as J_c is concerned, or any other technique that may be developed for the fabrication of the final components.

From the preparation techniques, solid state reaction is widely used and optimization of the starting materials using $BaCO_3$, BaO_2 or $Ba(OH)_2$ as a Ba precursor was performed. Chemical techniques were also examined, (evaporation of nitrates, freeze-drying, mist pyrolysis) in order to produce high quality ceramic powders.

Another possible method to improve the properties of the material is by chemical doping. Potassium doping was selected as the most promising since it could affect the orthorhombic to tetragonal (O–T) transition and its effect on the structure, microstructure and properties was examined in the 123 structure, using either Er, Y, Gd or Nd in the central rare earth ion site ($REBa_{2-x}K_xCu_3O_{7-\delta}$). Techniques such as X-ray and neutron diffraction were utilized.

As described in the literature survey, oxygen at stoichiometries near 7 is essential for superconductivity and since oxygenation was shown to be slow, determination of diffusivity is very important. Two electrochemical techniques were, therefore, developed as accurate, fast and relatively cheap methods to obtain oxygen conductivity and diffusion coefficient values. The work involved establishing the validity of the techniques as well as measurements of ceramic superconductors.

In the present thesis SI units are principally employed. However, following common usage, degrees C (instead of K) were utilized when referring to temperatures around or higher than room temperature and also centimetres were used as an operational convention in cases such as diffusion coefficient (cm^2/sec) or conductivity ($Ohm^{-1}cm^{-1}$).

3. EXPERIMENTAL PROCEDURES

3.1. Materials

The materials used for the preparation of YBCO samples were Y_2O_3 99.99%, Gd_2O_3 99.999% (Alfa Ventron Products), Nd_2O_3 and Er_2O_3 99.9% (Reacton), $BaCO_3$ Techn. Gr. (Ventron), BaO_2 purum, p.a. (Fluka), CuO ultrapure or 99.999% (Ventron) and $KC_8O_4H_5$ 99.95% (Aldrich).

The Yttria-stabilized Zirconia electrolytes used as blocking electrodes in the electrochemical characterization of oxygen conductivity, were fabricated from commercial powder (8% Y)-ZrO_2 ("8YSZ" or "YSZ") from Tosho (TZ-8Y).

The other electrolyte used in this study, $Bi_{1.75}Sm_{0.25}O_3$ ("BiSm") was fabricated from Bi_2O_3 99.9% (Aldrich) and Sm_2O_3 99.9% (Ventron).

For the $Bi_{1.7}Pb_{0.3}SrCa_2Cu_2O_x$ ("BPSCCO") compound starting materials were Bi_2O_3 as above, PbO 99.9% (Aldrich), CaO Lab. Reag. (BDH), $SrCO_3$ Lab. Reag. (Hopkins & Williams Ltd) and CuO as above.

The Ag sample used for DC/impedance measurements was of 99.95% purity.

3.2. Sample preparation

3.2.1. Grinding

When the starting materials were powders of the oxides/ carbonates, very good mixing and grinding was necessary in order to reduce the amount of second phases after sintering.

In most of the cases, grinding was performed with an agate mortar and pestle for times ranging from 15 min. to 1 hr. and 30 min., using either acetone or more usually ethanol to assist the mixing/grinding process.

Ball milling with ZrO_2 media was also used, for times between 12 and 24 hours. Alcohol was also added in the plastic container used for

milling. Contamination from the container (organic matter) was detected as insoluble remains, after dissolving the milled powder in acid. As a result, grinding by mortar and pestle was preferred.

3.2.2. Firing/annealing

In order to sinter the precursor powders, they were fired at around 950 C for YBCO, 850 C for BiSm and BPSCCO and 1500 C for YSZ. In some cases, heating of the samples was fast, however, a controlled rate of heating and cooling provided the best results. Typically, 5 or 10 degrees/minute were used, even though slow cooling (1–3 deg./min.) was preferred for the oxygenation of YBCO followed by an annealing step of 12–24 hrs. at 400 C. The atmosphere used was either air or oxygen.

Furnace calibration experiments showed constant temperature (+/– 3 deg.) along the hot zone area. Care was taken, so that samples were usually put in exactly the same place in the furnace. A difference in the real temperature, as compared to the one indicated by the furnace controller, was taken into account for the different furnaces, using higher (adjusted) values for the controller.

3.2.3. Polishing

Polishing was necessary for microstructural studies (SEM, optical) or in order to ensure the best contact between the electrodes and the material under examination in the electrochemical cells.

Different grades of Buehler–Met metallographic grinding paper were used, starting from P600 (coarse) to P1200 (fine). Polishing was then continued at the diamond polisher using 6, 3 and 1 μm paste. Usually polishing with 6 and 3μm paste was satisfactory.

3.3. Characterization techniques

3.3.1. Density measurements

The density (g/cm^3) was calculated applying the formula $\rho=m/V$, where m is the mass of the sample, weighted with an accuracy of ±0.0001 gr and V the volume which was calculated measuring the dimensions of the sample with a micrometer (±0.001 mm). An initial estimation of density was carried out measuring the dimensions of as-fired pellets. The average of four values taken at a cross pattern was used for radius, and the average of five values (four at the edge, one at the centre) for the height. This usually gave an underestimation of density for the as-sintered samples. A much more accurate measurement was done when repeating the measurements after polishing. The surface irregularities removed, the calculated density increased by 1-3 percentage units.

The estimation of X-ray density (6.39 g/cm^3) is based on cell parameters and stoichiometry of the ideal orthorhombic phase $YBa_2Cu_3O_7$. Since there is a possibility of the material being partially oxygenated, both the cell parameters and the oxygen stoichiometry can be different, resulting in lower values for X-ray density. This problem is expected to be present especially in the dense (>88%) samples, where oxygenation can be slow. As a result density values presented here as a percentage of X-ray density are subject to errors due to the reason presented above, therefore, density in g/cm^3 will be also quoted where necessary.

3.3.2. X-Ray diffraction

This technique was used for phase determination and for cell parameter measurements and peak intensities calculation. A Philips PW1710 diffractometer was used with $Cu_{K\alpha}$ (or $Co_{K\alpha}$) radiation. As expected, $Co_{K\alpha}$ radiation was found to give much better results (higher peaks and much lower background), but was not available for most of the time for this study. A slit of one degree was used with a graphite crystal crystal monochromator between the sample and the counter. The diffractometer was operated at 40kV and 40mA. For calculations, a weighted average value $\lambda(Cu_{K\alpha})$ = 1.54178 Å was taken when using Bragg's Law [178]:

$$\lambda = 2\ d\ \sin\ \theta \qquad (3.1)$$

where d is the atomic spacing in Å and θ is the angle between the incident X-ray beam and the normal to the sample surface.

For phase determination continuous scanning at a speed of 1 deg./min. was applied and the output was obtained via an integrated chart recorder. For accurate peak position or intensity measurements, a step scan mode of 0.005 deg step with a 20 sec. sampling time was employed. A $Bi_4Ge_3O_{12}$ (BGO) single crystal (for which the exact peak positions were known) was placed beside the samples to serve as an internal standard. A microcomputer controlled the diffractometer and stored the data on magnetic media (floppy disk). These were transferred to the main frame and processed there or in another microcomputer as shown in figure 3.1. The programs used in order to control the diffractometer through the microcomputer, store the data, determine the peak position (least square fitting to a second order equation) and calculate the cell parameters, had been formulated by Dr. X. Turrillas.

3.3.3. Neutron Diffraction

The neutron diffraction facilities at the Rutherford Appleton Laboratory were used in order to obtain high temperature *in-situ* information on the structure of the bulk of the material. The POLARIS instrument was used, utilizing neutrons from the pulsed neutron source ISIS [179]. The diffractometer, instead of measuring Bragg reflections by scanning a detector through a range of angles, uses the pulsed white beam nature of ISIS to measure reflections at fixed scattering angles, monitoring the time of arrival of the neutron after the initial neutron burst produced from the target [180]. This is called the time-of-flight method. The d-spacing is proportional to the time of flight (t-o-f), as can be shown by combining Bragg's Law (eq.3.1) with de Broglie's relationship (eq.3.2):

$$\lambda = h\ /\ p_n = h\ /\ m_n\ v_n \qquad (3.2)$$

where p_n, m_n and v_n are the momentum, mass and velocity of the neutrons respectively and h is Planck's constant. Therefore:

$$h\ /\ m_n\ v_n = 2\ d\ \sin\ \theta \qquad (3.3)$$

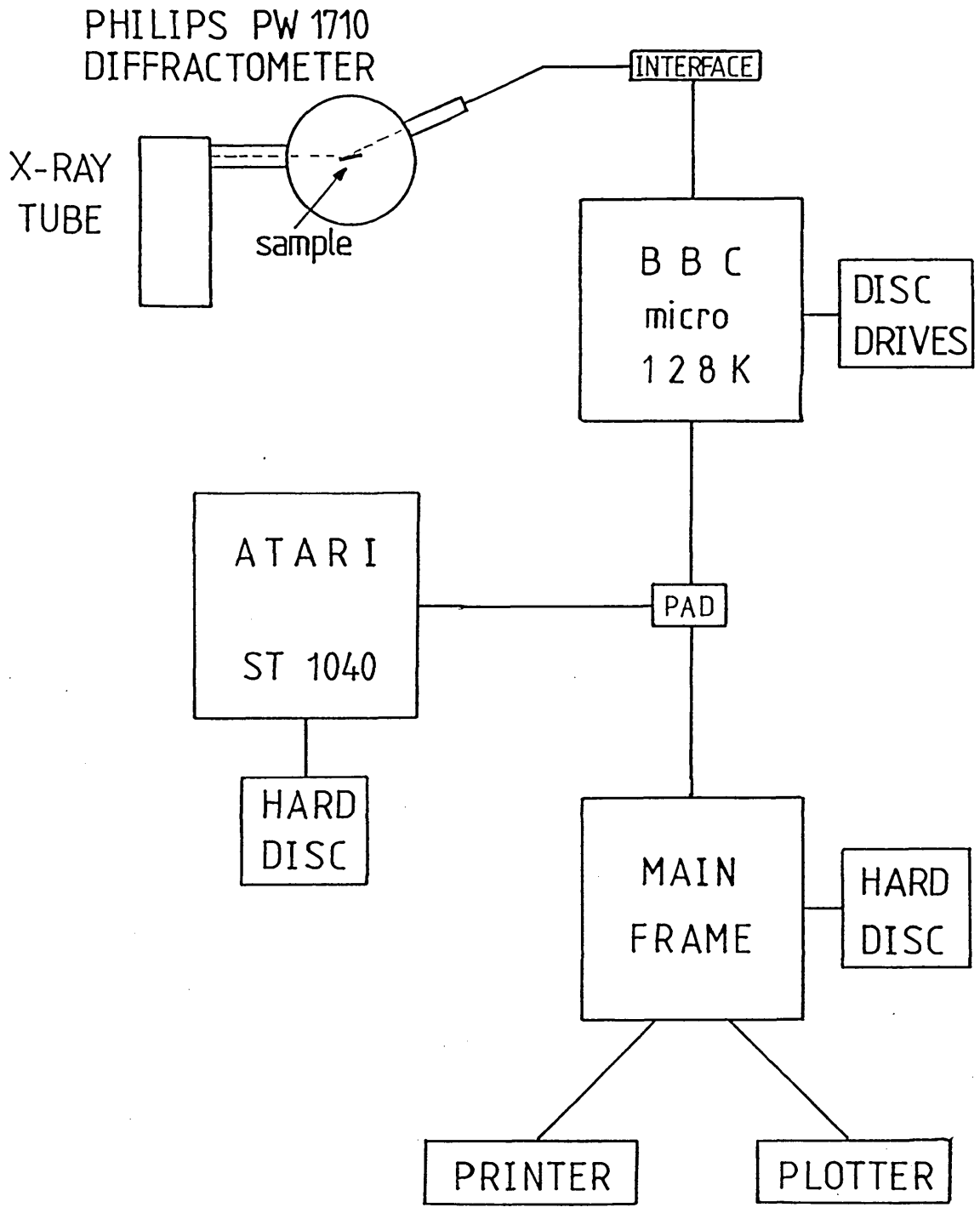

Figure 3.1: Schematic diagram for X-ray diffraction data collection and analysis equipment.

Substituting v_n by the ratio L/t, where L is the total flightpath of the neutrons and t the total time from the "source" to the sample and then to the detector, and rearranging eq. 3.3,

$$t = 2\ d\ L\ (m_n\ /\ h)\ \sin\ \theta \qquad (3.4)$$

Therefore, the d-spacing can be found from the t-o-f, when the position of the detector is defined (L,θ) in space.

In fact, in the experimental arrangement (see figure 3.2), there are 27 detectors arranged in 3 banks around the sample and the mini-computer controlling the experiments collects and processes data from all the detectors.

The profiles obtained were fitted with a Rietveld refinement method, where list squares fitting was applied to the entire profile, without intermediate extraction of structure factors or integrated intensities.

3.3.4. Scanning Electron Microscopy

The equipment used for SEM included the JEOL T-200, JEOL T220A and JEOL JSM35 CF microscopes equipped with backscattering detectors. EDAX (Energy Dispersive Analysis of X-Rays) is available for the T-200 for qualitative analysis and for the JSM35 where semi-quantitative information, element maps and point analysis can be performed.

3.3.5. Particle Size Measurements

The Malvern Laser Particle Sizer 3600D was used in order to measure particles of 1-100 μm. The powder was ultrasonically dispersed in ethanol or acetone during the measurements. Smaller particles could only be measured accurately by SEM.

3.3.6. Atomic Absorption

In order to examine the potassium content of the K-doped samples, chemical analysis was performed with a Perkin Elmer 2380 Atomic Absorption Spectrophotometer, at a wavelength of 766.5 nm using an

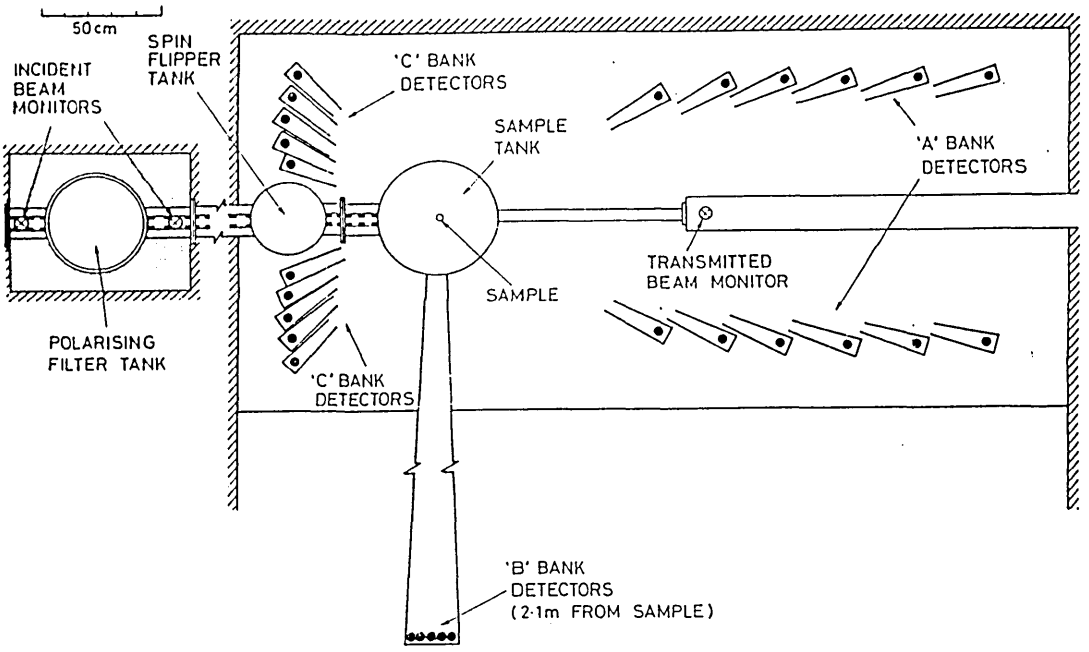

Figure 3.2: The POLARIS neutron diffraction experimental arrangement at Rutherford Appleton Laboratory.

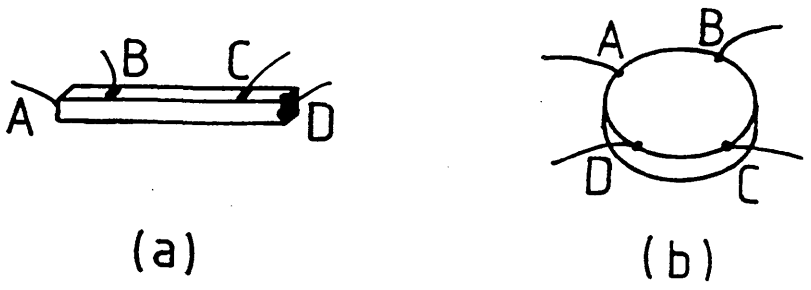

Figure 3.3: (a) Linear 4-point and (b) van der Pauw arrangements for resistivity measurements.

air–acetylene flame. Standards were fabricated and the samples were dissolved in 1:1 water solution of HNO_3 and diluted to reach the required approximate concentration. CsCl was used in the examined solution for ionization control.

3.3.7. Thermal Analysis

Thermogravimetric and differential thermal analysis were performed at a Stanton–Redcroft simultaneous thermal analyzer STA–780, controlled by a Commodore CBM 4032 microcomputer. The sample (~20mg) was placed in an alumina crucible and compared with another crucible containing alumina standard, under controlled atmosphere (air, N_2 or forming gas: 90%N_2–10%H_2). Heating rates of 5–10 deg/min were used.

3.3.8. Four–point resistivity/Superconductivity

DC resistivity was measured either using a linear 4–point arrangement in bar shaped samples or a van der Pauw arrangement for cylindrical pellets. Painted silver was used for contacts. In order to reduce the contact resistance the sample was annealed for 1 hr at 500 C in O_2, after the Ag contacts were being painted on.

For the measurement, the whole arrangement was cooled either under vacuum or in He gas, so that no vapour condensed on the sample. Values of resistivity of the sample and the resistor used for temperature control were collected with a microcomputer.

A. Linear contact arrangement.

As shown in figure 3.3a, four contacts are made, the current contacts (A,D) are made at the bar edges and the voltage contacts (B,C) in between at a distance L (cm). If the cross section of the bar is A in cm^2, the resistivity (Ohm cm) is:

$$\rho = R \frac{A}{L} = \frac{V_{BC}}{I} \frac{A}{L} \qquad (3.5)$$

B. Van der Pauw contact arrangement.

Assuming a uniform, flat sample of constant thickness d and four

point contacts at the edges, (A, B, C and D in figure 3.3b), the resistivity can be determined by measuring the resistance R_{AD}, passing current through B and C and the resistance R_{DC}, passing current through the A and B contacts.

The following relation exists between R_{AD} and R_{DC} [181]:

$$\exp(-\pi\, d\, R_{AD} / \rho) + \exp(-\pi\, d\, R_{DC} / \rho) = 1 \qquad (3.6)$$

where ρ is the resistivity, giving the solution:

$$\rho = \frac{\pi\, d}{\ln 2} \; \frac{(R_{AD} + R_{DC})}{2} \; f\left(\frac{R_{AD}}{R_{DC}}\right) \qquad (3.7)$$

where $f(R_{AD}/R_{DC})<=1$, with $f(1)=1$.

Other techniques such as AC susceptibility, and magnetization were used. AC susceptibility was measured using a Partshorne type mutual inductance bridge, while magnetization was measured with a vibrating sample magnetometer. These measurements took place in the Dept. of Physics and some of them were conducted with the help of R. Meisels and S. Bungre.

3.3.9. DC Polarization

In this electrochemical technique a mixed conductor sample is placed in between two electrically blocking, ionically conducting electrodes, such as YSZ or $Bi_{1.75}Sm_{0.25}O_3$ (BiSm). The blocking electrodes were coated with either sputtered or painted platinum (Pt) on the one side. Two Pt disc shaped foils, touching the Pt-coated electrodes serve as contacts. This electrochemical cell (figure 3.4) was also used for impedance spectroscopy.

The experimental arrangement is shown in figure 3.5. The electrochemical cell is in a furnace with controlled atmosphere (O_2) and it is connected with a constant current source and a digital voltmeter. Constant current of the order of 0.1–1 mA was used and the voltage was measured versus time until it was stabilized.

Provided that the oxygen conductivity (σ) of the blocking electrolytes is considerably larger than that of the mixed conductors, σ ($Ohm^{-1}cm^{-1}$) can be calculated from Ohm's law and the definition of resistance:

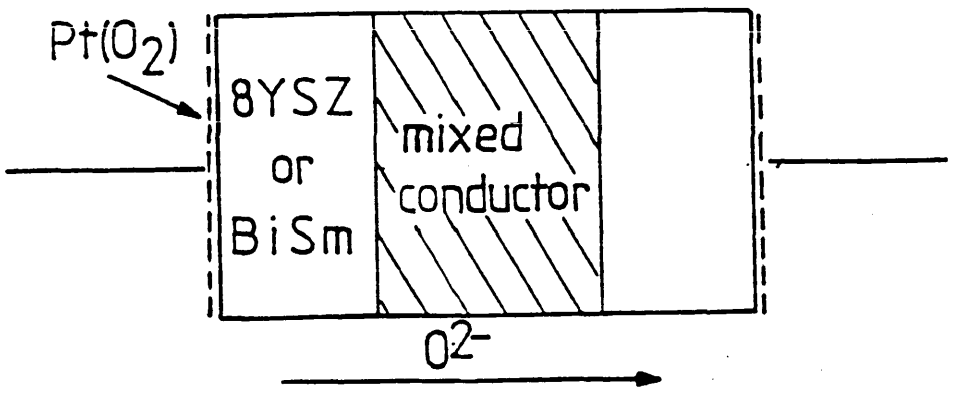

Figure 3.4: The electrochemical cell used in impedance spectroscopy / DC polarization experiments.

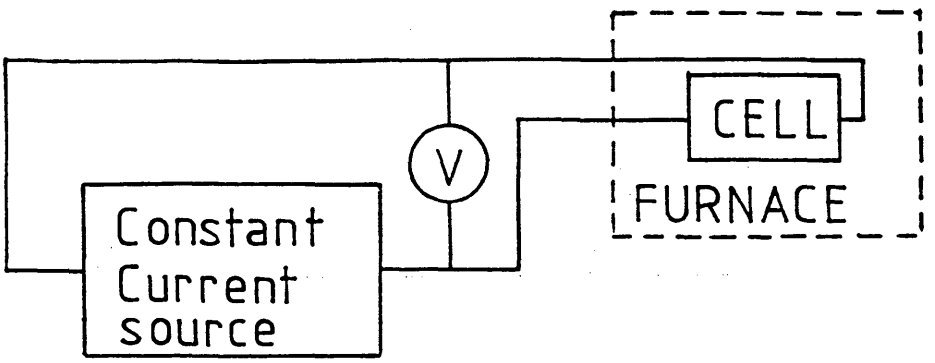

Figure 3.5: DC polarization experimental apparatus.

$$\sigma = \frac{I}{V} \frac{\ell}{A} \qquad (3.8)$$

where I is the amplitude of the current (A), V the equilibrium voltage (Volts), ℓ (cm) the thickness of the mixed conductor and A (cm^2) the contact surface of mixed conductor/blocking electrode. The conditions under which this relation can be used, as well as the various problems that may arise, are described in the appropriate results and discussion chapter.

3.3.10. Impedance Spectroscopy

This is a well known technique for the determination of conductivity of solid electrolytes such as zirconia. For this system, the typical arrangement is that shown in figure 3.6a where a YSZ pellet, both sides covered with Pt, is used.

If a periodic voltage V^*, with an angular frequency ω is applied to such a system,

$$V^* = V_m \exp(j\omega t) \qquad (3.9)$$

then the generated current will, in general, be of different phase:

$$I^* = I_m \exp(j\omega t + j\varphi) \qquad (3.10)$$

The resulting impedance (or "complex impedance"), Z^*, the ratio of the potential difference to the current flowing through the system, becomes:

$$Z^* = V^* / I^* = V_m / I_m \exp(-j\varphi) = |Z| \exp(-j\varphi) \qquad (3.11)$$

The impedance, therefore can be expressed as:

$$Z^* = |Z| \cos\varphi - j|Z| \sin\varphi = Z' - j\,Z'' \qquad (3.12)$$

where Z' and Z'' are the real and the imaginary parts of the impedance [182,183].

Results are usually represented in terms of the imaginary versus the

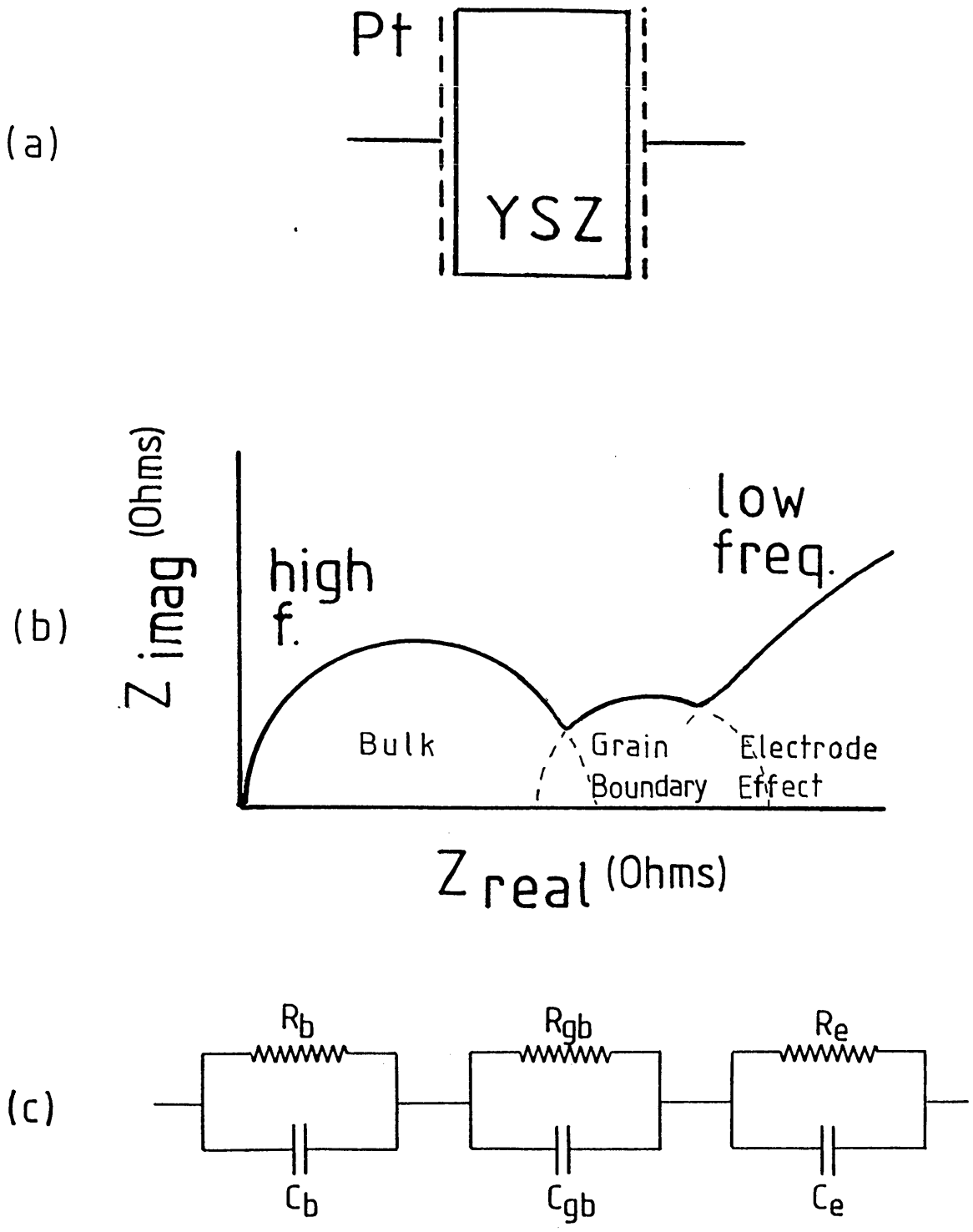

Figure 3.6: Typical application of impedance spectroscopy: (a) The cell Pt/YSZ/Pt, (b) Typical results and (c) Equivalent circuit.

real part of the impedance Z for each of the examined frequencies at the particular temperature.

It can be shown [184] that a parallel R-C circuit results in a semi-circle in the $Z' - Z''$ plane. This way, typical results which are in the form of semicircles, such as in figure 3.6b can be modelled using electrical circuit equivalents (fig.3.6c). In the particular, simple case of zirconia, the first semicircle is attributed to the conductivity of the bulk of the material, the second to the grain boundaries and the third to the $Pt(O_2)/YSZ$ interface (double layer or electrode effect).

From the frequency f (Hz) of the maximum of each semicircle and the resistance R (Ohms) (the radius of the semicircle), the capacitance C (F) can be calculated using the relation:

$$\omega C R = 2 \pi f C R = 1 \qquad (3.13)$$

and from the capacitance, the relative permittivity or dielectric constant ϵ can be found through:

$$C = \frac{\epsilon \epsilon_0 A}{d} \qquad (3.14)$$

where ϵ_0 is the permittivity of free space.

Different processes in solid electrolytes, usually have different capacitances and therefore the semicircles are clearly separated and can be identified. In the case of processes with similar capacitances, semicircles overlap and sometimes create depressed semicircles (with their centre below the Z'-axis).

The advantage of impedance spectroscopy is, therefore, that it can distinguish between the different contributions to the cell conductivity. Impedance spectroscopy is extensively covered in a book edited by J.R. MacDonald [185], where further information can be found.

The apparatus is shown in figure 3.7. The furnace and an HP 4192 A LF Frequency Response Analyser were controlled by a Hewlett-Packard microcomputer. The AC signal had an amplitude of 20-110 mV and a frequency which varied from 5 Hz to 13 MHz. The impedance measurements were conducted in oxygen, over a temperature range of 380-850 C. One hour equilibrium time was used before each measurement, after the furnace achieved the required temperature.

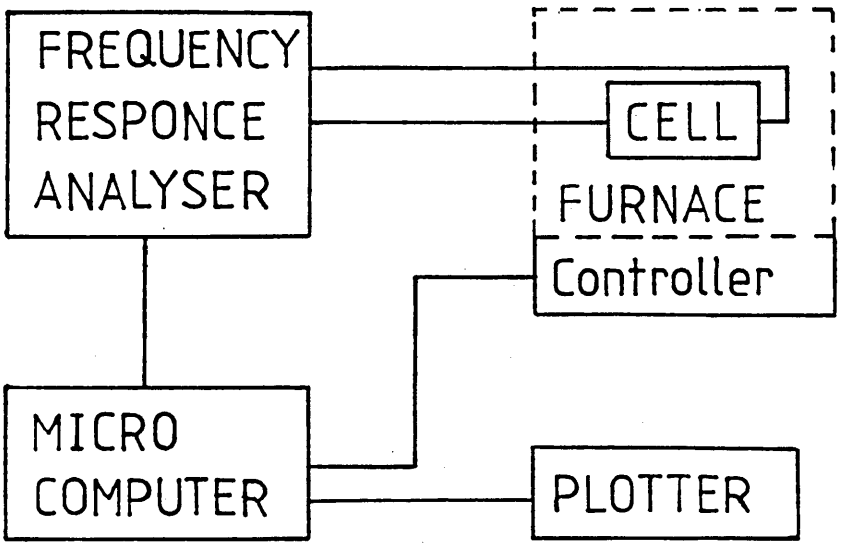

Figure 3.7: Experimental arrangement for impedance spectroscopy measurements.

4. PREPARATION AND CHARACTERIZATION OF YBCO

4.1. Phase Identification

The characterization of the prepared samples was initially carried out by X-ray diffraction in order to examine the phase purity and T_c was measured to confirm their quality.

The main phases of the $1/2Y_2O_3$-BaO-CuO pseudoternary diagram have been identified by the diffraction pattern. In figure 4.1 a,b and c the patterns for the 123 ($YBa_2Cu_3O_{7-\delta}$), 211 (Y_2BaCuO_5) and 132 ($YBa_3Cu_2O_x$) phases respectively can be seen, in agreement with literature reports [67,68,186].

A small quantity of 132 is usually present in typical YBCO samples. In the case of firing at higher or much lower temperatures than necessary, 211 and $BaCuO_2$ appear. CuO has also often been detected as an impurity in YBCO.

4.2. Solid State Reaction

The conventional preparation technique of mixing and firing the starting materials is a convenient method that can be easily applied. The quality of the obtained material, however, can vary significantly and optimization of the method was necessary. The starting materials is one of the parameters that can have an effect on the final properties of the superconductor. Most problems in YBCO are connected with Ba, which tends to react with CO_2 or H_2O and therefore the effect of the Ba-precursors $BaCO_3$, BaO_2 and $Ba(OH)_2$ on the final material was studied.

In order to have an homogeneous mixture the starting oxides/ carbonates were mixed and thoroughly ground for the preparation of YBCO.

An initial step of firing at 500-600 C was used when BaO_2 was used as starting material. After the decomposition the material was ground and pressed, followed by firing at 900-950 C in order to form the 123 phase. The resulting material was ground either by mortar and pestle or by ball milling, pressed into pellets of 13 mm diameter with a pressure of 75

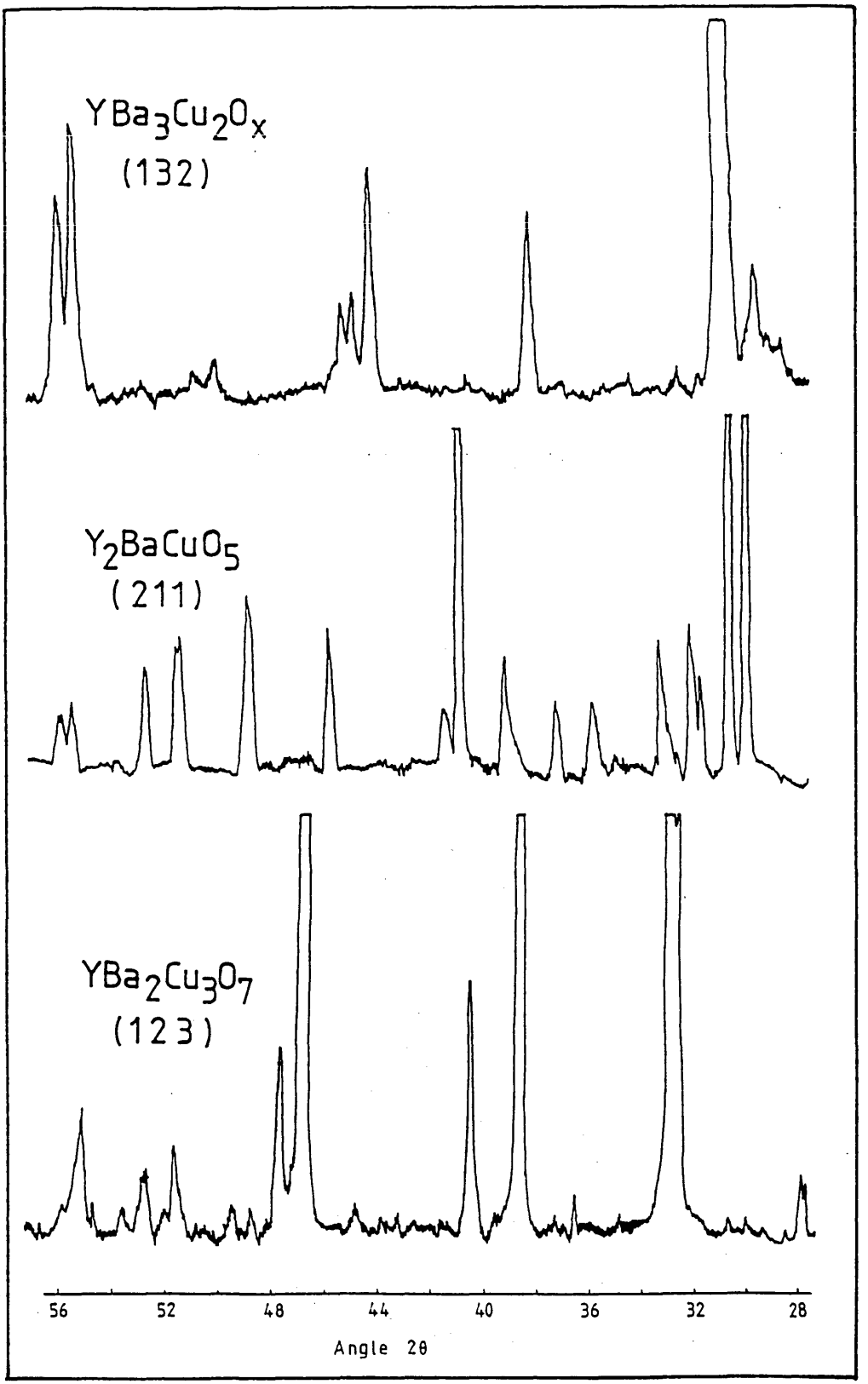

Figure 4.1: X-ray diffraction patterns of the main phases in the pseudoternary diagram $YO_{1.5}$–BaO–CuO ($Cu_{K\alpha}$ radiation).

MPa and fired at 900–980 C for sintering and densification. Phase characterization by XRD and microstructural examination by SEM were performed as well as critical temperature measurements.

4.2.1. $BaCO_3$ route

The formation of YBCO from $BaCO_3$ has been reported to occur at temperatures between 900 and 980 C, usually at 950 C. A number of grinding/firing cycles is required to obtain single phase material.

After firing the oxide/carbonate mixture at 950 C, full decomposition occurs, as indicated by weight loss measurements and also the components react to form the "123" phase (YBCO). This was confirmed by X–ray diffraction as shown in figure 4.2 where the diffraction pattern of unfired material is compared to the pattern of YBCO after firing at 950 C.

Even though the material after this first firing is single phase, the density achieved is usually 60–70% of the X–ray density. This low density is probably due to the fact that during the formation of YBCO, more than 10% of the mass of the sample is lost as CO_2. This represents a considerable volume and as a result large porosity remains since sintering cannot take place effectively.

The density of the samples in the case of a direct short firing and in the case of two firings with intermediate grinding is presented in table 4.1. From this table it can be observed that material fired for a second time had a density of 86% which was raised further to 92% using ball milling for size reduction of the powder particles. The effect of sintering time is also important since 7.5 h gave lower density (81%) than 15 h (86–92%) (table 4.1).

Firing for a second time, also improved significantly the superconducting properties of the material. Low temperature resistivity data presented in figure 4.3, show that T_c is less than 70 K for a directly fired sample and 88 K for a reground and refired sample. A possible explanation for the low T_c in the first material, is poor connectivity of the grains as a result of the low density.

Typical grains are elongated with a long axis of 10 μm and a short one of about 2–3 μm as can be seen from figure 4.4, where the surface morphology of a 92% dense pellet is shown. There is a network of cracks, part of which is shown in the micrograph, due to the thermal processing and anisotropic properties of the material.

EDAX analysis was carried out at several points in the same and

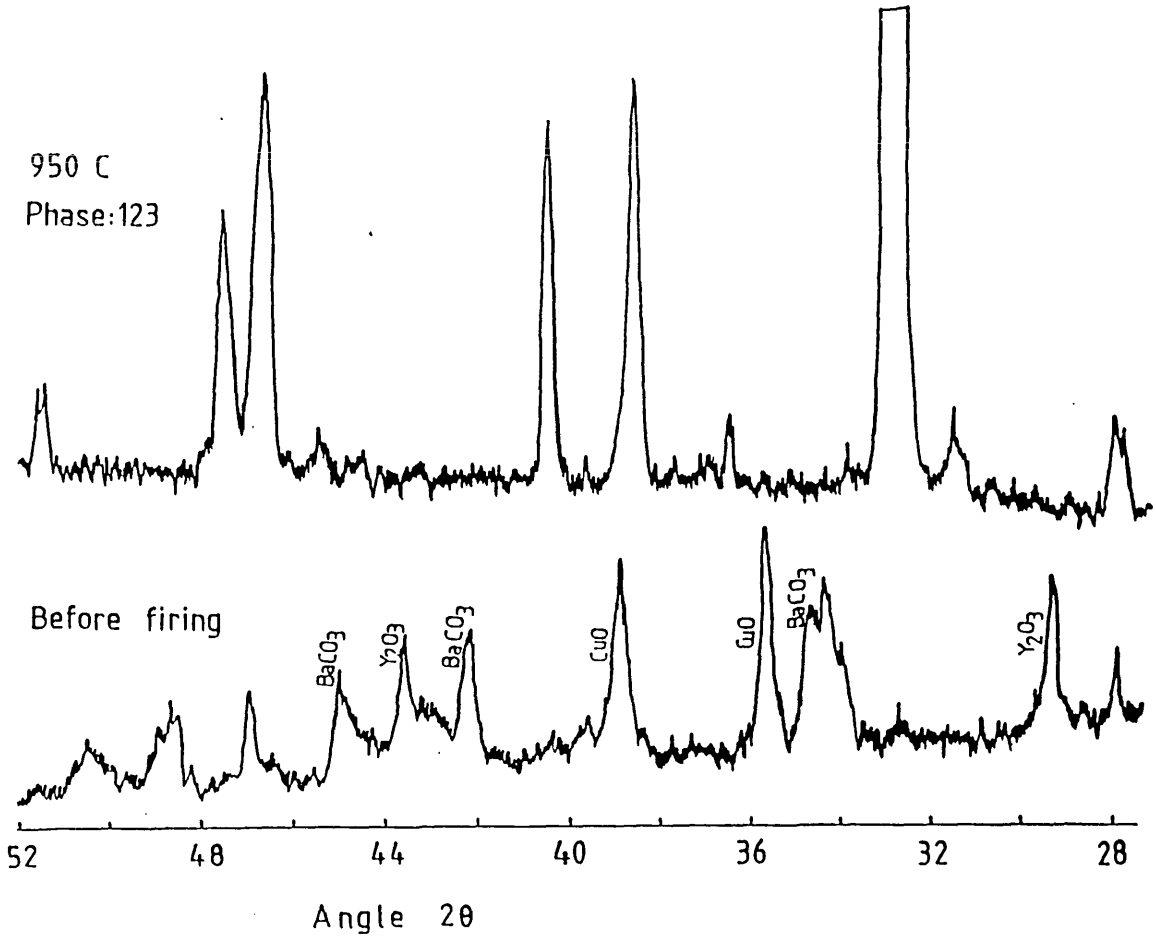

Figure 4.2: X-ray diffractograms for the unfired Y_2O_3, BaO_2, CuO mixture, compared to the fired material (YBCO) (Cu_{Ka} radiation).

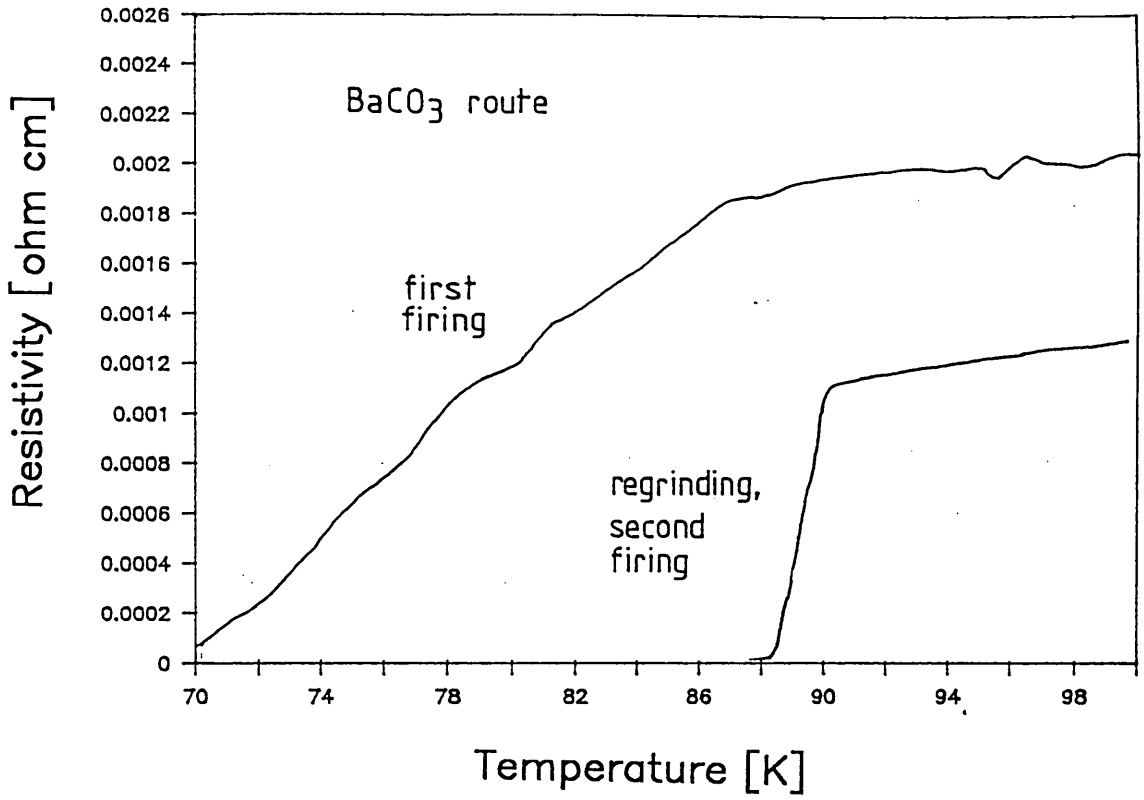

Figure 4.3: The superconductive transition for samples prepared from $BaCO_3$, after a first and a second firing at 950 C.

different samples and the ratio of Y:Ba:Cu peaks was found to be stable, indicating that the stoichiometry of the components of the superconductor is fixed (1:2:3). A typical graph is shown in figure 4.5. Small amounts of impurities such as CuO, $BaCuO_2$ and in one case an Y and Ba-rich phase were also detected as isolated grains, in agreement with X-ray diffraction, where a very small peak of CuO and barely distinguishable peaks for $BaCuO_2$ were identified, in a diffraction pattern which would be characterized as "single" phase according to the literature of HTS.

Table 4.1
Sample density dependence from preparation process

Step 1		Step 2		Density (% X-ray)
Temp.(C)	Time(h)	Temp.(C)	Time(h)	
950	4			69
950	5			58
950	5			58
920	12			52
950	12	950	15	86*
950	12	950	15	92
950	12	950	14	88
950	12	950	7.5	81

*grinding by mortar and pestle, the rest by ball milling

4.2.2. BaO_2 route

In the case of preparation from BaO_2, an initial firing step at 600 C is necessary to decompose it. After that it is ground and fired at 950 C for the formation of YBCO phase and then reground, pressed and fired for sintering since this was found to be the the optimum procedure.

The powder used for the final sintering stage, ground by mortar and pestle, is shown in figure 4.6. The particles have irregular, angular shape and a size that vary significantly. The particle size distribution in figure 4.7 obtained by a laser particle size analyser, shows that 90% wt. of the material has size between 2 and 10 μm.

The resulting density after sintering such powder is 88%, compared to

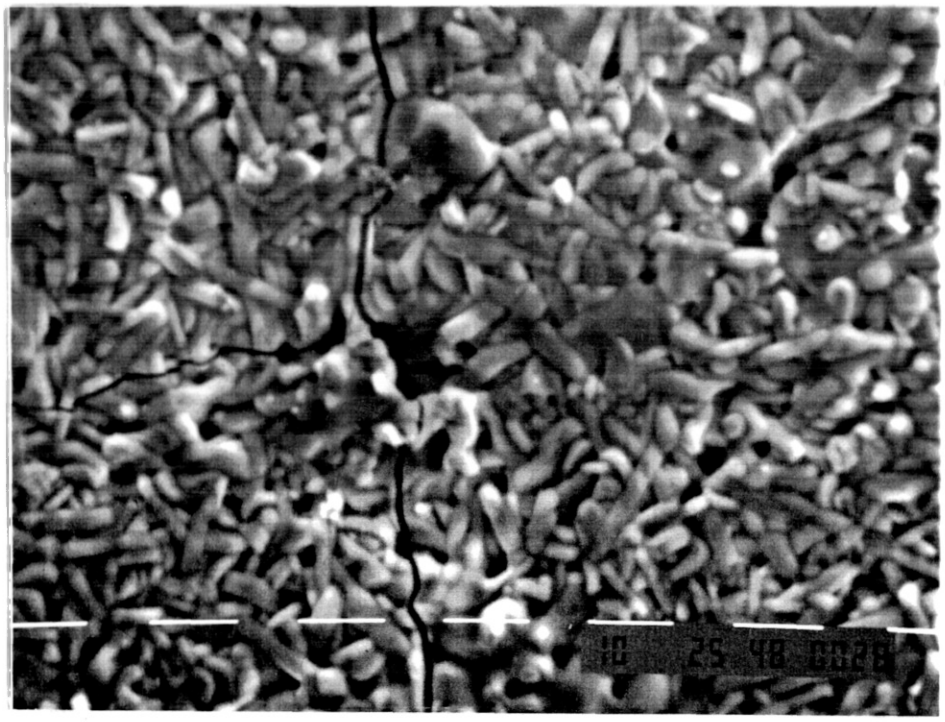

Figure 4.4: Typical surface morphology of a 92% dense sample prepared through solid state reaction from $BaCO_3$. Bar= 10 μm.

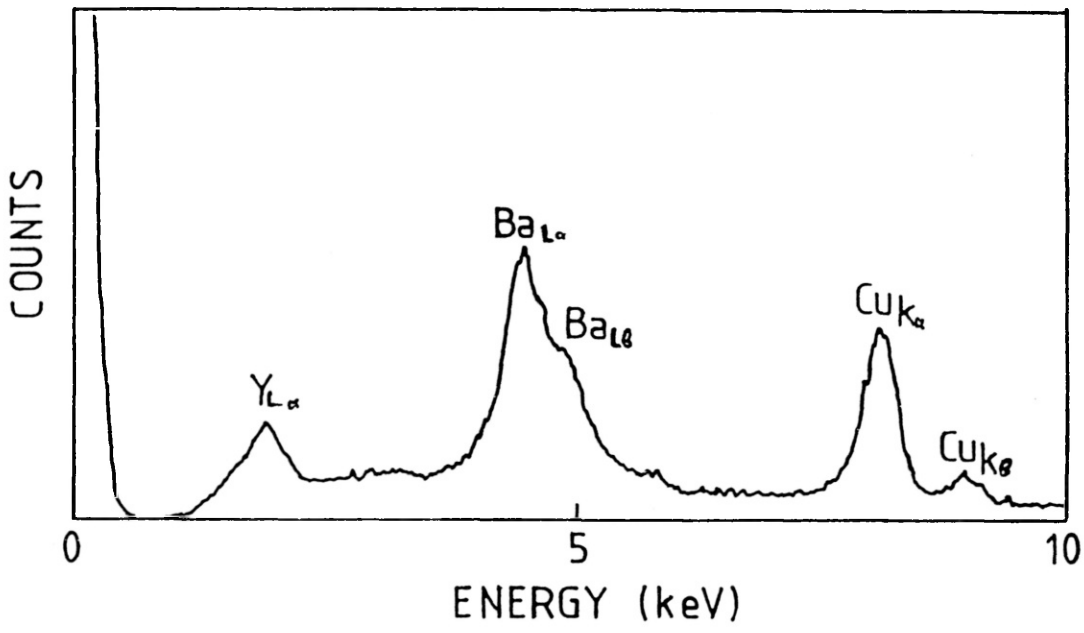

Figure 4.5: Typical EDAX (Energy Dispersive Analysis of X-rays) trace for $YBa_2Cu_3O_{7-\delta}$.

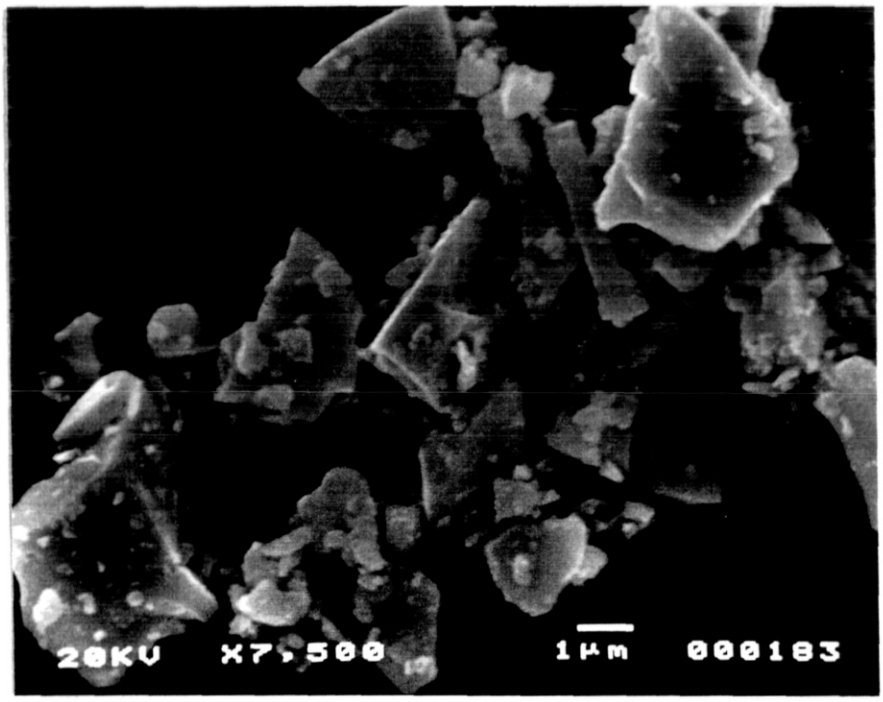

Figure 4.6: Morphology of YBCO powder after mortar and pestle grinding (solid state reaction, BaO_2 as a Ba-precursor). Bar= 1 μm.

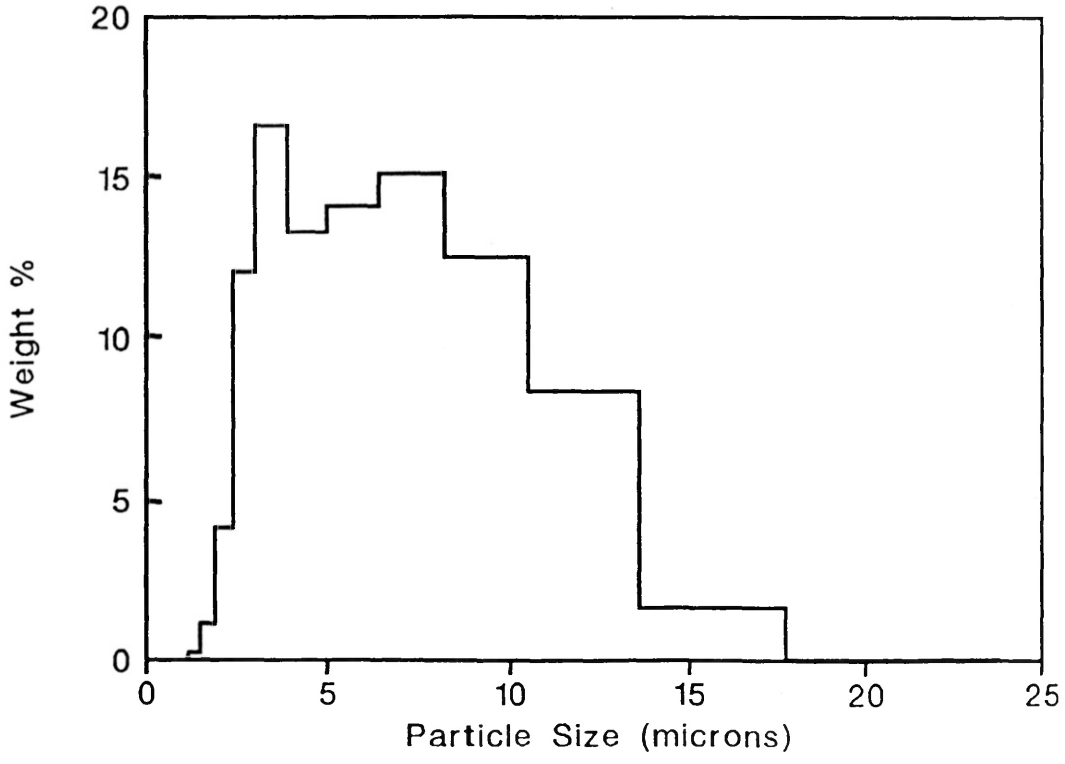

Figure 4.7: Particle size distribution for the powder shown in figure 4.6.

86% that the $BaCO_3$ route gave under the same conditions. Ball milling with ZrO_2 media in ethanol resulted in contamination from the polypropylene container (3% of the total weight as proved from the weight loss) and the material fabricated this way was of poor quality.

The material produced from BaO_2, was in general of higher quality than that from the $BaCO_3$ route. In figure 4.8 the superconductive behaviour of samples after a first and a second firing is presented. Comparing this with figure 4.3, a significant improvement of the material after the first firing can be observed and also a minor improvement on zero resistivity ($T_c^{R=0}$) which is 89 K for the BaO_2 route sample compared to 88 K for the $BaCO_3$ one. A more important improvement is that of the normal state resistivity which became 0.3 mOhm cm (at 100 K), compared to 1.2 mOhm cm in figure 4.3.

The 88% dense material that was produced had very few cracks unlike the $BaCO_3$ route samples, as characterized by SEM. XRD showed $BaCuO_2$ peaks of similar height to the one reported in 4.2.1 (just above the background) but no trace of CuO.

As a result, using BaO_2 instead of $BaCO_3$, seems to offer advantages in solid state conventional preparation as was also confirmed in the literature [135,136] later on.

4.2.3. $Ba(OH)_2$ route

$Ba(OH)_2$ was also used as an alternative precursor. The main problem in this case was the fact that it is very hygroscopic and reacts to form $BaCO_3$. The starting materials were ball milled and different batches were fired at 850,900 and 950 C. Examination of the samples by X-ray diffraction showed that multiphase material resulted in all cases. The main phase was 123 but there was also a considerable amount of 211 and some CuO. Regrinding and refiring of the above samples at 950 C did not improve their purity and most of the times resulted in partial melting. The morphology of the samples was different than usual. In figure 4.9a plate-like crystals of CuO (detected by EDAX) are shown, grown in a part of a sample and in figure 4.9b the surface morphology of another point can be observed. It is, therefore, clear both from SEM and XRD that multiphase, inhomogeneous material results from fabrication with $Ba(OH)_2$ as a Ba precursor.

T_c measurements have not been performed since the quality of the material was obviously not satisfactory.

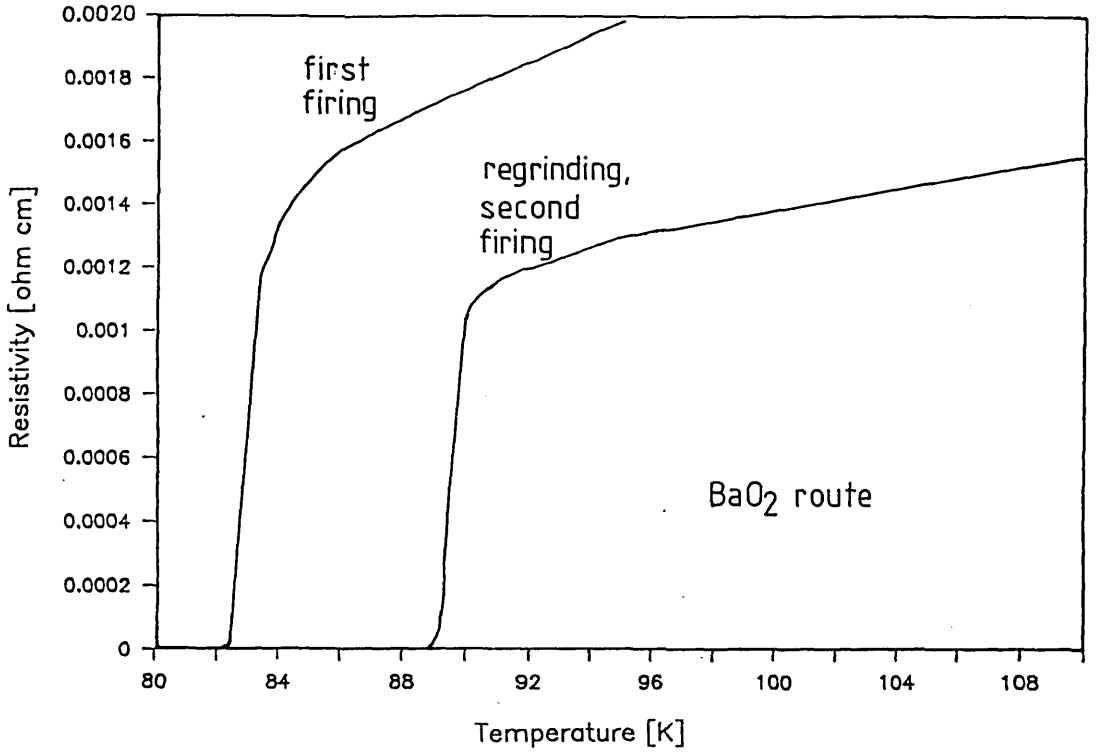

Figure 4.8: The superconductive transition for samples prepared from BaO_2, after a first and a second firing at 950 C.

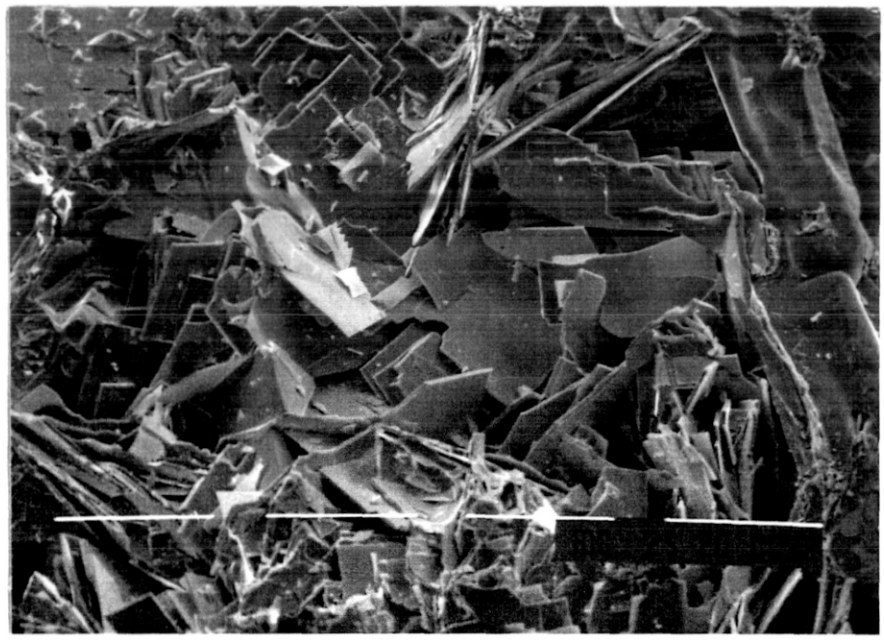

(a)

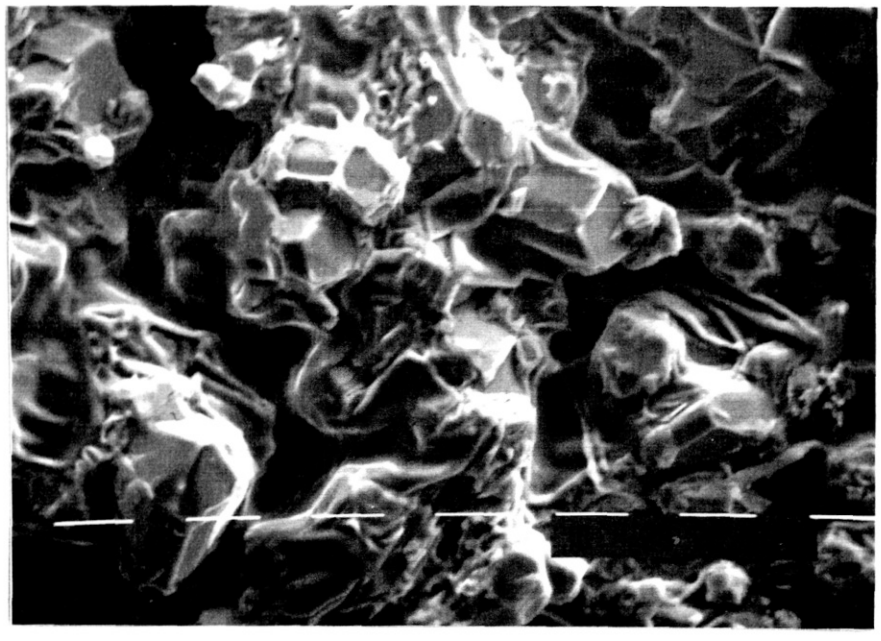

(b)

Figure 4.9: Surface morphology of samples prepared from the $Ba(OH)_2$ - solid state reaction route. (a) Bar= 100 μm, (b) Bar= 10 μm.

4.3. Evaporation of Nitrates

4.3.1. Experimental

The starting materials (Y_2O_3, BaO_2, CuO or Cu) were dissolved in a small excess of nitric acid and then the solution was boiled to evaporate all the water and the remaining acid. The nitrate salts were heated on a hot plate up to 300 C. After grinding they were fired at 500 C to decompose the nitrates and later on at 800–950 C for the formation of YBCO. A final grinding and pressing stage was followed by firing at 900–950 C for sintering.

4.3.2. Results

The evaporation of a nitrate solution was attempted for the production of a homogeneous powder. YBCO as well as 5,10 and 15% K–doped material was produced, where x% is the percentage of barium substitution by K. During the evaporation of the solution a white powder was originally precipitated, while the rest of the solution had the dark blue colour typical for the Cu nitrate. After the evaporation of the liquid, the remaining blue powder melted and gradually became black.

After the initial firing at 500 C for the decomposition of nitrates the formation of YBCO was attempted by firing at temperatures ranging from 800 C to 950 C. In all cases a multiphase material resulted when temperatures lower than 950 C were used. X–ray diffraction indicated that in some cases the material that was sintered at 950 C was single phase but the results were not reproducible, since fabrication by the same procedure, led to the appearance of large amounts of 211 and $BaCuO_2$. In other cases CuO and $BaCuO_2$ or 211 and CuO appeared. By examination of the phase diagram (figure 2.5), it can be concluded that the different batches/fractions used, had different stoichiometries around the 1:2:3 ratio.

It was also frequently observed that the 211 phase was formed in the centre of the sample at the contact with the substrate. Generally the pellets were deformed and sometimes cracked, clearly having areas of different composition.

4.3.3. Discussion

This method, therefore, presented the following problems: (a) The material produced was not homogeneous since Ba and Y nitrates precipitated first and Cu later as was obvious from the colour of the solution, (b) the powder did not have a small particle size since during the decomposition of the nitrates melting took place. As a result, there was non-reproducibility and usually poor quality of the produced samples, in disagreement with initial reports of good quality material obtained by this method [137,138]. There was also no indication of lowering of the YBCO formation temperature as claimed. Since 1987, however, no further publications were made on this fabrication route, something that indicates that careful examination of the results led to conclusions similar to those presented here on the applicability of this technique.

4.4. Freeze-Drying

4.4.1. Experimental

Freeze drying or lyophilization is a technique that can be used for the fabrication of high quality (homogeneous, small particle size) ceramic powders. It is essentially a means of drying, achieved by freezing the wet substance and causing the ice to sublime directly to vapour by exposing it to a low partial pressure of water vapour. The method requires four basic operations [187]: (a) Mixing, preparing a solution of the cations, (b) Freezing the solution abruptly, so that no fractional crystallization occurs and the random ordering of the ions in the solution is retained, (c) Sublimation of the ice under vacuum, until only a mixture of the salts remains and (d) Decomposition of the salts to form the oxides and subsequent calcination to form the required phase.

For preparation of YBCO, a solution of Y, Ba and Cu nitrates was prepared by dissolving the oxides with a small excess of nitric acid and sprayed on liquid nitrogen. The frozen droplets were collected and put in a precooled container which was put immediately in the freeze-dryer. Three types of freeze-dryers were used: (i) a big capacity laboratory multi-user commercial freeze-dryer, (ii) a home-made apparatus shown in figure 4.10 and (iii) a small capacity laboratory commercial unit.

When all the water was removed through sublimation, the sample was transported to a dry-box and heated on a hot plate (~300 C) and subsequently ground and fired at 500 C and/or at 800 C. The last stage was grinding, pressing and firing again at 900-950 C for sintering.

4.4.2. Results

The first two stages reported in the previous section, fabricating and freezing the solution, did not present any difficulties. During sublimation, however, melting of the frozen droplets was observed. This would result in the precipitation of the salts and loss of the expected chemical homogeneity and small particle size.

In order to avoid melting, the container of the frozen material was kept at low temperatures using dry ice (solid CO_2) when the big capacity

freeze-dryer was used. Since it was difficult to maintain dry ice overnight, a second device was set up, where the frozen solution container was kept at a low temperature using an "environment chamber" (-25 C max.), shown in figure 4.10. In both cases, very slow sublimation rates resulted since the vapour pressure of the water is much lowered at such temperatures. Freeze drying for 7-10 days was necessary in several experiments and even then, some melting occurred, especially at the final stage of the process when most of the water had been removed.

Investigation of the possible reasons that could result in lowering the melting point of the salt solution led to the conclusion that the remaining small excess of nitric acid, used to dissolve the oxides, was responsible for this effect. The melting point of HNO_3 is -42 C [188] and, therefore, a HNO_3-H_2O solution is bound to have a melting point lower than -4 C.

When the role of HNO_3 was realized, the solution was formed with the minimum excess of HNO_3 possible and then neutralized (pH=7) with the addition of dilute ammonia. The problem of melting was thus overcome and eventually the solution was freeze-dried in less than two days using a small laboratory apparatus, without having to keep the material at low temperatures.

The material produced after freeze-drying was very hygroscopic and it was transferred in a dry box before decomposition on a hot plate. As in the case of evaporation from a solution, melting of the nitrates occurred since $Cu(NO_3)_2$ $3H_20$ melts at 114 C [188].

One more problem that arose was the decomposition of ammonium nitrate that was formed during neutralization of the solution with ammonia. Ammonium nitrate decomposed violently producing a cloud of brown vapours and at the same time dispersing small particles of the powder around the hot plate.

Firing at 600 C was initially attempted but the decomposition was not completed as indicated from X-ray diffraction and the large weight loss after subsequent firing at 950 C. For this reason, a calcination temperature of 800 C was used in order to succesfully decompose the material.

The powder produced by this method had a wide size distribution ranging from 5 μm particles to 40 μm particles/agglomerates with irregular shape as can be seen in figure 4.11.

Pressing and firing of this powder at 950 C gave multiphase material, usually containing YBCO as a majority phase along with a considerable amount of $BaCuO_2$ and 211. A typical X-ray diffraction pattern is presented in figure 4.12. DC resistivity and AC susceptibility confirmed

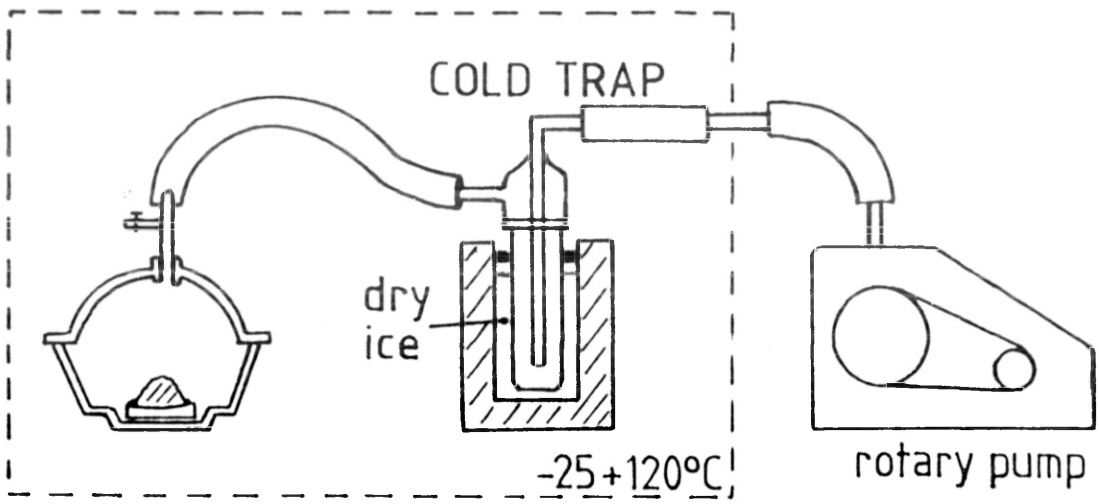

Figure 4.10: Apparatus constructed for the freeze-drying process.

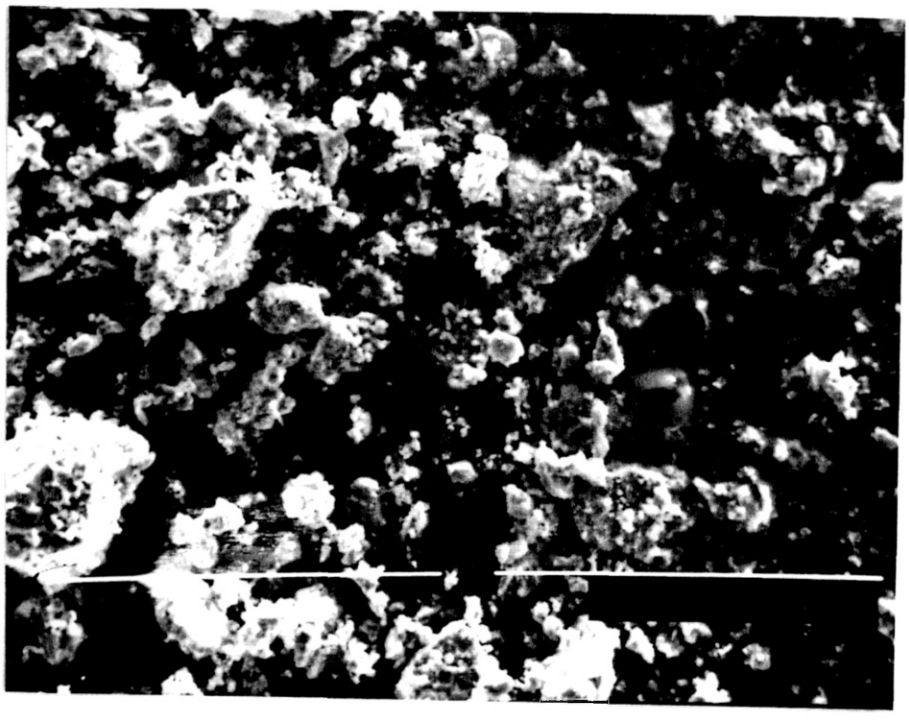

Figure 4.11: Scanning electron micrograph of powder produced by freeze-drying. Bar= 100 μm.

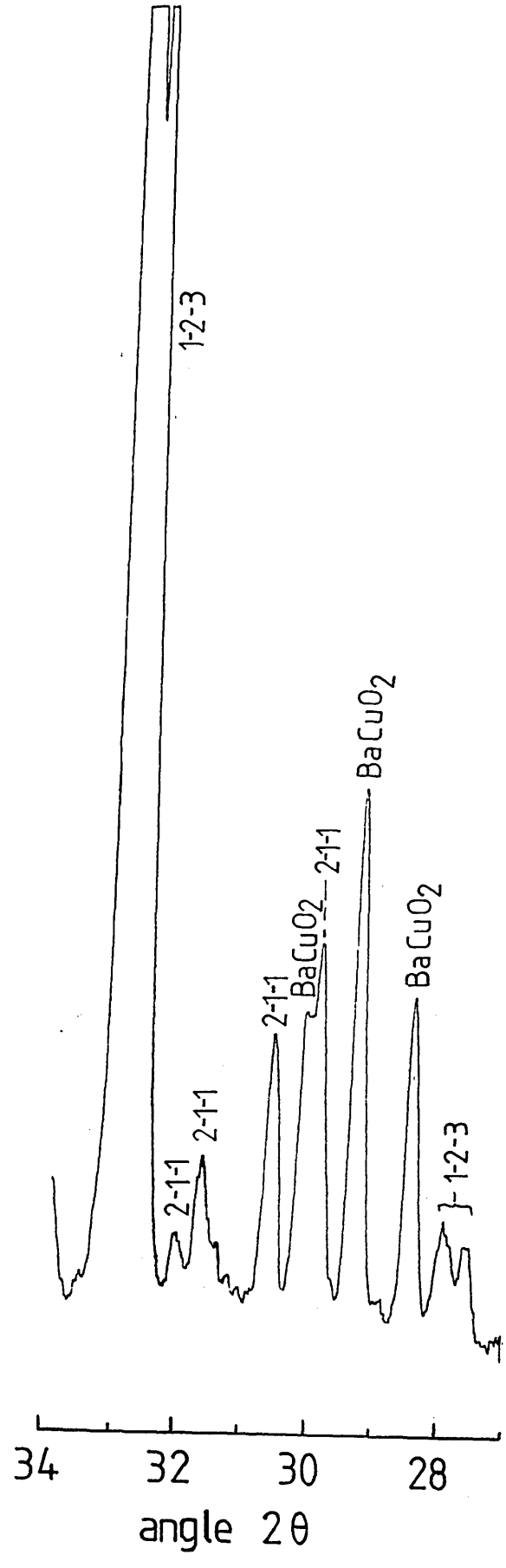

Figure 4.12: Typical X-ray diffraction pattern (Cu_{Ka} radiation) of the multiphase material produced by freeze-drying.

the results of X-ray diffraction, showing that the samples produced were of poor quality.

4.4.3. Discussion

The poor quality of the powder and bulk samples produced by freeze-drying can be explained by analyzing the problems presented during the fabrication process. Specifically, melting of the frozen material during the initial experiments resulted fractional precipitation of the nitrates and consequently, the loss of the expected homogeneity. Furthermore, when conditions were adjusted to avoid this effect, decomposition of the freeze-dried salts on a hot plate resulted in melting of the Cu nitrate and loss of homogeneity and small particle size.

A possible route to avoid these problems would be to heat the material in vacuum immediately after freeze-drying, so that the crystalline water of the nitrates can be removed by sublimation, thus avoiding melting, and heating at even higher temperatures, to decompose the nitrates. The first step of heating the nitrates to remove the crystalline water was attempted using the "environment chamber"; however, even though a temperature of 122 C (maximum for the apparatus) was reached, not all the water was removed. Further heating on a hot plate still resulted in melting, possibly indicating the existence of other hydrated forms melting at even higher temperatures.

Therefore, either heating in vacuum at higher temperatures or using something other than nitrate salts could possibly result in better results.

Work reported in the literature during and after the research presented here are contradictory. According to an initial report [141], the synthesized material was of very good quality, but in another publication Wang et al.[189] concluded that freeze-drying of nitrates gave highly aggregated material and resulted in low-density ceramics (<75%), in agreement with the results presented here. Medelius and Rowcliffe [142], came to the same conclusions as in this work, as far as pH control and problems created by nitrates are concerned, and using acetate-nitrate mixtures they achieved the fabrication of much better powders.

4.5. Mist Pyrolysis

4.5.1. Experimental

The mist pyrolysis process consisted of three steps: initial atomization of the starting solution into micron-sized droplets via an ultrasonic atomizer, transit of the generated aerosol through a hot zone where the decomposition and reaction processes took place and subsequent collection using a filter. The mist pyrolysis apparatus, which was constructed in collaboration with Mr. K. Ley to perform the process, is schematically shown in figure 4.13.

The potential advantages of using such a technique include close control of green microstructure; the method producing spherical, controllable size particles with uniform size distribution and enhanced chemical homogeneity relative to solid state approaches.

The starting solution for YBCO contained nitrates in the ratio 1:2:3 for the Y, Ba, Cu cations. $Y(NO_3)_3$ and $Cu(NO_3)_2$ were prepared by reaction of their 99.999% pure oxides with nitric acid. $Ba(NO_3)_2$ of analytical purity was also used. The solution had a concentration of 0.025 M and a pH adjusted to 7 (so as to minimize corrosion of the ultrasonic transducers).

The ultrasonic atomizer used, ("Electrosonic ES4 humidifier"), consisted of 4 piezoelectric transducers, operating at a frequency of 1.6 MHz. Atomization by ultrasonic means has two important advantages over nozzle (spraying) methods: (a) Very narrow droplet size distribution [190,191], (b) Droplet size and quantity of atomized solution can be indepedently controlled by adjusting the frequency and the power respectively, so that optimum conditions can be easily achieved [190].

The temperature of the furnace and the carrier gas (oxygen) flowrate could be used to control the phase formation reaction. A flowrate of 1.5-2.5 l $min.^{-1}$ was used, in a silica tube of active length 50 cm and internal diameter 3.1 cm. A residence time of 9-15 sec. was calculated, without taking into account, however, possible effects (such as expansion of carrier gas) due to the high temperature of the furnace. Temperatures between 900 and 1000 C were used.

The design of the filter had to provide adequate collection performance for submicron particles and at the same time be resistant to

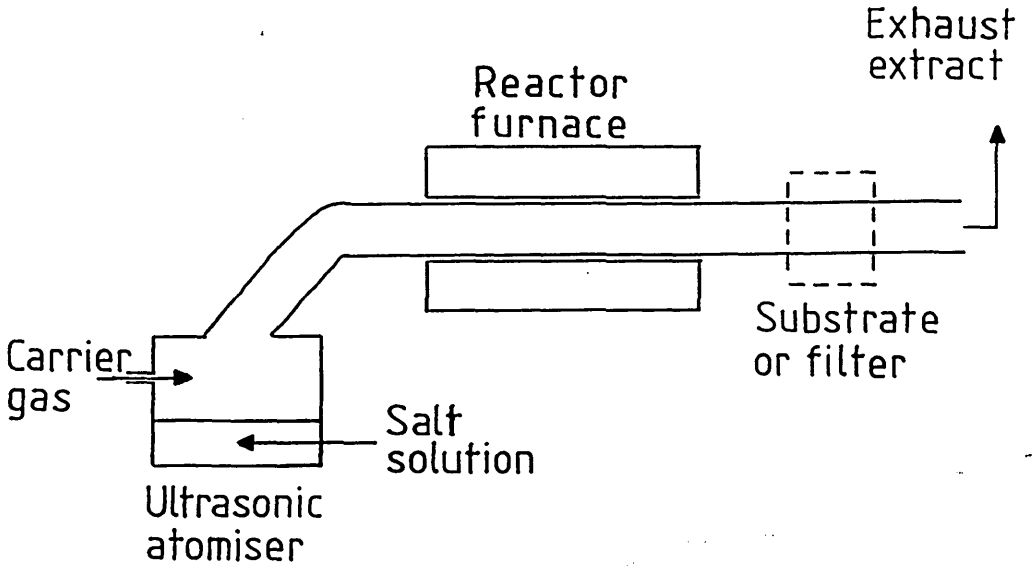

Figure 4.13: The apparatus constructed for mist pyrolysis.

high temperatures combined with water vapour. For this reason a Gelman Sciences Type A/E glass fibre filter was selected, with nominal 1μm pore size, being able, however, to retain 99.98% of 0.3 μm particles, operating at temperatures up to 550 C and high flowrates (32 lt/min.). A large pore sintered glass filter was used as a support for the glass fibre one.

For the production of bulk samples, the collected powder was pressed into 5 mm diameter pellets and subsequently fired up to 950 C for 4–12 hrs duration. The atmosphere of the furnace was oxygen and slow rates of heating and cooling were used (2–5 deg min^{-1}).

4.5.2. Particle size calculation

The expected powder particle size obtainable via this technique can be calculated from first principles using equation (4.1) [192], which gives an estimate of the diameter of the droplets that are generated through ultrasonic cavitation of a solution.

$$d = 0.969\left[\frac{\gamma}{\rho f^2}\right]^{1/3} \qquad (4.1)$$

In the above equation, d is the calculated droplet size (m), γ and ρ represent respectively the surface tension (N m^{-1}) and the density (Kg m^{-3}) of the solution, whilst, f represents the ultrasonic frequency (Hz) used.

Using a frequency of 1.6 MHz, a surface tension of 69.6×10^{-3} N m^{-1} and a calculated density of 1.03 g cm^{-3} for the YBCO precursor solution, equation (4.1) gives a droplet diameter of 2.9 μm. From the concentration of the solution (0.025 M), the mass of YBCO produced from each droplet is found to be 2.1×10^{-13} g. Supposing a density of 6.39 g cm^{-3} (X-ray density of orthorhombic YBCO), and spherical particle shape, the diameter of each particle is calculated to be approximately 0.4 μm.

These calculations may be summarized by the following equation (4.2):

$$d_p \simeq \left[\frac{c\, M_w\, \gamma}{10^6\, \rho\, \rho'\, f^2}\right]^{1/3} \qquad (4.2)$$

Here, d_p is the particle diameter (m), c is the concentration (moles l^{-1}), M_w the molar weight of the compound formed (g), ρ' the X-ray density

of the compound (g cm^{-3}) and γ (N m^{-1}), ρ (g cm^{-3}) and f (Hz) as defined for equation (4.1).

Consequently, control of particle size for a particular compound can be achieved via both the frequency of the transducers producing the fine mist and the concentration of the solution itself.

4.5.3. Results

Initial experiments with a furnace temperature of 900–950 C gave partially reacted (brown) powder. When a temperature of 1000 C was selected, the powder had the typical black colour of YBCO.

X–ray diffraction of the powder produced when the furnace was at 1000 C, indicated the formation of YBCO phase (figure 4.14). Broadening of the peaks due to the small particle size can be observed. No impurity peaks were detected, which is an important result since small amounts of CuO or Y_2BaCuO_5 are usually present in YBCO. Therefore, this method can be used to produce single phase powder *in one step*.

The collected powder was also examined by SEM which confirmed that the individual particles were of spherical shape (see figure 4.15). From figure 4.16, it can also be seen that the particle size distribution is quite narrow, with 97% of the particles between 0.1 and 0.5 μm, with a mean diameter of around 0.3 μm, thus confirming the theoretical estimate of 2.9 μm, calculated from equation (4.2).

Particles produced from processes such as mist or spray pyrolysis can be hollow [193], and this effect has been observed in YBCO [194]. Preliminary SEM work did not suggest the particles produced here were hollow. Agreement between the estimated and measured particle size suggest solid particles, however, the possibility of the particles being hollow cannot be excluded.

Pressing and firing of the powder resulted in bulk superconducting material. In figure 4.17 the resistive transition can be seen, with an onset of 92 K and zero resistance of ~89 K. A room temperature resistivity of ~1.8 mohm cm was observed.

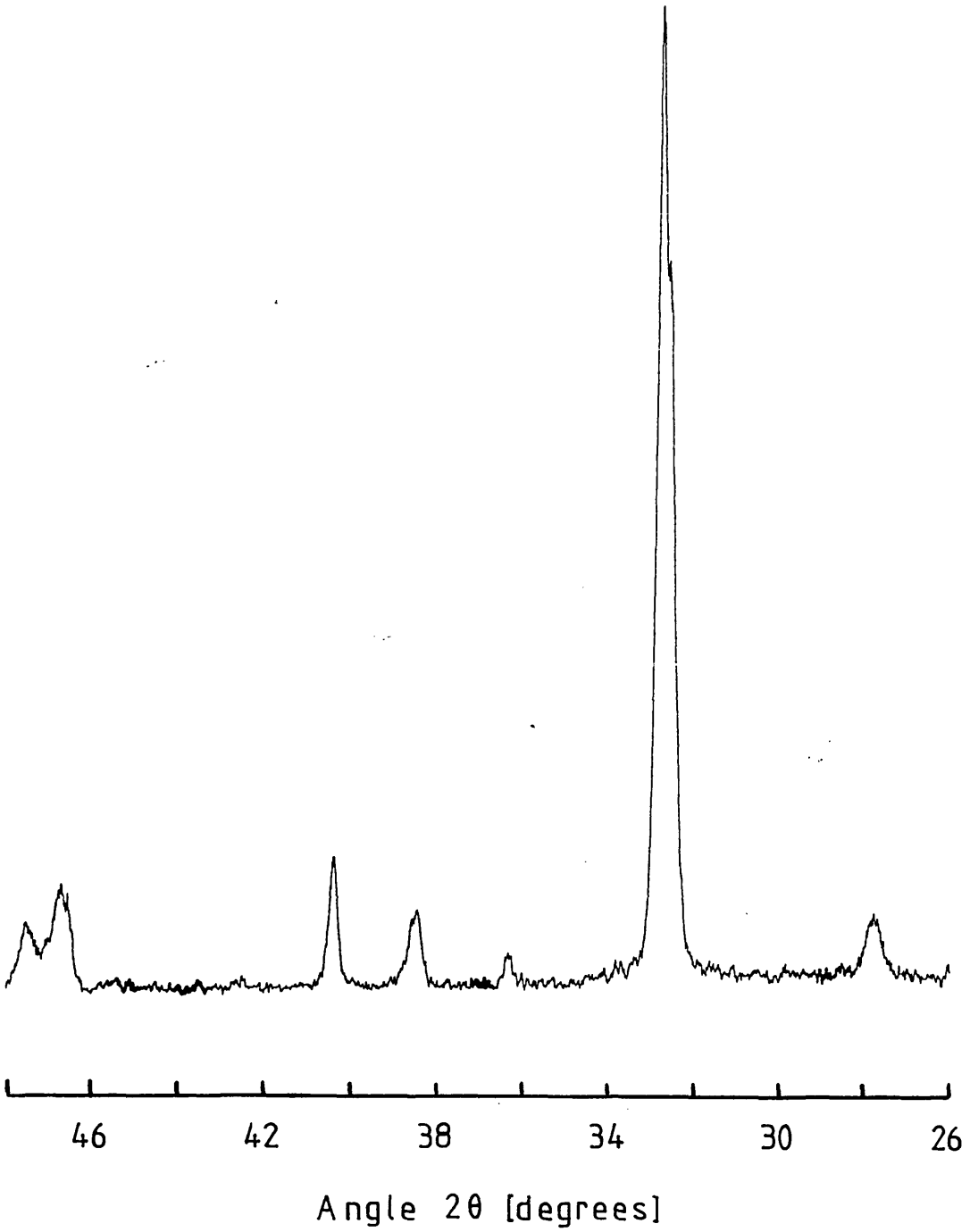

Figure 4.14: X-ray diffraction pattern (Cu_{Ka} radiation) for powder produced from mist pyrolysis.

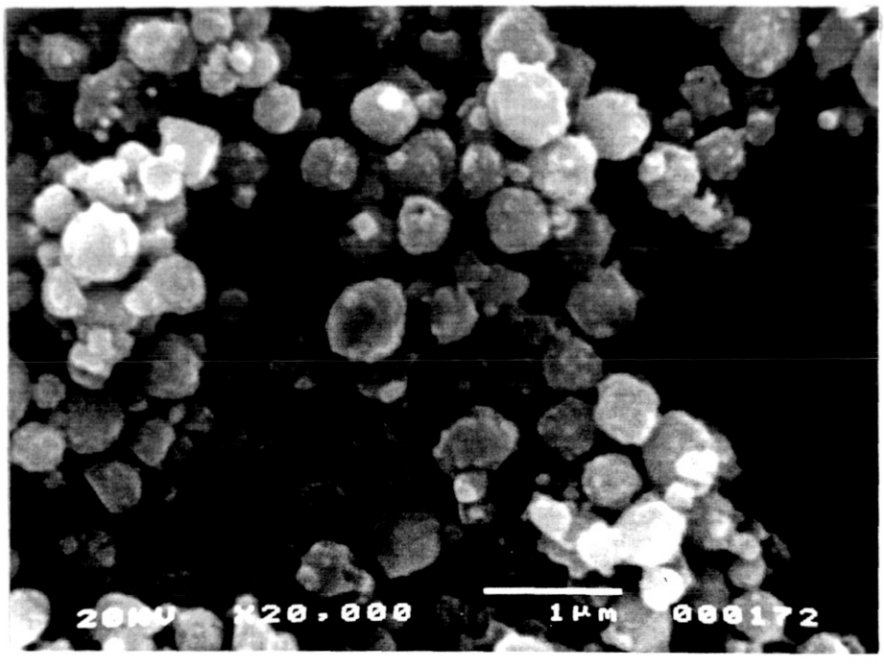

Figure 4.15: Scanning electron micrograph of YBCO powder prepared by mist pyrolysis. Bar= 1 μm.

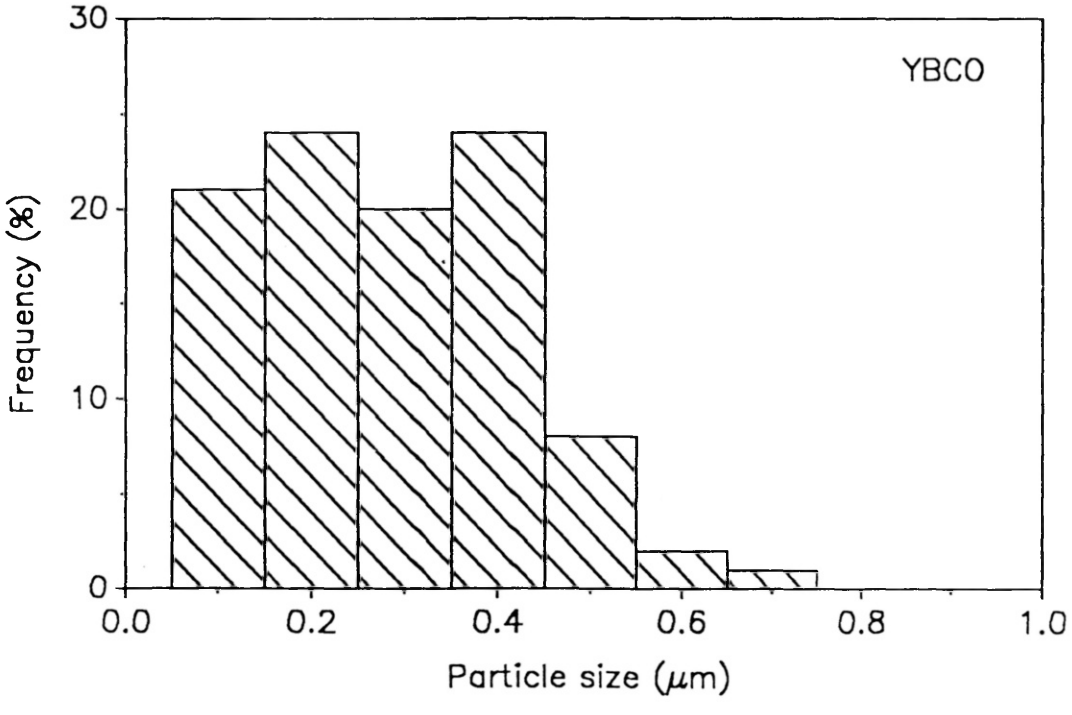

Figure 4.16: Particle size distribution for the powder shown in figure 4.15.

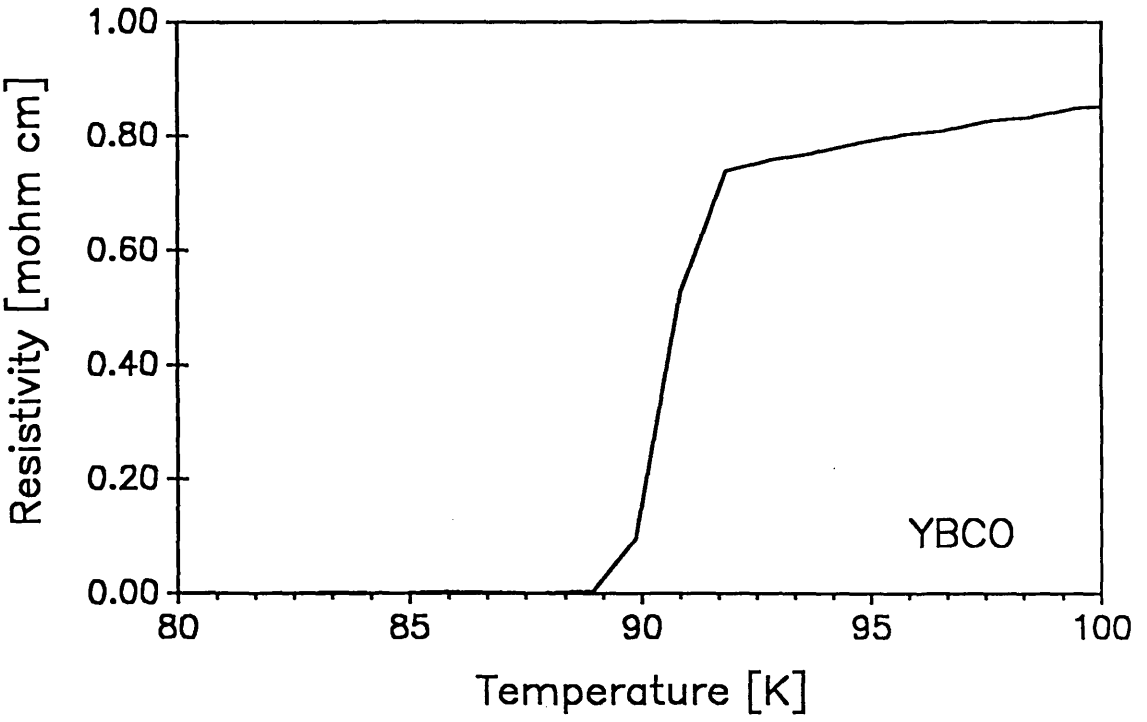

Figure 4.17: The superconductive transition of a bulk sample produced by mist pyrolysis powder.

4.5.4. Discussion

Mist pyrolysis has, therefore, been demonstrated to give single phase, submicron powders which lead to the fabrication of bulk superconducting material, following a simple procedure. Part of the experimental results presented here, will be published [195].

Other reseachers have also produced powders from mist pyrolysis; the particle size, however, is bigger and the distribution is wider, 2 μm [194], 0.5 - 2 μm [196] and "less than 1 μm" [143,197], than the powder presented in this work. Furthermore, even though the powders are claimed to be single phase YBCO, a small amount of CuO can be detected in figure 1 of reference [197].

Mist pyrolysis compares favourably with most of the other methods. Chemical techniques used for powder production such as co-precipitation of oxalates [86,144], sol-gel [145], freeze-drying [142] and hydroxycarbonates [198], further to the basic preparation step (which can be complex and time consuming itself), require calcination and usually light ball milling in order to obtain fine powder. On the other hand, this powder, ready for forming and sintering can be obtained directly from mist pyrolysis.

Scaling up of the apparatus is possible and design optimization for the mist producing ultrasonic equipment, furnace and filtering system could enable commercial development of this fabrication process. For collection of the produced powders electrostatic precipitation filtering is ideal since it is the only method that is efficient for submicron size particles. Both the ultrasonic electrostatic precipitation equipment and technology are commercially available, so that no basic technology has to be developed in order to produce large scale mist pyrolysis units.

4.6. Conclusions

There is a clear advantage of mist pyrolysis as a preparation technique, since very good particle size and distribution of single phase YBCO can be obtained. The simple experimental arrangement and the scaling up possibilities are promising for the application of this technique for high quality powder fabrication.

In comparison, the solid state preparation technique can produce reasonably "single" phase material (with very small amounts of impurities) which can be used for basic studies of the material. The particle size, however, depends on comminution, with problems such as contamination from the grinding media, irregular particle shape and wide size distribution. The best results were obtained using BaO_2 as a precursor for Ba, while using $BaCO_3$ resulted in material of slightly lower quality. Material prepared from $Ba(OH)_2$ was multiphase.

Application of the freeze-drying technique using Y, Ba and Cu nitrates was not successful; however, the problems involved were identified. It is, therefore, possible that adequate choice of materials and apparatus development could lead to successful application of freeze-drying.

Evaporation from nitrates did not lead to reproducible results since multiphase material was often obtained and even in the cases where single phase YBCO resulted, there was no advantage over the solid state preparation or other techniques.

5. RARE EARTH SUBSTITUTION, POTASSIUM DOPING AND O-T TRANSITION

Cation substitution/doping has been used to improve the properties of many modern ceramics. There are two main effects that doping cations can have: an effect on the structure and also on the electronic/ionic behaviour of the material.

In $YBa_2Cu_3O_{7-\delta}$, oxygenation to increase the stoichiometry to 7 is a very important problem, therefore, the rare earth substitution/ potassium doping work presented here had as an objective the investigation of the effect on parameters/properties connected with the behaviour of oxygen, as well as the microstructure of the material.

Initial investigations [163,164] on potassium substitution in the place of barium in YBCO, indicated a possible increase of the orthorhombic-to-tetragonal (O-T) transition temperature. In order to extent the limited information obtained from the literature, other rare earth ions (Er, Nd, Gd) were also used instead of Y.

The possible extent of K substitution without deterioration of the properties of the material (since only a partial substitution is expected for K with a valence of 1+, compared to Ba 2+) was investigated. The effect on the O-T transition was examined quantitatively by XRD, measuring the cell parameters after quenching from different temperatures as well as examining the material *in-situ* at high temperatures by neutron diffraction.

The elements Er, Y, Gd, Nd were selected so that they cover almost the whole range of ionic radii (Er=1.004 .. Nd=1.109 Å) of the rare earth cations which can substitute for Y in the 123. The prepared samples were examined by X-ray diffraction (phase identification/ cell parameters), low temperature resistivity measurements and also by neutron diffraction, atomic absorption, thermal analysis, scanning electron microscopy and energy dispersive X-ray analysis. The amount of doping will be referred to, either as x in the formula $REBa_{2-x}K_xCu_3O_{7-\delta}$ or as a percentage of barium atom substitution.

5.1. $ErBa_{2-x}K_xCu_3O_{7-\delta}$

Erbium samples with 0, 2.5, 5 and 10% K-doping (x= 0, 0.05, 0.1, 0.2) were prepared. Even though single phase 123 material was obtained for 2.5% doping, higher K contents had as a result the formation of the 211 phase (Er_2BaCuO_5), possibly along with another, potassium-containing, phase which was not identified. In figure 5.1 X-ray diffraction data are presented for the different doping levels. Peaks which do not belong to the 123 phase are shown hatched. It can be observed that for 5 and 10% K, the 123 phase has disappeared. Multiple attempts to prepare samples of these compositions always gave the same results.

The T_c is not significantly affected with 2.5% doping as is shown in figure 5.2 and the material remains a 90K superconductor. No attempt for low temperature resistance measurements of the 5 and 10% K doped materials was made since the 211 was the majority phase. A series of Ba deficient (non K-doped) samples, however, was prepared, with 5 and 10% Ba-deficiency ($ErBa_{2-x}Cu_3O_{7-\delta}$, x=0.1, 0.2). Both samples had 123 as the majority phase with a small amount of secondary phases as concluded from XRD, having a T_c(R=0) of 90-91 K, indicating that K-doping had a deleterious result as far as the Er-123 phase formation was concerned.

From cell parameter data listed in table 5.1, it can be seen that the a and b parameters do not change significantly for 2.5% doping but there is some decrease in the c parameter. The number in parenthesis is the accuracy of the last digit of each number.

Er has an atomic radius of 1.004 Å, the closest to Y (1.019 Å) compared to the other cations used in this study. However, unlike in the yttrium 123, it seems that potassium cannot substitute more than 2.5% the Ba in this structure, forming other compounds instead.

Fabrication of the Er-123 potassium doped samples was performed by X. Turrillas.

Table 5.1

Cell Parameters (Å) for $ErBa_{2-x}K_xCu_3O_{7-\delta}$

x	a	b	c
0.00	3.814(2)	3.8861(3)	11.6637(1)
0.05	3.818(2)	3.8840(3)	11.6519(1)

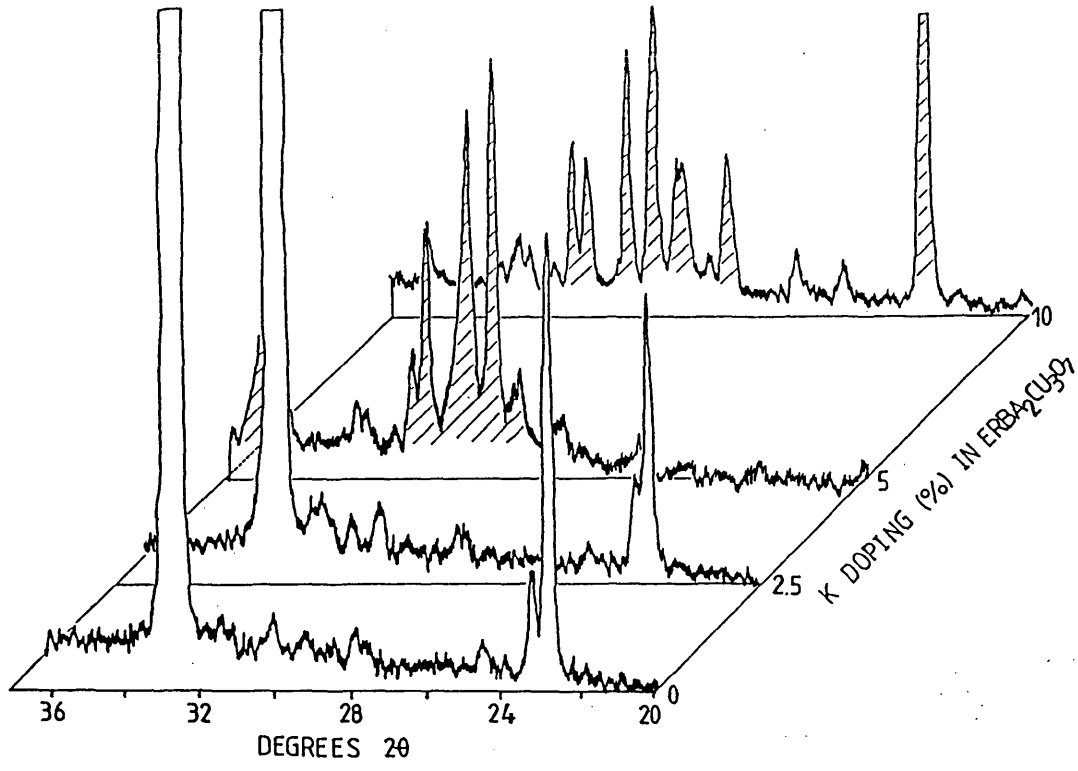

Figure 5.1: X-Ray diffraction patterns (Cu Kα radiation) for $ErBa_{2-x}K_xCu_3O_{7-\delta}$. For 0 and 2.5% substitution (x=0, 0.05), the 123 phase is formed while for 5 and 10% (x=0.1, 0.2), the 211 phase results.

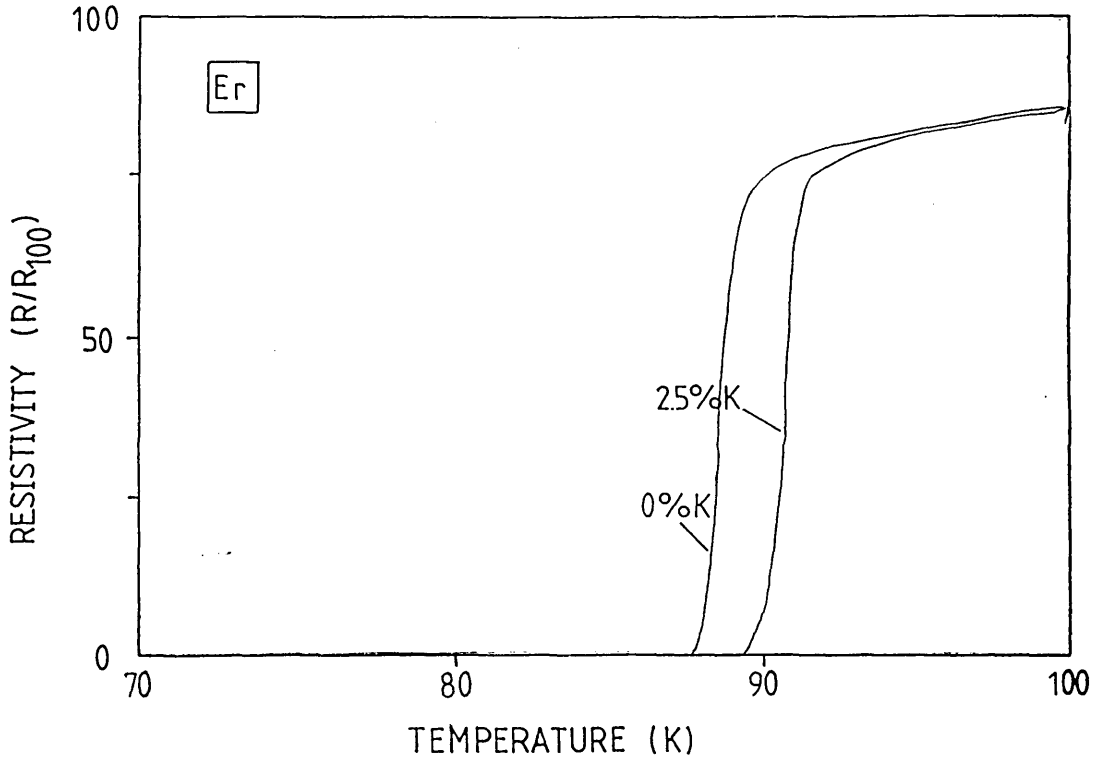

Figure 5.2: Normalised resistivity versus temperature for $ErBa_{2-x}K_xCu_3O_{7-\delta}$, x=0 and 0.5.

5.2. $YBa_{2-x}K_xCu_3O_{7-\delta}$

For $YBa_{2-x}K_xCu_3O_{7-\delta}$ samples with 0, 5, 7.5, 10, 15, 20 and 25% K-doping (or x=0, 0.1, 0.15, 0.2, 0.3, 0.4 and 0.5) have been prepared. Up to 25% the 123 phase was obtained with minor impurities, provided that the proper sintering conditions were followed. In figure 5.3 the X-ray diffraction plots are presented for different degrees of doping and it can be seen that even though the level of impurities (hatched areas) increases with the doping level, it is generally quite low.

There is no effect of doping on T_c up to 15% K as can be seen in figure 5.4. This is an important finding since for most ions that partially substitute either of the constituent cations of 123, a drop of T_c is usually found.

The cell parameters of material fully loaded with oxygen can be seen in table 5.2 and it is evident that the values do not change up to 15% K doping. A further experiment, therefore, was performed, fabricating a Ba-deficient sample $YBa_{1.6}Cu_3O_7$, identical to a 20% K doped sample, but without potassium. In figure 5.5 it can be seen that in the case of the Ba-deficient sample, the impurity level is slightly larger than for the 20% K doped 123 which even though might indicate a partial K substitution, offers no conclusive evidence.

Sample density was found to decrease with K-doping when the optimum conditions for phase formation were employed, in accordance with Moure et al. [166], despite claims by Chen et al. [163] that potassium acted as a densification aid. In figure 5.6 there is a definite trend for lower densities with increased K content. In this figure, the highest densities obtained from each series of samples are given (all samples prepared by solid state processing).

The microstructure was affected and depending on the sintering conditions, different effects could be seen. In figure 5.7 the surface morphology of a 10% K-doped sample fired at 950 C for 18 hours (slow heating and cooling rates) is presented. Grains were estimated to have dimensions of 15-25 x 3-8 μm which are larger than the typical YBCO grains (such as in figure 4.4 with dimensions of approximately 10 x 2-3 μm). In this particular case, therefore, a grain size enhancement was obtained.

If the firing temperature is increased to 970 C, a significant amount of CuO is formed. In figure 5.8 the microstructure of a sample treated at this temperature for 10 hours can be seen in a backscattered electrons

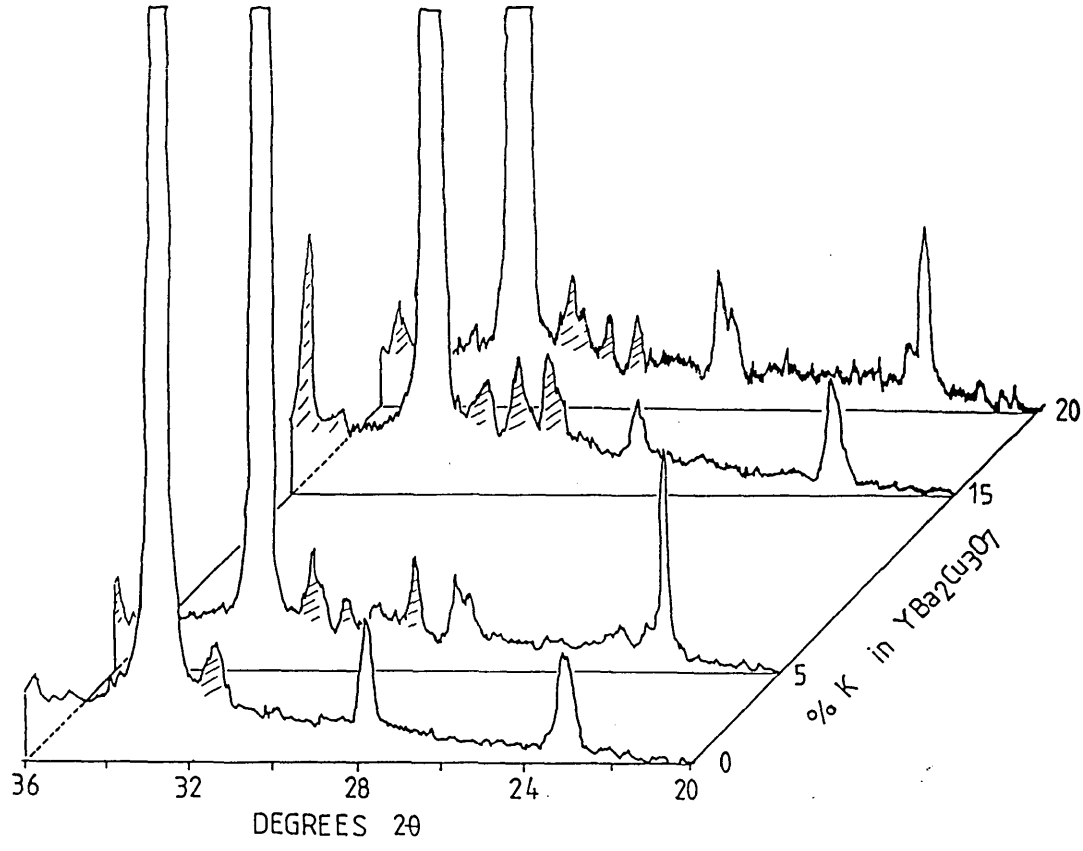

Figure 5.3: X-Ray diffraction patterns (CuKα) for $YBa_{2-x}K_xCu_3O_{7-\delta}$ for x=0, 0.1, 0.3 and 0.4 (0, 5, 15 and 20% K doping).

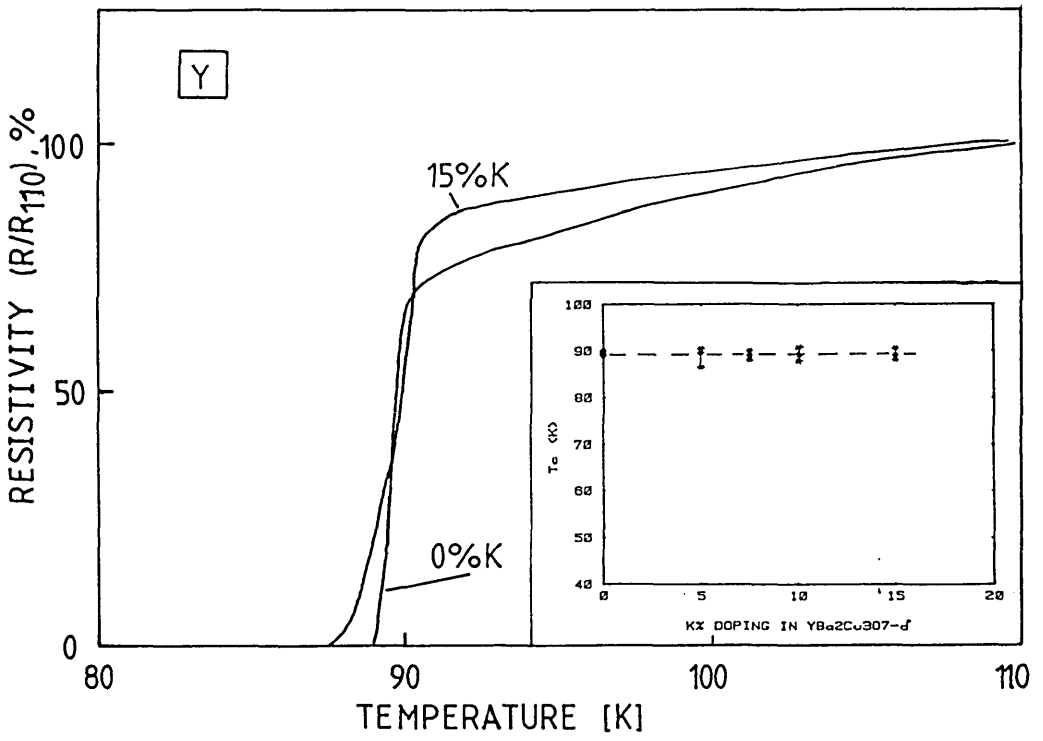

Figure 5.4: Normalized resistivity versus temperature for $YBa_{2-x}K_xCu_3O_{7-\delta}$, x=0, 0.3 (0, 15% K doping). Inset: Tc versus K doping (%). Tc does not drop with doping up to 15%. Bars represent onset,midpoint and zero resistivity.

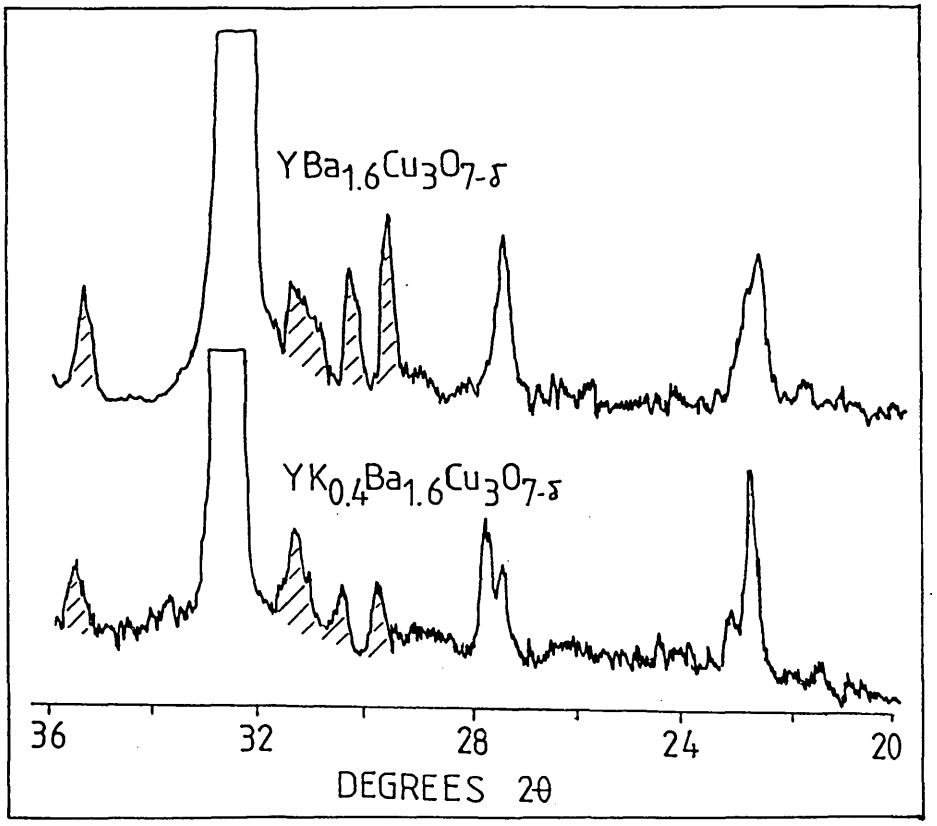

Figure 5.5: Comparison between the XRD traces of a 20% K-doped and a Ba deficient (same cation ratio but without potassium) sample.

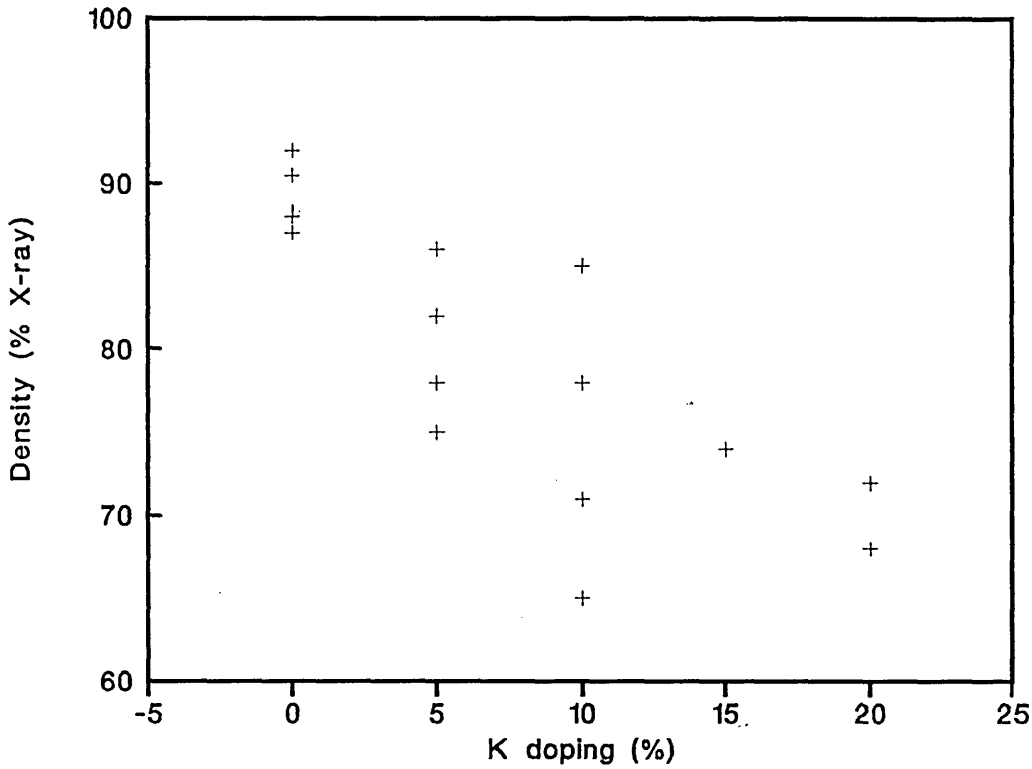

Figure 5.6: Sample densities versus K–doping (%) for $YBa_{2-x}K_xCu_3O_{7-\delta}$.

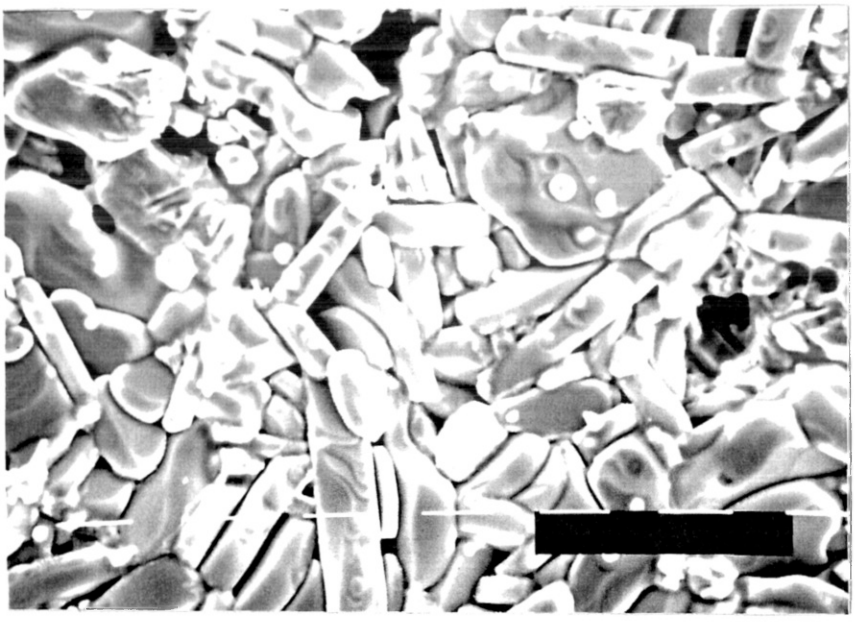

Figure 5.7: Scanning electron micrograph of enhanced grain size in $YBa_{1.8}K_{0.2}Cu_3O_{7-\delta}$ (10% K-doped) fired at 950 C. Bar= 10μm.

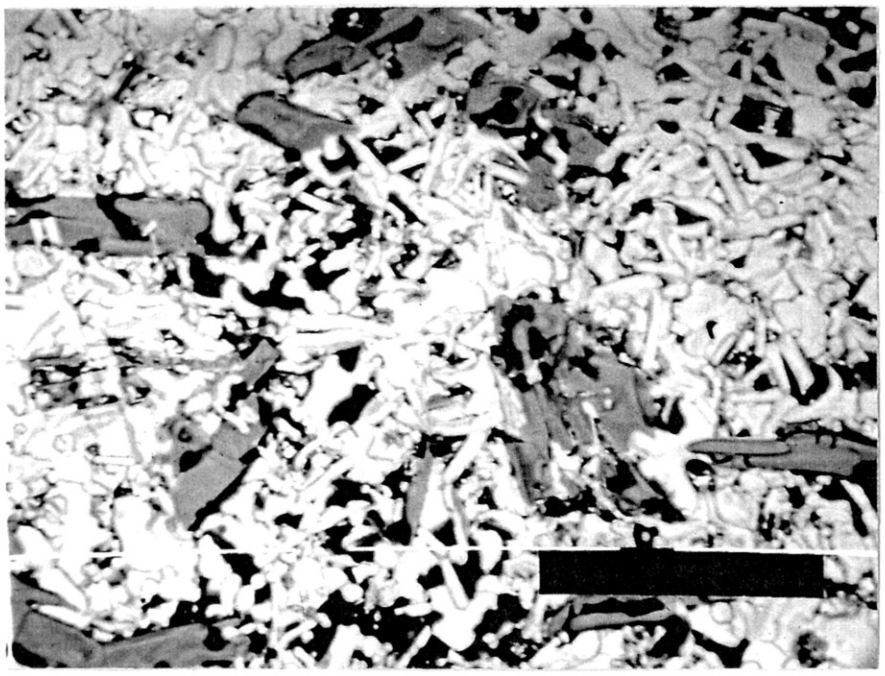

Figure 5.8: Backscattered electron micrograph of a $YBa_{1.8}K_{0.2}Cu_3O_{7-\delta}$ sample fired at 970 C. Dark areas are CuO. Bar= 100 μm.

micrograph. The large, darker grains (CuO according to EDAX) are randomly distributed among the YBCO phase grains (white in the micrograph), occasionally filling spaces between them, as observed in other micrographs.

A eutectic mixture rich in K and Cu was formed, but it had a negative effect since it appeared as a liquid phase wetting the crucible when heating at temperatures near 950 C. As a result, the rest of the material became non stoichiometric and second phases observed by SEM and X-ray diffraction, appeared. In order to avoid the formation of this phase the sintering temperature had to be lowered depending on the amount of doping. For the maximum doping, 20%K (x=0.4), the optimum temperature was found to be 920 C.

Table 5.2

Cell Parameters (Å) for $YBa_{2-x}K_xCu_3O_{7-\delta}$

x	a	b	c
0.00	3.826(2)	3.8922(4)	11.6767(1)
0.10	3.826(1)	3.8944(2)	11.6833(1)
0.15	3.819(2)	3.9839(4)	11.6818(2)
0.20	3.824(1)	3.8930(3)	11.6790(1)
0.30	3.820(1)	3.8915(3)	11.6754(1)

5.3. $GdBa_{2-x}K_xCu_3O_{7-\delta}$

Samples of $GdBa_{2-x}K_xCu_3O_{7-\delta}$ with compositions of x=0, 0.1, 0.2 and 0.3 were prepared by the solid state method, using two grinding/sintering cycles. A sintering temperature of 940-960 C in air for times ranging from 4-15 hours was found to be sufficient for the formation of the 123 phase. A further annealing step at 400 C in oxygen was employed, as for all 123 samples, in order to increase the oxygen stoichiometry and improve the superconductive properties.

Potassium doping up to 5% seems to have no effect on the phase formation and 123 remains the only phase. However, a small amount of second phases appears at 10% doping which becomes even more for 15% doping. The X-ray diffraction data presented in figure 5.9, suggest,

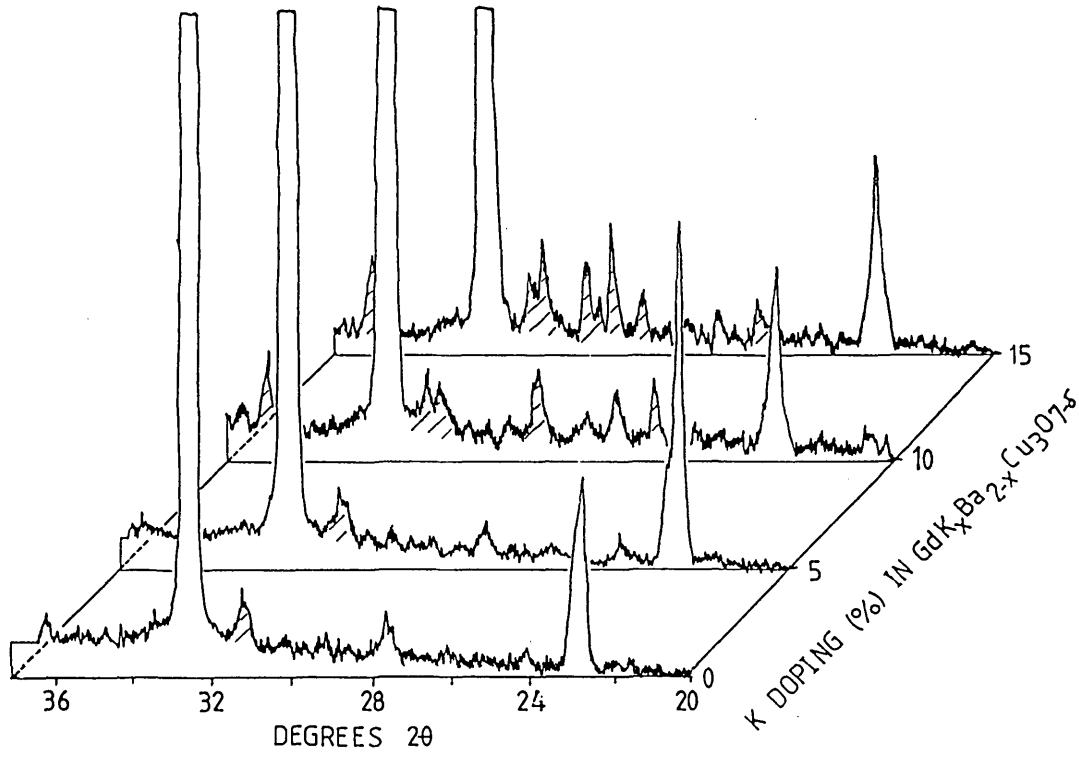

Figure 5.9: X-Ray diffraction patterns (CuKα) for $GdBa_{2-x}K_xCu_3O_{7-\delta}$, for x= 0, 0.1, 0.2 and 0.3 (0, 5, 10 and 15% K)

therefore, that 5% potassium substitution for Ba is possible.

The resistivity versus temperature results shown in figure 5.10, are in accordance with XRD data, since there is no effect on T_c by a 5% doping level. In the case of 10 and 15% doping the T_c is lowered to or below 60K, in comparison with a T_c of approximately 90 K obtained for 0 and 5% doping. It is worth mentioning, however, that all samples display a metallic behaviour from room temperature to 100 K.

Cell parameters decrease slightly with increasing K content as shown in table 5.3. The effect of K-doping to the density and sinterability of the samples is similar to that of Y-123. No accuracy estimation was possible due to software problems, allowing only the refinement of three out of the four available peaks.

Examination of a sample of stoichiometry $GdBa_{1.8}Cu_3O_{7-\delta}$ showed that no second phases could be detected by X-ray diffraction. The transition temperature $T_c(R=0)$ is 70 K compared to 60 K for the K-doped sample. This indicates that even though T_c drops considerably due to Ba deficiency, addition of potassium results in a further deterioration of the properties of the material. Comparison of the Ba-deficient Gd-123 with Er- and Y-123 shows that the Gd-based material is more sensitive to non-stoichiometry than the other compounds.

Fabrication of the K-doped samples was performed by K. Ley, as part of his final year research project.

Table 5.3

Cell Parameters (Å) for $GdBa_{2-x}K_xCu_3O_{7-\delta}$

x	a	b	c
0.00	3.847	3.904	11.711
0.10	3.844	3.898	11.691
0.20	3.840	3.897	11.695

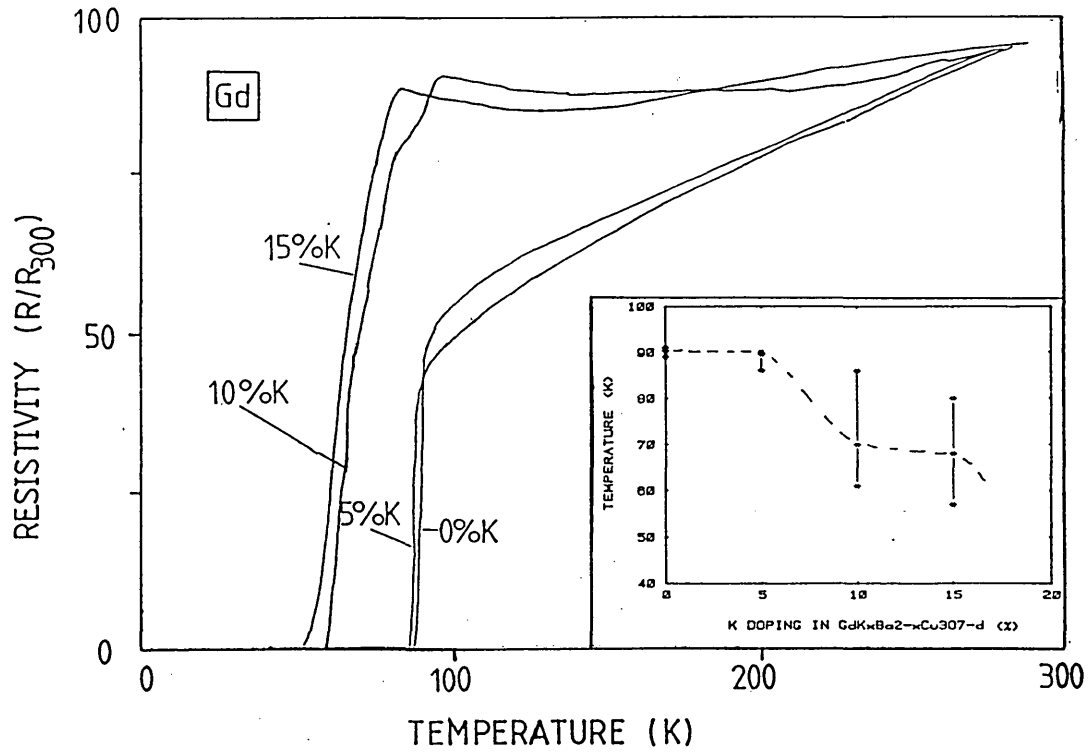

Figure 5.10: Normalised resistivity versus temperature for K-doped Gd samples. x=0, 0.1, 0.2 and 0.3 for $GdBa_{2-x}K_xCu_3O_{7-\delta}$. Inset: Tc versus K doping.

5.4. $NdBa_{2-x}K_xCu_3O_{7-\delta}$

The compositions prepared for $NdBa_{2-x}K_xCu3O_{7-\delta}$ where x=0, 0.1, 0.15 and 0.2 (i.e. 0, 5, 7.5 and 10% K-doping). The optimum firing temperature was found with the help of X-ray diffraction for each composition before examining the superconductive properties of the samples. Diffractograms from 20 to 36 degrees 2θ versus firing temperature are presented in figure 5.11a,b for 0 and 5% K-doped material and in figure 5.12a,b for 7.5 and 10% doping respectively. The peaks shown hatched belong to other phases such as $BaCuO_2$, $NdBa_3Cu_2O_x$ (Nd-132) or Nd_2BaCuO_5 (Nd-211).

The Nd-123 phase (undoped) is found to be most stable at 950 C as can be seen in figure 5.11a. Firing at lower temperatures results in the formation of Nd-132 along with 123, while at higher temperatures $BaCuO_2$ is formed. K-doping of 5% appears, from figure 5.11b, to stabilise the 123 phase over the range 890 to 980 C, since minor impurity peaks are detected. In the case of 7.5% K-doping, two effects can be observed from figure 5.12a. First, that even for temperatures as low as 800 C, the Nd-123 is the majority phase and second, that the optimum formation temperature for this compound is 920. It seems, therefore, that K-doping favours the formation of the Nd-123 phase, while at the same time, lowering the firing temperature by 30 degrees. Increasing the potassium content at 10% has as a result the appearance of considerable amount of second phases, indicating that K does not take the place of Ba at this doping level (figure 5.12b). The optimum XRD results for each doping level are summarized in figure 5.13, where it can be seen that a very small amount of impurities can be detected up to 7.5% K-doping, which increase considerably at 10% K.

T_c measurements in figure 5.14 for materials with different amounts of doping show a considerable decrease of the critical temperature for the potassium doped samples. Examination of a similarly prepared sample with a stoichiometry of $NdBa_{1.9}Cu_3O_{7-\delta}$ resulted in a $T_c(R=0)$ of 82K. Therefore, potassium doping in the 5% K-doped compound results in lowering of the T_c despite positive effects on the phase formation observed by XRD.

Cell parameters decrease slightly for 5% doping (x=0.1) but there is no effect for 7.5% K-doping (table 5.4) which indicates that K substitution can only occur at smaller doping levels.

Table 5.4

Cell Parameters (Å) for $NdBa_{2-x}K_xCu_3O_{7-\delta}$

x	a	b	c
0.00	3.877(2)	3.9252(4)	11.7757(1)
0.10	3.868(2)	3.9164(4)	11.7492(1)
0.15	3.868(1)	3.9157(3)	11.7471(1)

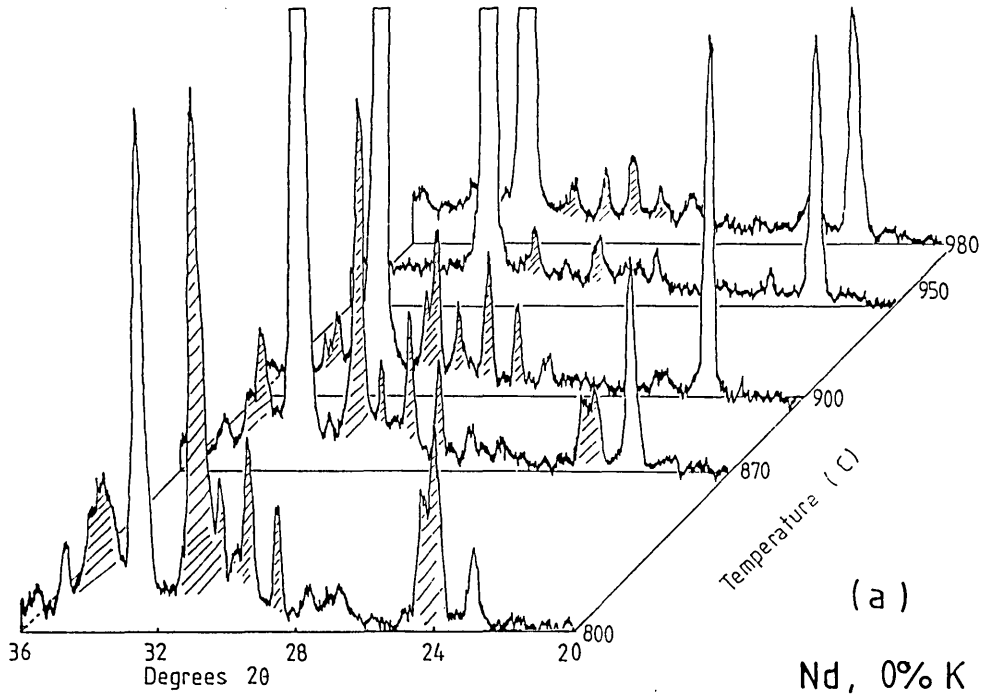

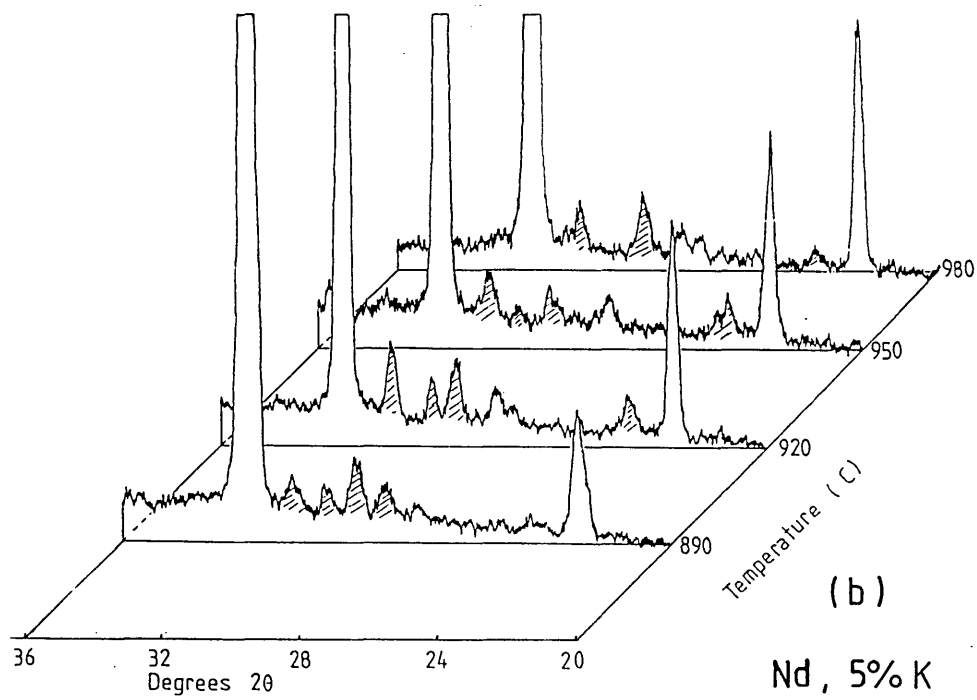

Figure 5.11: X-Ray diffraction patterns (Cu Kα radiation) at different temperatures for $NdBa_{2-x}K_xCu_3O_{7-\delta}$.(a) x=0, (b) x=0.1 (0 and 5% K doping respectively).

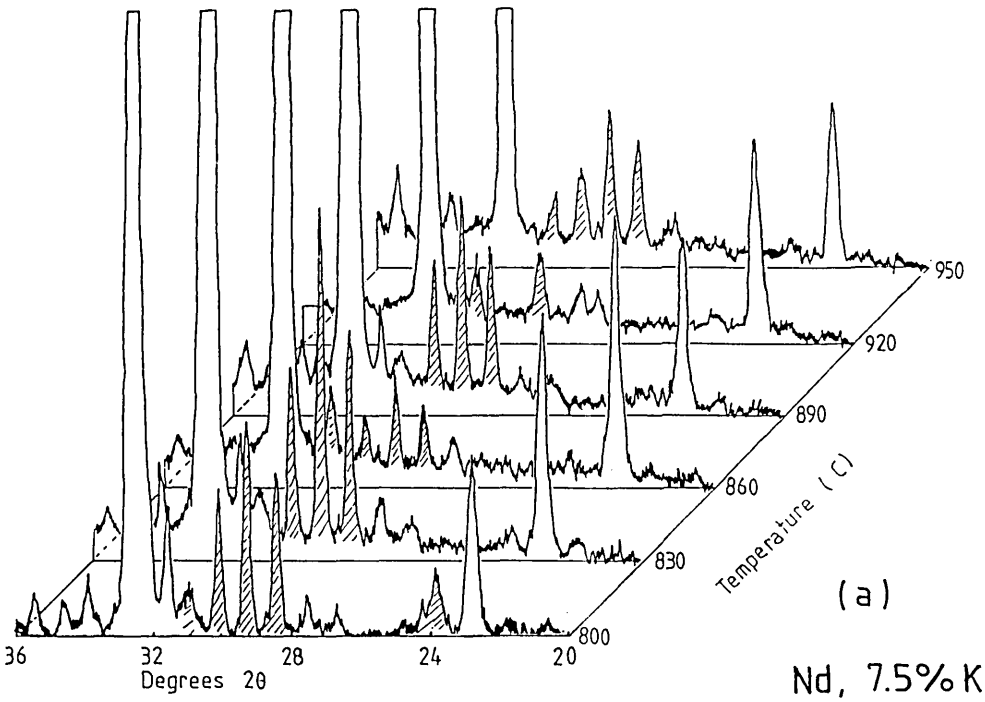

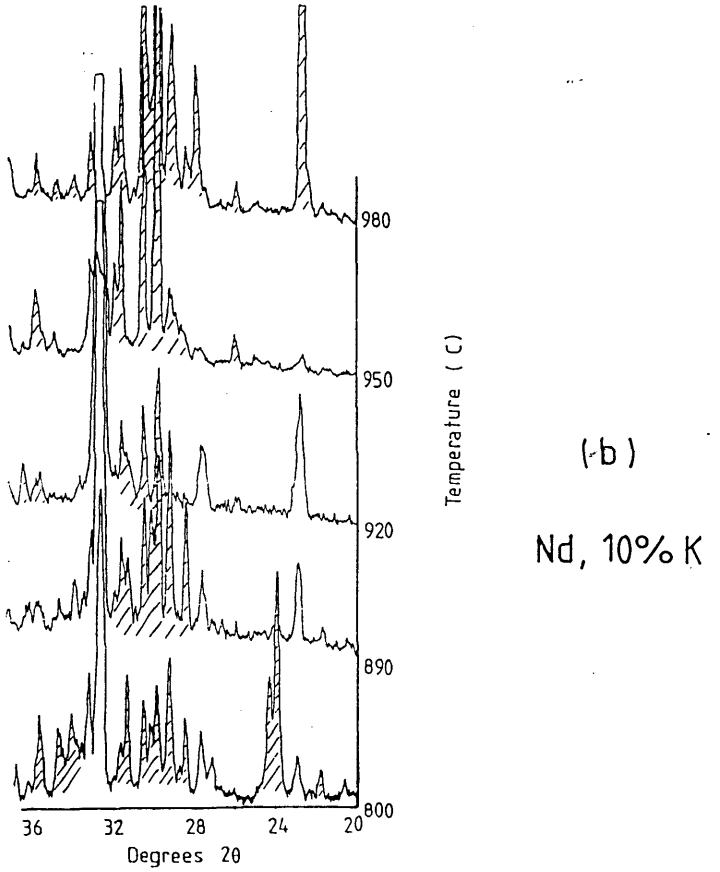

Figure 5.12: X-Ray diffraction patterns (Cu Kα radiation) at different temperatures for $NdBa_{2-x}K_xCu_3O_{7-\delta}$.(a) x=0.15, (b) x=0.2 (7.5 and 10% K doping respectively).

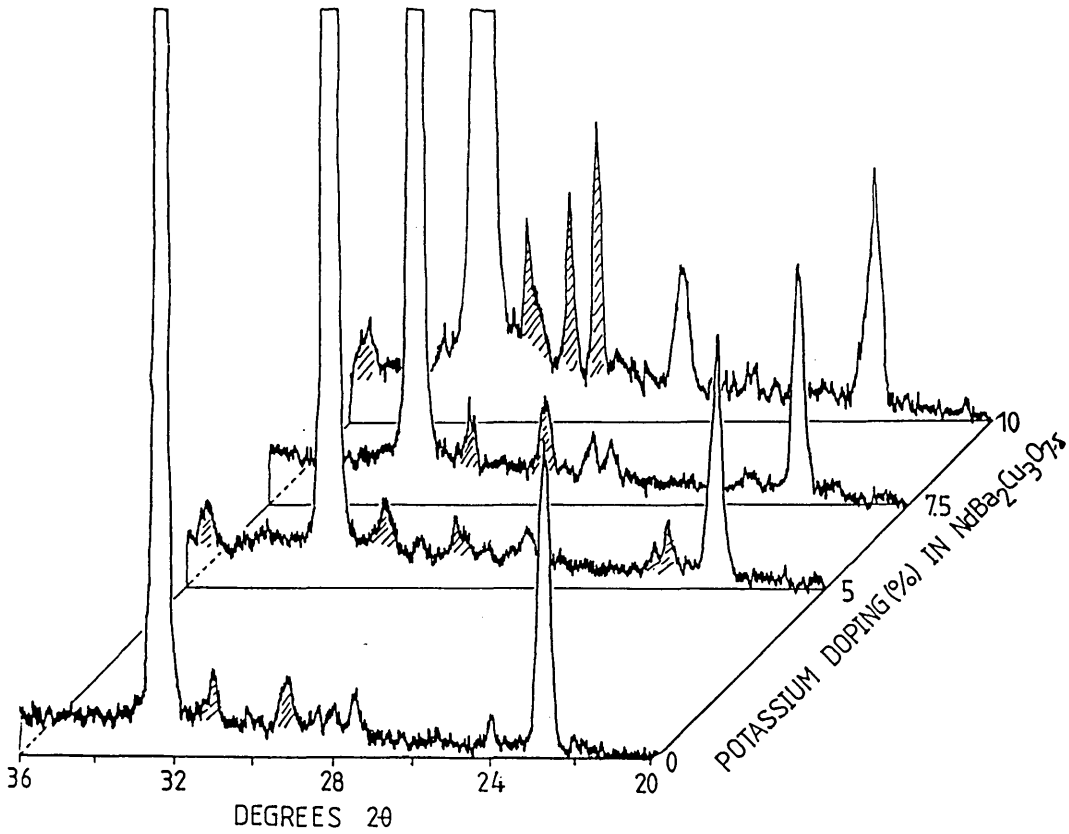

Figure 5.13: X-Ray diffraction patterns (Cu Kα radiation) for $NdBa_{2-x}K_xCu_3O_{7-\delta}$ x=0, 0.1, 0.15 and 0.2 (0, 5, 7.5 and 10% K doping respectively), after firing temperature optimization.

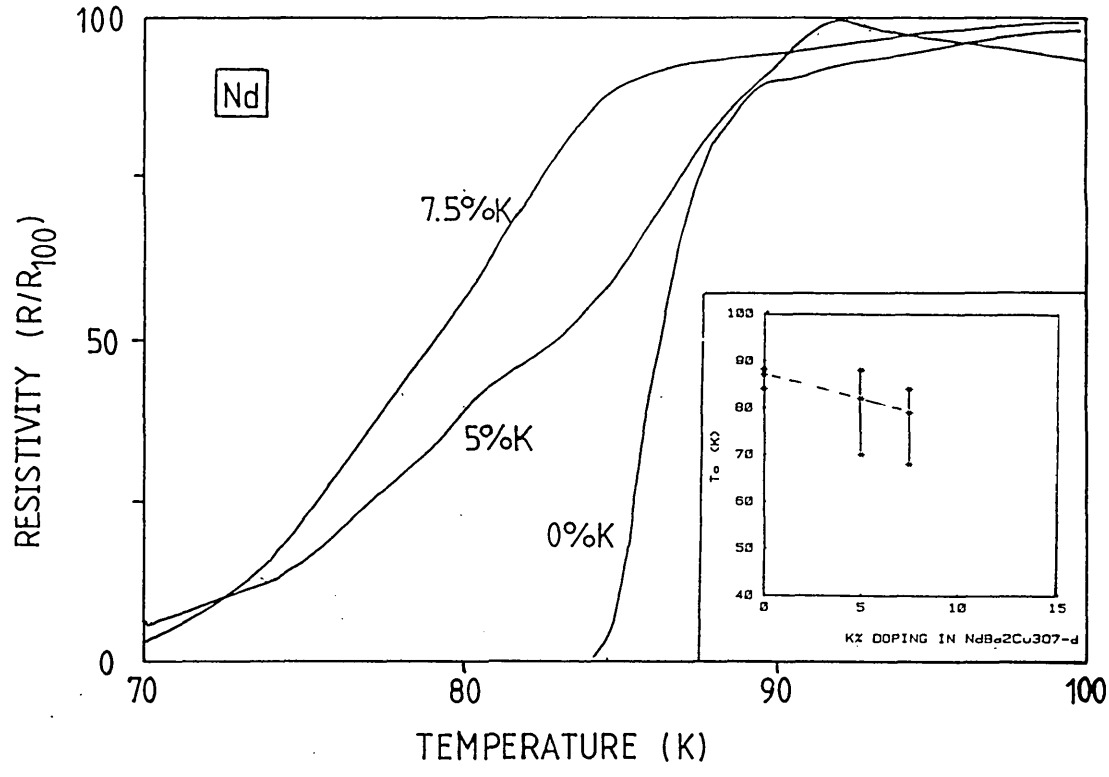

Figure 5.14: Normalised resistivity versus temperature data for $NdBa_{2-x}K_xCu_3O_{7-\delta}$, showing the effect of potassium doping. x=0, 0.1 and 0.15.

5.5. The Role of Potassium

Potassium substitution in $YBa_2Cu_3O_{7-\delta}$ was found not to affect T_c up to 15% doping. According to the literature, in most cases this result is confirmed [163–166], even though a small decrease in T_c is claimed by Saito et al. [167]. There is no information available for Er, Gd and Nd potassium doping.

Comparing the results for the Er, Y, Gd and Nd–123, one would expect them to relate with the ionic radius of the rare earth (R.E.) cations.

Considering Ba and O atoms as spheres touching one another on the Ba–O1 plane, the available space for Ba was calculated using the cell parameters given by Tarascon et al. [153] for $R.E.Ba_2Cu_3O_7$ and the effective ionic radii calculated by Shannon [159]. The coordination number of Ba is 10 and for O1 (Ba–O plane) is 6 and so the corresponding ionic radii are 1.52 and 1.4 Å respectively. In table 5.5, calculated values for the R.E. superconductors used in this study are shown.

Table 5.5: Comparison between the available space for Ba/K and the ionic radii of Ba and K ions (distances in Angstroms).

Cation	Radius	O1–O1 distance	Avail.radius	Eff.ion.radii
Er	1.004	5.449	1.32	Ba^{2+}_{X}= 1.52
Y	1.019	5.453	1.33	
Gd	1.053	5.472	1.34	K^{1+}_{X}= 1.59
Nd	1.109	5.494	1.35	

There is a considerable disagreement between the calculated available "space" for Ba and its ionic size according to Shannon [159]. This could be attributed to the fact that the calculated effective ionic radii are slightly different for different materials and bonds. Especially in the case of 123, bonds like the Cu–O ones are far from the ideal ionic model of Cu^{2+}–O^{2-} causing O1 and Ba radii to vary.

The conclusion that can be drawn qualitatively from this table is that since K^+ has a bigger ionic radius than Ba^{2+}, it would be expected to

have an increasing solubility with increasing R.E. cation size. The experimental results (phase relations, T_c), however, show a behaviour that does not appear to have a correlation with ionic radii.

The cell volume for the K-doped compounds is shown in figure 5.15. A small decrease for Nd and Gd-123 cell volume is a possible indication that initially some potassium enters the structure, but further doping is not accepted and second phases start to appear instead. For Y and Er compounds, however, there is no effect on the cell volume, which indicates a possibility of K not entering their structure.

An examination of potassium content was therefore necessary, since in most samples no K could be detected by EDAX. In table 5.6 atomic absorption results are presented for K-doped samples. Even though there is a large variation of the results, it is obvious that a significant amount of potassium evaporates (due to its high vapour pressure) during sintering. As a result, it is clear that the actual potassium content can vary from 1 to 52% of the starting composition and therefore, doping levels referred to in this chapter are nominal.

Examination of the Y-123 potassium stoichiometry indicates a general trend for lower content when higher annealing temperatures or longer annealing times are used. An attempt to examine the influence of different K-precursors ($KC_8O_4H_5$ or K_2CO_3) initially indicated that K_2CO_3 had as a result increased K-content, however, the results overall are inconclusive. *

Table 5.6: Potassium content in $R.E.Ba_{2-x}K_xCu_3O_{7-\delta}$

R.E.	x nominal	x Atom.Abs.	Temp(C)	Time(h)	Precurs.
Er	0.05	0.005 ± 0.002	950	18	$KC_8O_4H_5$
Y	0.2	0.135 ± 0.002	900	5	K_2CO_3
Y	0.2	0.009 ± 0.001	940	17	K_2CO_3
Y	0.2	0.112 ± 0.002	950	7	K_2CO_3
Y	0.2	0.086 ± 0.003	950	7	$KC_8O_4H_5$
Y	0.2	0.058 ± 0.002	950	46	$KC_8O_4H_5$
Gd	0.2	0.002 ± 0.001	960	10	$KC_8O_4H_5$
Nd	0.1	0.008 ± 0.001	980	5	$KC_8O_4H_5$

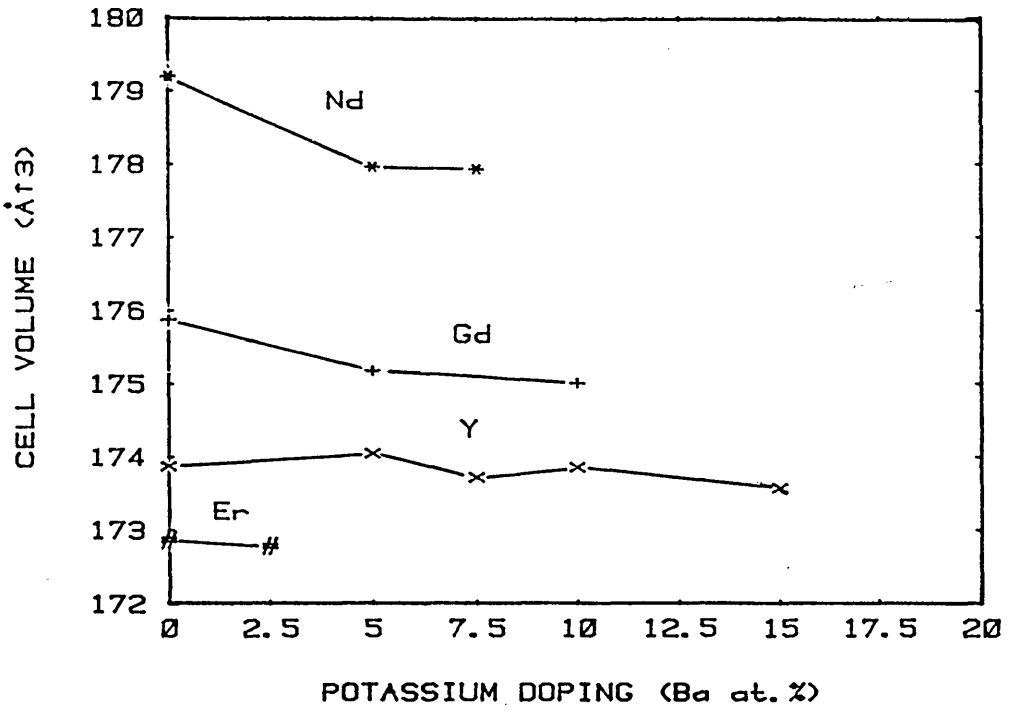

Figure 5.15: Cell volume versus K–doping (%) for $REBa_{2-x}K_xCu_3O_{7-\delta}$, (RE= Nd, Gd, Y, Er).

Thermogravimetric analysis (TGA) was used in order to examine the oxygen content of the samples. Heating in a reducing environment up to 900 C, the material loses oxygen and eventually decomposes to rare earth oxide and barium oxides, while copper and potassium are reduced to their metallic state. The oxygen content at that temperature is therefore known and the initial stoichiometry can be calculated using the weight loss found from TGA.

In table 5.7 the oxygen stoichiometry is listed for Y, Gd and Nd–123 superconductors, previously annealed at 400 C. It can be seen that the calculated oxygen content for K–doped samples is lower than the non–doped ones, apart from the Nd K–doped 123. In view of the previous results (Atomic Absorption), indicating that potassium evaporates during high temperature treatment and also that different amounts of potassium can remain in the samples, the value of 7.65 for oxygen stoichiometry of Nd K–doped 123 sample can be explained. If an amount of potassium in the sample evaporated during TGA, the weight loss would be interpreted as if it was due to oxygen, resulting in higher than expected calculated values for oxygen stoichiometry.

Table 5.7: Oxygen content in R.E.$Ba_{2-x}K_xCu_3O_y$

Formula	Weight% at 900 C	Oxygen content (y)
$YBa_2Cu_3O_y$	92.20	6.73
$YK_{0.1}Ba_{1.9}Cu_3O_y$	91.98	6.66
$NdK_{0.1}Ba_{1.9}Cu_3O_y$	90.58	7.65
$GdBa_2Cu_3O_y$	92.22	7.08
$GdK_{0.2}Ba_{1.8}Cu_3O_y$	91.78	6.96

Even though, therefore, small amounts of potassium remain in the doped materials, the T_c can be affected as in the case of Nd and Gd–123. In the case of Er–123, addition of K has as a result the formation of other phases, while no effect on T_c or the structure was detected for Y–123 (only the microstructure was affected).

5.6. O-T Transition Temperature by XRD on K-doped YBCO

The results of K-doping in $REBa_2Cu_3O_{7-\delta}$ superconductors (RE= Er, Y, Gd, Nd) showed that the Y-123 superconductors are the most promising since T_c was not affected even with 15% K at. substitution. For this reason $YK_xBa_{2-x}Cu_3O_{7-\delta}$ material was quenched from different temperatures and the cell parameters were measured to monitor the O-T transition. Some of the results presented here, have been reported in [199,200].

The compositions x=0.1, 0.2, 0.4 (5,10 and 20%K doping respectively) were examined. The samples were fired at the required temperature for at least 30 minutes (longer for temperatures lower than 550-600 C) in air and quenched in liquid nitrogen in a metallic container. The X-ray diffractometer was operated in a step scan mode, scanning from 40 to 48 degrees 2θ ($Cu_{K\alpha}$ radiation). The position of the (113), (006), (020) and (200) peaks of YBCO, as well as the (420) peak of BGO (internal standard), were determined. Using these values, the cell parameters of YBCO were found.

In figure 5.16 the variation of a, b and c/3 cell parameters is presented versus temperature for 5, 10 and 20% K doping. The accuracy found was of similar order of the one presented in the tables 5.1, 5.2, 5.4 and therefore too small to be recorded on this graph.

The O-T transition temperature increased from 700 C for 5% doping to 800 C for 10%, while there was only an increase to 825 C for 20% doping. Potassium, therefore, affects the behaviour of the material and the structure remains orthorhombic at higher temperatures.

This is in agreement with initial results of Chen et al. [163] and Tallon et al. [164] reporting an effect on the orthorhombic-to-tetragonal transition temperature by K-doping. Another effect of K-doping, an increased speed in oxygen uptake at the final low temperature O_2-annealing stage, was observed by Moure et al [166], indicating that oxygen dependent properties are affected.

Minimization of microcracking due to the higher temperature of O-T transition for K-doped samples was initially proposed as one of the possible advantages since the change of the thermal expansion coefficient of the tetragonal to the orthorhombic phase (from 20 to $25x10^{-6}K^{-1}$ [94,110]) would happen at higher temperatures, at which some of the alleviation of stresses could possibly occur by plastic deformation rather than microcracking. However, the anisotropy of the thermal expansion

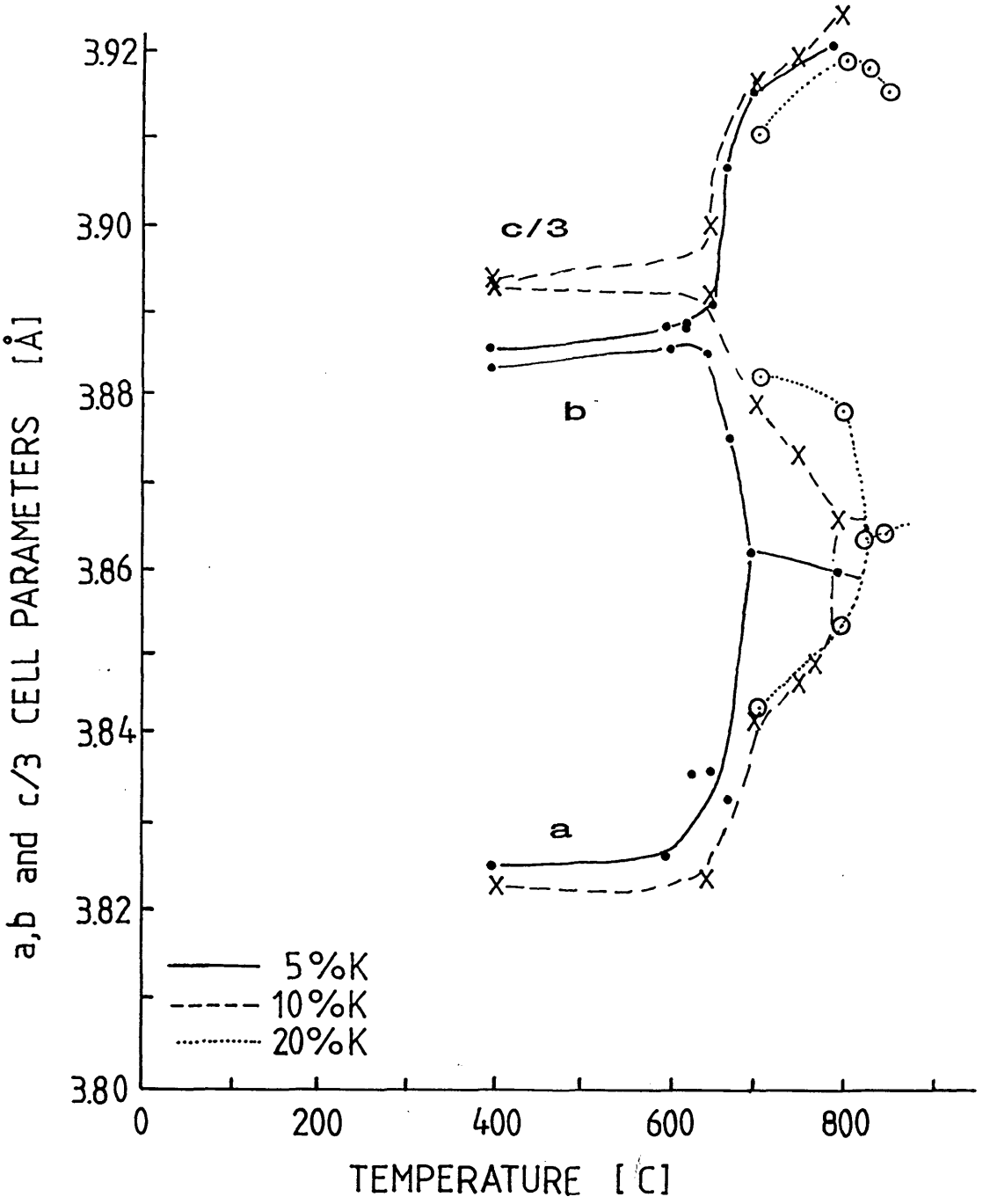

Figure 5.16: The variation of cell parameters a, b and c/3, determined by X-ray diffraction, versus quenching temperature for 5,10 and 20% doped material ($YK_xBa_{2-x}Cu_3O_{7-\delta}$, x=0, 0.1, 0.2).

coefficient over the a, c and b-axis, which is the main reason for microcracking, cannot be avoided and therefore no improvement from this point of view is expected.

Considering the defect chemistry of potassium substitution in the Ba site it is likely that oxygen vacancies are created (eq. 5.1):

$$K_2O(BaO) \longrightarrow 2K'_{Ba} + O_O^X + V_O^{\cdot\cdot} \qquad (5.1)$$

It would also be possible that oxygen is introduced to reduce these vacancies according to eq. 5.2:

$$V_O^{\cdot\cdot} + \tfrac{1}{2}O_2 \longrightarrow O_O^X + 2h^{\cdot}(Cu^{3+}) \qquad (5.2)$$

If (eq. 5.2) occurs, an increase in oxygen stoichiometry compared to the undoped material would be expected and the increase of the temperature at which the O-T transition occurs could possibly be justified. From table 5.7, however, a small decrease of oxygen content is observed instead. According to this result, equation 5.1 seems to occur and an increase of oxygen vacancies is expected in the material. Examination of the structure (figure 2.9) indicates that the oxygen site likely to be affected is O1, in the same plane as Ba. It is not clear, however, how this could have an effect on the O-T transition. Decrease of the c-axis, on the other hand, as observed in the case of Nd and Gd, can be justified.

Since the amount of potassium found in the material is small (from half to a very small fraction of the nominal composition -see table 5.6-), a small effect would normally be expected on the properties of the material.

In order to examine further the effect of potassium doping on the structure of the material, an *in-situ* investigation by neutron diffraction was performed.

5.7. O-T Transition Temperature by Neutron Diffraction

Examination of the K-doped YBCO samples by *in-situ* neutron diffraction presented the following advantages: results are indicative of the bulk of the material (not just the surface as for X-rays), since the samples are practically transparent to neutrons; and *in situ* measurements permit elimination of problems that might arise by quenching. By using the Rietveld refinement method, the cell parameters were obtained. This method could also provide information on the exact place and site occupancies of the different atoms. However, the very small amount of potassium present makes it practically impossible to estimate the site occupancies for it. Furthermore, impurities (CuO and 211) resulted in unsatisfactory goodness-of-fit parameters, and so results on site occupancies have not been used.

Three oxygen loaded samples of 0, 5 and 10% K-doping were examined ($YK_xBa_{2-x}Cu_3O_{7-\delta}$, x=0, 0.1, 0.2). They were inserted in powder form in SiO_2-glass tubes, contained in a cylindrical stainless steel holder which was placed in the on-stage furnace in an oxygen atmosphere. Due to the short time allocated for these experiments, only 20 min. were allowed for equilibration for all temperatures before the measurements took place. An experiment performed in order to examine the effect of the equilibration time, however, showed that there is only a small difference of the results after 20 and 180 min.

Spectra for the stainless steel holder were recorded at all temperatures examined and later on were subtracted from the spectra of the samples, so that eventually only the contribution from material itself was obtained. In figure 5.17, the spectra of the empty steel holder along with the steel holder when containing an $YBa_2Cu_3O_{7-\delta}$ sample at room temperature are showed.

The neutron diffraction spectra obtained for YBCO over the temperature range 25-725 C are shown in figure 5.18. The separation, merging or inversion of intensities of peaks due to the structural transition from the orthorhombic to the tetragonal phase can be observed. The temperature steps were chosen so that the transition temperature could be traced within 25 degrees.

The O-T transition temperature observed when heating the samples from 25 C compared to that when cooling them from higher temperatures (700-800 C), presented a hysteresis of the order of 30 degrees centigrade. This was probably due to the slow kinetics of oxygen and the relatively

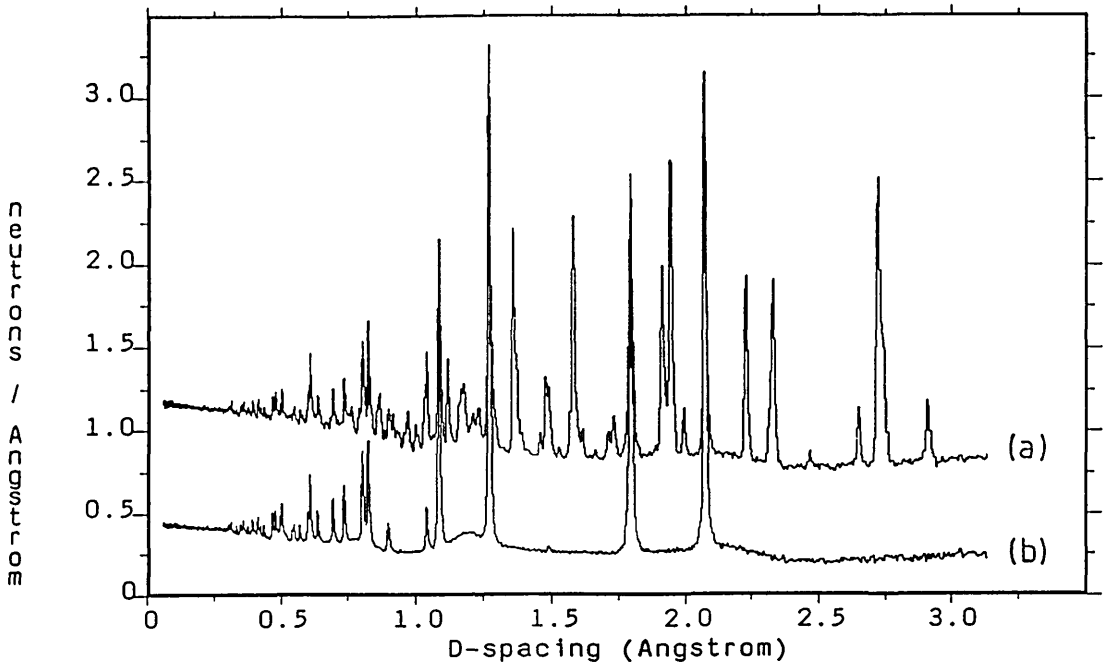

Figure 5.17: Neutron diffraction patterns at room temperature: (a) $YBa_2Cu_3O_{7-\delta}$ sample in a steel holder, (b) the steel holder by itself.

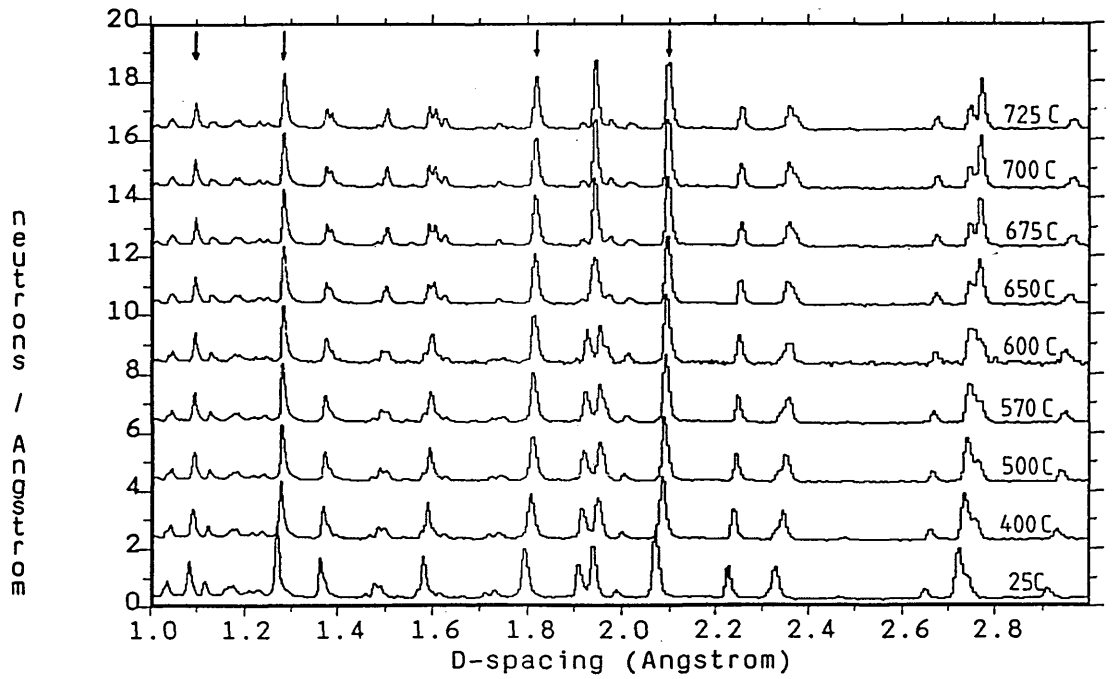

Figure 5.18: The variation of the $YBa_2Cu_3O_{7-\delta}$ peaks over 25-725 C, by neutron diffraction. Peaks indicated by an arrow are due to the steel holder.

short equilibration time that was used before each measurement. The evolution of three of the peaks of YBCO and 5% K-doped YBCO during the O-T transition is shown in figure 5.19. The merging of the (200) and the (020) peaks of the orthorhombic phase to the single (200) reflection of the tetragonal phase is clearly shown. The peaks appear to be flat due to the scaling.

The cell parameters were obtained by fitting the data and a typical accuracy of 0.0003-0.0006 Å was obtained. The cell parameters for 0, 5 and 10% K-doped YBCO at different temperatures shown in figure 5.20 do not indicate any effect as that observed by XRD on quenched material. Comparing this figure with 5.15, a different behaviour of the c-axis can be noticed. It changes abruptly on the quenched material near the O-T transition, while a gradual increase is observed *in-situ*. Also, a general increase of all cell parameters can be noticed for the neutron diffraction results. This is a normal consequence since *in-situ* measurements include the effect of thermal expansion, irrespectively of other structural changes. A very clear illustration of this is the change of cell parameters between 25 and 400 C. The structure remains the same since the oxygen stoichiometry is maintained near 7, but an increase on all cell parameters is recorded.

The orthorhombic to tetragonal transition occurs at approximately 675, 650 and 650 C (the last value is an estimate since measurements only up to 635 C were performed) for 0, 5 and 10% K-doped material. This result and the data shown in figure 5.20 indicate that within experimental errors, there is no difference in the behaviour of doped as opposed to that of the undoped material.

This contradicts the results from X-ray diffraction of quenched material. Neutron diffraction provides results from the bulk of the material, while XRD only from a certain thickness below its surface. As far as the bulk of the material is concerned, the O-T transition temperature is not affected by K-doping and there is no indication of the applicability of the models (eq.5.1-5.2) in this situation, especially because of the small existing amount of potassium.

It might be argued that K-doping could have an effect on the surface exchange process, facilitating oxygen intake during the very short cooling time before quenching. Such an effect would be detectable by XRD but not by neutron diffraction. Possible intake of oxygen before quenching is also indicated by the fact that transition temperatures are in general lower when estimated by *in-situ* examination (650-675 C) than from quenched samples (700-820 C).

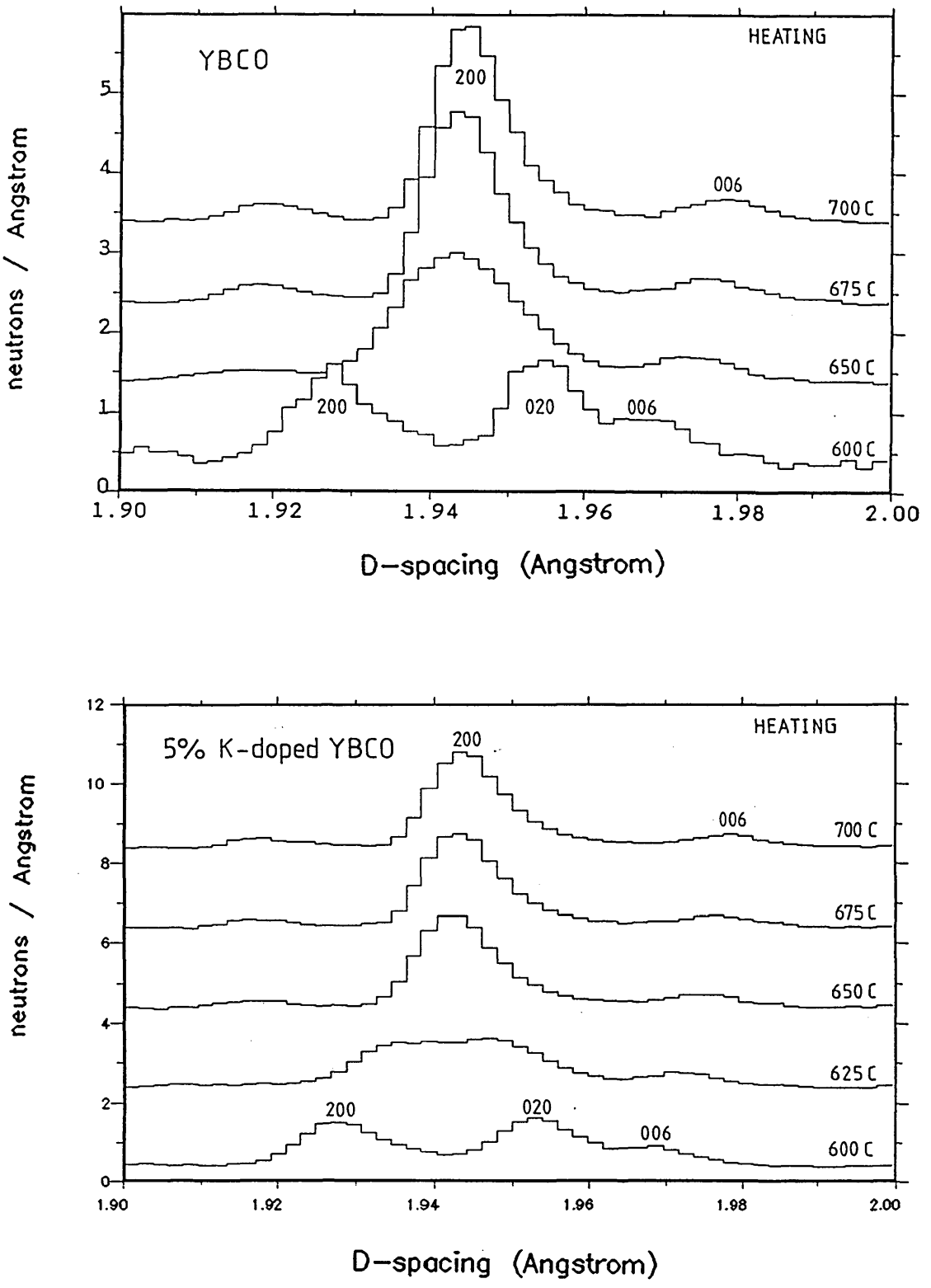

Figure 5.19: The evolution of the 200, 020 and 006 peaks for different temperatures for the 0 and 5% K-doped YBCO samples.

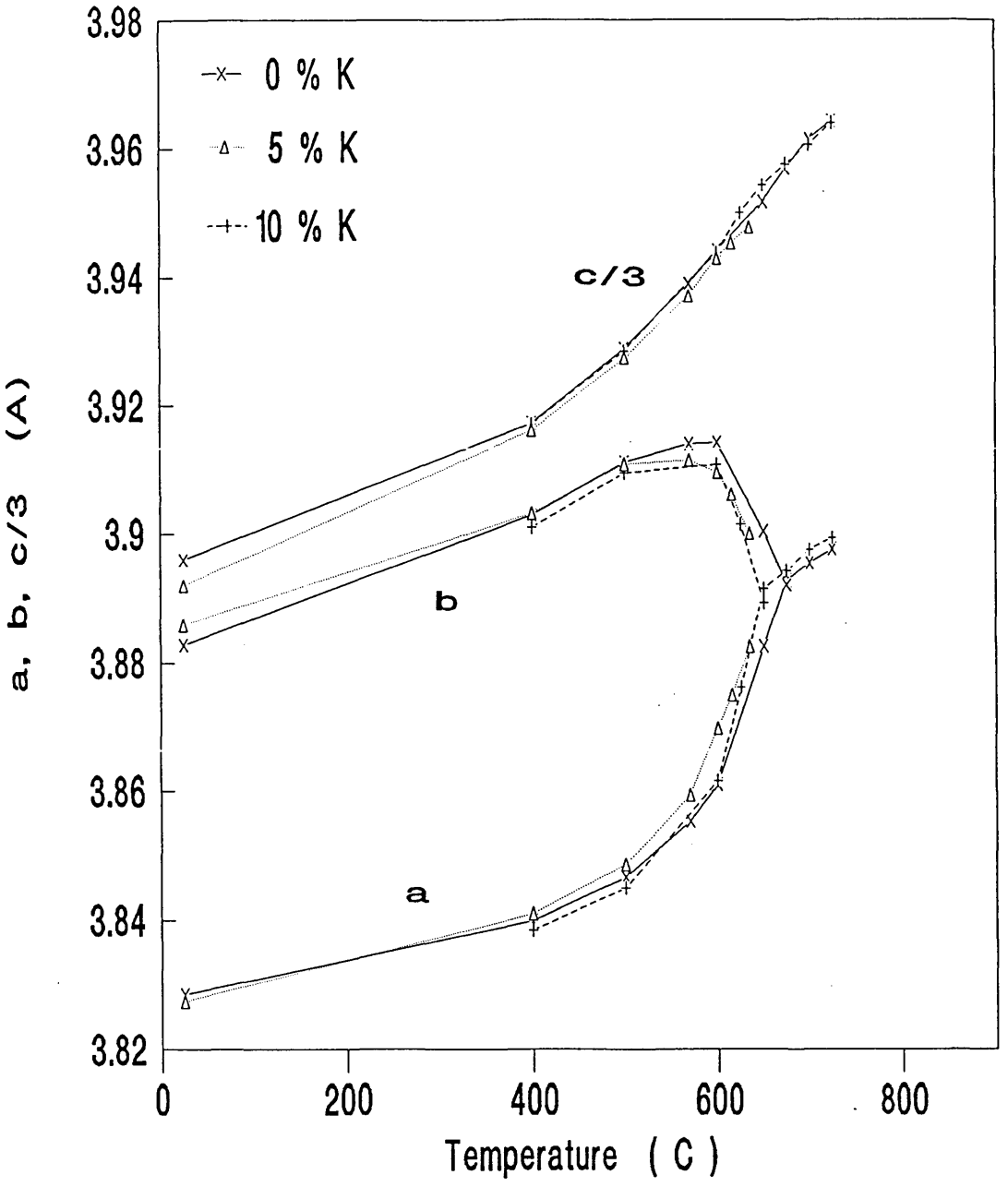

Figure 5.20: The variation of cell parameters a,b and c/3, determined *in-situ* by neutron diffraction, versus temperature for 0, 5 and 10% K-doped material ($YK_xBa_{2-x}Cu_3O_{7-\delta}$, x=0, 0.1, 0.2).

The neutron diffraction experiments were performed in collaboration with Dr. W. Cywinski and Dr. S. Kilcoyne from the University of Reading (Physics Dept.).

5.8. Conclusions

Examination of K-doping of the 123 structure showed a deterioration of the superconducting properties when Er, Gd and Nd were used as the R.E. cation, even though a very small amount of potassium remained, the rest evaporating during sintering. Y-123 did not show any effect on T_c for nominal doping up to 15% K, microstructural changes were, however, observed.

Grain enlargement or partial decomposition of the YBCO phase to CuO and 211 or $BaCuO_2$ resulted for different firing temperatures. This is an interesting property since large-grain YBCO could be useful in combination with preferred orientation in order to obtain high J_c material, a route followed by Murugaraj et al. [201,202]. In these publications it is claimed that the a-b plane growth is larger for $YBa_{2-y}K_xCu_3O_{7-\delta}$ (y=0.15-0.2, x-very small) samples, resulting in oriented bulk ceramics.

Results on the orthorhombic to tetragonal (O-T) transition temperature differ for investigations *in-situ* and on quenched material. *In-situ* neutron diffraction indicated that the doped material has the same transition temperature (650-675 C) as undoped YBCO. On the other hand, an increase from 700 to 800 C was found for quenched 0 and 10% K-doped YBCO respectively by X-ray diffraction. These contradictory results could possibly be due to surface effects, since bulk properties, as indicated by neutron diffraction, are not affected.

6. OXYGEN MASS TRANSPORT

6.1. Oxygen conductivity by electrochemical techniques

Solid state electrochemical techniques had been used extensively in the past for characterizations of ionic or mixed ionic and electronic conductive ceramics [203,204]. Using these techniques, thermodynamic and transport quantities are transformed into electrical quantities (voltage, current) which can be measured accurately. The equipment required, therefore, is not necessarily expensive and measurements can be performed in a relatively short time in most cases.

The most complicated measurements involve mixed conductors, since in that case auxiliary electrolytes have to be used. In this work, the objective was to measure oxygen conductivity in the YBCO and BSCCO mixed conductor materials, where holes are the majority carriers.

In the case of YBCO, oxygen diffusion can be calculated from the conductivity measurements and, therefore, the process time for low temperature (400–450 C) oxygen annealing can be accurately found. Measurements on BSCCO can also give information on the mass transport and indicate the applicability for ceramic electrochemical reactors.

Possible disadvantages and limitations on the application of the electrochemical techniques are also examined and discussed.

6.1.1. The electrochemical cell

The main problem concerning measurements of YBCO or BSCCO is that electronic conductivity is much larger than the oxygen ion conductivity. In order, therefore, to isolate the ionic contribution, auxiliary electrolytes that would block electronic current had to be selected.

The cell employed (figure 3.4) is simple in design and ideally the partial ionic conductivity of the material to be examined should be two orders of magnitude lower than that of the blocking electrodes. In this way the contribution of the electrodes will be very small compared to that of the material to be measured.

Since conductivity values have not been established for either YBCO or BSCCO, silver, a well characterized mixed conductor, was used in order to verify the applicability of the electrochemical technique using this cell. The temperature range for these measurements is 300–850 C.

6.1.2. Electron blocking electrodes

The choice of the blocking electrodes is dictated from the magnitude of their oxygen conductivity at the required temperature range. Two kinds of electrodes were used:

i) Yttrium Stabilized Zirconia (YSZ or 8YSZ)

At a stoichiometry of 8% Y, good conductivity can be obtained. It can operate in a temperature range of 300–1200 C, even though at 300–400 C it has a rather small conductivity. Attention must be paid to the working atmosphere, since at either very high or very low oxygen pressures, electronic conductivity becomes similar or larger than the ionic one [205].

ii) Samarium doped bismuth oxide ($Bi_{1.75}Sm_{0.25}O_3$ or BiSm)

Doping with Sm, the δ–Bi_2O_3 phase is stabilized. This phase has an oxygen conductivity which is much higher than that of YSZ, however, the operation temperature is limited to a maximum of approximately 800 C. On the other hand, BiSm can be used at temperatures between 300–500 C providing much better conductivity than YSZ. Apart from the possible appearance of electronic conductivity at extremes of partial oxygen pressure [206] (as for YSZ), reduction of the $Bi_{1.75}Sm_{0.25}O_3$ to metallic Bi and Bi–Sm oxide can occur at reducing conditions, even with small voltages/ currents [207].

The conductivity σ of both materials is presented in figure 6.1. Results for σ(bulk+grain boundary) 8YSZ over the temperature range 288–783 C, from [184] were used. For the experiments performed here, the same commercial powder (TZ–8Y) and the same firing procedure were employed. A series of impedance spectroscopy measurements over 245–395 C was performed in order to find the conductivity of BiSm presented in this figure.

6.1.3. Possible contributions to the conductivity

A number of different processes can affect electrochemical measurements and therefore they have to be taken into account in order to analyze the results and to take the necessary precautions.

In figure 6.2 the cell and the possible contributions to the conductivity are presented:

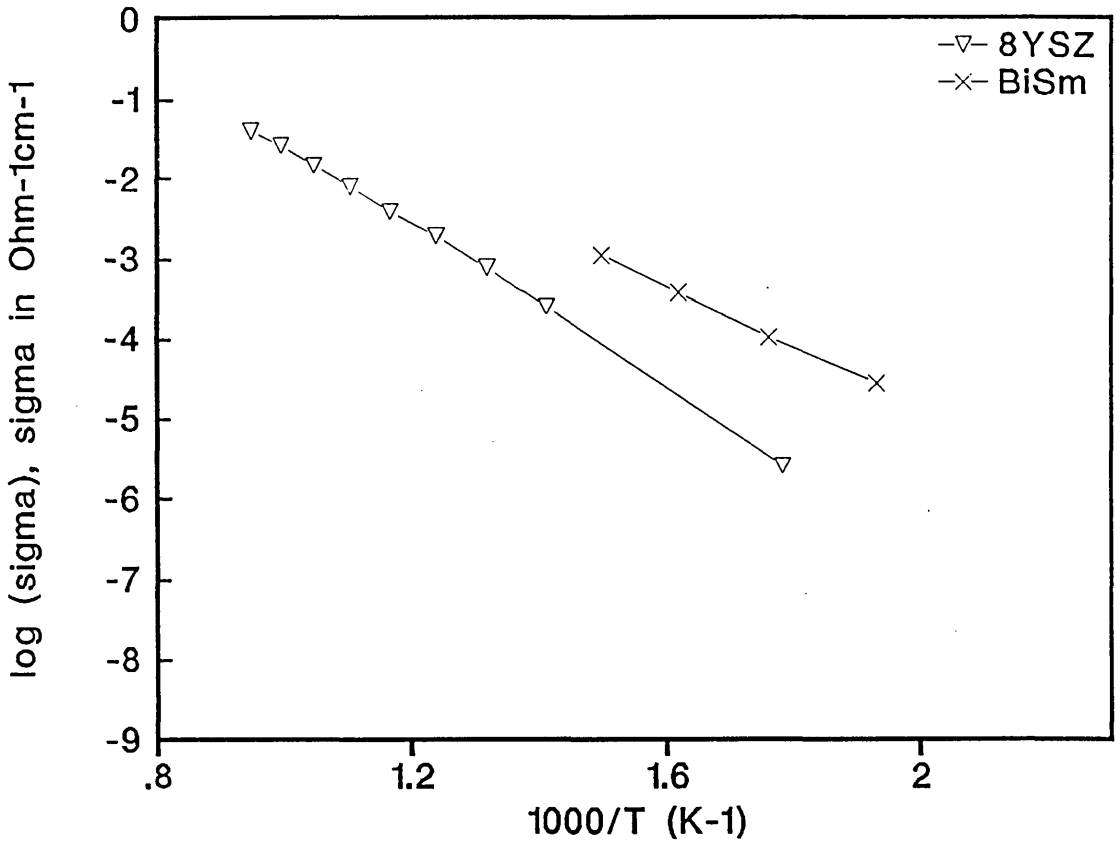

Figure 6.1: The conductivity of 8YSZ (bulk+grain boundary) and $Bi_{1.75}Sm_{0.25}O_3$ (bulk) versus temperature.

1. Pt(O2)/ Blocking electrolyte interface

This interface gives rise to the 'electrode effect' which can be detected by impedance spectroscopy even in the simple Pt/YSZ/Pt system (see figure 3.6).

2. Blocking electrolyte/ Mixed conductor interface

Depending on the quality of the interface, different values of resistance will be obtained. In order to minimize this value, all touching surfaces were polished using 2 μm diamond paste and measurements were performed cooling the cell assembly from high temperatures. This had as a result better contacts since at these temperatures (800–850 C) some of the materials soften slightly. In many cases after this treatment the three pellets were stuck together and it was difficult to separate them.

3. Leaking or short circuit routes for oxygen

Due to the high activity of triple points (atmosphere, blocking electrolyte, mixed conductor) it is possible that oxygen ions with two holes from the mixed conductor are freed as oxygen atoms to form molecules on one hand,

$$2\,O^{2-} + 4\,h^{\cdot} \longrightarrow O_2 \qquad (6.1)$$

while on the other hand, oxygen from the atmosphere can be decomposed to oxygen ions that enter zirconia and holes moving through the mixed conductor, so that the opposite reaction to (6.1) occurs. If this effect occurs and is large enough, it can cause short circuiting since it would be easier to leak through the contacts instead of passing through the material.

In an attempt to prevent this effect from happening the sides of the assembly were sealed with glass. After the measurements, however, it was observed that glass penetrated in some extent the area between the blocking electrolyte and the mixed conductor. Because of this effect, using the cell without glass sealing was preferred instead. Measurements with glass sealing were performed by Maier et al. [208].

4. Oxygen conductivity in both the mixed conductor and the blocking electrolyte

The oxygen conductivity of the mixed conductor is the required value, while that of the blocking electrodes can be either subtracted from the total value or ignored if it is less than 2 orders of magnitude smaller (<1%).

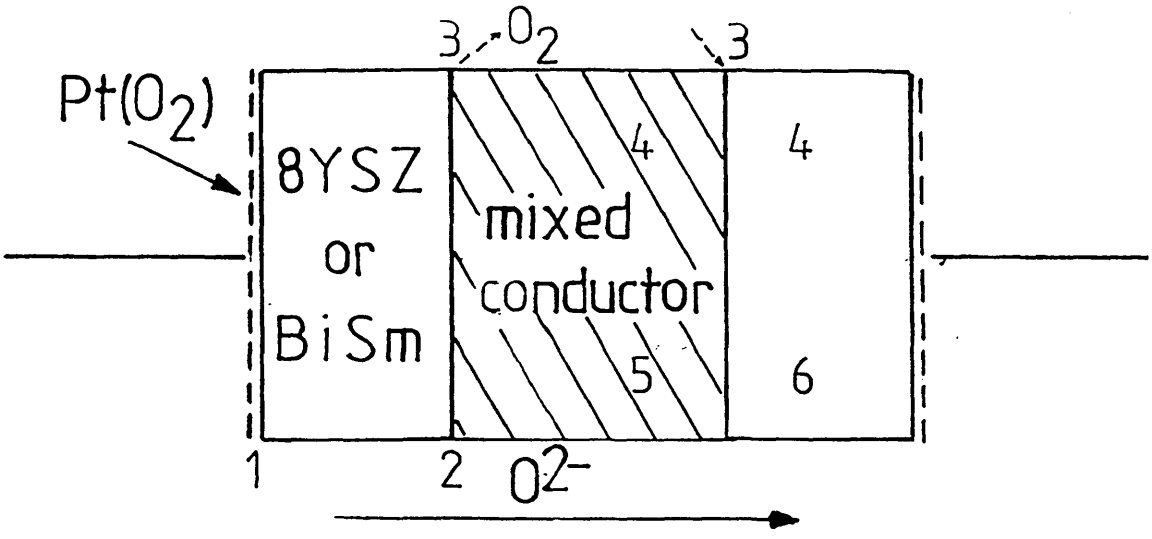

Figure 6.2: The possible contributions to the conductivity of the electrochemical cell employed here.

It should also be mentioned that grain boundary conductivity can be another factor influencing these measurements, especially since it gives different capacitances and therefore different semicircles than the bulk conductivity in the real vs. imaginary impedance plots. The grain boundary conductivity of the YSZ used here, however, is very small, while no such contribution was detected by examination of the Pt/BiSm/Pt cell.

5. Porosity / Inhomogeneities

If porosity is present, the conductivity of the material at X-ray density (σ_O) can be found from the relation [209]:

$$\sigma = \sigma_O (1-P)^x \qquad (6.2)$$

where σ is the actual conductivity, and P is the pore fraction in the sample. Values for x range between 1.5 and 3. With a density of around 90% (so that 1-P= 0.9), the $(1-P)^x$ parameter could take values between 0.85-0.73. However, since no information for x was available for the materials examined here, no attempt was made to estimate σ_O values.

Inhomogeneities and impurities can have considerable effects on conductivity/ diffusion coefficients. For this reason high quality starting materials were used. In the case of BSCCO, the sample was multiphase and therefore the oxygen conductivity found can only be considered as an average of different contributions.

6. Possible hole conductivity of blocking electrolytes under certain conditions.

The conditions employed here were a temperature range of 350-850 C and an atmosphere of air or oxygen. Voltages applied did not exceed 4 V (usually 1-2 V) and no blackening of the BiSm was observed. Under these conditions, an electronic (hole) conductivity of 2-4 orders of magnitude lower than the ionic conductivity of the BiSm electrolyte is expected [206]. This might interfere with the measurement of the ionic conductivity of the mixed conductors, therefore, BiSm was mainly employed at temperatures lower than 500 C, at which hole conductivity will be at least 3 orders of magnitude smaller than the ionic.

6.1.4. The case of Ag

Oxygen diffusion in silver has been studied extensively in the past and a number of electrochemical techniques has been employed. In table 6.1 the available results (chemical diffusion coefficients) are listed.

Results are based either on gas-liquid diffusion cells or on electrochemical investigations. Potentiostatic, potentiometric or galvanostatic techniques have been used, [204] but as can be seen from table 6.1, there is a satisfactory agreement of the results. It can also be seen that the activation energy for temperatures higher than 950 C (silver is molten) is around 0.3-0.4 eV, while for lower temperatures (solid silver) the activation energy is around 0.5 eV.

In order to examine the applicability of the electrochemical technique suggested here, solid silver was examined and the results were compared to [216].

Table 6.1: Oxygen diffusion coefficient in Ag.

Workers	Diffusion coefficient	Temp. range
Eichenauer & Muller 1962 [210]	$D= 3.66\times10^{-3}\ \exp[(\ 0.48eV\ )/kT]$	(412–862 C)
Mizikar et al. 1963 [211]	$D= 1.47\times10^{-3}\ \exp[(\ 0.31\pm0.14eV\ )/kT]$	(1000–1200 C)
Masson & Whiteway, 1967 [212]	$D= 5.15\times10^{-3}\ \exp[(\ 0.43\pm0.11eV\ )/kT]$	(970–1200 C)
Rickert & El Miligy, 1968 [213]	$D= 2.63\times10^{-3}\ \exp[(\ 0.32eV\ )/kT]$	(990–1220 C)
Velho et al. 1969 [214]	$D= 2.20\times10^{-3}\ \exp[(\ 0.34\pm0.06eV\ )/kT]$	(1000–1150 C)
Sano et al. 1970 [215]	$D= 3.00\times10^{-3}\ \exp[(\ 0.38\pm0.02eV\ )/kT]$	(1000–1200 C)
Ramanarayanan & Rapp 1972 [216]	$D= 4.90\times10^{-3}\ \exp[(\ 0.50\pm0.06eV\ )/kT]$	(750–950 C)
Otsuka & Kozuka 1973 [217]	$D= 1.81\times10^{-3}\ \exp[(\ 0.33\pm0.06eV\ )/kT]$	(1000–1150 C)
Park 1990 [218]	$D= 3.20\times10^{-3}\ \exp[(\ 0.50eV\ )/kT]$	(740–915 C)

6.2. Impedance spectroscopy: Calculations and reproducibility

6.2.1. Calculation of conductivities for the complex cell

For the resistivity/ conductivity of the different processes, semicircles were graphically fitted to the $Z'-Z''$ plots and the values were obtained from the intersection of the semicircles with the real (Z') axis. From two to four semicircles were found to be present in the impedance plots. Some of them, especially at higher temperatures (>600 C), were depressed, their centre being under the real axis. Examining the impedance plots over the temperature range, it can be observed that high frequency semicircles which are well-defined at low temperatures, become too small to be observed at higher temperatures, while other, lower frequency semicircles appear fully. As a result, in all cases, impedance spectroscopy at lower temperature gives information on different processes rather than higher temperature measurements, a behaviour that is typical even in simple cells such as Pt/YSZ/Pt.

The wiring from the measurement apparatus, through the sample holder, leading to the sample, gives a resistance of approximately 2 Ohms at 600 C and 4 Ohms at 800 C. The obtained values from impedance spectroscopy were, therefore, corrected if they were of a similar order of magnitude (<100 Ohms).

In order to examine the reproducibility of the results, a number of parameters were considered and their effect was observed for typical cell arrangements.

6.2.2. The AC signal oscillating level

The oscillating level (amplitude) of the AC signal was examined during preliminary measurements for the cell Pt/BiSm/YBCO/BiSm/Pt at 412 C and for the cell Pt/BiSm/BiSm/Pt between 450-475 C. No effect can be detected in the impedance plots for oscillating levels of 20 and 110 mV. In some cases, low frequency data were slightly better defined if an oscillating level higher than 20 mV was employed. As a result, an oscillating voltage of an amplitude of 35 mV was chosen for the rest of the impedance measurements.

6.2.3. Equilibration

Three cells were examined in order to find the effect of time allowed for equilibrium. Impedance values for the cell BiSm/YBCO/BiSm, at 412 C, in air, decreased by 25% in 80 min, as shown in figure 6.3. For the cell BiSm/Ag/BiSm, at 515 C, in air, impedance values for one semicircle remained constant, while for the other decreased by 12% in 126 min. Finally for the cell YSZ/YBCO/YSZ, at 400 C, in air, a drop of 40% was observed in 82 min.

Not all contributions were found to have the same behaviour with time. It would be expected that interface processes are affected with time since better contacts might be achieved through slow creep, or since improvement of the Pt electrodes with firing might occur. Another possibility is also the equilibration of the sample itself. Very long times should have been used in order to achieve full equilibrium, especially for YBCO and BSCCO, which are expected to have lower oxygen conductivity values than Ag. On the other hand, other contributions like the conductivity of the blocking electrolytes are expected to remain constant.

A general trend of decrease of the obtained impedance values with time has been observed, but from these results, there is no clear indication of an equilibration time. As a result, one hour was decided to be used as a conventional time for achieving equilibrium.

6.2.4. Results on heating/cooling the cell

Examination of the impedance when heating/cooling the cell showed a systematic trend for lower impedance values when measurements were performed during cooling.

A typical example is given in figure 6.4 where two conductivity contributions of the cell BiSm/BPSCCO/BiSm are shown. In order to avoid the discrepancies present due to the different behaviour during heating/cooling, all measurements to be compared were performed when cooling. It can also be seen that the contribution represented by triangles is affected, while the other one (circles) is not. It seems possible, therefore, that this information can contribute to the interpretation and the assignment of the different contributions to physical processes.

In particular, improvement of the quality of the contacts as observed

by firing the cell at higher temperatures (see also section 6.1.3(2)) suggests that the second contribution might be connected with the transport through the blocking electrolyte/mixed conductor interface. Another possibility is also that the mixed conductor behaves differently since it might not be fully equilibrated.

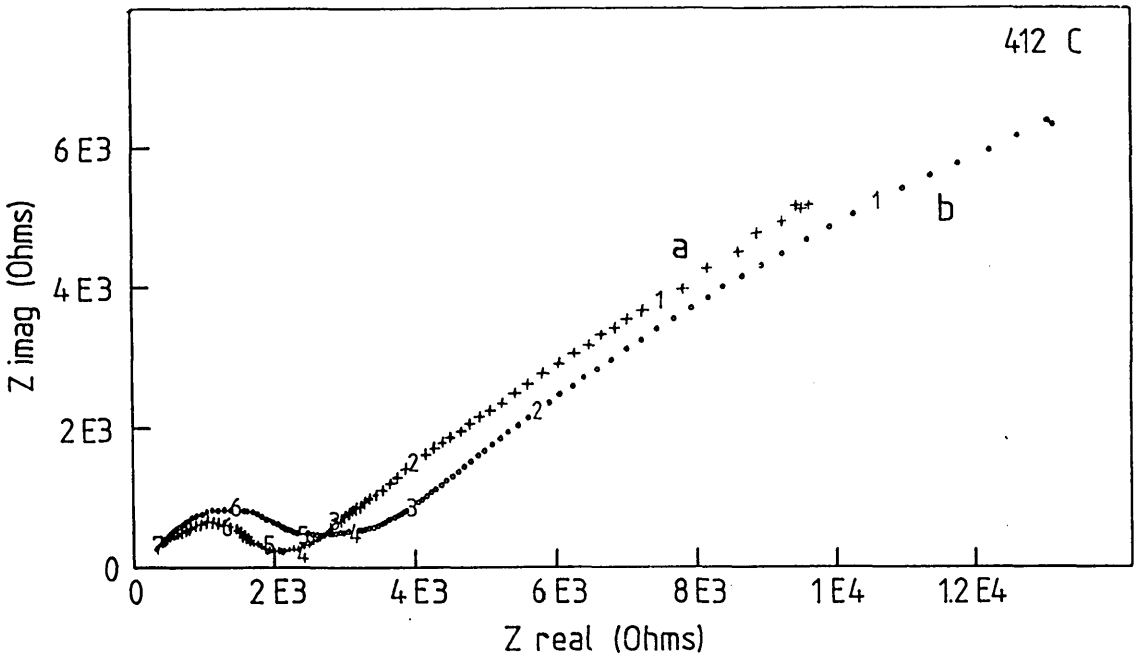

Figure 6.3: Impedance spectra of the cell BiSm/YBCO/BiSm at 412 C in air. The spectrum a (points shown as +) was obtained 80 min later than the b (points shown as o). Numbers (1–7) on the impedance plots indicate the logarithm of the frequency at these points (10^1–10^7 Hz).

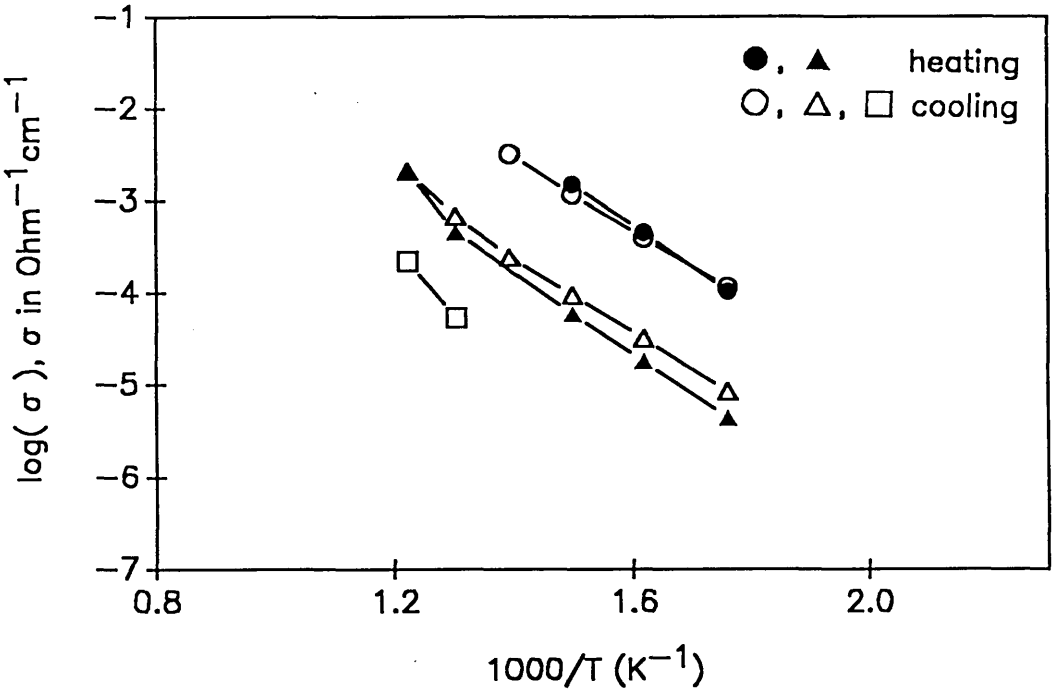

Figure 6.4: Conductivities of the contributions of the cell BiSm/BPSCCO/BiSm when heating (filled symbols) and cooling (empty symbols).

6.3. Impedance spectroscopy results

6.3.1. The Pt/YSZ/YSZ/Pt and Pt/BiSm/BiSm/Pt cells

The YSZ/YSZ and BiSm/BiSm cells were examined as a reference. Since they are much simpler than the complex cells for the measurements of mixed conductors, the aim of these measurements was to observe the effect of the electrode-to-electrode interface and to provide a model to describe this behaviour.

Impedance spectroscopy of the BiSm/BiSm cell resulted in $Z'-Z''$ plots with three semicircles. A spectrum of this cell at 295 C in air can be seen in figure 6.5. The conductivities for these contributions were calculated and their temperature dependence is shown in figure 6.6. The solid line represents the conductivity of BiSm, obtained by the cell Pt/BiSm/Pt. It can be seen that the highest conductivity contribution (semicircle A in figure 6.5) corresponds to the $Bi_{0.25}Sm_{0.75}O_3$. The contribution B can, therefore, be assigned to the electrode-to-electrode (BiSm/BiSm) interface and C to the BiSm/Pt electrode effect.

Examination of the YSZ/YSZ cell resulted in plots containing two semicircles (figure 6.7), however, the conductivities calculated, were found to be very small. As can be seen from figure 6.8, there is a very large difference between the conductivity of YSZ and the calculated conductivities of the cell.

A similar investigation by Fabry et al. [219], resulted in a model identical to that presented here for BiSm/BiSm. The interface contribution was identified as a semicircle similar to the B semicircle in figure 6.5 and was ascribed to a simple two-plate capacitor model with a calculated distance of 1.5 μm between the two plates.

The only way to explain the results shown in figure 6.8 is a very badly shaped contact between the two samples, so that the surface area used to convert resistance to resistivity should be considerably smaller than the one employed. This argument is supported by the fact that the first contribution has the same slope (activation energy) as the conductivity of YSZ. Another observation leading to the same conclusion is the large degree of depression of the semicircle of the second contribution seen in figure 6.7. This depression can be explained if instead of a fixed distance (as in Fabry's model), a largely varying distance between the two surfaces of the capacitor is considered. Each area of a constant distance would give a semicircle, displaced in comparison to one

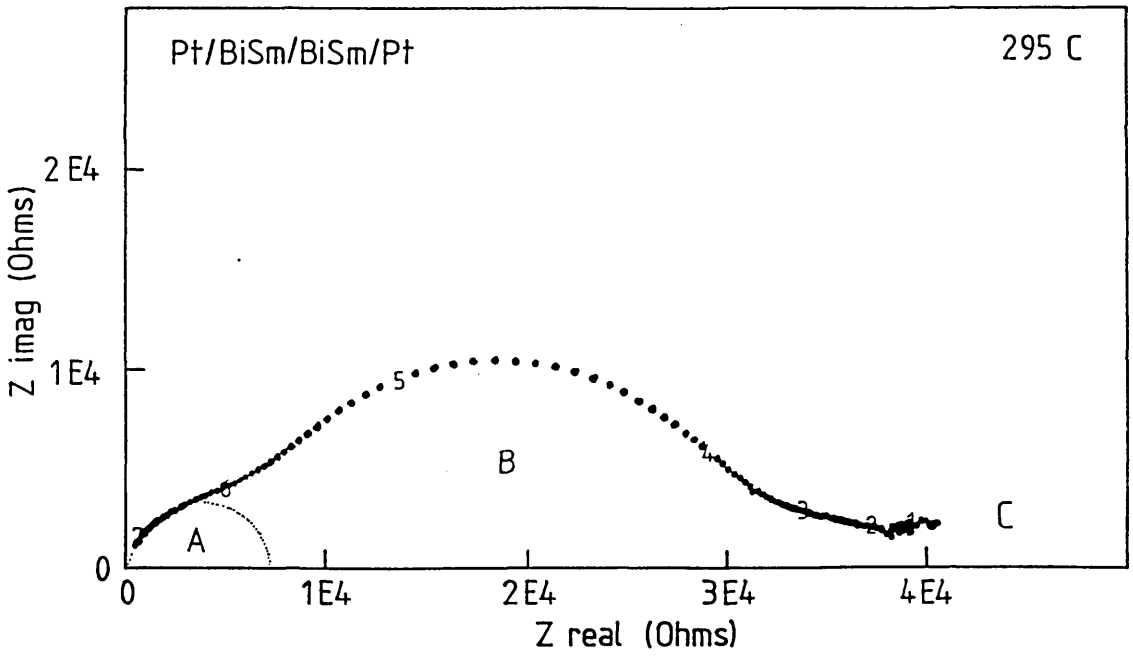

Figure 6.5: Impedance spectrum of the cell Pt/BiSm/BiSm/Pt at 295 C, in air. Two semicircles and the beginning of a third one appear.

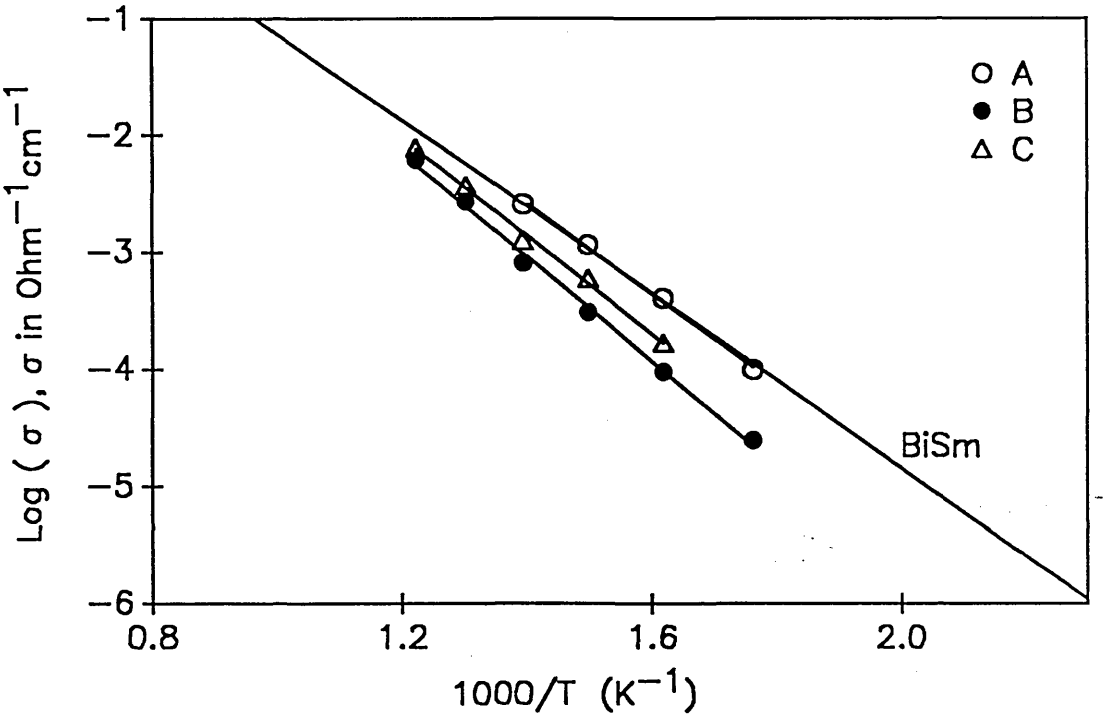

Figure 6.6: The temperature dependence of the conductivity contributions of the cell Pt/BiSm/BiSm/Pt. The contribution A coincides with the conductivity of BiSm.

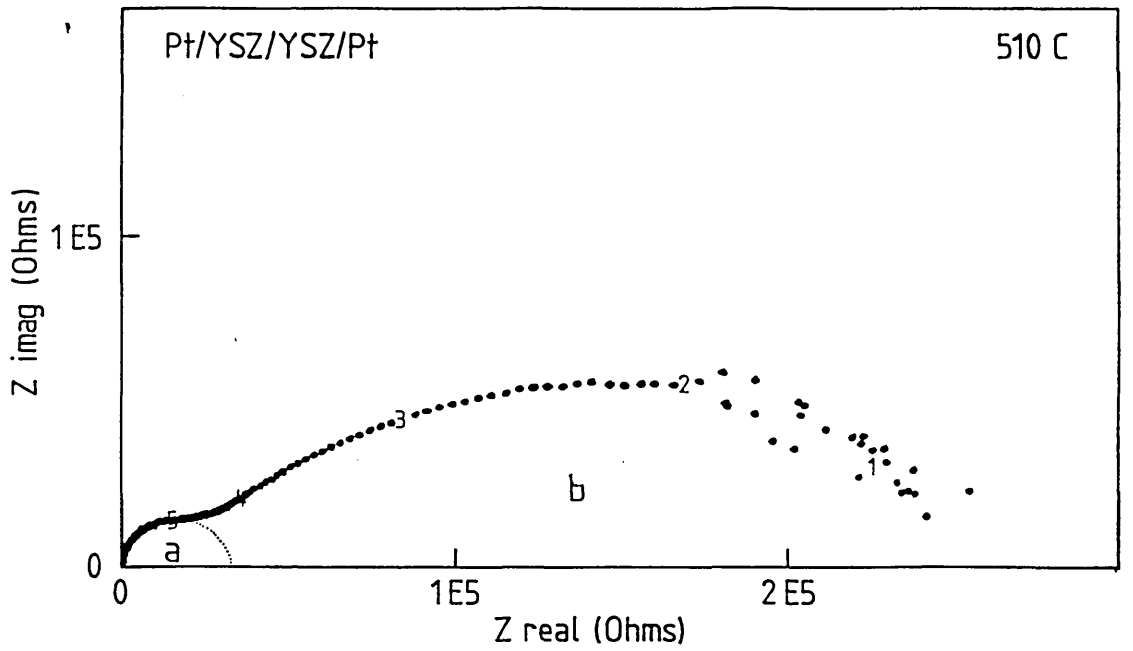

Figure 6.7: Impedance spectrum for the cell Pt/YSZ/YSZ/Pt at 510 C, in air.

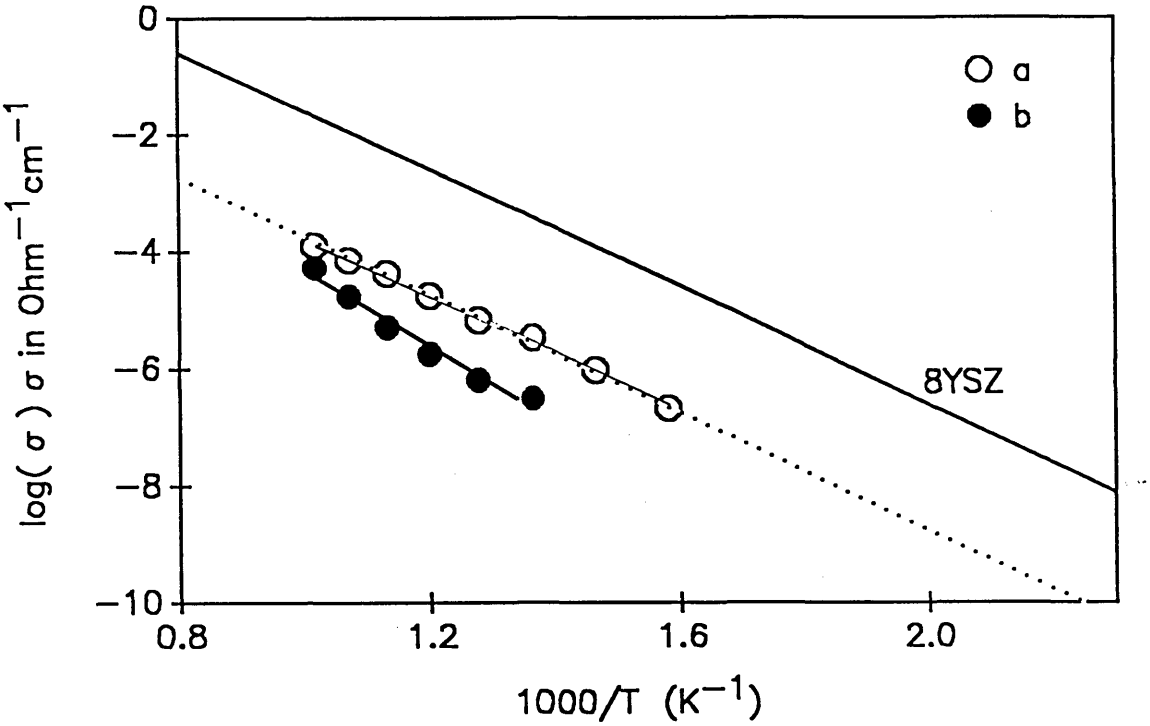

Figure 6.8: The temperature dependence of the conductivity contributions of the cell Pt/YSZ/YSZ/Pt. The dotted line has the same slope as 8YSZ, but is displaced to demonstrate the agreement with the slope of the conductivity of the contribution a .

from another area. Many of these semicircles compose what appears in figure 6.7 as a largely depressed semicircle. This is also the description of the distributed elements used for the modelling of depressed semicircles.

Measurements on the YSZ/YSZ cell were performed by J. Kajda.

6.3.2. Ag

Both YSZ and BiSm were used as blocking electrodes in order to examine Ag by impedance spectroscopy. All the measurements were performed in an oxygen atmosphere. In figure 6.9 a typical plot for the cell BiSm/Ag/BiSm at 445 C is presented. Examination of the results for both cells employed, showed the existence of four semicircles, some of them partially overlapping and, therefore, not clearly distinguishable.

The temperature dependence of the conductivity of the different contributions is shown in figure 6.10 for the BiSm/Ag/BiSm cell. The highest conductivity semicircle was again identified as the contribution of BiSm, however, none of the other contributions correlates with the expected conductivity for Ag and they could be attributed to some of the processes presented in 6.1.3. Contribution b has the same slope as contribution B of the BiSm/BiSm cell and it is possible, therefore, that is due to the BiSm/Ag interface.

Similarly, the results for the cell YSZ/Ag/YSZ are compared in figure 6.11. Again, the contribution of YSZ is identified and comparison of the rest of the contributions with the conductivity of Ag, shows a possible relation with contribution d. However, there are not enough points and data on this contribution can only be obtained at high temperatures/low frequencies, which practically means that the impedance values approach the DC conditions.

It seems, therefore, that it is difficult to obtain the conductivity of the mixed conductor with impedance spectroscopy at this range of temperatures (300-750 C) and frequencies (13MHz-5Hz). There is an indication, however, that at lower frequencies more information can be obtained.

6.3.3. YBCO

The cells BiSm/YBCO/BiSm and YSZ/YBCO/YSZ were examined. In figure 6.12, the evolution of the impedance spectra for the first cell from

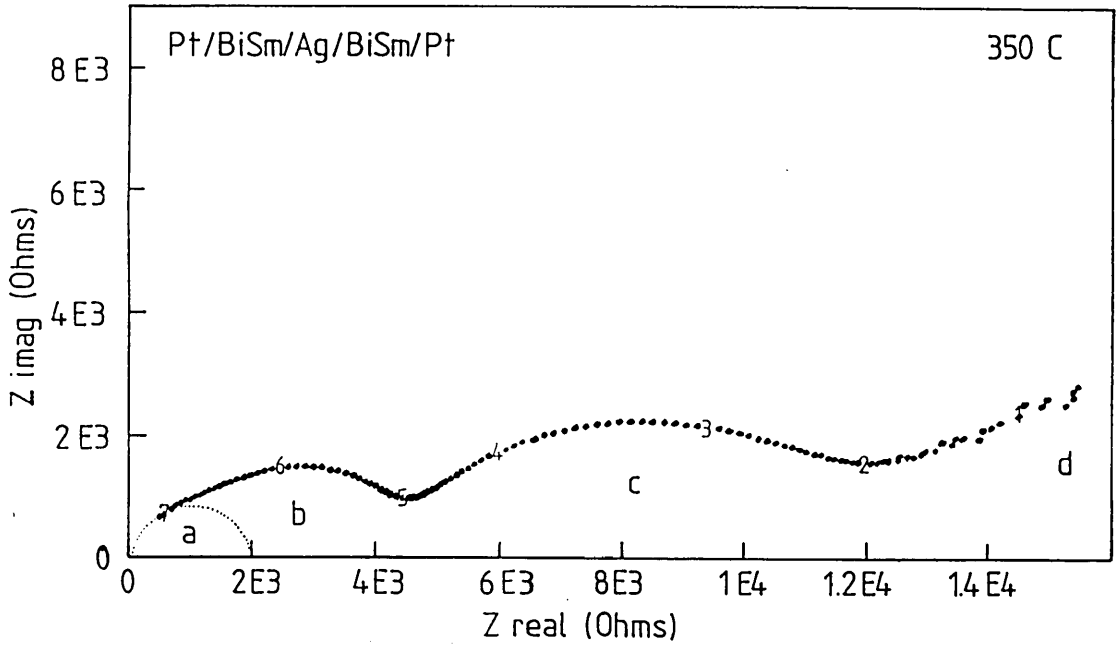

Figure 6.9: Impedance spectrum for the cell Pt/BiSm/Ag/BiSm/Pt at 350 C, in oxygen.

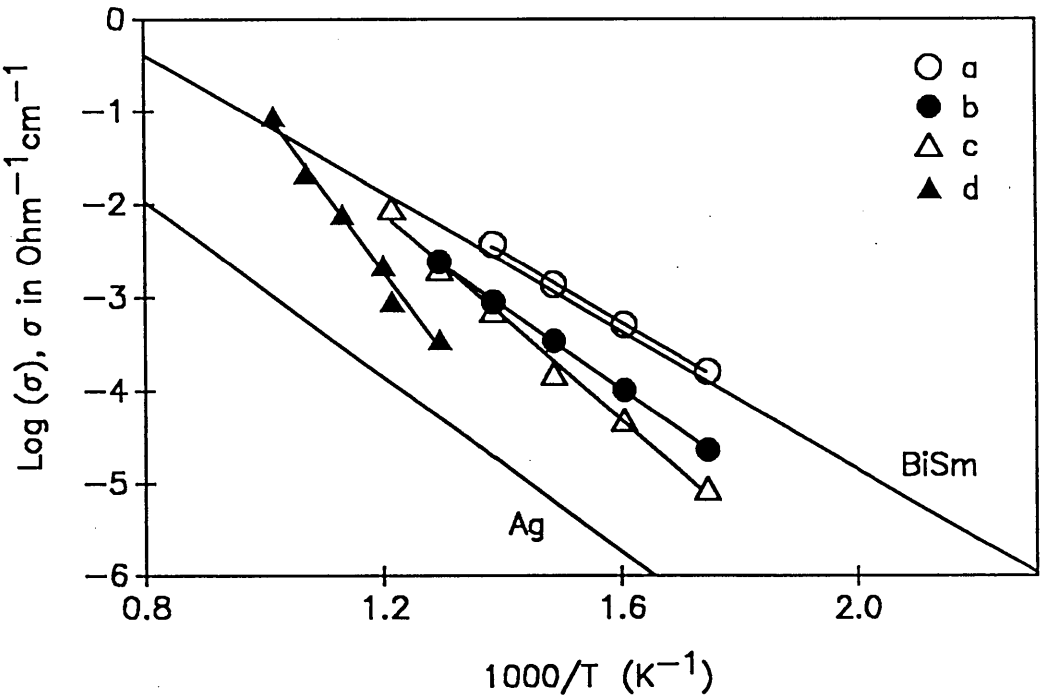

Figure 6.10: Temperature dependence of the conductivity contributions of the cell Pt/BiSm/Ag/BiSm/Pt. The conductivities of BiSm and Ag are also shown.

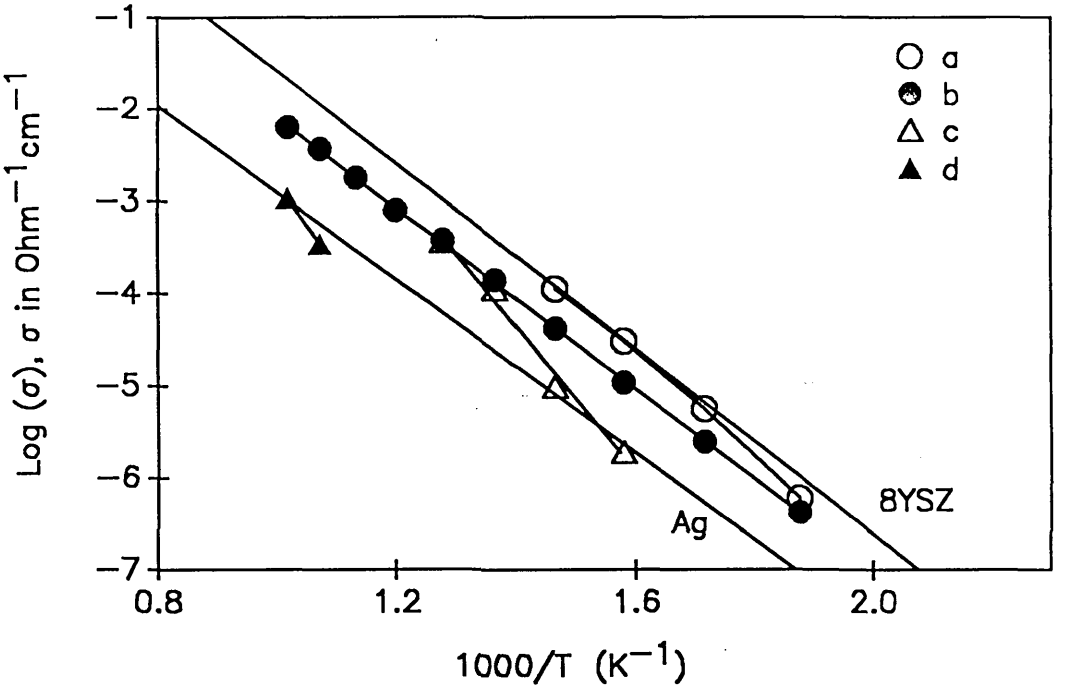

Figure 6.11: Temperature dependence of the conductivity contributions of the cell Pt/YSZ/Ag/YSZ/Pt. The conductivities of YSZ and Ag are also shown.

300 to 700 C are shown. At lower temperatures the a, b and c semicircles can be distinguished, while at higher temperatures information for the semicircles b and d only can be obtained. The conductivity values obtained from these plots are shown in figure 6.13. The contribution a can be clearly attributed to BiSm, while comparison of the contribution b with contribution B of figure 6.6 (section 6.3.1, BiSm/BiSm cell) reveals that they have almost identical values. This indicates that contribution b can possibly be attributed to the contact resistance of the BiSm/YBCO interface and if this is so, this interface behaves very similarly to the BiSm/BiSm interface.

Examination of the YSZ/YBCO/YSZ cell shows that the spectra obtained (figure 6.14) have impedances of at least one magnitude larger than that for the cell using BiSm as blocking electrodes. From the conductivity values shown in figure 6.15, the contribution a agrees well with YSZ. The second contribution b, has the same slope as the second one of the cell YSZ/Ag/YSZ (figure 6.11) which might indicate that they are both due to similar processes. Attention is also drawn to b and d (figure 6.13) and b and c (figure 6.15) contributions. They have similar slopes and it is, therefore, possible that they describe the same processes, but it is not apparent to what processes they refer.

6.3.4. BPSCCO

Examination of the BiSm/BPSCCO/BiSm and YSZ/BPSCCO/YSZ cells was performed so that not only information for BPSCCO would be obtained, but a comparison of the behaviour of the electrochemical cells would also be possible.

Conductivity data from the first cell indicate the existence of three processes (see figure 6.4) out of which the first is attributed to the ionic conductivity of BiSm. The second has the same values as contribution B of the cell BiSm/BiSm and b of the cell BiSm/YBCO/BiSm. It seems, therefore that it is due to a common characteristic of these cells such as the interface between the pellets, in this case the BiSm/BSCCO interface.

The data on the YSZ/BPSCCO/YSZ cell are shown in figure 6.16. Four processes contribute to the conductivity of the cell. The first is due to YSZ, showing that this behaviour is consistent for all the cells, whether the blocking electrodes are YSZ or BiSm. Comparison of the contribution b with the second one of the cell YSZ/YBCO/YSZ (figure 6.15) shows that they have the same values (and also the same slope as

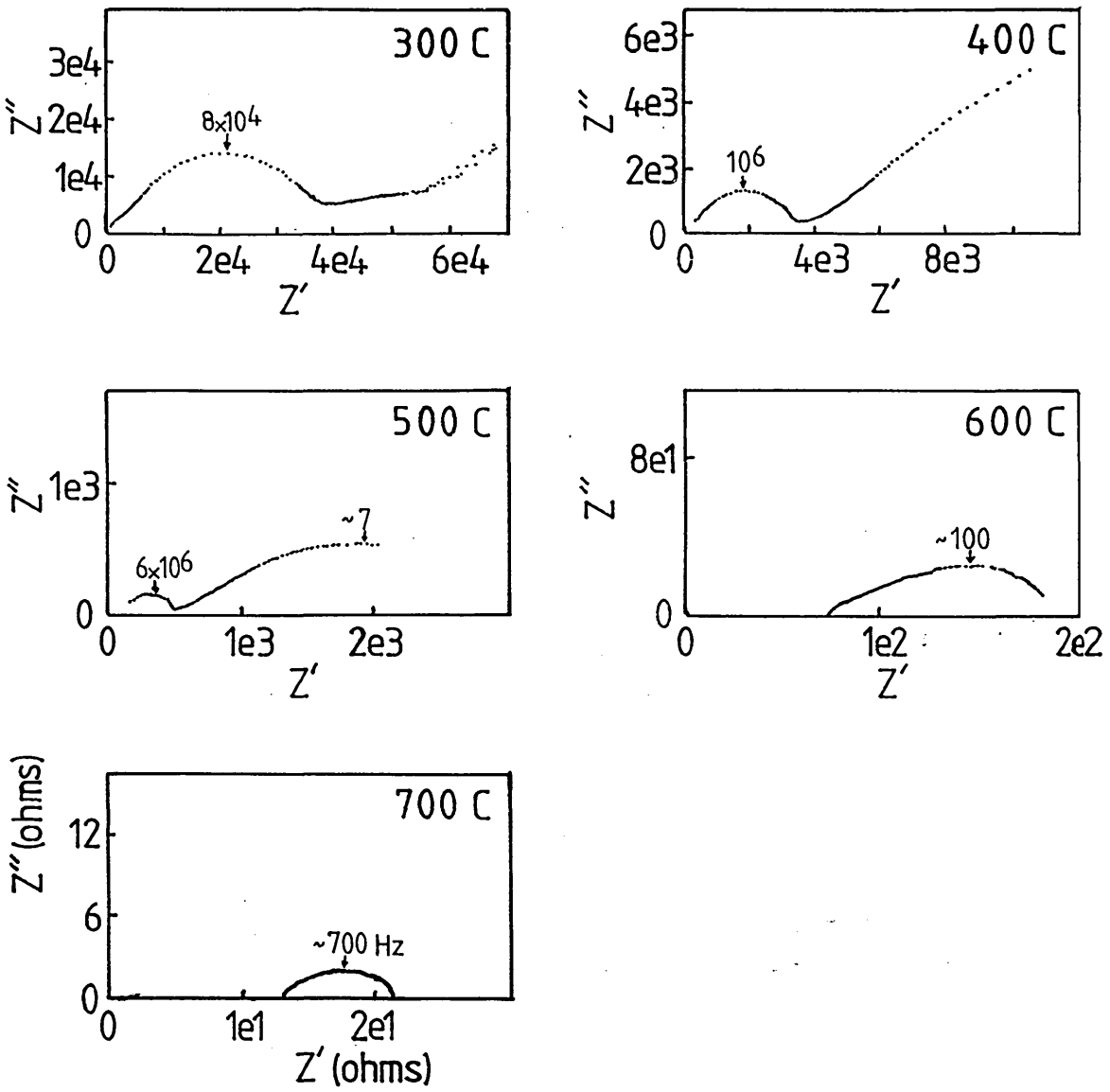

Figure 6.12: Impedance spectra for the Pt/BiSm/YBCO/BiSm/Pt cell in the range 300–700 C, in oxygen.

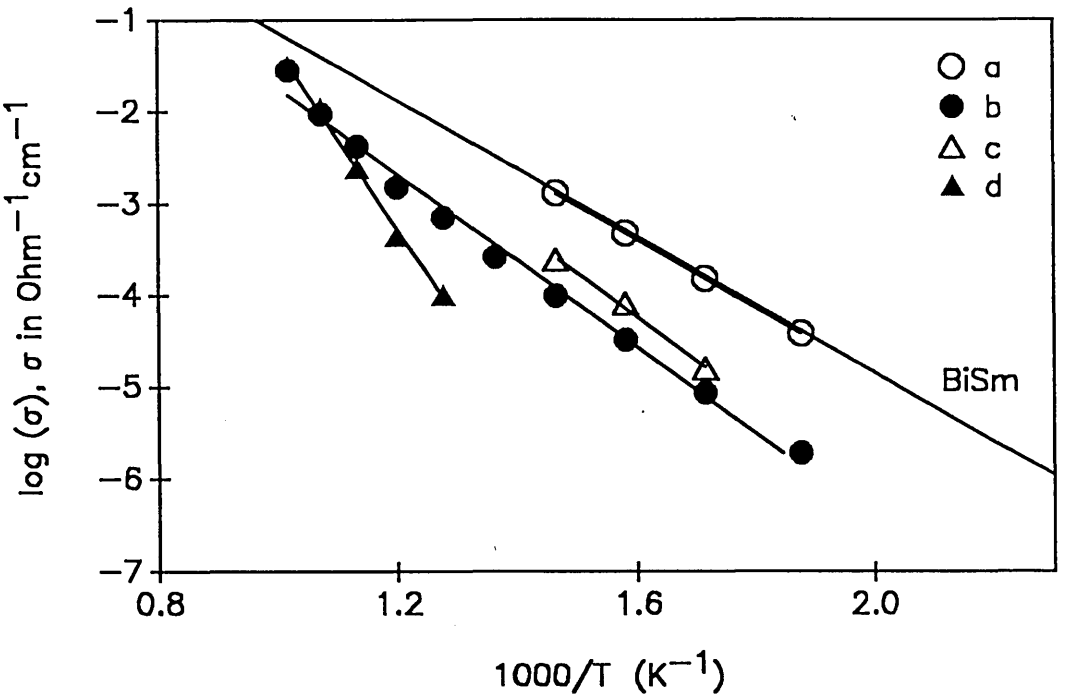

Figure 6.13: Temperature dependence of the conductivity contributions of the cell Pt/BiSm/YBCO/BiSm/Pt. The conductivity of contribution a is the same as that of BiSm.

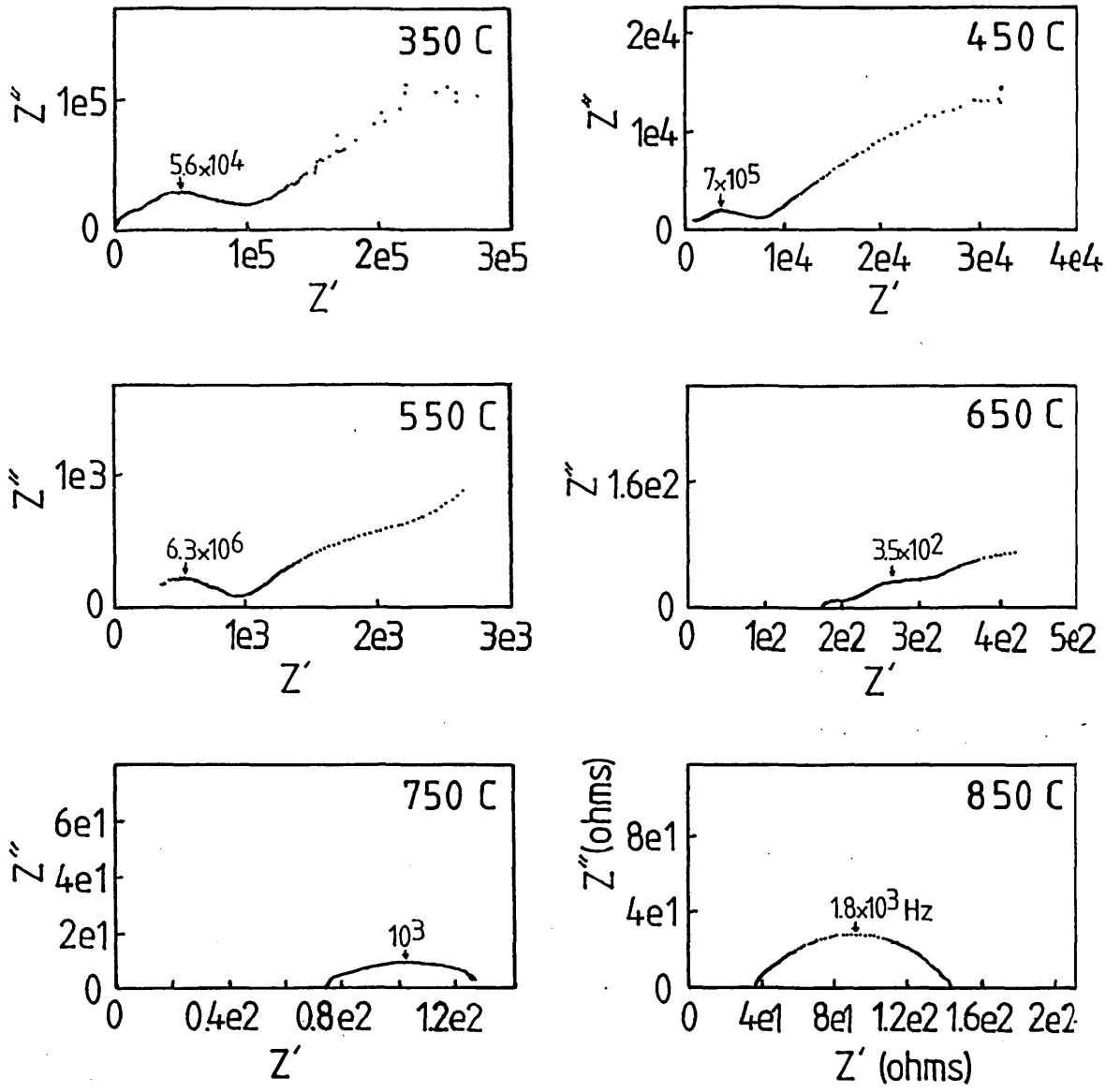

Figure 6.14: Impedance spectra for the Pt/YSZ/YBCO/YSZ/Pt cell in the range 350–850 C, in oxygen.

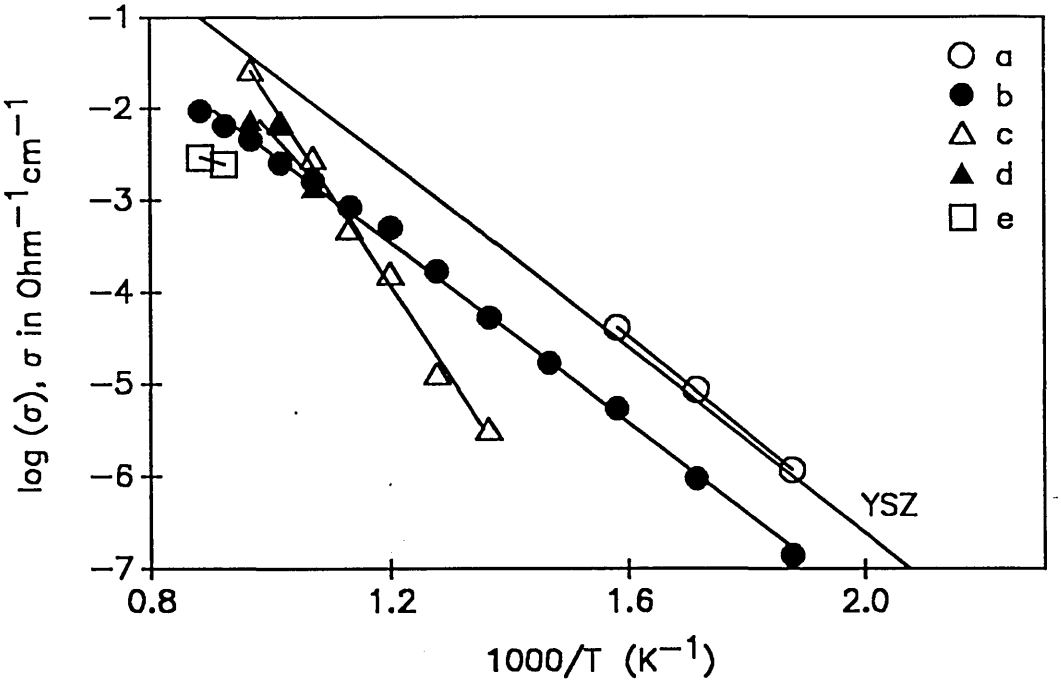

Figure 6.15: Temperature dependence of the conductivity contributions of the cell Pt/YSZ/YBCO/YSZ/Pt. The conductivity of YSZ is also shown.

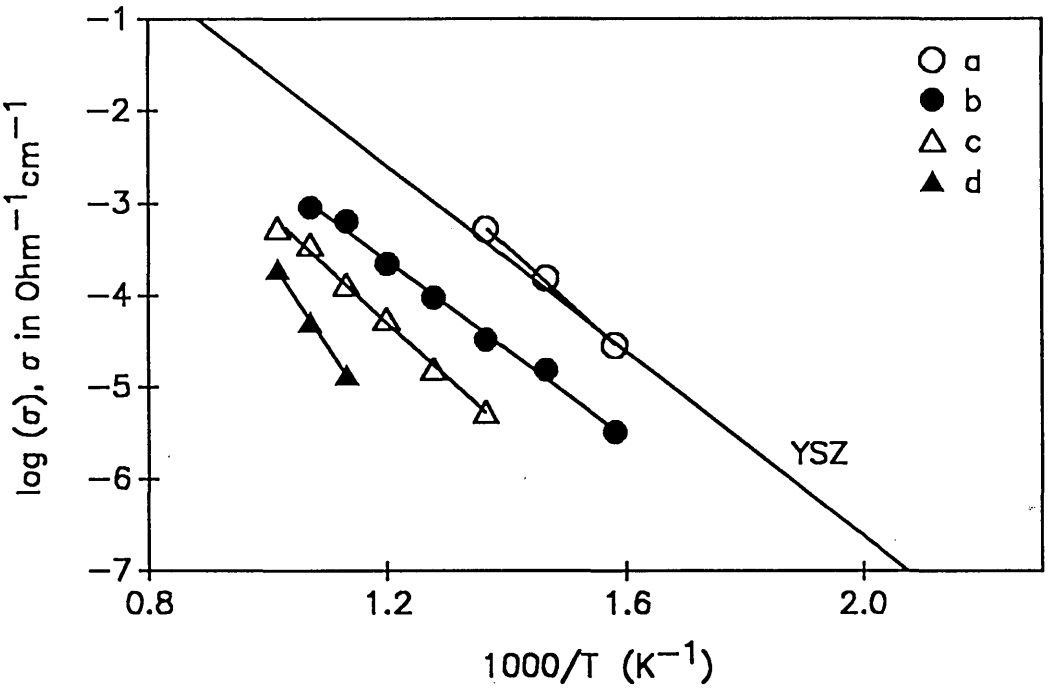

Figure 6.16: Temperature dependence of the conductivity contributions of the cell Pt/YSZ/BPSCCO/YSZ/Pt. The conductivity of YSZ coincides with that of contribution a.

the contribution b of the cell YSZ/Ag/YSZ). In this case, the same argument as for the BiSm cell, can be put forward; the YSZ/BPSCCO interface behaves exactly like the YSZ/YBCO and in a similar way to the YSZ/Ag interface.

Nevertheless, the conclusion from comparison of the results of the two cells having BPSCCO as the mixed conductor is that none of the other contributions have the same values in the two assemblies, in which case they would attributed to the conductivity of BPSCCO.

Measurements on the YSZ/BPSCCO/YSZ cell were performed by X. Turrillas.

6.3.5. Model for AC data

The information obtained from the impedance spectroscopy measurements using different blocking electrodes and different mixed conductors provides a basis for the interpretation of the observed conductivity contributions.

A general consideration of the number of conductivity contributions (semicircles in $Z'-Z''$ plots) for the different cells examined, shows that (table 6.2):

(i) One more contribution is obtained when YSZ is used instead of BiSm in the YBCO and BSCCO containing cells, and

(ii) One contribution more than when BSCCO is used, appears when YBCO is the mixed conductor.

Table 6.2: Number of conductivity contributions for the different cells

Mixed conductors	Blocking electrodes BiSm	YSZ
Ag	4	4
YBCO	4	5
BSCCO	3	4

An explanation for (i) can be that the Pt/YSZ interface is much more resistive than the Pt/BiSm which cannot be distinguished since there are other, possibly overlapping contributions.

From (ii), the cells containing YBCO obviously have an extra characteristic that should be taken into account for further consideration. It could be due to a secondary conductivity route like short circuiting through triple contacts, grain boundary conductivity or conductivity

through cracks or other imperfections.

Examination of the conductivity contributions showed that in the cells examined here, the highest conductivity (and highest frequency) semicircle was due to the blocking electrodes. Attention has to be paid in the calculation of resistivity from resistance, so that the dimensions of the blocking electrolytes are used for this contribution. On the other hand, in order to calculate resistivity values that are or might be related with the mixed conductor, its thickness was considered.

The contribution usually described as b has been attributed to the blocking electrode/mixed conductor interface. In all the BiSm containing cells (without mixed conductor, with YBCO, BPSCCO) it has the same values versus temperature, while in the case of Ag, it has the same slope but higher values. In the YSZ cell with YBCO it also has the same values as the YSZ with BPSCCO. Similarly, higher values are obtained when Ag is used, but the slope is the same as that in the other YSZ containing cells.

Using either YSZ or BiSm, Ag makes a better contact probably because of plastic deformation, since it has a very low melting point of 962 C [188]. After the measurements, Ag was found to have adhered firmly to the YSZ or BiSm pellets. Higher conductivity values for contribution b in the cells containing Ag is thus justified.

The same contribution has been attributed to the interface by Fabry et al. [219] for the YSZ/YSZ cell and also by Maier et al. [217] using the YSZ/YBCO/YSZ cell.

For the other contributions, one is probably due to the electrode effect (Pt/YSZ interface). Since, however, there was no agreement of any of the contributions when comparing cells with the same mixed conductor but different blocking electrodes and since the Ag conductivity could not be determined, it seems that impedance spectroscopy applied under the present conditions cannot assist in the determination of the oxygen conductivity of mixed conductors.

On the other hand Vischjager et al. [127] and Maier et al. [208,220] claim that they determined the oxygen conductivity of YBCO; there is no agreement, however, between their results. In one case [127] the a and b conductivity contributions are assigned to bulk and grain boundary conductivities of the mixed conductor (YBCO). In the other case [208,220] not enough information is given as to how the oxygen conductivity was calculated. Preliminary AC data collected in collaboration with Delft University will be published [221].

6.4. DC polarization experimental considerations

6.4.1. Non-linearity of I-V curves

When an electrical circuit or in the particular case, an electrochemical cell, has ohmic behaviour, the resulting resistance is constant irrespective of the currents/voltages used.

Examination of the cells employed here, showed that under certain conditions, application of DC currents of different intensities resulted in resistances varying by a factor of 4 or in some cases even more.

In terms of current versus voltage behaviour, an ohmic system gives a straight line. A typical example of the behaviour that can arise using complex electrochemical cells, is shown in figure 6.17. At small currents/voltages there is a large deviation from linearity which becomes smaller as the current/voltage is increased. For the cell YSZ/Ag/YSZ, small deviations were detected at higher temperatures (700-800 C), which became larger at lower temperatures (<=600 C). Taking into account that the voltage cannot be increased considerably since the potential created might affect the electrolytes, it seems that there is a temperature-voltage "window" of ranges, under which measurements can be performed so that the system will display ohmic behaviour. When the overall conductivity of the cell becomes very small, large voltages are necessary in order to enter the linear range of I-V plots and therefore a lower temperature limit exists for these measurements.

When 8YSZ is used as the blocking electrolyte, the cell will display linear (ohmic) behaviour if it is operated at temperatures higher than 500 C, since its conductivity drops significantly below this temperature. On the other hand, BiSm is a better oxygen conductor and can be used at even lower temperatures, employing reasonably small voltages (1 V max), so that no problem, such as blackening (reduction) of the electrolyte occurs.

6.4.2. Voltage vs. time behaviour

Before each measurement, a time of one hour was allowed for equilibration of the cells at each temperature.

In the way that the DC technique is applied here, steady state measurements are necessary for the calculation of conductivity. On the application of a current, however, the voltage developed along the

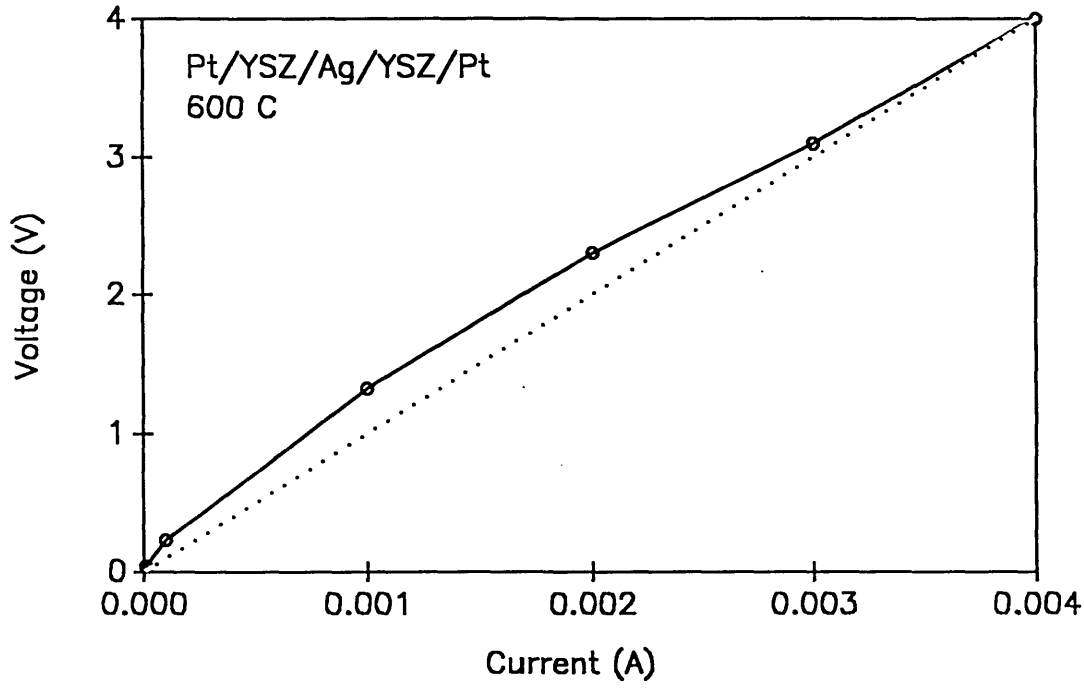

Figure 6.17: The deviation of the I–V (current–voltage) curve from linearity for the cell Pt/YSZ/Ag/YSZ/Pt at 600 C in air. At high voltages, values approach Ohm's law (dotted line).

complex cell is only stabilized after a certain time.

The behaviour of the voltage of the YSZ/YBCO/YSZ cell at different temperatures can be seen in figure 6.18. At 812 C the voltage decreases and about 20 min. are enough to reach equilibrium. At lower temperatures the voltage drops and and even after 45 min., equilibrium was not reached. Measurements were stopped at that point since after studying another cell for 2 days, it was estimated that the error would be less than 5%.

Examination of the voltage of the cell YSZ/Ag/YSZ (figure 6.19) shows that since Ag is a faster conductor than YBCO, equilibrium is achieved in a much shorter time. It has to be noted that even though at both 600 and 800 C the voltage increases to reach a steady value, at 700 C it increases initially only to start decreasing after the first 3–5 min. Other measurements on Ag performed over 1–4 h. indicated either a very small change (increase/decrease) or fluctuation of the voltage around a certain value.

As a result, the time used in order to obtain equilibrium values for the voltage across the cell varied for the different cell assemblies, depending on the temperature and the materials examined (both the blocking electrode and the mixed conductor).

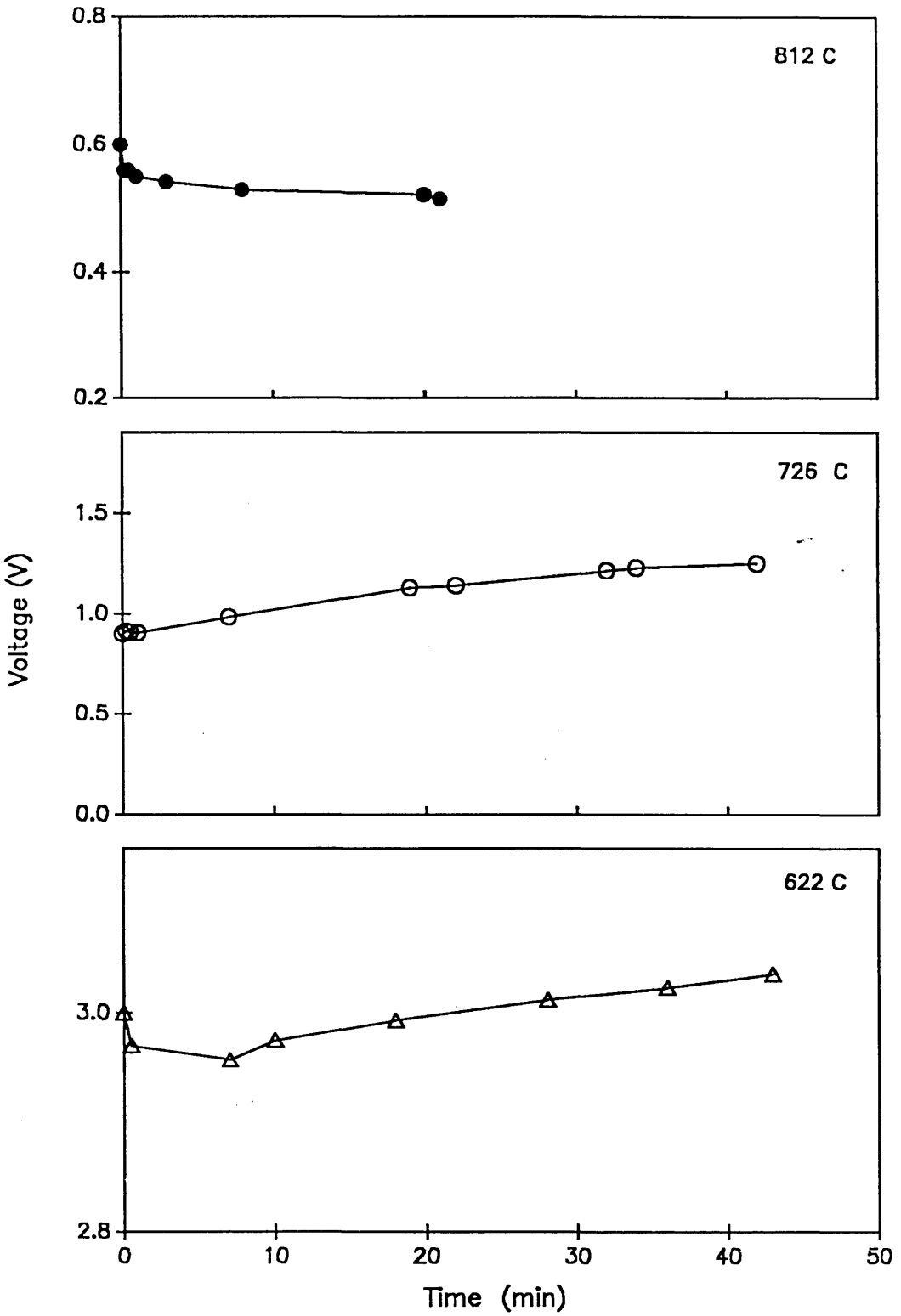

Figure 6.18: The time dependence of the voltage across the YSZ/YBCO/YSZ cell at different temperatures in oxygen. Current= 1 mA.

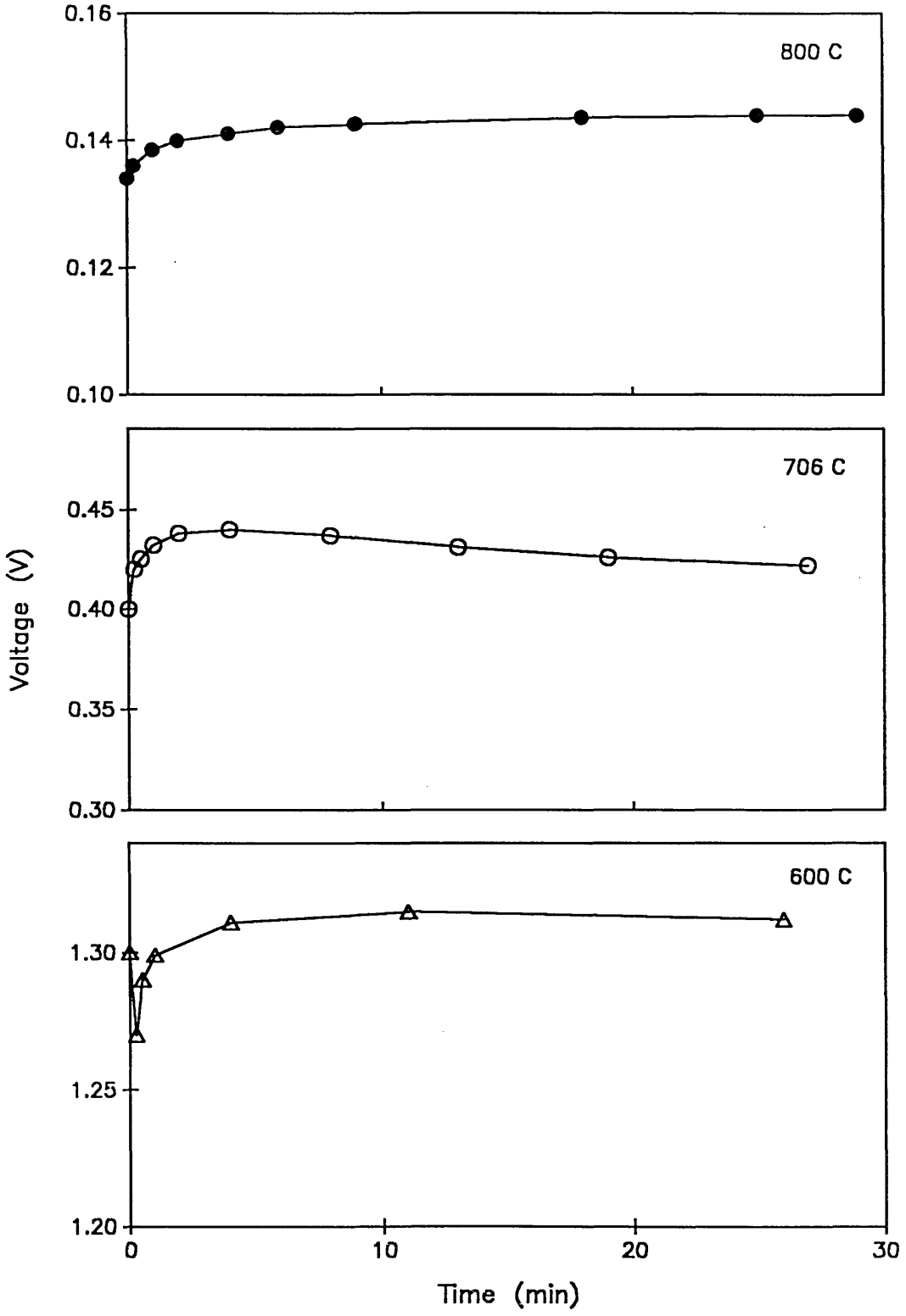

Figure 6.19: The time dependence of the voltage across the YSZ/Ag/YSZ cell at different temperatures in air. Current= 1 mA.

6.5. DC results

6.5.1. Ag results

Ag was examined by the DC polarisation technique, in air. When the YSZ/Ag/YSZ cell was employed, a time of 30 min. was shown to be enough for equilibrium in the range 600-800 C, when a current of 1 mA was used. For the BiSm/Ag/BiSm cell, times between 60 and 100 min. were used, even though changes of less than 2% occurred after the first 10 min. at 450 and 475 C, using a current of 10 μA.

The conductivity of oxygen in Ag versus temperature is presented in figure 6.20. It can be seen that values determined from the BiSm/Ag/BiSm cell at lower temperatures agree with those determined using the YSZ/Ag/YSZ cell at higher temperatures. This is an important finding since it signifies that the same property is measured in both cells. Even more significantly, these results agree with the conductivity data (solid line) calculated using the results of Ramanarayanan and Rapp [216].

6.5.2. YBCO results

DC measurements were similarly performed in YBCO, in O_2, using YSZ as the blocking electrolyte. A series of measurements in the range 480-600 C, using a current of 0.1 mA, resulted in voltages between 0.7 and 4 V. The cell voltage was monitored over long times (24-55 hours) in order to examine the cell behaviour. It was concluded that after approximately two hours, the voltage was stabilized at a certain value and subsequently fluctuated around it in a range of 0.3 to 2%. The YBCO sample used had a density of 5.51 g/cm^3 (86% of X-ray).

The second series of measurements was performed with different YSZ and YBCO samples (YBCO density 4.42 g/cm^3 - 69% of X-ray), in the range 622-812 C. A current of 1mA was employed and voltages between 0.5 and 3 V were obtained. A time of approximately 20-45 min. was allowed for equilibration as seen in figure 6.18.

In figure 6.21 the diffusivity of YBCO versus temperature is shown. It can be seen that results from the two different assemblies cannot be distinguished. One measurement, performed with BiSm electrodes, resulted in a conductivity value of 3.4×10^{-5} Ohm^{-1}cm^{-1} at around 600 C which is near the values obtained with the YSZ electrodes.

6.5.3. BPSCCO results

A BPSCCO sample was also examined over the range 500–705 C, using a YSZ/BPSCCO/YSZ cell. The oxygen diffusivity results are shown in figure 6.21, in comparison with the diffusivity of YBCO. BPSCCO has a higher diffusivity than YBCO, even though it does not have an oxygen deficiency or stoichiometry variations as does YBCO.

It has to be mentioned, however, that since the BPSCCO sample was multiphase (with 2212 as the majority phase), the oxygen diffusivity obtained here represents an average of all the phases present.

Preliminary measurements for YBCO and BPSCCO oxygen mass transport have been published [222].

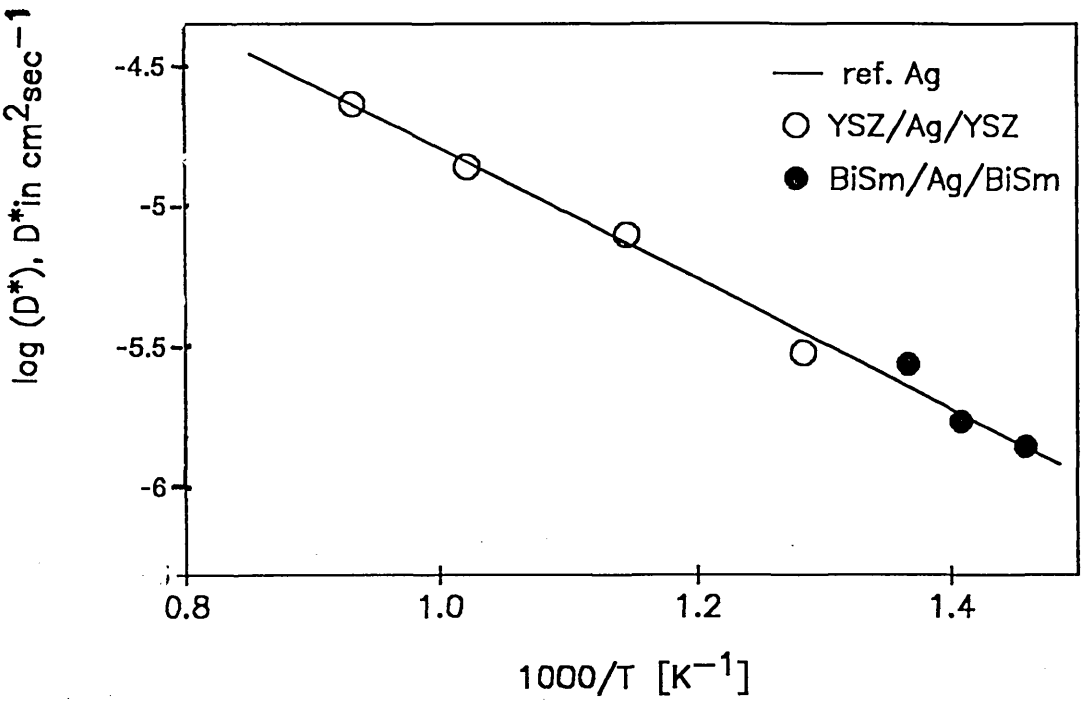

Figure 6.20: The oxygen diffusivity of Ag from the DC polarisation method versus temperature, in air. Solid line represents results calculated from reference [216].

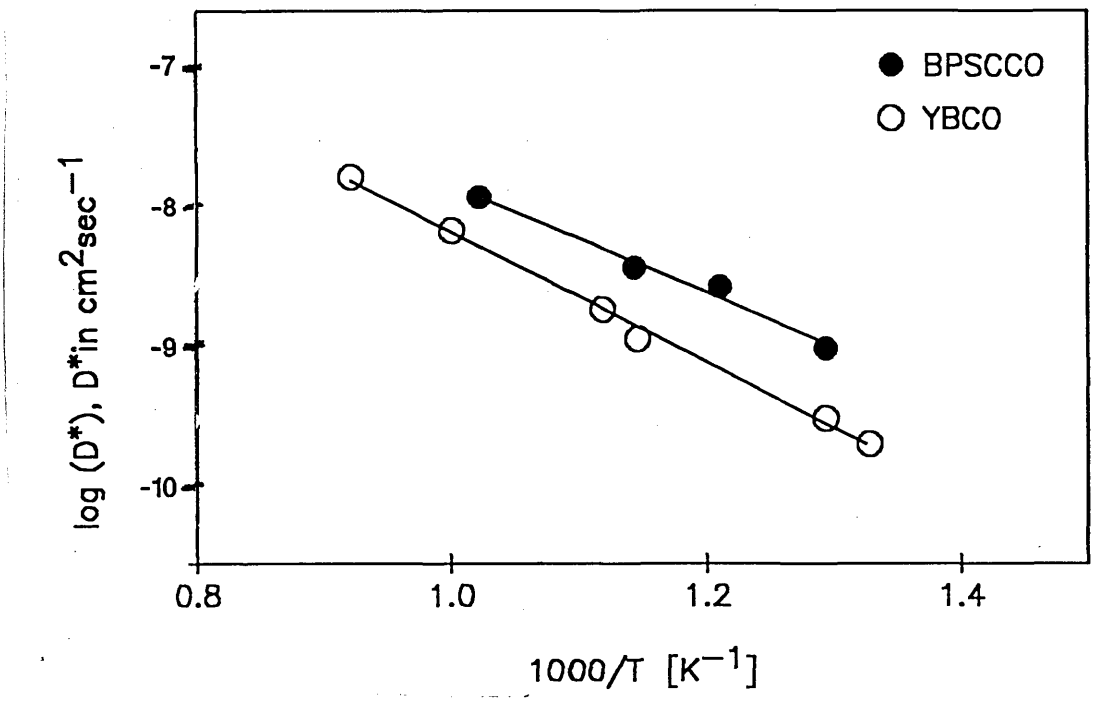

Figure 6.21: Oxygen diffusivity versus temperature for YBCO and BPSCCO by the DC polarisation technique.

6.6. Discussion: conductivity and diffusion coefficient

6.6.1. Ag

For the calculation of conductivity (σ_O), oxygen diffusion (D_O) and solubility (n_O) data were used in the relation (6.3):

$$\frac{\sigma_O}{D_O^*} = \frac{n_O\, q_O^2}{k\, T} \qquad (6.3)$$

Since the moving species are oxygen ions, the charge q_O is equal to the charge of two electrons (q_O=2e). The problem in the application of this equation for Ag is that the self diffusion coefficient (D_O^*) is necessary, while only chemical diffusion coefficient data are available. From oxygen solubility data in liquid silver in oxygen pressures up to 1 atm. [223], it was shown that Sievert's Law (Henry's Law) is obeyed. This implies that in solid silver, where oxygen solubility is even lower, Henri's Law will be followed too. It would be, therefore, safe to assume that the thermodynamic factor that would enable the conversion of chemical to self diffusion coefficient values is equal to 1. As a result, direct comparison of the (self) diffusion coefficients calculated from conductivity data with the (chemical) ones from the literature is possible.

Using the conductivity data from the DC technique applied here in equation 6.3, the oxygen diffusion coefficient in Ag can be calculated to give:

$$D^* = 4.98\times10^{-3} \exp[\ (\ 0.50 \pm 0.13\ \text{eV})\ /\ kT\ ]$$

The pre-exponential factor can be expressed as exp(−5.3 ± 2.0). A confidence level of 95% was considered for the calculation of the confidence interval. Comparing this with results from [210, 216, 218] from table 6.1, a very good agreement can be observed, as is also shown in figure 6.20.

It can be concluded that the DC method gives satisfactory results, especially since cell assemblies provide consistent data irrespectively of the blocking electrodes employed.

6.6.2. YBCO

In order to apply the equation 6.3 for the calculation of the self diffusion coefficient of YBCO from oxygen conductivity data, the charge (q_O) and the available sites (n_O) for the moving species have to be used.

As in the case of Ag, a charge of two electrons has been assumed. The available sites for oxygen, taking into account that conduction takes place on the basal plane (see chapter 2.4), are the O5 sites, therefore, one site per cell is available. Using the cell volume of YBCO, this is calculated to be $n_O = 5.78 \times 10^{21}$ sites/cm^3. It can be argued that the oxygen deficiency at temperatures higher than 400–450 C should be taken into account; however this would not affect the results significantly. Instead of one site, 1.6–1.7 sites would be available at the highest temperatures which is not a significant factor when exponentially varying values are considered.

Calculation of the self diffusion coefficients from the conductivity data presented in figure 6.21 and fitting, results in the following relation:

$$D^* = 5.8 \times 10^{-4} \exp [(0.99 \pm 0.11 \text{ eV})/ kT]$$

for the diffusion coefficient of oxygen in YBCO. The pre-exponential factor can be expressed as exp(−7.44 ± 1.5) for a 95% confidence level.

Comparison of this diffusion coefficient with the available literature data in figure 6.22 indicates considerable agreement with the data of Routbort et al. [119] and Sabras et al. [224], which are considered to be reliable since the $^{16}O/^{18}O$ exchange/SIMS method was used to obtain them.

A large spread of data (± 2 or even 3 orders of magnitude) from different measurements can also be observed especially when different experimental techniques have been used. In some cases, even the same techniques give different results. This could be due to the fact that different processes might be measured. Routbort et al. [119], apart from the average diffusion coefficient shown in figure 6.22, measured a slow diffusion component in the c-axis direction of single crystals, while on the other hand, Sabras et al. [224] also measured a much faster diffusion component attributing it to grain boundary diffusion. It is also possible that surface exchange might be influencing some of the other measurements and in this way the largely different values and activation energies obtained can be explained.

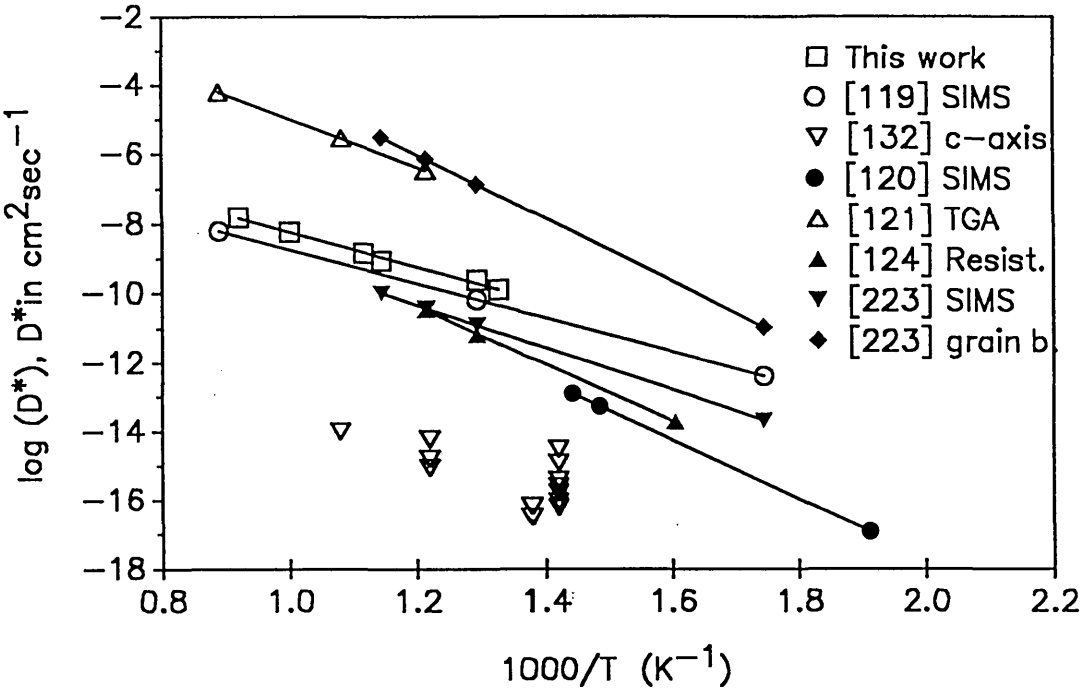

Figure 6.22: The oxygen diffusion coefficient of YBCO versus temperature. Comparison with literature results.

6.7. Conclusions

Two measurement techniques have been employed, using a complex electrochemical cell assembly, in order to measure the oxygen conductivity in mixed conductors and especially in Ag, YBCO and BSPCCO.

Impedance spectroscopy measurements were performed with either YSZ or BiSm as the electron blocking electrolytes. The magnitude of the AC signal oscillating level was found to have practically no effect between 20-110 mV. The time allowed for equilibration was set at one hour since no systematic behaviour could be observed to the increase of some of the conductivity contributions. Also, conductivity values were found to be higher when cooling a sample rather than when heating it and that was attributed to either the establishment of better contacts at high temperatures or to the fact that the mixed conductors were only partially equilibrated. Measurements were performed when cooling the cell.

Examination of the spectra obtained from the Pt/BiSm/BiSm/Pt and Pt/YSZ/YSZ/Pt cells, showed that the conductivity of the blocking electrolyte could be identified and a second conductivity contribution was attributed to the resistance of the electrolyte-electrolyte interface.

For the complex cells Pt/BiSm/Ag/BiSm/Pt and Pt/YSZ/Ag/YSZ/Pt, several conductivity contributions were obtained but none of them could be attributed to the conductivity of Ag. Using YBCO or BPSCCO in the place of the mixed conductor in these cells, the conductivity contributions of the blocking electrolyte and possibly of the blocking electrolyte/mixed conductor interface were identified, however, there was no indication that any of the other contributions were due to the mixed conductor. It was, therefore, concluded that in the range which these measurements were performed (temperature 300-800 C, frequency 13MHz-5Hz) no information on the oxygen conductivity of the mixed conductors could be obtained.

Measurements of the complex cells by DC polarisation presented a problem because of non-linearity of I-V curves (non-ohmic behaviour) and selection of current/voltage in the linear region was necessary. The time required for the stabilization of the voltage developed across the cell had also to be taken under consideration. For the cell containing Ag, a shorter time was necessary than for the YBCO or BPSCCO containing ones. In general, higher temperatures also resulted in shorter stabilization times.

DC polarization gave consistent results using either BiSm or YSZ blocking electrodes and the oxygen conductivity of Ag was successfully determined. The diffusion coefficient was calculated from conductivity results for YBCO and it was found to agree well with some of the results presented in the literature. Results for BPSCCO are the first to be presented and a slightly higher oxygen conductivity than for YBCO was found for this multiphase sample.

Problems inherent to the techniques applied here were presented, such as a contribution of the blocking electrolyte/ mixed conductor interface, short circuiting routes for oxygen, a possible interference from the hole conductivity of the blocking electrolytes, sample equilibrium and problems because of porosity/ inhomogeneity of the materials to be examined. These problems have to be taken under consideration when the DC or impedance techniques are applied. A four-point ionic arrangement, instead of the two point employed here, could be used to eliminate sources of error such as contact resistances, as suggested by Dudley and Steele [225].

7. FINAL CONCLUSIONS

The development of fabrication technologies, as well as the knowledge of the behaviour and the properties of the material are necessary in order to produce commercial applications using the unique properties of ceramic high T_c superconductors.

A number of fabrication techniques for YBCO were examined and compared as part of this work. Optimization of the starting materials for Ba for the solid state preparation method, where a mixture of the precursors is ground and fired in order to give the right phase, showed that BaO_2 gives very good results, while $BaCO_3$ results in material of slightly lower quality when the final product was examined by XRD, SEM and T_c measurements. $Ba(OH_2)$ as a precursor for Ba, results in multiphase material.

Evaporation of nitrates was a second technique employed and it resulted in non-reproducible results, without offering any advantage over the solid state route.

Application of freeze-drying gave poor results, steps were made, however, in order to identify the reasons. Adjustment of the pH of the solutions used, made the stage of removing the water from the frozen droplets possible without melting. The remaining salts incorporated water in the crystalline state and when heating, they melted, losing any advantages over the particle size or chemical homogeneity, compared to other methods. Changing the nitrates to other salts, or modifying the apparatus would, therefore, be necessary in order to apply this method successfully.

Mist pyrolysis, using an ultrasonic atomizer and passing the fine mist through a furnace, resulted in very good, single phase YBCO powders, with particle size ranging from 0.2-0.6 μm. The bulk material produced had good superconductive properties. Further work should be concentrated on the development of this technique, optimization of the use of equipment and scaling-up of the production to pilot plant (and later on to commercial) scale.

Potassium doping in the place of Ba in $REBa_2Cu_3O_{7-\delta}$ resulted in a different behaviour when different rare earths (RE) were used in the central cation site. There was little or no effect when Y was used (apart from grain enlargement under certain conditions), while a depression of T_c and appearance of second phases was observed for Er, Gd and Nd. In most cases, only a small amount of the potassium, originally included in

the sample, remained after firing. The grain enlargement observed can be beneficial for producing samples with large, oriented grains.

The orthorhombic-to-tetragonal transition was determined to occur between 650 and 675 C. An attempt to influence the transition temperature by potassium doping had, according to *in-situ* neutron diffraction, no result, even though X-ray diffraction on quenched material indicated an increase of the O-T transition temperature of 100 degrees for 10% K-doping.

Oxygen mass transport is important for YBCO, since superconductivity depends on oxygen stoichiometry. Two electrochemical techniques, impedance spectroscopy and DC polarization were employed, in order to determine the oxygen conductivity and diffusion coefficient in mixed conductors. Ag was examined as a reference material, in order to evaluate these techniques. The BSCCO superconductor was also examined.

A number of conductivity contributions from the complex cells employed was observed by impedance spectroscopy. Some of these contributions were identified, none of them, however, could be attributed to the conductivity of the mixed conductors. Further work is needed so that the various contributions can be unambiguously attributed to specific physical processes. This work should include the comparison of dielectric constants for each contribution, the measurement of the "electrode effect" by examination of the Pt/YSZ/Pt cell with Pt electrodes of the same quality and also the examination of some of the common characteristics of the behaviour of conductivity contributions of different cells versus temperature.

DC polarisation measurements were successful in the determination of the oxygen conductivity for Ag and results for YBCO agree well with some of the results presented in the literature. The measurements for BPSCCO show an average oxygen conductivity of the multiphase sample, which is higher than that for YBCO.

Examination of Ag in different atmospheres is necessary, and four-point contact assemblies can be used in order to obtain more accurate measurements. $^{16}O/^{18}O$ exchange and SIMS can provide self diffusion coefficients to be compared with those calculated using the electrochemical techniques.

Experimental precautions and problems inherent to the electrochemical techniques employed here were also presented. Equilibrium of the samples, contact resistances short circuiting routes and other possible sources of interference have to be taken under consideration when these techniques are applied.

APPENDIX 1: The relation between chemical and self diffusion coefficient

If the relation 2.4.18 is considered and the following equation A1.1 is used instead of 2.4.19 (activity is not considered equal to concentration),

$$d\mu_i = R\ T\ d\ln a_i \qquad \text{(A1.1)}$$

the following results:

$$J_i = - c_i B_i \frac{R\ T}{N} \frac{d\ln a_i}{dx} \qquad \text{(A1.2)}$$

Substituting B_i from the Nerst–Einstein equation (2.4.21) and c_i from A1.3:

$$c_i = \frac{dc_i}{d\ln c_i} \qquad \text{(A1.3)}$$

the relation obtained is:

$$J_i = - \frac{dc_i}{d\ln c_i} \frac{D^*}{kT} \frac{RT}{N} \frac{d\ln a_i}{dx} \qquad \text{(A1.4)}$$

By rearranging, it can be observed that it takes the form of the first law of Fick:

$$J_i = - D^* \frac{d\ln a_i}{d\ln c_i} \frac{dc_i}{dx} \qquad \text{(A1.5)}$$

where the chemical diffusion coefficient is:

$$\tilde{D} = D^* \frac{d\ln a_i}{d\ln c_i} \qquad \text{(A1.6)}$$

The expression $(d\ln a_i / d\ln c_i)$ is called the *thermodynamic factor.*

APPENDIX 2: The calculation of the thermodynamic factor dlna/dlnc for YBCO

Assuming that oxygen diffusion takes place through the oxygen sites in the Cu1 plane, as suggested by figure 2.14 and that the atomic jump is isotropic, neglecting the site distribution in the orthorhombic phase, the following relation can be derived:

$$\tilde{D} = D^* \frac{d\ln a_O}{d\ln c_O} = D^* \frac{d\log P_{O_2}}{d\log y} \qquad (A1.7)$$

where P_{O_2} is the partial oxygen pressure and c_O is the concentration of oxygen atoms in the Cu1 plane in $YBa_2Cu_3O_{6+y}$. Using the ($\log P_{O_2}$) vs. ($\log y$) data obtained by Kishio et al. [121] from thermogravimetric measurements (see figure A.1), the thermodynamic factor can be calculated from the slopes of the curves at $\log P_{O_2}=0$. The results are given below in the table A.1. This derivation assumes a very simple relationship between the vacancy concentration and the oxygen partial pressure. More complicated relationships can be derived [226].

Table A.1: The thermodynamic factor at different temperatures.

T(C)	Therm.factor
350	113
400	86.3
450	66.5
500	36
550	22.8
600	15.4
650	10.8
700	9.82
750	8.16
800	6.5
850	5.7
900	4.34

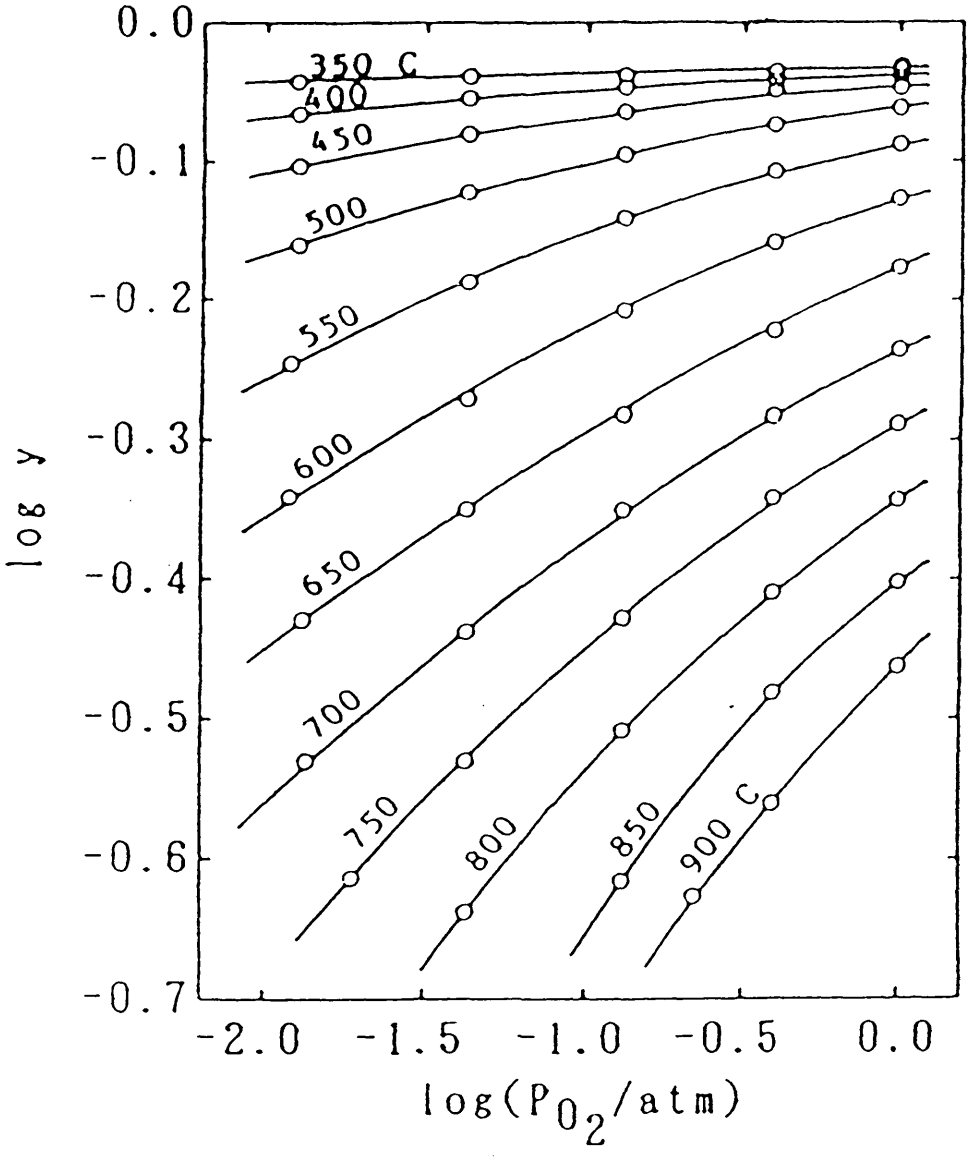

Figure A.1: The relation between log y and log P_{O2} for $YBa_2Cu_3O_{6+y}$. The thermodynamic factor, connecting chemical and self diffusion coefficients, can be obtained from the slope of these curves.

APPENDIX 3: Typical Impedance Spectroscopy Data

These data were collected by the microcomputer controlling the HP frequency response analyser as described in section 3.3.10 (fig.3.7).

File : BISM27AG.DAT
Cell : Pt/BiSm/Ag/BiSm/Pt
Furnace Temperature : 500 C
Sample Temperature : 467 C
Atmosphere : O_2

Frequency (Hz)	Z real (Ohms)	Z imag. (Ohms)
5.0000000000E+00	1.1400000000E+03	-3.5000000000E+02
5.0110000000E+00	1.1400000000E+03	-3.5000000000E+02
5.6230000000E+00	1.1100000000E+03	-3.5000000000E+02
6.3090000000E+00	1.0800000000E+03	-3.4000000000E+02
7.0790000000E+00	1.0600000000E+03	-3.4000000000E+02
7.9430000000E+00	1.0300000000E+03	-3.3000000000E+02
8.9120000000E+00	1.0100000000E+03	-3.2000000000E+02
1.0000000000E+01	9.8000000000E+02	-3.1000000000E+02
1.1220000000E+01	9.6000000000E+02	-3.0000000000E+02
1.2589000000E+01	9.4000000000E+02	-3.0000000000E+02
1.4125000000E+01	9.2000000000E+02	-2.9000000000E+02
1.5848000000E+01	9.0000000000E+02	-2.8000000000E+02
1.7782000000E+01	8.8000000000E+02	-2.7000000000E+02
1.9952000000E+01	8.6000000000E+02	-2.6000000000E+02
2.2387000000E+01	8.4000000000E+02	-2.6000000000E+02
2.5118000000E+01	8.2000000000E+02	-2.5000000000E+02
2.8183000000E+01	8.0000000000E+02	-2.4000000000E+02
3.1622000000E+01	7.8000000000E+02	-2.3000000000E+02
3.5481000000E+01	7.7000000000E+02	-2.2000000000E+02
3.9810000000E+01	7.5000000000E+02	-2.2000000000E+02
4.4668000000E+01	7.4000000000E+02	-2.1000000000E+02
5.0118000000E+01	7.2000000000E+02	-2.0000000000E+02
5.6234000000E+01	7.1000000000E+02	-2.0000000000E+02
6.3095000000E+01	7.0000000000E+02	-1.9000000000E+02
7.0794000000E+01	6.8000000000E+02	-1.8000000000E+02
7.9432000000E+01	6.7000000000E+02	-1.8000000000E+02
8.9125000000E+01	6.6000000000E+02	-1.7000000000E+02
1.0000000000E+02	6.5000000000E+02	-1.6000000000E+02
1.1220100000E+02	6.4000000000E+02	-1.6000000000E+02
1.2589200000E+02	6.3000000000E+02	-1.5000000000E+02
1.4125300000E+02	6.2000000000E+02	-1.5000000000E+02
1.5848900000E+02	6.1000000000E+02	-1.4000000000E+02
1.7782700000E+02	6.0000000000E+02	-1.4000000000E+02
1.9952600000E+02	5.9000000000E+02	-1.3000000000E+02
2.2387200000E+02	5.8000000000E+02	-1.3000000000E+02
2.5118800000E+02	5.7000000000E+02	-1.2000000000E+02
2.8183800000E+02	5.6000000000E+02	-1.2000000000E+02
3.1622700000E+02	5.6000000000E+02	-1.1000000000E+02
3.5481300000E+02	5.5000000000E+02	-1.1000000000E+02
3.9810700000E+02	5.4000000000E+02	-1.0000000000E+02
4.4668300000E+02	5.3500000000E+02	-9.9000000000E+01
5.0118700000E+02	5.2900000000E+02	-9.5000000000E+01
5.6234100000E+02	5.2300000000E+02	-9.2000000000E+01
6.3095700000E+02	5.1700000000E+02	-8.8000000000E+01
7.0794500000E+02	5.1100000000E+02	-8.5000000000E+01
7.9432800000E+02	5.0500000000E+02	-8.1000000000E+01

8.9125000000E+02	5.0000000000E+02	−7.8000000000E+01
1.0000000000E+03	4.9500000000E+02	−7.5000000000E+01
1.1220180000E+03	4.9000000000E+02	−7.2000000000E+01
1.2589250000E+03	4.8500000000E+02	−6.9000000000E+01
1.4125370000E+03	4.8100000000E+02	−6.7000000000E+01
1.5848930000E+03	4.7600000000E+02	−6.4000000000E+01
1.7782790000E+03	4.7200000000E+02	−6.1000000000E+01
1.9952620000E+03	4.6800000000E+02	−5.9000000000E+01
2.2387210000E+03	4.6400000000E+02	−5.7000000000E+01
2.5118860000E+03	4.6100000000E+02	−5.4000000000E+01
2.8183820000E+03	4.5800000000E+02	−5.2000000000E+01
3.1622770000E+03	4.5400000000E+02	−5.0000000000E+01
3.5481330000E+03	4.5100000000E+02	−4.8000000000E+01
3.9810710000E+03	4.4800000000E+02	−4.6000000000E+01
4.4668350000E+03	4.4500000000E+02	−4.4000000000E+01
5.0118720000E+03	4.4200000000E+02	−4.2000000000E+01
5.6234130000E+03	4.3900000000E+02	−4.0000000000E+01
6.3095730000E+03	4.3700000000E+02	−3.9000000000E+01
7.0794570000E+03	4.3400000000E+02	−3.7000000000E+01
7.9432820000E+03	4.3200000000E+02	−3.5000000000E+01
8.9125090000E+03	4.3000000000E+02	−3.4000000000E+01
1.0000000000E+04	4.2800000000E+02	−3.3000000000E+01
1.1220180000E+04	4.2600000000E+02	−3.1000000000E+01
1.2589250000E+04	4.2400000000E+02	−3.0000000000E+01
1.4125370000E+04	4.2200000000E+02	−2.9000000000E+01
1.5848930000E+04	4.2000000000E+02	−2.7000000000E+01
1.7782790000E+04	4.1800000000E+02	−2.6000000000E+01
1.9952620000E+04	4.1700000000E+02	−2.5000000000E+01
2.2387210000E+04	4.1500000000E+02	−2.4000000000E+01
2.5118860000E+04	4.1400000000E+02	−2.3000000000E+01
2.8183820000E+04	4.1200000000E+02	−2.2000000000E+01
3.1622770000E+04	4.1100000000E+02	−2.1000000000E+01
3.5481330000E+04	4.1000000000E+02	−2.1000000000E+01
3.9810710000E+04	4.0900000000E+02	−2.0000000000E+01
4.4668350000E+04	4.0800000000E+02	−1.9000000000E+01
5.0118720000E+04	4.0700000000E+02	−1.9000000000E+01
5.6234130000E+04	4.0600000000E+02	−1.8000000000E+01
6.3095730000E+04	4.0500000000E+02	−1.8000000000E+01
7.0794570000E+04	4.0400000000E+02	−1.7000000000E+01
7.9432820000E+04	4.0300000000E+02	−1.7000000000E+01
8.9125090000E+04	4.0200000000E+02	−1.7000000000E+01
1.0000000000E+05	4.0100000000E+02	−1.7000000000E+01
1.1220180000E+05	4.0000000000E+02	−1.7000000000E+01
1.2589250000E+05	4.0000000000E+02	−1.7000000000E+01
1.4125370000E+05	3.9900000000E+02	−1.7000000000E+01
1.5848930000E+05	3.9800000000E+02	−1.7000000000E+01
1.7782790000E+05	3.9800000000E+02	−1.8000000000E+01
1.9952620000E+05	3.9700000000E+02	−1.8000000000E+01
2.2387210000E+05	3.9600000000E+02	−1.9000000000E+01
2.5118860000E+05	3.9600000000E+02	−2.0000000000E+01
2.8183820000E+05	3.9500000000E+02	−2.0000000000E+01
3.1622770000E+05	3.9400000000E+02	−2.2000000000E+01
3.5481330000E+05	3.9400000000E+02	−2.3000000000E+01
3.9810710000E+05	3.9300000000E+02	−2.4000000000E+01
4.4668350000E+05	3.9200000000E+02	−2.6000000000E+01
5.0118720000E+05	3.9100000000E+02	−2.8000000000E+01
5.6234130000E+05	3.9000000000E+02	−3.1000000000E+01
6.3095730000E+05	3.8900000000E+02	−3.3000000000E+01
7.0794570000E+05	3.8800000000E+02	−3.6000000000E+01
7.9432820000E+05	3.8700000000E+02	−3.9000000000E+01

8.9125090000E+05	3.8500000000E+02	−4.3000000000E+01
1.0000000000E+06	3.8300000000E+02	−4.7000000000E+01
1.1220180000E+06	3.8100000000E+02	−5.1000000000E+01
1.2589250000E+06	3.7800000000E+02	−5.6000000000E+01
1.4125370000E+06	3.7600000000E+02	−6.1000000000E+01
1.5848930000E+06	3.7200000000E+02	−6.7000000000E+01
1.7782790000E+06	3.6800000000E+02	−7.3000000000E+01
1.9952620000E+06	3.6300000000E+02	−8.0000000000E+01
2.2387210000E+06	3.5600000000E+02	−8.7000000000E+01
2.5118860000E+06	3.4900000000E+02	−9.4000000000E+01
2.8183820000E+06	3.4100000000E+02	−1.0100000000E+02
3.1622770000E+06	3.3200000000E+02	−1.0800000000E+02
3.5481330000E+06	3.2000000000E+02	−1.1500000000E+02
3.9810710000E+06	3.0800000000E+02	−1.2100000000E+02
4.4668350000E+06	2.9400000000E+02	−1.2600000000E+02
5.0118720000E+06	2.7900000000E+02	−1.3000000000E+02
5.6234130000E+06	2.6200000000E+02	−1.3200000000E+02
6.3095730000E+06	2.4500000000E+02	−1.3300000000E+02
7.0794570000E+06	2.2600000000E+02	−1.3100000000E+02
7.9432820000E+06	2.0700000000E+02	−1.2600000000E+02
8.9125090000E+06	1.8900000000E+02	−1.1900000000E+02
1.0000000000E+07	1.7200000000E+02	−1.1100000000E+02
1.1220185000E+07	1.5500000000E+02	−1.0000000000E+02
1.2589254000E+07	1.4000000000E+02	−8.8000000000E+01
1.3000000000E+07	1.3600000000E+02	−8.4000000000E+01

REFERENCES

1. Kingery,W.D., p.31 in **High Tech Ceramics** (Materials Science Monographs, 38A), Ed. Vincenzini,P., Elsevier Sci.Publ., Amsterdam, 1987.

2. Schober,M., *Ceramic Bulletin*, 66,1698(1987)

3. Newnham,R.E., *Adv.Ceram.Mat.* 3,12(1988)

4. Kittel,C., p.51 in **Introduction to Solid State Physics**, (2nd ed., New York John Wiley & sons, Inc., 1956)

5. Bednorz, J.G. and Müller, K.A., *Z.Phys.* B64,189(1986)

6. **CRC Handbook of Chemistry and Physics** (1986-1987) 67th ed., pp.E92-E100, CRC Press Inc., Baca Raton, Florida.

7. Sleight,A.W, Gillson, J.L. and Bierstedt, P.E., *Solid St. Commun.* 17,27(1975)

8. Cava, R.J., Van Dover, R.B., Batlogg, B. and Rietman, E.A., *Phys.Rev.Lett.* 58,408(1987)

9. Tarascon, J.M., Greene, L.H., Mc Kinnon, W.R., Hull, G.W. and Geballe, T.H., *Science*, 235,1373(1987)

10. Wu,M.K.,Ashburn,J.R., Torng,C.J., Hor,P.H., Meng,R.L., Gao,L., Huang,J.L., Wang,Q. and Chu,C.W., *Phys.Rev.Lett.* 58,908(1987)

11. Maeda,H., Tanaka,Y., Fukutomi,M. and Asano,T., *Jpn.J.Appl. Phys.Lett.*, 27,L209(1988)

12. Sheng,Z.Z. and Herrmann,A.M., *Nature*, 332,138(1988)

13. Wyatt,O.H. and Dew-Hughes,D. pp.526-528 in **Metals, Ceramics and Polymers**, Cambridge Univ.Press (1974)

14. Rosenberg,H.M., p.126 in **The Solid State**, 3rd ed. Oxford University Press (1989)

15. Blakemore,J.S., p.270 in **Solid State Physics**, 2nd ed. W.B.Saunders Co., Philadelphia (1974)

16. Bardeen,J., Cooper,L.N. and Schrieffer,J.R., *Phys.Rev.* 108,1175(1957)

17. Mott,N., *Nature*, 327,185(1987)

18. Campbell,P., *Nature*, 330,21(1987)

19. Anderson,P.W. and Abrahams,E., *Nature*, 327,363(1987)

20. Tarascon,J.M., Barboux,P., Micheli,P.F., Greene,L.H., Hull,G.W.,

Eibschultz,M. and Sunshine,S.A. *Phys.Rev.* B37,7458(1988)

21. Emery,V.J. *Nature*, 328,756(1987)

22. Bray,J.W. and Hart,H.R.Jr. p.516 in Electronic Ceramics/ Properties, Devices and Applications, ed. Levinson,L.M., Marcel Dekker Inc. NY (1988)

23. Kingery,W.D., Bowen,H.K., Uhlmann,D.R., pp.847-912 in Introduction to Ceramics, (2nd ed., John Willey & Sons, Inc., New York 1976)

24. Schooley,J.J., Hosler,W.R., Cohen,M.L., *Phys.Rev.Lett.* 12,474 (1964)

25. Hulm,J.K., Jones,C.K., Mazelsky,R., Hein,R.A., Gibson,J.W., p.600 in *Proceedings of the 9th International Conference on Low Temperature Physics*, Eds. Daunt,J.G., Edwards,D.O., Milford,F.J., Yaqub,M. (1965)

26. Robin,M.B., Andres,K., Geballe,T.H., Kuebler,N.A., McWhan,D.B., *Phys.Rev.Lett.* 17,917(1966)

27. Sweedler,A.R., Raub,C., Matthias,B.T., *Phys.Lett.* 15,108(1965)

28. Sleight,A.W., Bither,T.A., Biersted,P.E., *Solid State Commun.* 7,299(1969)

29. Johnston,D.C., Prakash,H., Zackariasen,W.H., Viswanathan,R., *Mat.Res.Bull.* 8,777(1973)

30. Cava,R.J., Batlogg,B., Krajewski,J.J., Farrow,R., Rupp Jr,L.W., White,A.E., Short,K., Peck,W.F. and Kometani,T. *Nature*, 332,814(1988)

31. Tokura,Y., Takagi,H. and Ushida,S. *Nature*, 337,345(1989)

32. Sawa,H., Suzuki,S., Watanabe,M., Akimitsu,J., Matsubara,H., Watabe,H., Uchida,S., Kocusho,K., Asano,H., Izumi,F., Takayama-Muromachi,E. *Nature*, 337,347(1989)

33. Cava, R.J., Batlogg, B., Krajewski, J.J., Rupp, L.W., Schneemeyer, L.F., Siegrist, T., Van Dover, R.B., Marsh, P., Peck, W.F., Gallagher P.K., Glarum, S.H., Marshall, J.H., Farrow, R.C., Waszczak, J.V., Hull, R., Trevor P., *Nature,* 336,211(1988)

34. Markert,J.T., Seaman,C.L., Zhou,H. and Maple,B., *Solid St.Commun.* 66,387(1988)

35. Fueki,K., Kitazawa,K., Kishio,K., Hasegawa,T., Ushida,S., Hidenori,T. and Tanaka,S., p.38 in Chemistry of High-Temperature Superconductors, Ed. Nelson,D.L., Whittingham,M.S., George,T.F., ACS Symposium Series 351 (American Chemical Society, Washington DC, 1987)

36. Hor,P.H., Meng,R-.L., Wang,Y.Q., Gao,L., Huang,Z.J., Bechotold,J.,

Forster,K. and Chu,C.W., *Phys.Rev.Lett.* 58,1891(1987)

37. Michel,C., Hervieu,M., Borel,M.M., Grangin,A., Deslandes,F., Provost,J. and Raveau,B., *Z.Phys.* B68,421(1987)

38. Sheng,Z.Z. and Herrmann,A.M., *Nature*, 332,814(1988)

39. Leary,K.J., Loye,H.C., Keller,S.W., Faltens,T.A., Ham,W.K., Michaels,J.N. and Stacy,A.M. *Phys.Rev.Lett.* 59, 1236(1987)

40. Mattauch,H., Bauhofer,W. and Simon,A. *Supercond.Sci. Techn.* 1,167(1988)

41. Lin,Q., Wei,Y., Yan,Q., Chen,G., Zhang,P., Shen,Z., Ni,Y., Yang,Q., Liu,C., Ning,T., Zhao,J., Shao,Y., Han,S. and Li.J. *Sol.Stat.Commun.* 65,869(1987)

42. Takabatake,T., Ishikawa,M., Nakazawa,Y., Oguro,I., Sakakibara,T. and Goto,T., *Jap.J.Appl.Phys.* 26,L978(1987)

43. Ousset,J.C., Ravet,M.F., Maurer,M., Durant,J., Ulmet,J.P., Rakoto,H. and Askenazy,S., *Europhys.Lett.* 4,743(1987)

44. Kupfer,H., Apfelstedt,I., Schauer,W., Fliikiger,K., Meier-Hirmer,R. and Wiihl,H., *Z.Phys.B*, 69,159(1987)

45. Iye,Y., Tamegai,T., Takeya,H. and Takei,H., *Jap.J.Appl.Phys.* 26,L1057(1987)

46. Worthington,T.K., Gallagher,W.J. and Dinger,T.R., *Phys.Rev.Lett.* 59,1160(1987)

47. Sakakibara,T., Goto,T., Iye,Y., MIura,N., Takeya,H. and Takei,H., *Jap.J.Appl.Phys.* 26,L1892(1987)

48. Malozemoff,A.P. pp.71-150 in **Physical Properties of High Temperature Superconductors I** ed. Ginsberg,D.M. World Scientific, Singapore, London (1989)

49. Williams,J.E.C. p.66 in **Superconductivity and its Applications** Pion Ltd, London (1970)

50. Collings,E.W. pp.22-28 in **Applied Superconductivity, Metallurgy and Physics of Titanium Alloys** Vol.2: Applications, Plenum Press, New York, London (1986)

51. Collings,E.W. p.218 in ref. 50

52. Ekin,J.W., Braginski,A.I., Panson,A.J., Janocko,M.A. Capone II,D.W., Zalucek,N.J., Flandermeyer,B., de Lima,O.F., Hong,M., Kwo,J. and Liou,S.H. *J.Appl.Phys.* 62,4821 (1987)

53. Kupfer,H., Green,S.M., Jiang,C., Mei,Y., Luo,H.L., Meier-Hirmer,R. and Politis,C., *Z.Phys.B*, 71,63(1988)

54. Satchell,J.S., Humphreys,R.G., Chew,N.G., Edwards,J.A. and Kane,M.J.,*Nature*, 334,331(1988)

55. Zhang,L., Chen,J., Chan,H. and Harmer,M.P. *J.Am.Ceram.Soc.* 72,1997(1989)

56. Chaudhari,P., Mannhart,J., Dimos,D., Tsuei,C.C., Chi,J., Oprysko,M.M. and Scheuermann,M., *Phys.Rev.Lett.* 60,1653(1988)

57. Dimos,D., Chaudhari,P., Mannhart,J. and LeGoues,F.K. *Phys.Rev.Lett.* 61,219(1988)

58. Ekin,J.W., Peterson,R.L. and Bray,S.L. "Critical Currents of High-Tc Superconductors", invited paper presented at the Materials Research Society International Meeting on Advanced Materials, Tokyo, Japan, May 30 - June 3, 1988.

59. Collings,E.W. pp.423,491 in **Applied Superconductivity, Metallurgy and Physics of Titanium Alloys** Vol.1: Applications, Plenum Press, New York, London (1986)

60. Alford,N.McN., Button,T.W. and Birchall,J.D. *Supercond.Sci.Techn.* 3,26(1990)

61. Miska,K.H., *J.of Metals*, 40(1),14(1988)

62. Dew-Hughes,D. *Metals and Materials*,4,741(1988)

63. Polushkin,V.N. and Vasiliev,B.V. "Investigation of R-F SQUIDs at Liquid Nitrogen Temperatures" presented in "High Temperature Superconductors", Univ. of Birmingham Sept. 19-21, 1989

64. Matsuzawa,H., Osada,T., Ishibashi,Y., Irikura,K., Okamoto,K., Mochizuki,A., Wada,H. and Akitsu,T. *Jap.J.Appl.Phys.* 28,L717(1989)

65. Roth,S.R., Davis,K.Land Dennis,J.R., *Adv.Ceram.Mat.* 2,3B, Special Issue,"Ceramic Superconductors", 303(1987)

66. Frase,K.G. and Clarke, D.R., p.295 in ref. 65

67. Wang,G., Hwu,S.-J., Song,S.N., Ketterson,J.B., Marks,L.D., Poeppelmeier,K.R. and Mason,T.O. p.313 in ref. 65

68. Wong-Ng,W. Roth,R.S., Swartzendruber,L.J., Bennett,L.H., Chiang,C.K., Beech,F. and Hubbard,C.R., p.565 in ref. 65

69. Takada,J., Kitaguchi,H., Osaka,A., Miura,Y., Takahashi,K., Takano,M., Ikeda,Y., Bando,Y., Yamamoto,N., Oka,Y and Tomii,Y.,

Jpn.J.Appl.Phys. 26,L1684(1987)

70. Wagner,G.R., Panson,A.J. and Braginski,A.I., *Phys.Rev.* B36,7124(1987)

71. Kogachi,M., Nakahigashi,K., Nakanishi,S., Fukuoka,N., Sasakura,H., Minamigarra,S., Skibuya,I, Demizu,F., Sawai,H., Tsuboi,T. and Yanase,A., *Jap.J.Appl.Phys.* 26,L1684(1987)

72. Collin,G., Audier,A.C. and Romes,R., *J.Phys.France*, 49,383(1988)

73. Ginley,T.S., Venturini,E.L., Kwak,J.F., Baughman,R.J. and Morosin,B. *J.Mater.Res.* 4,496(1989)

74. Karpinski,J., Kaldis,E. and Rusiecki,S. *J.Less Comm.Met.* 150,207(1989)

75. Cava, R.J., Krajewski,J.J., Peck Jr,W.F., Batlogg,B., Rupp,L.W., Fleming,R.M., James,A.C.W.P. and Marsh,P. *Nature*, 338,328(1989)

76. Miyatake,T., Gotoh,S., Koshizuka,N. and Tanaka,S. *Nature*, 341,41(1989)

77. Licci,F., Tissot,P. and Scheel,H.J. *J.Less Comm.Met.* 150,201(1989)

78. Tripathi,R.B., Singh,S., Khullar,S.M., Khurana,B.S., Kotnala,R.K., Jain,K., Reddi,B.V., Goel,R.C., Nagpal,K.C., Singhal,S. and Das,B.K. *Sol.Stat.Commun.* 69,1165(1989)

79. Capponi,J.J., Chaillout,C., Hewat,A.W., Lejay,P., Marezio,M., Nguyen,N., Raveau,B., Soubeyroux,J.L., Tholence,J.L. and Tournier, *Europhys.Lett.*3, 1301(1987)

80. Galasso,F., *J.of Metals*, 39(6),8(1987)

81. Murfy,D.W., Sunshine,S.A., Gallagher,P.K., O'Bryan,H.M., Cava,R.J., Batlogg,B., Van Dover,R.B., Scheemeyer,L.F. and Zahurak,S.M., p.181 in ref. 65

82. Cox,D.E., Moodenbaugh,A.R., Hurst,J.J. and Jones,R.H., *J.Phys.Chem.Solids*, 49,47(1988)

83. David,W.I.F., Harisson,W.T.A., Gunn,J.M.F., Moze,O., Soper,A.K., Day,P., Jorgensen,J.D., Hinks,D.G., Beno,M.A., Soderholm,L., Capone,D.W., Schuller,I.K., Segre,C.U., Zhang,K. and Grace,J.D., *Nature*, 327,310(1987)

84. Kajitani,T., Oh-Ishi,K., Kikuchi,M., Syono,Y. and Hirabayashi,M., *Jpn.J.Appl.Phys.* 26,L1144(1987)

85. Kikuchi,M., Syono,Y., Tokiwa,A., Oh-Shi,K., Arai,H., Hiraga,K., Kobayashi,N., Sasaoka,T. and Muto,Y., *Jpn.J.Appl.Phys.* 26,L1066(1987)

86. Torardi,C.C., McCarron,E.M., Subramanian,M.A., Horowitz,H.S.,

Michel,J.B., Sleight,A.W. and Cox,D.E, p.152 in ref. 65

87. Collin,G., Audier,A.C. and Romes,R., *J.Phys.France*, 49,383(1988)

88. Beno,M.A., Soderholm,L. Capone,D.W., Hinks,D.G., Jorgensen,J.D., Grace,J.D., Schuller,I.K., Segre,C.U. and Zhang,K., *Appl.Phys.Lett.* 51,57(1987)

89. Beech,F., Miraglia,S., Santoro,A. and Roth,R.S., *Phys.Rev.* B35,8778(1987)

90. Renault,A., McIntyre,G.J., Collin,G., Pouget,J.-P. and Comes,R., *J.Physique*, 48,1407(1987)

91. Hewat,A.W., *Neutron News*, 1,28(1990)

92. Sleight,A.W., *Science*, 242,1519(1988)

93. Jorgensen,J.D., Beno,M.A., Hinks,D.G., Soderholm,L., Volin,K.J., Hitterman, R.L.,Grace,J.D., Schuller,I.K., Segre,C.U., Zhang,K. and Kleefisch,M.S., *Phys.Rev.*B36, 3608(1987)

94. Gallagher.P.K., O'Bryan,H.M., Sunshine, S.A. and Murphy,D.W., *Mat.Res.Bull.* 22,995(1987)

95. Harris,D.C. and Hewston,T.A., *J. Solid State Chem.* 69,182(1987)

96. Appelman,E.H., Morss,L.R., Kini,A.M., Geiser,U., Umezawa,A., Crabtree,G.W. and Carlson,K.D., *Inorg.Chem.* 26,3237(1987)

97. Matacotta,F.C., Nobile,G., Serrini,G., Giardina,M.D. and Merlini,A.E. *Mat.Res.Soc.Symp.Proc.* 99,561 (Materials Research Society, Pittsburgh, PA, 1988).

98. Dou,S.X., Liu,H.K., Bourdillon,A.J., Savvides,N., Zhou,J.P. and Sorrell,C.C. *Solid St.Comm.* 68,221(1988)

99. Tao,Z., Alburger,D.E., Jones,K.W., Yao,Y.D. and Kao,Y.H. *Appl.Phys.Lett.* 53,1440(1988)

100. Kawamura,G. and Hiratani,M. *J.Electrochem.Soc.*, 134,3211(1987)

101. Cava,R.J., Batlogg,B., Chen,C.H., Rietman,E.A., Zohurak,S.M. and Werder,D., *Phys.Rev.* B36,5719(1987)

102. Chaillout,C., Alario-Franco,M.A., Capponi,J.J., Chenavas,J., Hodeau,J.L. and Marezio,M., *Phys.Rev.* B36,7118(1987)

103. Alario-Franco,M.A., Chaillout,C. *Solid State Ionics*, 32/33,1056(1989)

104. Chaillout,C., Alario-Franco,M.A., Capponi,J.J., Chanavas,J., Strobel,P. and Marezio,M., *Solid State Commun.* 65,283(1988)

105. Mei,Y., Jiang,C., Green,S.M., Luo,H.L. and Politis,C., *Z.Phys.*B69,11(1987)

106. Van Den Berg,J., Van Der Beek,C.J., Kes,P.H., Nieuwenhuys,G.J., Mydosh,J.A., Zandbergen,H.W, Van Berkel,F.P.F., Steens,R. and Ijdo,D.J.W., *Europhys.Lett.*4, 737(1987)

107. Wong-Ng,W. and Cook,L.P. p.624 in ref. 35

108. Jorgensen,J.D., Veal,B.W., Kwock,W.K., Crabtree,G.W., Umezawa,A., Nowicki,L.J. and Paulikas,A.P., *Phys.Rev.Lett.*B36, 5731(1987)

109. LaPlaca,S.(courtesy of) in: Clarke,D.R. p.273 in ref. 65

110. O'Bryan,H.M. and Gallagher,P.K. p.640 in ref. 65

111. Viegers,M.P.A., de Leeuw,D.M., Mutsaers,C.A.H.A., van Hall,H.A.M., Smoorenburg,H.C.A., Hengst, J.H.T., de Vries,J.W.C. and Zalm,P.C.,*J.Mat.Res.*2,743(1987)

112. Button,T.W., Ward,P.J., Rand,B., Sharp,J.H., Messer,P.F. and Harris,E.A., *Brit.Ceram.Proc.*40,93(1988)

113. Sleight,A.W., "Copper and Bismuth Based High Temperature Superconductors", presented in the 7th International Conference in Solid State Ionics (SSI-7), Hakone (Japan), Nov. 5-11, 1989, to be published in the proceedings

114. Kaiser,D.L., Gayle,F.W., Roth,R.S. and Swartzendruber,L.J. *J.Mater.Res.* 4,745(1989)

115. Alford,McN.N., Birchall,J.D., Clegg,W.J., Harmer,M.A., Kendall,K. and Jones,D.H, *J.Mat.Sci.*23,761(1988)

116. Fiory,A.T., Gurvitch,M., Cava,R.J. and Espinosa,G.P. *Phys.Rev.*B36,7262(1987)

117. Freitas,P.P. and Plaskett,T.S., *Phys.Rev.*B36,5723(1987)

118. Han,Y.H. and Monroe,D.W., *Mat.Res.Soc.Symp.Proc.* 99,753 (Materials Research Society, Pittsburgh, PA, 1988).

119. Rothman,S.J., Routbort,J.L. and Baker,J.E., *Phys.Rev.*B40,8852(1989)

120. Ikuma,Y. and Akiyoshi,S., *J.Appl.Phys.*64,3915(1988)

121. Kishio,K., Suzuki,K., Hasegawa,T., Yamamoto,T., Kitazawa,K. and Fueki,K. *J.Solid State Chem.* 82,192(1989)

122. Glowacki,B.A., Highmore,R.J., Peters,K.F., Greer,A.L. and Evetts,J.E. *Supercond.Sci.Techn.*1,7(1988)

123. O'Bryan, H.M. and Gallagher, P.K., *J.Mater.Res.*3,619(1988)

124. Tu,K.N., Yeh,N.C., Park,S.I. and Tsuei,C.C. *Phys.Rev.*B39,304(1989)

125. Ottaviani,G., Nobili,C., Nava,F., Affronte,M., Manfredini,T., Matacotta,F.C., Galli,E., *Phys.Rev.*B39,9069(1989)

126. O'Sullivan,E.J.M. and Chang,B.P., *Appl.Phys.Lett.*52,1441(1988)

127. Vischjager,D.J., Van Der Put,P.J., Schram,J. and Schoonman,J. *Sol.St.Ionics*,27,199(1988)

128. MacManus,J.L., Fray,D.J. and Evetts,J.E. *Supercond.Sci.Techn.*1,291(1989)

129. Min,B.-J., Yoo,H.-I. and Park,Y.K. *Mater.Lett.*7,325(1989)

130. Shi,D., Zhang,K. and Capone,D.W. *J.Appl.Phys.*64,1995(1988)

131. Alford,N.McN., Clegg,W.J., Harmer,M.A., Birchall,J.D., Kendall,K. and Jones,D.H. *Nature* 332,58(1988)

132. Rothman,S.J., Routbort,J.L., Liu,J.-Z., Downey,J.W., Thompson,L.J., Fang,Y., Shi,D., Baker,J.E., Rice,J.P., Ginsberg,D.M., Han,P.D. and Payne,D.A. "Anisotropy of oxygen tracer diffusion in $YBa_2Cu_3O_{7-\delta}$ single crystals", invited paper at the TMS Fall Meeting, Indianapolis, IN, Oct. 1-5, 1989. To be published in the proceedings.

133. McColm,I.J. and Clark,N.J. p.60 in **Forming,Shaping and Working of High Perfomance Ceramics** (Blackie 1988)

134. Grader,G.S., O'Bryan,H.M. and Rhodes,W.W. *Appl.Phys.Lett.* 52,1831(1988)

135. Costa,G.A., Ferretti,M., Fornasini,M.L. and Olcese,G.L. *Sol.St.Commun.*65,469(1988)

136. Hepp,A.F., Gaier,J.R., Philipp,W.H., Warner,J.D., Garlick,R.G., Pouch,J.J. and Hambourg,P.D. *Mat.Res.Soc.Symp.Proc.* 99,615 (Materials Research Society 1988)

137. Davison,S., Smith,K., Zhang,Y-C., Liu,J-H., Kersaw,R., Dwight,K., Rieger,P.H. and Wold,A. p.65 in ref. 35

138. Keller,S.W., Kevin,J.L., Faltens,T.A., Michaels,J.N. and Stacy,A. p.114 in ref. 35

139. Johnson,D.W.Jr., Gallagher,P.K., Schrey,F. and Rhodes,W.W. *Ceram.Bull.*55,520(1976)

140. Tseung,A.C.C. and Bevan,H.L. *J.Mat.Sci.*5,604(1970)

141. Johnson,S.M., Gusman,M.I., Rowcliffe,D.J., Geballe,T.H. and Sun,J.Z. *Adv.Cer.Mat.*2(3B),337(1987)

142. Medelius,H and Rowcliffe,D.J., *Mat.Sci.Eng.*A109,289(1989)

143. Kodas,T.T., Engler,E.M., Lee,V.Y., Jacowitz,R., Baum,T.H., Roche,K., Parkin,S.S.P., Young,W.S., Hughes,S., Kledar,J and Auser,W. *Appl.Phys.Lett.*52,1622(1988)

144. Manthiran,A. and Goodenough,J.B.,*Nature*,329,701(1987)

145. Ravindranathan,P., Komarneni,S., Bhalla,A., Roy,R. and Cross,L.E., *J.Mater.Res.*3,810(1988)

146. Yurek,G.J., Vander Sande,J.B., Rudman,D.A. and Chiang,Y.-M. *J.Metals* 40(1),16(1988)

147. Murr,L.E., Hare,A.W. and Eror,N.G., *Nature*,329,37(1987)

148. Lee,D.F. and Salama,K., "Mechanical and Superconducting Properties of $YBa_2Cu_3O_{7-\delta}$-Ag Composites", presented in 92nd Ann.Meeting, Am.Ceram.Soc., Dallas, Texas, 22-26 April 1990.

149. Sen,S., Chen,I.-G., Chen,C.H. and Stefanescu,D.M., *Appl.Phys.Lett.* 54,766(1989)

150. Several papers presented in the 92nd Annual Meeting, American Ceramic Society, Dallas, Texas, 22-26 April 1990

151. Alford,N.McN., Button,T.W. and Birchall,J.D. "Processing, Properties and Devices in High-T_c Superconductors", presented in "High Temperature Superconductors", Univ. of Birmingham, 19-21 Sept. 1989

152. Selvamanickam,V. and Salama,K. "Effects of Microstructural Defects and Grain Orientation on Current Density of $YBa_2Cu_3O_{7-\delta}$ Superconductor", as in ref. 150.

153. Tarascon,J.M., McKinnon,W.R., Greene,L.H., Hull,G.W. and Vogel,E.M. *Phys.Rev.*B36,226(1987)

154. Kistenmacher,T.J. *Sol.St.Commun.*65,981(1987)

155. Greaves,C and Slater,P.R. *Supercond.Sci.Techn.*2,5(1989)

156. Fartash,A. and Oesterreicher,H., *Sol.St.Commun.*66,39(1988)

157. Dalichaouch,Y., Torikachvili,Early,E.A., Lee,B.W., Seaman,C.L., Yang,K.N., Zhou,H. and Maple,M.B. *Sol.St.Commun.*65,1001(1988)

158. p.B-128 in ref. 6

159. Shannon,R.D., *Acta Cryst.*A32,751(1976)

160. Liang,R., Inaguma,Y., Takagi,Y. and Nakamura,T. *Jap.J.Appl.Phys.* 25,L1150(1987)

161. Cabtree,G.W., Downey,J.W., Flandermeyer,B.K., Jorgensen,J.D., Klippert,T.E., Kupperman,D.S., Kwok,W.K., Lam,D.J., Mitchell,A.W., McKale,A.G., Nevitt,M.V., Nowicki,L.J., Paulikas,A.P., Poeppel,R.B., Rothman,S.J., Routbort,J.L. Singh,J.P., Sowers,C.H., Umezawa,A. and Veal,B.W. p.444 in ref. 35

162. Wu,M.K., Ashburn,J.R., Higgins,C.A., Loo,B.H., Burns,D.H., Ibrahim,A., Rolin,T.D., Chien,F.Z. and Huang,C.Y., *Phys.Rev.*B37,9765(1988)

163. Chen,I-.W. Keating,S., Keating,C.Y., Wu,X., Xu,J., Reyes-Morel,P.E. and Tien,T.Y. p.457 in ref. 35

164. Tallon,J.L., Huang,M., Turrillas,X., Meisels,R. and Bungre,S. poster presented in the Conference on High Temperature Superconductivity, 14-15 Dec. 1987, Univ. of Bristol, Bristol, The Institute of Physics.

165. Felner,I. and Barbara,B. *Sol.St.Commun.*66,205(1988)

166. Moure,C., Fernandez,J.M., Duran,P., Vieira,S. and Aguilo,A. presented in Strasbourg,France, Europe-Materials Research Society, May 31- June 2(1988)

167. Saito,Y., Noji,T., Endo,A., Higuchi,N., Fujimoto,K., Oikawa,T., Hattori,A. and Furuse,K., *Physica*,148B,336(1987)

168. Markert,J.T., Dalichaouch,Y. and Maple,M.B. p.312 in ref. 48

169. Maeno,Y., Tomita,T., Kyogoku,M., Awaji,S., Aoki,Y., Koshino,K., Minami,A. and Fujita,T. *Nature*,328,512(1988)

170. Shindo,D., Hiraga,K., Hirabayashi,M., Tokiwa,A., Kikuchi,M., Syono,Y., Nakatsu,O., Kobayashi,N., Muto,Y. and Aoyagi,E. *Jap.J.Appl.Phys.*26,L1667(1988)

171. Yao,Y.D., Krol,A., Kao,Y.H., Waltus,C., Spagna,S., Althoff,J., Woronisk,S., Jang,L.Y. and Xu,F. *Mat.Res.Soc.Symp.Proc.* 99,407 (Materials Research Society, 1988)

172. Pan,K.K., Mathias,H., Rey,C.M., Moulton,W.G., Ng,H.K., Testardi,L.R. and Wang,Y.L. *Phys.Lett.*A125,147(1987)

173. Dominec,J., Smrcka,L., Vasec,P., Geurten,S., Smrckova,O., Sykorova,D. and Hajek,B. *Sol.St.Commun.*65,373(1988)

174. Dexin,Z., Mingshan,X., Ziqing,Z., Shubin,Y., Huansui,Z. and

Shuxia,S. *Sol.St.Commun.*65,339(1988)

175. Barns,R.L. and Laudise,R.A. *Appl.Phys.Lett.*51,1373(1987)

176. Hill,D.M., Meyer,III,H.M. and Weaver,J.H. *Appl.Phys.Lett.*53,1657(1988)

177. Jin,S.-G., Liu,L.-G. Zhu,Z.-Z and Huang,Y.-L. *Sol.St.Commun.* 69,179(1989)

178. Cullity,B.D. p.86 in **Elements of X-ray Diffraction**, 2nd ed., Addison-Wesley Publ.Co.Inc. (1978)

179. "ISIS User Guide: Experimental Facilities at ISIS", Rutherford Appleton Laboratory Report 88-030(1988)

180. David, W.I.F., Akporiaye,D.E., Ibberson,R.M. and Wilson,C.C. "The High Resolution Powder Diffractometer at ISIS - An Introductory Guide, Version 1.0", Rutherford Appleton Laboratory (1988)

181. Blumenthal,R.N. and Seitz,M.A. p.109 in **Electrical Conductivity in Ceramics and Glass. Part A.** Tallan,N.M. ed. Marcel Dekker, Inc., New York (1974)

182. Bottelberghs,P.H. pp.145-172 in **Solid Electrolytes: General principles, characterization, materials, applications**, Hagenmuller,P., ed., Academic Press (1978)

183. Kilner,J.A., *Materials Science Forum*,7,205(1986)

184. Khan,N., **Ionic conductivity microstructure relationships in the ternary Zr-Ce-Y-O systems**, Doctorate Thesis, Imperial College, Univ. of London (1990)

185. MacDonald,J.R. ed., **Impedance Spectroscopy. Emphasizing Solid Materials and Systems**, John Wiley & Sons Inc.(1987)

186. Bell,A.M.T., *Supercond.Sci.Techn.*3,559(1990)

187. Schnettler,F.J., Monforte,F.R. and Rhodes,W.W. p.79 in **Science of Ceramics**,vol.4, Edi. by Steward,G.H., British Ceramic Society, Henry Blacklock &Co Ltd, Manchester, UK, 1968

188. **CRC Handbook of Chemistry and Physics** (1986-1987) 67th ed., pp.B68-B146, CRC Press Inc., Baca Raton, Florida.

189. Wang,C.T., Lin,L.S., Lin,J.H., Su,J.Y., Yang,S.J. and Hsu,S.E., *Mat.Res.Soc.Symp.Proc.* 99,257 (Materials Research Society 1988)

190. Spitz,J. and Viguie,J-C. British patent no. 1 362 803, (1974).

191. Blandenet,G., Court,M. and Lagarde,Y. *Thin Solid Films*,77, 81(1981)

192. Lang,R.J. *J.Acoust.Soc.Am.*34,6(1962).

193. p.81 in ref.133.

194. Stroumbos,H. Univ. Paris-Sud., Lab. de Physique de Solides, Personal communication (1989).

195. Ley,K., Kontoulis,I. and Steele,B.C.H. "Preparation of bulk and thick films high temperature superconductors by mist pyrolysis", to be published in *Brit.Ceram.Proc.* (1990/91)

196. Tsuchida,K., Tsudo,H. and Kato,A. *J.Mat.Sci.Lett.* 8,222(1989)

197. Kodas,T., Datye,A., Lee,V. and Engler,E. *J.Appl.Phys.* 65,2149(1989)

198. Voigt,J.A., Buncer,B.C., Doughty,D.H., Lamppa,D.L. and Kimball,K.M. *Mat.Res.Soc.Symp.Proc.* 99,635(MRS, Pittsburgh, PA, 1988).

199. Turrillas,X., Tallon,J.L., Huang,M., Meisels,R., Kontoulis,I. and Steele,B.C.H., *Brit.Cer.Proc.* 41,273 (1989)

200. Kontoulis,I., Turrillas,X., Meisels,R., Bungre,S., Steele,B.C.H. *J. Less Common Met.* 151,229 (1989)

201. Murugaraj,P., Maier,J. and Rabenau,A. *Sol.St.Comm.*66, 735(1988)

202. Murugaraj,P., Maier,J. and Rabenau,A. *Sol.St.Ionics* 32/33, 1183(1989)

203. Weppner,W., Huggins,R.A., *Ann.Rev.Mat.Sci.*8,269(1978)

204. Rickert,H., pp.168-214 in **Electrochemistry of Solids. An introduction**, Springer-Verlag, Berlin 1982.

205. p.37 in ref.184

206. Takahashi,T., Esaka,T. and Iwahara,H. *J.Appl.Electrochem.* 7, 303(1977)

207. Takahashi,T., Esaka,T. and Iwahara,H. *J.Appl.Electrochem.* 7, 299(1977)

208. Maier,J., Murugaraj,P. and Pfundtner,G. to be printed in *Sol.St.Ionics*, 1990.

209. Baumgartner,C.E., Arendt,R.H., Iacovangelo,C.D. and Karas,B.R. *J.Electrochem.Soc.*131,2217(1984)

210. Eichenauer,W. and Müller,G. *Z.Metalkde*,53,321(1962)

211. Mizikar,E.A., Grace,R.E. and Parlee,N.A.D. *Trans.ASM*,56,101(1963)

212. Masson,C.R. and Whiteway,S.G. *Can.Met.Quart.*6,199(1967)

213. Rickert,H. and El Miligy,A.A. *Z.Metalkde*,59,635(1968)

214. Velho,L.R., El-Tayeb,N.M., Gani,J. and Parlee,N.A.D. *Trans.Met.Soc.AIME*,245, 184(1969)

215. Sano,N., Honma,S. and Matsushita,Y. *Metal.Trans*.1,301(1970)

216. Ramanarayanan,T.A. and Rapp,R.A. *Metal.Trans*.3,3239(1972)

217. Otsuka,S. and Kozuka,Z. *J.Jap.Inst.Met*.37,364(1973)

218. Park,J.H. *Mater.Let*.9,313(1990)

219. Fabry,P., Schouler,E. and Kleitz,M. *Electrochem.Acta* 23,539(1978)

220. Maier,J., Murugaraj,P., Pfundtner,G., Sitte,W. *Ber.Bunsenges.Phys.Chem.* 93,1350(1989)

221. Vischjager,D.J., van Zomeren,A.A., Schoonman,J., Kontoulis,I. and Steele,B.C.H., "Ionic Conductivity of Ceramic Superconductors", in "Solid State Ionics-7", Hakone (Japan), Nov. 1989. To be published in the proceedings.

222. Turrillas,X., Kilner,J., Kontoulis,I. and Steele,B.C.H., *J. Less Common Met.* 150,139 (1989)

223. Diaz,C., Masson,C.R. and Richardson,F.D. *Trans.Instn.Min.Metall.* 75,C183 (1966)

224. Sabras,J., Dolin,C., Ayache,J., Monty,C., Maury,R. and Fert,A. *Colloque de Physique*, 51,C1-1035 (1990)

225. Dudley,G.J. and Steele,B.C.H., *J.Solid State Chem.* 31,233(1980)

226. Sabras,J., Peraudeau,G., Berjoan,R. and Monty,C. CNRS Lab. de Phys. des Materiaux, Bellevue, 92190 MEUDON, France. "Oxygen diffusion, oxygen vacancy concentrations and chemical diffusion in $Y_{1-u}Ba_{2-v}Cu_{3-w}O_{7-\delta}$", to be published.